KINETIC TRAJECTORY SIMULATION MODEL FOR MAGNETIZED PLASMA SHEATH

A THESIS SUBMITTED TO THE

CENTRAL DEPARTMENT OF PHYSICS

INSTITUTE OF SCIENCE AND TECHNOLOGY

TRIBHUVAN UNIVERSITY

NEPAL

FOR THE AWARD OF

DOCTOR OF PHILOSOPHY

IN PHYSICS

BY

BHESHA RAJ ADHIKARI

SEPTEMBER 2020

KINETIC TRAJECTORY SIMULATION MODEL FOR MAGNETIZED PLASMA SHEATH

A THESIS SUBMITTED TO THE

CENTRAL DEPARTMENT OF PHYSICS

INSTITUTE OF SCIENCE AND TECHNOLOGY

TRIBHUVAN UNIVERSITY

NEPAL

FOR THE AWARD OF

DOCTOR OF PHILOSOPHY

IN PHYSICS

BY

BHESHA RAJ ADHIKARI

SEPTEMBER 2020

DECLARATION

Thesis entitled **"KINETIC TRAJECTORY SIMULATION MODEL FOR MAGNETIZED PLASMA SHEATH"** which is being submitted to the Central Department of Physics, Institute of Science and Technology (IOST), Tribhuvan University, Nepal for the award of the degree of Doctor of Philosophy (Ph.D.), is a research work carried out by me under the supervision of Prof. Dr. Raju Khanal, Central Department of Physics, Tribhuvan University, Kirtipur, Kathmandu, Nepal and co-supervised by Dr. Hari Prasad Lamichhane, Central Department of Physics, Tribhuvan University, Kirtipur, Kathmandu, Nepal.

This research is original and has not been submitted earlier in part or full in this or any other form to any university or institute, here or elsewhere, for the award of any degree.

Bhesha Raj Adhikari

RECOMMENDATION

This is recommended that **Mr. Bhesha Raj Adhikari** has carried out research entitled **"KINETIC TRAJECTORY SIMULATION MODEL FOR MAGNETIZED PLASMA SHEATH"** for the award of Doctor of Philosophy (Ph.D.) in **Physics** under our supervision. To our knowledge, this work has not been submitted for any other degree.

He has fulfilled all the requirements laid down by the Institute of Science and Technology (IOST), Tribhuvan University, Kirtipur for the submission of the thesis for the award of Ph.D. degree.

. . . . . .

Dr. Raju Khanal
Supervisor
(Professor)
Central Department of Physics
Tribhuvan University
Kirtipur, Kathmandu,
Nepal

. . . . . .

Dr. Hari Prasad Lamichhane
Co-supervisor
(Associate Professor)
Central Department of Physics
Tribhuvan University
Kirtipur, Kathmandu,
Nepal

APRIL 2019

LETTER OF APPROVAL

[Date: 03/04/2019]

On the recommendation of Prof. Dr. **Raju Khanal** and Dr. **Hari Prasad Lamichhane**, this Ph.D. thesis submitted by **Bhesha Raj Adhikari**, entitled **"KINETIC TRAJECTORY SIMULATION MODEL FOR MAGNETIZED PLASMA SHEATH"** is forwarded by Central Department Research Committee (CDRC) to the Dean, IOST, T.U..

. . . . . .

Dr. Binil Aryal
Professor,
Head,
Central Department of Physics,
Tribhuvan University
Kirtipur, Kathmandu
Nepal

ACKNOWLEDGMENTS

At first, I am very pleased to extend my gratefulness to all respected persons who provided me motivation, support and guidance for the completion of this research work.

I would like to express my sincere thanks and appreciation to my supervisors Prof. Dr. Raju Khanal and Dr. Hari Prasad Lamichhane, Central Department of Physics, Tribhuvan University, Kirtipur for their valuable suggestions, motivation, time and effort for completing this research work. Their guidance, constant support, monitoring and encouragement throughout this research work leads to the successful completion of this work.

I would like to express my heartfelt thanks to Prof. Dr. Binil Aryal, Head of the Central Department of Physics, Tribhuvan University, Kirtipur, for his encouragements and suggestions. He matained homely and academic environment in Central Department of Physics for research works.

I would like to express my sincere gratitude to Prof. Dr. Lok Naryan Jha, Prof. Dr. Sitaram Prasad Byahut, Prof. Dr. Shekhar Gurung, Prof. Dr. Mukunda Mani Aryal, Prof. Dr. Jeevan Jyoti Nakarmi, Prof. Dr. Narayan Prasad Adhikari, Prof. Dr. Ram Prasad Regmi, Prof. Dr. Om Prakash Niraula, Dr. Bal Ram Ghimire, Dr. Ghanashyam Thakur, Dr. Arjun Kumar Gautam, Dr. Ajay Kumar Jha, Dr. Sanju Shrestha, Dr. Gopi Chandra Kaphle for their valuable support throughout the journey of my research work.

My special thanks go to Mr. Suresh Basnet and Mr. Rajesh Kumar Bachchan for their continuous support and suggestions to complete this research work. I also want to thank Mr. Roshan Chalise, Ms. Shanti Thagunna, Mr. Vijay Kumar Singh Kshetri and other family members of CDP for their evergreen support and encouragement during the research work.

I would like to thank Kathmandu University, Dhulikhel, St. Xavier's College, Kathmandu, Amrit Science Campus, Kathmandu, Ravenshaw University, Cuttack, India, Amity University, Lucknow, India, VIT University, Chennai, India for opportunity to present my research work in international conferences.

I am thankful to Bhaktapur Multiple Campus, Bhaktapur, Institute of Science and Technology for granting me study leave to do my research work. I would also like to thank University Grants Commission for providing the Ph.D. fellowship.

At last but not the least, I would like to thank my parents and family members for their encouragement, patience and regular support. My special thank goes to Mrs. Rita

Adhikari, Ms. Rachana Adhikari and Mr. Parikshit Adhikari who are always supportive.

Bhesha Raj Adhikari
April, 2019

ABSTRACT

Plasma wall interaction is an important phenomenon in all applications, where plasma comes into contact with a material wall. The understanding of plasma sheath, a thin layer that is formed between the core plasma and the wall, is crucial in understanding as well as controlling the particle and energy fluxes reaching the surface. Because of sharp gradients in the sheath region the fluid approach, which is usually used to explain the core plasma and presheath region, does not yield accurate results in the sheath region. In order to understand the characteristics of the sheath formed in a magnetized plasma the method of kinetic trajectory simulation (KTS) has been used and also the coupling of presheath-sheath has been extended. Assuming that, at the sheath entrance distribution functions of ion and electron to be cut-off Maxwellian the final self consistent states are obtained by solving the governing kinetic equations, iteratively. In order to satisfy the Bohm-Chodura condition, initial velocity of ions entering the sheath region is taken equal to the ion acoustic velocity. As the plasma sheath region is small compared to the collision mean free path and also the particle densities are less compared to the presheath region, the sheath region is assumed to be collisionsless.

It has been observed that the presheath electron temperature affects the Child-sheath thickness and the space charge density reaching the wall. Furthermore, improved distribution of electrons, i.e., consideration of cut-off by the negative wall yields our simulation result to deviate from earlier works without cut-off by about 3%. The coupling scheme, developed, provides a basis for smooth transition of plasma parameters in presheath-sheath interface. Ion velocity at presheathsheath boundary is also affected by obliqueness of the field. Velocity of ion increases towards the wall as the obliqueness of the field increases.

In the presence of oblique magnetic field in the plasma sheath, the damping of ion velocity with time has been observed. It is shown that the velocity waves are damped in plasma without collisions in the time scale of the order of seconds. As the obliqueness of the field changes the separation of the mean values as well as the maximum amplitude of all the three components of the velocity also change. Mean value of $x-$component of velocity is nearly equal to zero for all angles at magnetic field 2.5 mT, but the mean value of y and $z-$components of velocity varies with nearly equal amplitudes. When the field is greater than zero, the mean value of $x-$component is almost equal to zero, but the mean values of y and $z-$components of velocities are both nearly equal to 10^3 m/s at zero field. But for the greater value of magnetic field, the two components of velocities are split with different mean values. The frequency of oscillations of three component

of velocity of ions changes as the magnetic field changes. The maximum amplitude of $x-$component of velocity is almost independent of the magnetic field but the maximum amplitudes of y and $z-$components of velocity change and show oscillating nature as the magnetic field changes also.

As the obliqueness of the field changes the mean values, beat frequency as well as the maximum amplitude of the three components of the velocity also change but frequency of oscillation almost remains same at magnetic field 2 mT. Modulation frequency of ions in a magnetized plasma sheath has been observed for different angles at constant magnetic field 6 mT. Also, by varying angle average values, maximum amplitude, damping factor as well as frequency of oscillation of the velocities are studied. For y and $z-$components of velocity maximum amplitudes change but for $x-$component the maximum amplitude remains constant. However, there is a quite change observed in the values of damping factor and modulation frequency for all component of velocity. Frequency of oscillation of all velocity components of ions remains same. At 30° and 60°, shoulder is not seen but at 75°, shoulder in the velocity profile is obtained around 0.05 second for each component of velocity. The amplitude of the oscillating velocity decreases with time and the mean values of different component of velocity changes as well. The computed and fitted values of the vector sum of oscillatory part of all three components of velocities match. At angle 30°, damping rate of vector sum of oscillatory part of total velocity increases with the magnetic field increases from 1 mT to 5 mT. On the other hand vector sum of oscillating part of initial velocity is almost equal for magnetic field 1 mT, 3 mT and 5 mT at the same angle 30°. But for different obliqueness of the magnetic field, the initial velocity of the vector sum of oscillating part at 90° is greater than that at 30° and 60°.

The input physical parameters taken are consistent with earlier previous works and comparison reveal that our results agree well. The present magnetized plasma wall transition study provides a basis for proper understanding of the plasma sheath, which has useful applications in fusion devices as well as in many industrial applications of plasma.

LIST OF ACRONYMS AND ABBREVIATIONS

DFA	Distribution Function Approach
D-T	Deuterium-Tritium
ICF	Inertial Confinement Fusion
JET	Joint European Torus
ITER	International Thermonuclear Experimental Reactor
KTS	Kinetic Trajectory Simulation
MCF	Magnetic Confinement Fusion
PWT	Plasma Wall Transition
SOL	Scrape Off Layer
TFTR	Tokamak Fusion Test Reactor

LIST OF SYMBOLS

B	Magnetic field
C_{s}	Ion-acoustic velocity
E	Electric field
$f_{\mathrm{st}}^{\mathrm{e}}$	Starting distribution function of electron
$f_{\mathrm{st}}^{\mathrm{i}}$	Starting distribution function of ion
F	Lorentz force
k_{B}	Boltzmann constant
L	Dimension of the plasma system
m^{i}	Mass of ion
n^{e}	Electron density
n^{i}	Ion density
n	Plasma density
N_{D}	Number of particles in a Debye sphere
$r_{\mathrm{st}}^{\mathrm{e}}$	Starting configuration of electron
$r_{\mathrm{st}}^{\mathrm{i}}$	Starting configuration of ion
T^{i}	Temperature of ion
$T_{\mathrm{ps}}^{\mathrm{e}}$	Electron temperature at the presheath side of the sheath edge
$T_{\mathrm{ps}}^{\mathrm{i}}$	Ion temperature at the presheath side of the sheath edge
$u_{\mathrm{ps}}^{\mathrm{e}}$	Electron fluid velocity at the presheath side of the sheath-presheath boundary
$u_{\mathrm{ps}}^{\mathrm{i}}$	Ion fluid velocity at the presheath side of the sheath-presheath boundary
$v_{\mathrm{st}}^{\mathrm{e}}$	Starting velocity of electron
$v_{\mathrm{st}}^{\mathrm{i}}$	Starting velocity of ions
ϵ_0	Permittivity of free space
$\lambda_{\mathrm{D}}^{\mathrm{e}}$	Electron Debye length
τ	Mean time between collisions of electron with neutral atom
γ^{e}	Electron polytropic constant
γ^{i}	Ion polytropic constant
ω	Frequency of plasma oscillation
Ω	Cyclotron frequency or gyrofrequency

LIST OF TABLES

Page No.

Table 1: The observed data of mean value, amplitude, damping constant, frequency of oscillation and phase angle at magnetic field 2.5 mT. . 79

Table 2: The observed data of average value, amplitude, damping constant, frequency of oscillation and beat frequency at magnetic field 2 mT. 84

Table 3: The observed data of average value, amplitude, damping constant, frequency of oscillation and modulation frequency at magnetic field 6 mT 87

LIST OF FIGURES

Page No.

Figure 1: Physical concept of Debye shielding. 2
Figure 2: Existence of plasma in diverse ranges of temperature and density. . 3
Figure 3: Schematic diagram representing the D-T fusion reaction. 4
Figure 4: Progress in the confinement performence of plasma. 5
Figure 5: Schematic diagram of ITER. 5
Figure 6: Different stages of inertial confinement fusion. 6
Figure 7: Variation of the potential in front of the negative absorbing material wall. 7
Figure 8: Damped Oscillation in which its amplitude is decreasing exponentially. 9
Figure 9: Diagram of carrier signal, modulating sine wave signal and amplitude modulated signal. 11
Figure 10: Larmor gyration in uniform magnetic field. 36
Figure 11: In space the real orbit of the gyrating particle. 38
Figure 12: Plasma sheath model. 47
Figure 13: Potential profile monotonically decreasing from $x = L$ to $x = 0$. . . 52
Figure 14: Schematic representation of the phase-space griding. 56
Figure 15: The iteration scheme 67
Figure 16: Ion velocity distributions function (a) at the sheath entrance and (b) at the wall 71
Figure 17: Potential profile as the function of normalized distance 72
Figure 18: Child-sheath thickness as the function of presheath electron temperature 72
Figure 19: Ion flux as the function of potential for different values of presheath electron temperature 73
Figure 20: Electron flux as the function of potential for different values of presheath electron temperature 73
Figure 21: Presheath ion velocity as the function of presheath ion temperature for different values of presheath electron temperature 73
Figure 22: Variation of ion temperature as the function of presheath ion temperature 74

Figure 23: Potential profile as the function of normalized distance 74
Figure 24: Variation of velocity with time at constant magnetic field 2.5 mT for different values of obliqueness (a) at angle 0°, (b) at angle 30°, (c) at angle 45°, (d) at angle 60°, (e) at angle 75° and (f) at angle 90° 76
Figure 25: Damping of x- component of velocity with time at magnetic field 2.5 mT and angle 30°. 77
Figure 26: Damping of y- component of velocity with time at magnetic field 2.5 mT and angle 30°. 77
Figure 27: Damping of z- component of velocity with time at magnetic field 2.5 mT and angle 30°. 77
Figure 28: Damping of x- component of velocity with time at magnetic field 2.5 mT and angle 45°. 78
Figure 29: Damping of y- component of velocity with time at magnetic field 2.5 mT and angle 45°. 78
Figure 30: Damping of z- component of velocity with time at magnetic field 2.5 mT and angle 45°. 78
Figure 31: Variation of mean values of velocity with respect to angles at magnetic field 2.5 mT. 80
Figure 32: Variation of maximum amplitude of velocity with respect to angles at magnetic field 2.5 mT. 80
Figure 33: Variation of velocity with time at constant obliqueness 30° for different values of magnetic field (a) at 1.5 mT, (b) at 4.5 mT, (c) at 7.5 mT and (d) at 10.5 mT. 81
Figure 34: Variation of mean value of velocity with respect to magnetic field at angle 30° 82
Figure 35: Variation of maximum amplitude of velocity with respect to magnetic field at angle 30° 82
Figure 36: Variation of velocity with time at constant magnetic field 2 mT for different values of obliqueness (a) at 30°, (b) at 60° and (c) at 75°. 84
Figure 37: Variation of velocity with time at constant magnetic field 6 mT for different values of obliqueness (a) at 30° , (b) at 60° and (c) at 75° . 86
Figure 38: Velocity variation with time at magnetic field 3 mT and angle 30°. 87
Figure 39: Oscillatory part of total velocity with respect to time at magnetic field 3 mT and angle 30°. 88
Figure 40: Velocity variation with time at magnetic field 3 mT and angle 60°. 88
Figure 41: Oscillatory part of total velocity with respect to time at magnetic field 3 mT and angle 60°. 89
Figure 42: Velocity variation with time at magnetic field 3 mT and angle 90°. 89

Figure 43: Oscillatory part of total velocity with respect to time at magnetic field 3 mT and angle 90°. 90
Figure 44: Variation of vector sum of Oscillatory part of total velocity with respect to time at magnetic field 3 mT and different angle 90
Figure 45: Velocity variation with time at magnetic field 1 mT and angle 30°. 91
Figure 46: Oscillatory part of total velocity with respect to time at magnetic field 1 mT and angle 30°. 91
Figure 47: Variation of velocity with time at magnetic field 5 mT and angle 30°. 92
Figure 48: Oscillatory part of total velocity with respect to time at magnetic field 5 mT and angle 30°. 93
Figure 49: Variation of vector sum of Oscillatory part of total velocity with respect to time at angle 30° and different magnetic field. 93

TABLE OF CONTENTS

Page No.

Declaration i
Recommendation ii
Letter of Approval iii
Acknowledgements iv
Abstract vi
List of Acronyms and Abbreviations viii
List of Symbols ix
List of Tables x
List of Figures xi

CHAPTER 1 1

1. INTRODUCTION 1
1.1 Introduction to plasma 1
1.2 Sheath 7
1.3 Presheath 7
1.4 Damping of wave 9
1.5 Beats of wave 10
1.6 Modulation of wave 10
1.7 Motivation 11
1.8 Objectives 11
1.9 Outline 12

CHAPTER 2 13

2. LITERATURE REVIEW 13

CHAPTER 3 34

3. MATERIALS AND METHODS 34

3.1 Single particle model 34
3.2 Fluid model 37
3.2.1 Continuity equation 38
3.2.2 Momentum equation 39
3.2.3 Boltzmann relation 40
3.2.4 Poisson's equation 40
3.3 Basic concept of kinetic trajectory simulation 41
3.4 Basic equations 42
3.5 Plasma sheath model 47
3.6 Presheath-sheath coupling 51
3.7 Bohm-Chodura criterion 52
3.8 Electron density distribution 55
3.9 Discretization of the simulation region 55
3.10 Discretizing ion velocity 57
3.11 Ion trajectories 57
3.12 Ion velocity distribution function 61
3.13 Ion density distribution 61
3.14 Solution of Poisson's equation 62
3.15 Relaxation scheme 63
3.16 Electric field calculation 64
3.17 Iteration scheme 66
3.18 Introduction to Runge-Kutta method 66

CHAPTER 4 70

4. RESULTS AND DISCUSSION 70
4.1 Distribution function of ions 71
4.2 Potential profile 71
4.3 Child-sheath thickness 72
4.4 Ion and electron fluxes 72
4.5 Presheath ion velocity profile 73
4.6 Comparison of kinetic approach and fluid approach 74
4.7 Temporal ion velocity profile for different obliqueness of the magnetic field 75
4.8 Temporal ions velocity profile for different magnitude of magnetic field 80
4.9 Beat frequency of temporal ion velocity profile for different obliqueness of the magnetic field 83
4.10 Modulation frequency of temporal ion velocity profile for different obliqueness of the field 85

4.11 Vector sum of oscillatory part of temporal velocity for different obliqueness of the magnetic field 87
4.12 Vector sum of oscillatory part of temporal velocity for different value of magnetic field 91

CHAPTER 5 94

5. CONCLUSION AND RECOMMENDATIONS 94
5.1 Conclusion 94
5.2 Recommendations 96

CHAPTER 6 97

6. SUMMARY 97
6.1 Summary 97

REFERENCES 99

APPENDIX 107
A. Publications 107
B. Oral presentations 107
C. Poster presentations 108
D. Research visits 108
E. Participation in research methodology lectures 108

CHAPTER 1

1. INTRODUCTION

1.1 Introduction to plasma

Our universe consists of different types of matter, and the ones we encounter most are solid, liquid, and gas. On increasing the temperature of the substance which is initially in the solid state, it changes phase from solid to liquid and then to gas. On further increasing the temperature of a gas beyond a definite limit, it does not stay in the gaseous state; it enters a regime in which the thermal energy of its constituent particle overcomes the electrostatic interaction which ordinarily binds electrons to the atomic nuclei. Instead of hot gas composed of electrically neutral atoms, plasmas have a mixed population of charged and neutral particles. The number of ionized particle increases as the temperature is increased and different behavior is shows by the ionized gas rather than gaseous state. As the ionized particles have sufficiently high fraction, the ionized gas starts exhibiting collective behavior and the state of matter is plasma and it is neither solid nor liquid nor gas. Thus, a quasineutral gas of charged and neutral particles which shows collective behavior is plasma (Chen, 2016). The quasineutral property of plasma refers that the ion and electron densities are nearly equal i.e., $n^{\mathrm{i}} \simeq n^{\mathrm{e}} \simeq n$; where n is the plasma density. The collective behavior of plasma inferred that the motion of particles depend not only on the local conditions but also on the condition of the plasma far away from the point of interest. The term "plasma" originates from Greek, and denotes something molded or fabricated. Crookes (1879) discovered the existence of "the fourth state of matter", although the word plasma was coined by Langmuir (1928) to explain the state of matter in the positive column of glow discharge tube. Plasma is thus an ionized gas, satisfying definite criteria; however any ionized gas cannot be called plasma.

The main property of plasma is its capability to shield out any external electric field applied to it. In plasma, the given external field is shielded within a very small distance called Debye length and such phenomenon is called the Debye shielding. The representative relation of electron Debye length with the temperature of electron T^{e} and the

plasma density n is given as:

$$\lambda_{\mathrm{D}}^{\mathrm{e}} = \sqrt{\frac{\epsilon_0 k_{\mathrm{B}} T^{\mathrm{e}}}{e^2 n}}. \tag{1.1}$$

where ϵ_0 and k_{B} are the permittivity of free space and Boltzmann constant respectively. Debye shielding, which is shown in Figure 1 is statistically valid if there are large number of particles in the Debye sphere. Obviously, if there are only few particles in the sheath region, Debye shielding cannot be a statistically reasonable conception.

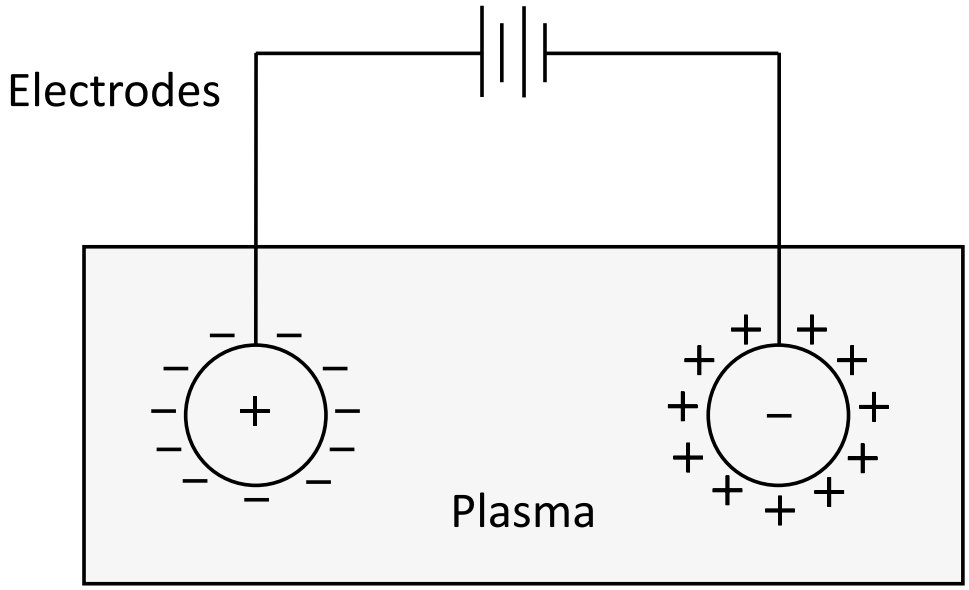

Figure 1: Physical concept of Debye shielding. (Source: Chen, 2016)

If the electrons in the plasma are displaced from a steady framework of ions, electric field will be set up in such a way as to restore the quasineutrality of the plasma by pulling the electrons back to their previous position. Due to their inertia, the electrons will overshoot and oscillate around their equilibrium position with a characteristic frequency termed as the plasma frequency. As previously stated, all the plasma are ionized gases, but not all ionized gases are plasma. The conditions that must be followed by an ionized gas to be called plasma are:

(a) The electron Debye length should be much smaller than the dimension of the system, i.e. $\lambda_{\mathrm{D}}^{\mathrm{e}} << L$.

(b) The number of particles in a Debye sphere should be very large, i.e. $N_{\mathrm{D}} >> 1$.

(c) If ω be the frequency of plasma oscillation and τ is the mean time between the collision with neutral atoms, then $\omega\tau > 1$.

In the universe, it is estimated that nearly 99 % of the visible material is in the plasma state. The stellar interiors and atmospheres, gaseous nebula, interstellar hydrogen, solar

winds and many more are plasmas. In the earth lightning is the high temperature plasma which occurs naturally. Plasma can also be created artificially by using high voltage sources to ionize the gases. As we go outside from the surface of the earth, e.g., the ionosphere, most of the space is totally dominated by plasma. Even though on the earth, plasma state is very few, but it is noticed that our solar system is dominated by plasma, as the sun is totally in plasma state.

It is often believed, due to misconception, that plasma is always formed only at very high temperature but it exists in various ranges of temperature as well as density as shown in Figure 2. Low temperature plasma which is applicable in surface modification as well as organic cleaning, are ionized gases created at pressures between 0.1 Torr and 2 Torr. Due to its diverse nature plasma has applications in different fields such as controlled thermonuclear fusion, surface treatment, bio-medical applications, lighting, medicine, electronics, transportation and space propulsion, display technology, space physics, solid state plasma, gas lasers, etc.

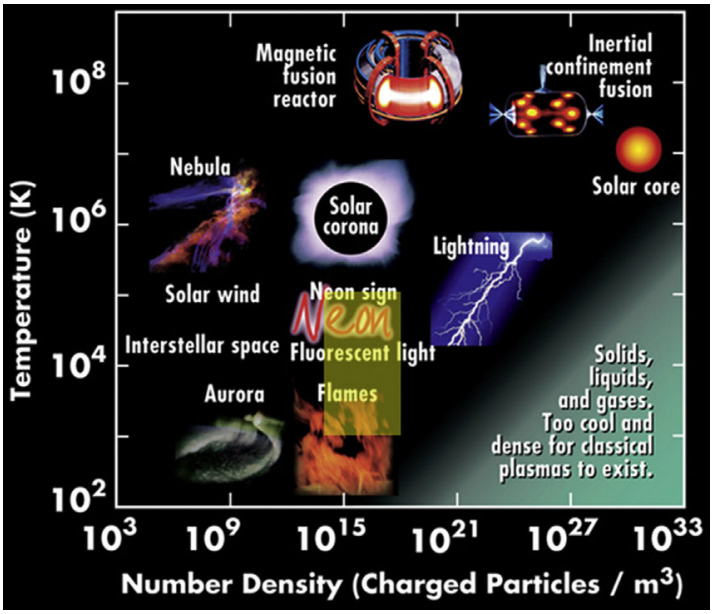

Figure 2: Existence of plasma in diverse ranges of temperature and density. (Source: https://www.lasers .llnl.gov/science/understanding-theuniverse/plasma-physics)

Nuclear fusion as the source of energy of the sun and stars is known since a long ago. Fusion energy is the potential sources of virtually limitless energy for mankind, since it can potentially supply immense amount of energy. However, it is still one of the most challenging scientific problems. According to Lawson criterion the three important parameters of fusion; temperature, confinement time and density must attain certain critical value whereby the temperature must be in the order of 10^8 K. This is much higher than the temperature at the core of the sun and hence it is not easy confining the fusion fuels. This is in fact the major issue in thermonuclear fusion experiments which is

not yet fully resolved, and hence the fusion power could not be produced for commercial application, so far. On the other hand, the problem of heating and containing such plasma is accountable for the fast growth of plasma physics, since 1950s. The nuclear fusion reaction between deuterium (D) and tritium (T) is shown in Figure 3. The D-T fusion is most conveniently attainable because the collision cross-section of the D-T fusion reactions is the highest, and occurs at the lowest temperature (Kaw & Bandyopadhyay, 2012).

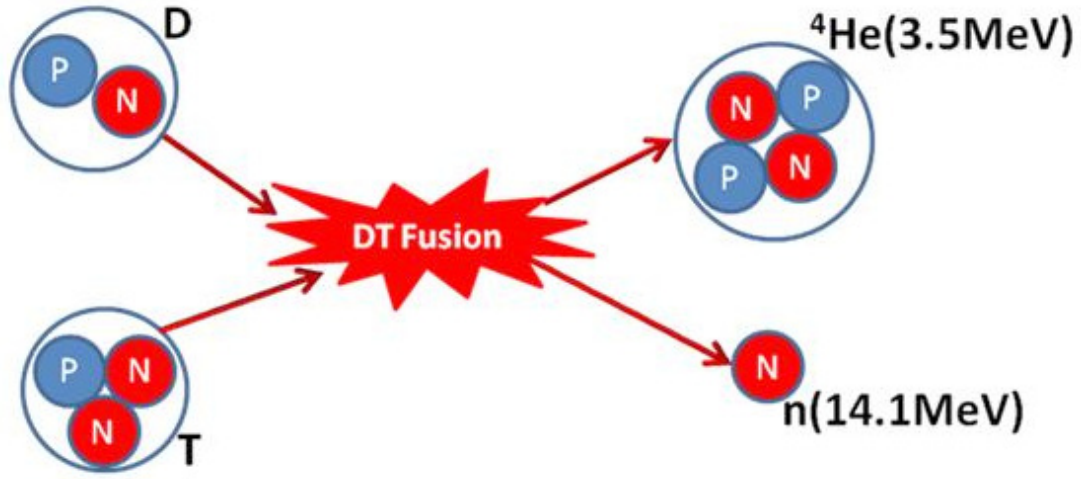

Figure 3: Schematic diagram representing the D-T fusion reaction. (Source: Kaw & Bandyopadhyay, 2012)

Different techniques for the terrestrial realization of fusion energy can be classified as: Magnetic Confinement Fusion (MCF) and Inertial Confinement Fusion (ICF). In MCF, plasma is confined by applying magnetic fields where low density plasma is confined for a longer interval of time. Among different magnetic confinement schemes, the most successful device so far is 'tokamak', a doughnut shaped magnetic chamber initiated in former Soviet Union in early 50s. The term is obtained from the Russian words for "toroidal chamber magnetic coil", toroidalnaya kamera magnitnaya katuska (Wesson, 1997). The progress in MCF research is depicted in Figure 4, which shows that since the start of tokamak experiments in the 1960s, the triple product has increased by more than three orders of magnitude. Thus, tokamaks are nowadays the most successful of the toroidal confinement systems, which makes them the most promising candidate, for the first generation of fusion reactors. The next generation tokamak named "International Thermonuclear Experimental Reactor (ITER)", an international nuclear fusion research project, is recently under construction at Cadarache in France which is shown in Figure 5. When ITER becomes operational, expected around 2030, it will become the greatest magnetic confinement plasma physics experiment. The first commercial demonstration of fusion power plant to bring the fusion energy to the commercial market will follow after the ITER project.

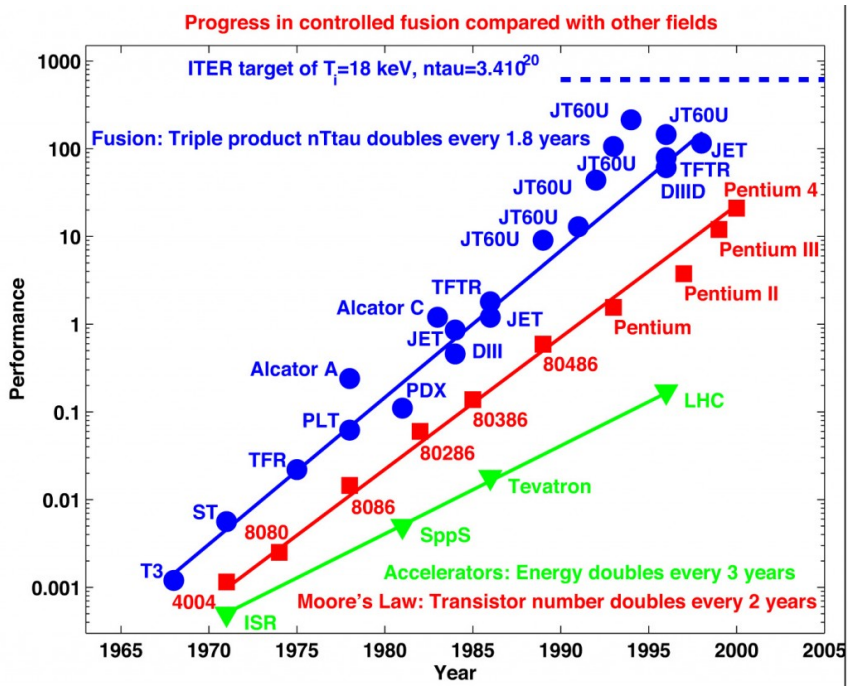

Figure 4: Progress in the confinement performence of plasma. (Source: https://www.iter.org/newsline/53/1589)

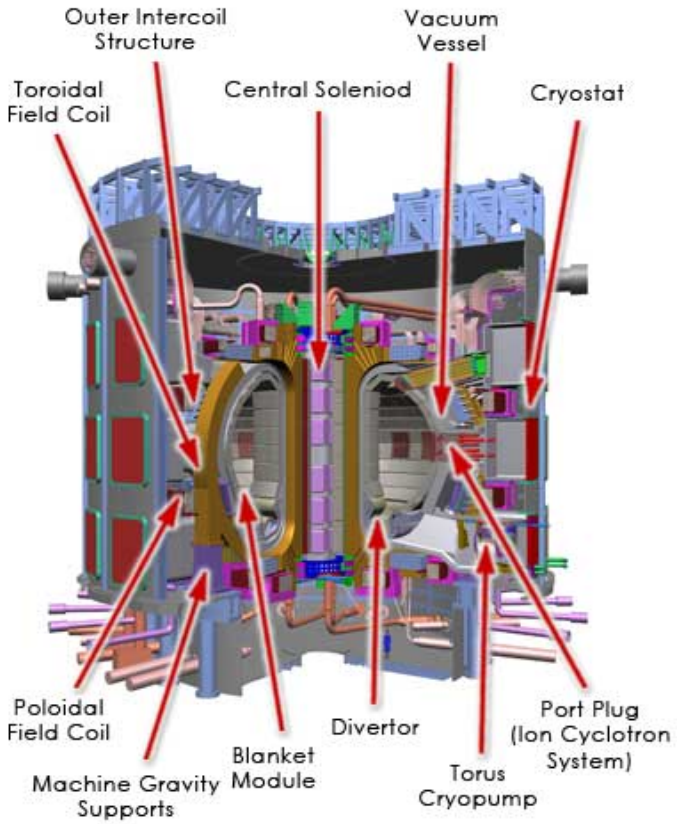

Figure 5: Schematic diagram of ITER. (Source: https://www.iter.org/mach)

The approach of ICF is totally different from MCF and aims to initiate nuclear fusion reactions by heating and compressing a fuel target, typically in the form of a pellet, that

hold deuterium and tritium mixture (Atzeni et al., 2004). In ICF, laser beams are applied to compress tiny pellet of plasma fuel to very high densities, for a small period of time (Atzeni et al., 2004). In this approach, the confinement is not attained by external fields, but by the inertia of the hot fuel, that keeps it jointly for a finite time (due to this, it is named as inertial confinement). To compress and heat the fuel, energy is delivered to the outer surface of the target, using high energy beams of laser light. The heated outer layer detonates outward, making a reaction force against the remainder of the target, accelerating it inwards, compressing the target. This process is designed to create shock waves that move inward through the target. A sufficiently strong set of shock waves can compress and heat the fuel, at the center so high that fusion reactions arise (Lindl, 1998). Figure 6 shows the different phases of inertial confinement fusion. At first, the laser beams quickly heat the outer layer of the fusion target and form a plasma corona. The unperturbed fuel is then compressed by the rocket-like blow-off of the hot surface matter. The fuel core then attains very high density (around 20 times the density of solid lead) and hence it ignites. Finally, thermonuclear burn spreads quickly through the compressed fuel, producing many times the input energy (Lindl, 1998).

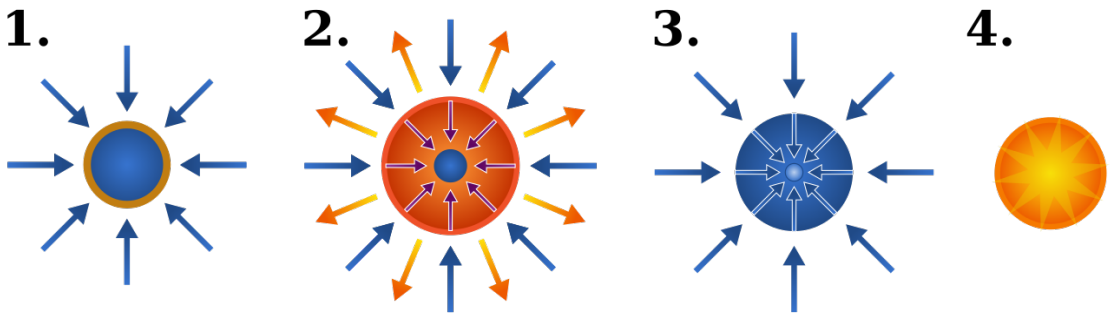

Figure 6: Different stages of inertial confinement fusion. (Source: https://en.wikipedia.org/wiki/Inertial_confinement_fusion)

Our interest is to understand how plasma interacts with a material wall when they come into contact in the presence of a magnetic field. In this work, the magnetized plasma sheath that separates the core plasma from the wall has been studies for different strength as well as obliqueness of the magnetic field using kinetic approach, namely the kinetic trajectory simulation (KTS) method. Due to the sharp gradient in the sheath region we have employed the kinetic approach, which is superior compared to fluid model as it deals with the complete distribution of plasma species whereas the fluid approach considers only the average macroscopic quantities. As this work is continuation of developing the KTS method the broad title looks similar to earlier works in our Group (Khanal, 2003; Chalise and Khanal, 2012), however, we have extended the existing 1d1v model to 1d3v model by including the effect of the magnetic field in presheath-sheath coupling scheme. In addition, the velocity profile of ions in the presence of different magnetic field strength as well as its obliqueness has been studied. Likewise, temporal components of velocity

of ions, beat frequency, modulation frequency and damping constant are also studied numerically following the Runge-Kutta method.

1.2 Sheath

Whenever plasma faces a material surface, because of the higher thermal mobility of electrons as compared with that of the ions the wall is charged up negatively with respect to the plasma. The negative potential which is developed on the wall attracts the ions, and part of the electrons is repelled thereby forming a positive-space-charge region in front of the wall. This positive space charge region is the 'sheath' which separates the negatively charged wall from the 'presheath' plasma as shown in Figure 7. The sheath structure is accountable for the flow of particles and energy towards the wall.

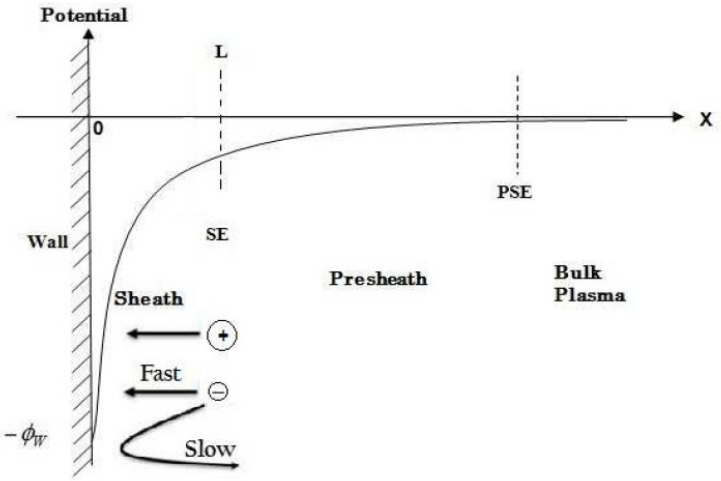

Figure 7: Variation of the potential in front of the negative absorbing material wall. (Source: Khanal, 2003)

Due to the shielding effect of plasma, the effect of negative wall potential is confined within a small distance (a few Debye lengths) away from the wall. Within the sheath region, the plasma is significantly non-neutral, however becoming practically quasineutral at the sheath edge also called "sheath entrance". The potential falls off quickly as we move towards the wall so that the electric field is comparatively strong, and there is domination of the motion of the plasma particles by electric force rather than magnetic force.

1.3 Presheath

Development of weak gradient region from where the ions accelerate, and enter into the sheath is the presheath region. In this region, the potential as well as other physical

variables have weak gradients as compared to that of the sheath. The negative potential of the wall has strong effect only in the sheath region but a residual electric field pierce beyond the sheath edge deep into the bulk plasma. This electric field is accountable for acceleration of the ions and helps to fulfill criteria which is required for the formation of plasma sheath. Therefore, to exist sheath, the instreaming ions at the sheath edge have to satisfy "Bohm criterion" and this criterion in kinetic form reads (Riemann, 1991):

$$\left\langle \frac{1}{v^2} \right\rangle \leq \frac{1}{C_s^2}\,, \tag{1.2}$$

where $\langle\rangle$ indicates average and

$$C_s = \sqrt{\frac{k_B(\gamma^i T_{ps}^i + \gamma^e T_{ps}^e)}{m^i}} \tag{1.3}$$

is the ion-acoustic velocity at the presheath side of the sheath edge. Here γ^i and γ^e are the ion and electron polytropic constants respectively and T_{ps}^i and T_{ps}^e are the ion and electron temperatures at the presheath side of the sheath edge respectively. This criterion demands that ions enter the sheath region with a high velocity which cannot be achieved only by the thermal motion of the ions. As a result, the ions must be accelerated by an electric field piercing the presheath region.

In the presence of oblique magnetic field the presheath consists of two distinct regions: "collisional presheath" and "magnetic presheath". The collisional presheath is adjacent to the bulk plasma where the electron pressure gradient accelerates electrons along magnetic field lines, there by generating an electric field which accelerates the ions. The acceleration results in a quasineutral ambipolar flow of electrons and ions along the magnetic field at sound speed. The "magnetic presheath"is adjacent to the sheath where, the electric field is powerful to deflect the ions from their motion along the magnetic field. The dimension of this region depends on the ion gyroradius and the angle of the magnetic field perpendicular to the wall (Chodura, 1982).

The above mentioned Bohm criterion, Equation (1.2), is valid for cases without magnetic field or magnetic field perpendicular to the wall. In the case of oblique magnetic field, the condition is modified as Bohm-Chodura condition (Chodura, 1982).

$$v \geq C_s \cos\theta\,, \tag{1.4}$$

where θ is the angle made by magnetic field with normal to the wall.

1.4 Damping of wave

The ions which satisfy Bohm-Chodura criteria show temporal oscillation in velocity at the sheath entrance. The ions oscillation also undergoes the damping phenomenon as there is collisions among the ions (Mathur, 2012). The variation of amplitude with time in damped oscillation is shown in Figure 8.

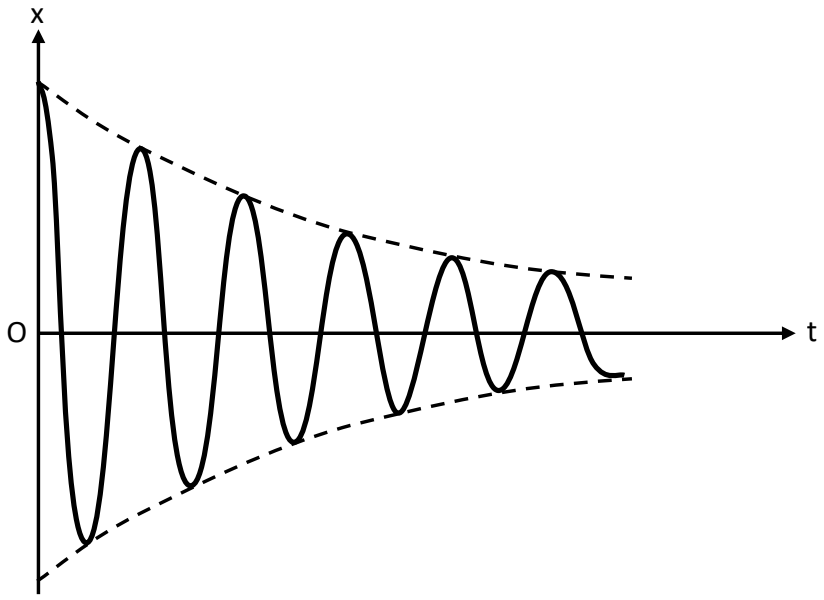

Figure 8: Damped oscillation in which amplitude is decreasing exponentially.

There are three different cases of the damping phenomenon of ions velocity wave:

In the case of over damping, if ω_0 is the oscillating particle's natural frequency, damping constant $k > \omega_0$; The displacement after attaining its maximum value, exponentially dies off with time without changing the direction of motion. Hence, there is no oscillation and then the motion is called overdamped.

In the case of under damping, the damping constant $k < \omega_0$, and this type of damping produces two types of effects: damping decreases the frequency or increases the time period of oscillator and the amplitude of oscillation gradually dies out. In actual practice specially in the case of musical instruments the damping is small and therefore its effect on the frequency or time period of the oscillator is negligible.

In the case of critical damping the damping constant $k = \omega_0$, the oscillator's motion is just non-oscillatory, i.e., it ceases to oscillate. It has application in different pointer type instruments, like galvanometers.

1.5 Beats of wave

The periodic variation in the intensity of charge particle at a point due to the superposition of two waves of slightly different frequencies traveling in the same direction is the beat. Each rise and fall in the intensity of wave is one beat. The time interval in which one beat occurs is the beat period, while the number of beats per second is the beat frequency. The number of beats produced per second is found to be equal to the difference in frequencies of two superposing waves. If f_1 and f_2 are the frequencies of two, then the beat frequency is equal to $f_1 - f_2$. However, for beats to be audible the beat frequency should not exceed 10 or beat period should not be less than 1/10 second. If the second wave comes before 1/10 second of the first wave, then we cannot distinguish between two sounds due to the persistence of hearing (Mathur, 2012).

The beat phenomenon is used by musicians in tuning their instruments. If an instrument is palyed to produce sound against the standard frequency, it is tuned until the beat disappears. In water beat phenomenon is used by dolphins, to observe the surrounding activities. When sound signals are sent by dolphin, there is production of beat between the original and reflected sound, from the surrounding substances. No beat is produced if there is no relative motion between the dolphin and the objects reflecting the sound, as both have same frequency. If there is relative motion, echo having different frequency produce beats with the original sound.

1.6 Modulation of wave

Modulation is the process of changing shape or frequency of a signal according to audio signal. In the case of radio transmission, this is the process of superimposing the periodic signal characteristics, on to the carrier wave, so that in the signal, there is transmission of information by the wave. Analog modulation and digital modulation are the types of modulation. The process of converting an analog input signal in to a signal which is suitable for RF transmission is the analog modulation. Amplitude modulation and angle modulation are the types of analog modulation. In amplitude modulation, carrier signal strength is varied with modulating signal as shown in Figure 9. Frequency modulation and phase modulation are the types of angle modulation. In frequency modulation there is variation of carrier signal with modulating signal, whereas in the case of phase modulation, the phase of the carrier signal is varied with the signal of modulation. In digital modulation, there is conversion of analog signal of carrier by the digital data, bit stream. Pulse code modulation, differential pulse code modulation, delta modulation and adaptive delta modulation are the types of digital modulation. In communication system, there is necessity of modulation due to the various reasons: to avoids signal mixing, to increase the communication range, for wireless communication, to reduce the

antenna height, to reduce the noise effects and many more.

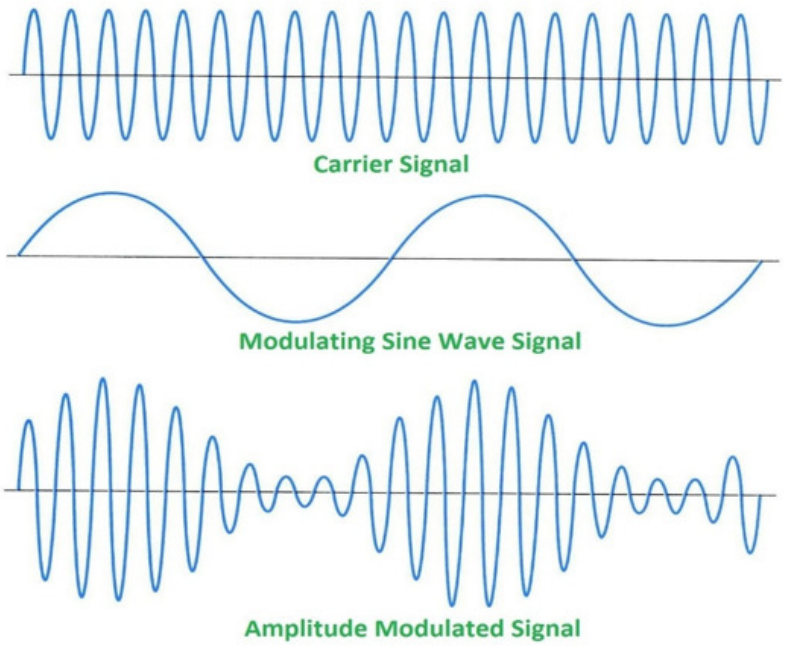

Figure 9: Diagram of carrier signal, modulating sine wave signal and amplitude modulated signal. (Source: https://www.pcmag.com/encyclopedia/term/37737/amplitude-modulation)

1.7 Motivation

The problem of sheath formation at the plasma boundary is important for all possible applications of plasma where the plasma is confined in a finite volume. It is one of the oldest problems in plasma physics but not yet fully understood. Because of its particular importance in plasma technology and fusion research, it remains undiminished or even growing interest (Chodura, 1982; Morales Crespo 2018). The understanding of plasma wall transition mechanism has great importance not only for tokamaks but also for electric discharges, Langmuir probes etc. In presence of magnetic field the analysis of the scrape-off layer is complicated because of the strong inhomogeneities. This is because of the transition from collision dominated plasma at the centre of a device to a collision free space charge sheath at the vicinity of the wall (Riemann, 1981). In order to understand the plasma-wall interactions in tokamaks and other fusion devices, it is necessary to study the properties of the edge plasma since it controls the heat loading to limiters or diverter plates, sputtering rate from these surfaces, etc.

1.8 Objectives

The objectives of the present work are:

- To develop presheath-sheath coupling scheme for magnetized plasma-wall transition
- To analyze beat frequency and velocity variation of ions in a magnetized plasma sheath for different obliqueness of the magnetic field
- To obtain the ion velocity profiles in a magnetized plasma sheath for different obliqueness and strength of the magnetic field.
- To understand the variation of mean velocity and amplitude of ions in a magnetized plasma sheath for different obliqueness of the magnetic field
- To study modulation frequency and velocity variation of ions in a magnetized plasma sheath for different obliqueness of the field

1.9 Outline

This dissertation is organized as follows: Chapter 1 is the Introduction, which gives an overview of the problem, its background and objectives. The review of relevant literatures is given in Chapter 2, and Chapter 3 explains the adopted methodology with the theoretical background. All the results of our work are presented in chapter 4, and their discussions are presented. Conclusion and recommendations are presented in Chapter 5, and finally the work is summarized in Chapter 6, which is followed by the references cited and appendix, where additional information related to the work are listed.

CHAPTER 2

2. LITERATURE REVIEW

Sheath formation issue in the boundary of plasma is significant for almost applications where plasma is confined to the limited volume. Previous works relating to the plasma wall transition gives the information about the assess of study of plasma sheath. Review and discussion of these previous works plays important role to understand the fundamental terminologies encountered in our existing work. It helps to make new prospective as well as interest to the issue. At the materials wall, the study of the plasma sheath problem still is not fully known. However, various experimental as well as theoretical research have been done till now (Langmuir, 1928; Franklin, 1989; Riemann, 1991; Oksuz & Hershkowitz, 2002).

Langmuir (1929) was the first study of plasma by the basic features of the plasma sheath transition . The interaction of electron and positive ion space charges in sheath region is studied. It was observed that in the plasma the potential distribution determines the motion of the ions and hence fixes the rate at which the ions reaches at the sheath. In his research, the essence of Bohm criterion was applied in an implicit form. Bohm (1949) formulated and explained the sheath formation criterion explicitly.

With collision less plasma the findings on the plasma-sheath transition were concerned. By the artificial cut-off into the diffusion-controlled theory of collision-dominated plasma, Boyd (1951) launched the "Bohm Criterion". (Persson, 1962) was the first to recognize the universal role of ion inertia in the bounded region called the presheath. Riemann (1981) was given the first self-consistent kinetic analysis of collisional presheath. The word 'presheath' is due to Hu & Ziering (1966) was actually marked to the Knudsen layer of collision-dominated plasma. It was applied by Franklin (1976) with a dissimilar sense to designate a transition layer needed for a smooth matching of plasma as well as sheath. As in the case of bounded collisionless plasma, the word 'presheath' mention to the whole plasma. Such types of coincidence may have increased some confusion in the nomenclature explained by Franklin (1989).

Godyak & Sternberg (1990) solved the dynamic model for radio frequency (rf) sheaths

in the range of the electron and ion plasma frequencies. In the case of floating dc sheaths having no rf voltage and for collisionless as well as rf sheaths for highly collisional, the solution obtained for the sheath dc voltage, and the capacitive sheath width coverage to the certain limits. The results obtained by them are in good agreement, with the experiment but, varies from using high voltage approximation. The relations which are obtained between the characteristics of sheath, show that the rf sheath capacitance as well as the equivalent sheath resistance are not dependent of the discharge current and the rf voltage.

Riemann (1991) analyzed that the boundary layer of plasma leads to the two scale problem i.e., collision free sheath and quasi-neutral presheath. For the sheath formation, close to the absorbing material wall, Bohm expresses the required condition. The fundamental feature of plasma-sheath transition was discussed, as well as their relation to the "Bohm criterion". The sheath condition is fulfilled marginally, and this condition is related to the field singularity of sheath edge. Finally, previous work have been reviewed, which was related to the specific problem of plasma sheath transition.

In collisional case Franklin (2000); Riemann (1997) attempted to generalize the Bohm criterion. Their attempts were based on an arbitrary meaning of presheath and sheath. The well-known subdivision of the boundary layer of a collision dominated plasma into a collisionless sheath and quasineutral presheath established by Riemann (1997). This subdivision is exactly valid only in the case when $\lambda_{\mathrm{D}}/\lambda \rightarrow 0$, where λ is the mean free path of ion and λ_{D} is the electron Debye length Riemann (1991). The sheath edge separating the presheath and sheath is mentioned by Bohm criterion. To report for collisions and space charges in boundary layer, Riemann used a simple fluid model of ions to explicit the controversial statements on the validity of plasma sheath idea as well as on the role of Bohm criterion for limited value of $\lambda_{\mathrm{D}}/\lambda$.

One dimensional self consistent plasma column that includes both the sheath and the presheath was explained by Goswami & Ramachandran (1999). The analytic solution for interesting limit where the collision operator is not dependent on the flow of velocities was derived. To balance electron and ion flux loss, it was claimed that the most conspicuous characteristic of the boundary potential profile is the plasma sheath which is normally formed at plasma boundary. At sheaths electric fields are normally more stronger compared to bulk plasma electric fields. For collisionless as well as feeble collisional systems, sheath scale lengths depend on Debye length, λ_D, and are normally more smaller as compared to the dimension of the plasma region, L.

Plasma sheath magnetization problem is worked by Chodura (1982). The effect on plasma wall transition region by applying oblique magnetic field was observed. To simulate the motion of particles of plasma in the magnetic as well as electric field,

Bohm's criterion is generalized to exist the monotonic profile of the layer. This profile of the layer have double structure i.e., the quasineutral magnetic presheath followed by electrostatic Debye sheath as well as potential drop between plasma and absorbing wall.

Ahedo (1999) studied the plasma-wall interaction structure in the case of oblique magnetic field. Chodura (1982) and Riemann (1994) recovered the model as specific cases like intermediate magnetic field and weak magnetic field respectively and compared with the powerful magnetic field case. In the case of intermediate magnetic field only collisional presheath, sheath and Chodura layer exists. Also the significance of the collisional presheath to characterize the perturbation region was completely explained. In the case of weak magnetic field, he presented and compared the results for whole range of incidence angles. Likewise for powerful magnetic field, he analyzed the local behavior around the sheath entrance point and for the specific range of angle of incidence to cross with regular solution as well as the internal singular point of the equation of sheath.

The characteristics of sheath and presheath was studied by Beilis et al. (1997) in the transition layers of plasma wall which is located in a magnetic field. By the application of the model of hydrodynamic, their force lines obliquely incident on the wall is calculated. At the sheath edge, they determined the limited electric field as well as critical velocity of ion for the presence of positive space charge steady state electrical sheath. The ion velocity is less as compared to the sound velocity of ion that depends on the magnetization of presheath plasma parameters. Also, by the use of ion to electron current ratio, Hall parameter of ion and Debye length to Larmor radius ratio, the dependencies of thickness and potential distribution of the presheath on the incidence angle of magnetization was determined. Likewise, it was observed that there is strong increment of the critical velocity with the Hall parameter, whereas the critical velocity increases monotonically for the field magnetization parallel to the absorbing wall.

For different current regimes as well as various emission coefficients of secondary electron on magnetized plasma sheath, Tskhakaya et al. (2002) worked on the action of active electrons. It was showed that few electrons having much energy may remarkably affect the energy flux to the wall as well as the potential drop across the sheath. For parameters of plasma, the fast moving electron, with smaller density across the sheath which is less then 0.1% can double the potential drop and the flux of energetic electrons to the wall. There is decrease in the effect of fast moving electrons, as the secondary-electron emission coefficient increases, as well as there is increase in the current towards the wall. For the fast moving electrons having low temperature, this effect is strong so much that, with the increase in density of fast moving electron, there is decrease in the energy flux towards the wall.

To study the space charge sheath adjoining to the electron absorbing wall, Khanal (2003) worked in the progress and understanding of the sheath by developing a kinetic model. Kinetic sheath problem is coupled by him to a two-fluid presheath one. The Kinetic Trajectory Simulation (KTS) model was explained and how to get the final self consistent time-independent state. The model designed is only for 1d1v, time-independent and collisionless cases and used this model to specific cases of a 1d1v single emitter plasma diode due to the testing and comparison purposes. To explain the space charge sheath near the electron absorbing wall, he used the KTS model and bordering his work in a two-fluid model. Also, the solution of presheath-sheath coupling problem was developed. Briefly how the solution is iterated and how the distribution function of the species of particle are computed by solving the corresponding kinetic relations in the collisionless trajectories was explained.

By finding the associated time-independent as well as collisionless kinetic relation along the particle trajectories, Dhakal (2013) calculated the distribution function of the particle species. The self consistent ion density, electron and charge density, potential as well as electric field profile was analyzed. Accordingly, the magnetic field has important effect on the plasma sheath and there forms three distinct regions; near the entrance of the sheath by the field magnetization, particles of plasma are dominated. For different species of plasma, difference in Larmor radius results in the separation of charge. On moving the charge particles towards the wall, there is increment of electric field and there appears greater quasi-neutral region. Also, in the closeness of the wall, electrostatic Debye Sheath appears which have dimension of few Debye length, where there is fully dominant of powerful electric field.

Mishra (2006) studied the structure of the plasma sheath which is formed near the absorbing wall for various densities of the presheath plasma. It was monitered that with the decrease in electron and ion density at the presheath region, there is increase in plasma density. At the absorbing material wall, ion and the electron density are minimum but the charge density becomes maximum. There is decrease in electron density very faster as compared to that of ions, therefore towards the wall, there is increase in the total charge density. Finally, it was found that at the wall potential was same but at the sheath entrance, plasma density increased at the presheath side. Near to the material wall, the electric field has gradient. By one order of magnitude at the wall, the density of ion exceeds the density of electron.

Zheng-Xiong et al. (2003) investigated the structure of sheath that have low pressure electronegative plasma in the steady state condition. It was assumed cold positive ions as well as hot negative ions by applying collisionless approximation. Bohm criterion in the modified form is obtained, with Sagdeev potential, by introducing the sound velocity of ion in the modified form. Electric potential, net space charge as well as densities of

particles in the sheath in the various cases of temperature ratio of electrons to negative ions was analyzed.

Tskhakaya et al. (2004) studied the problem of plasma-wall transition layer in the non-magnetized plasma without the normally splitting in to a sheath and presheath region. Considering electrons were to be Boltzmann distributed, while by the kinetic theory, they explained ion dynamics which includes recombination, ionization and charge exchange. IT was derived the condition that was satisfied by the velocity of ion throughout the whole plasma wall transition region to exclude the oscillatory nature of the electrostatic potential. For different physical conditions, the system of resulting equations is answered numerically. A comparison between current experimental results with a numerical equation was presented and hence tells that the model exactly explain the transition from the bulk plasma to the free electron plasma sheath.

In the absence of applied field magnetization, Shoucri et al. (2004) used the one dimensional, Eulerian, Vlasov code, to study the self consistent, plasma facing floating collector. The ion flow acceleration at the entrance of the Debye sheath with the formation of electric field was observed which was negative in front of the floating collector. The electric field acts to move the ions which is positive towards the plate. In such condition, electrons are pushed back so that at constant state, the collected current is to be zero at the plate. Finally, by using various parameters, it was observed the regular oscillations having constant amplitude. The oscillations become damps with the increase in collision of electron, which helps the system to obtain equilibrium.

Riemann et al. (2005) studied the plasma-sheath matching issue. The problem is solved clearly both analytically and numerically by the explicit construction of a matched asymptotic utterance and comparison with accurate solutions for the hydrodynamic plane Tonks- Langmuir issue. With the numerical potential curves, the approach acquired by consistent matching exhibit good agreement.

The effect of negative and positive ions is found by Stamate & Sugai (2005) by solving in three dimensions, the distribution of potential, as well as kinetic energy of ions. It was observed that, superposition of discrete focusing effect increases significantly the complexity of ions flux on the surface of electrode. Finally, the observed results is expected the importance of this study for the investigation of finite structure of plasma sheath.

For the cases in which the positive ion temperature is higher as compared to that of particles having negative charge, Amemiya & Bhattacharjee (2006) investigated the criterion for the sheath formation of particles having negative charge. It was observed the situations which recently came up, for instant, in the case of tokamak fusion plasma boundary, the beam of ion which is cooled by cold electrons and dusty plasmas when

cold dust having negative charge floats within hotter positive ions. The conditions for the velocity distribution of particles having negative charge to achieve the stable electron sheath was investigated. At last, the obtained result is valid only for negative ions, electrons and dust particles having negative charge.

Without magnetic field in plasma, the activity of acoustic waves of ions was investigated by Tiwari (2006), which was propagated from presheath to the sheath region. The model of wave turbulence was assumed for solving acoustic wave turbulence to cause flow of ion from sub-sonic to speed of supersonic. It was concluded that the space charge layer which was non neutral not serve for reflection of acoustic waves. Close to the sheath edge, reflection of the waves is strong. The nature of the coefficients of reflection were complex. The activity of incident wave shows singular activity at the presheath side, that propagating mode is not physically applicable solution in the background of presheath. Numerically, the length of wave which is shorter as compared to the scale length of presheath was observed which are less susceptible for reflection. Scales size which is short of the fluctuations of acoustic waves would be of fluctuations of short scale wave.

Schupfer et al. (2006) studied the action of particle induced electron emission on the voltage of plasma sheath. The new model in a collisionless kinetic sheath was developed, and coupled to the presheath fluid. The analysis for magnetized as well as unmagnetized case is valid for plasmas in which Debye length is very small as compared to the characteristic length of presheath. The ions which are majority as well as impurity are accelerated from the bulk plasma towards the boundary of material. These ions releases electrons moving back to the plasma, due to this, giving to the lower plasma sheath voltage as compared to without emission of electron. Finally, assuming specific plasma boundary conditions as well as the data of emission of particle induced electron, it was calculated self consistently the plasma sheath voltage and show the effect of particle induced electron emission.

Yu et al. (2007) developed the method for the measurement of thickness of sheath, in hall type stationary plasma thrusters. Numerically, the wall surface effect on the sheath was studied. It was described the dynamic process of electron in the plasma by the method of test particle and enters the electron randomly to the sheath from the discharge channel, and reflected back wards. According to their observation, the temperature of reflected electron is affected by the wall surface, if the depth of groove is very less as compared to that of thickness of sheath. Furthermore, there is increase in the temperature of reflected electron, as there is greater groove depth, as compared to the thickness of sheath. Finally, there is sharp jump of the temperature of reflected electron, if the groove depth is of the order of thickness of sheath.

Oblique magnetic field effect, in the state of liberation of dust particle from plasma

facing material wall is studied by Smirnov et al. (2007). They coupled Magnetized presheath, as well as Debye sheath to get the quantities of plasma at the material wall. The release of spherical dust increases, approaching field magnetization, parallel to the material wall. Furthermore, for shallower potential drop case, there is disappearance of critical radius for certain angle of field magnetization. Finally, they observed that the liberated dust particle's size may be controlled by calibrating the parameters of plasma like; density, temperature etc.

Joung et al. (2007) study the plasma parameters variation in boundary condition, and measured the plasma potential to create hyper thermal beam which is neutral. It was observed that the plasma potential which is negative is obtained from the limited current of space charge. The reflector surface ion energy is the difference between the reflector bias voltage as well as the potential of plasma. The potential of plasma positive, and not changed with the reflector bias voltage was supposed. On the other hand, plasma potential will be negative for maintaining quasinutrality, which affects the energy of ion on the surface of reflector.

The effectiveness of the ion densities ratio on a plasma sheath of electrons and two species of positive ions due to the consequences of magnitude and direction of oblique magnetic field was observed by Hatami, Niknam, et al. (2008). The positive ions have different masses, whereas the ionization ratio is same. Due to the action of electrostatic and Lorentz forces, it has been observed that the velocity of the heavier and lighter ion species as well as the density distribution begin to fluctuate as the ratio of electron Debye length to lighter ion species Larmor radius becomes more than 1 and 3 respectively. Likewise, it is observed that the fluctuations of velocity of lighter ion species are much greater as compared to those of the heavier ion species. Moreover, the results acquired in the existence of heavier ion are compared with the reported outcome of the plasma sheath magnetization comprising single species of positive ions. It has also been monitored that, due to the existence of heavier ion, density distribution as well as the velocity of species of lighter ion in the presence of plasma sheath magnetization decreases as well as increases respectively.

In the region of sheath, Hatami, Shokri, & Niknam (2008) studied the behavior of kinetic energy and density distribution of the charged particles. It was assumed that in the sheath region, there is exertion of weak external magnetic field. Ignoring ionization as well as recombination and applying the approach of hydrodynamics numerically, it is observed that, in the plasma by increasing the negative ions density the density distribution of species of both positive ions as well as the kinetic energy of these ion species decreases and increases respectively. Likewise, they observed that, due to the existence of the negative ions, there is change in normalized electrostatic potential of the region of sheath. Due to the increment of the negative ion densities, the normalized

electrostatic potential in the sheath increases. Also, the effect of ratio of density of both positive ion species, temperature and density of the negative ions are observed. Finally, the magnitude of external magnetic field on the net density distribution of the charged particles in the sheath region was studied.

By applying the magnetic field obliquely, Pandey et al. (2008) investigated the structure of plasma sheath. For the magnetic field having different orientations, the effectiveness of plasma ionization, plasma magnetization as well as plasma neutral collisions on the sheath region was studied. Also, plasma sheath width depends not only on the frequency of collision and magnetic field of plasma but also with the orientation of obliqueness of magnetic field. As the angle between the field magnetization and wall is increased, there is decrease in the sheath layer size. If the magnetic field is perpendicular with the wall as compared to the wall parallel, the grain in side the sheath acquires positive charge more. At last, the implication of the consequences for the measurement of the characteristics of sheath was discussed.

With a fluid model, in the oblique magnetic field, the density distribution of ion of the plasma sheath is explained by Zou et al. (2008). It was observed that on the plasma sheath, the magnetic field has important effects, including space charge density as well as ion density distribution and performed numerical simulations of the sheath. Here they assumed two cases of ion incidence, in the ion density there occurs fluctuations due to Lorentz force and the magnetic field parallel to the board is accountable for these changes. Because of the fluctuations of ion density, in some regions space charge density is quite higher. Therefore, due to the external magnetic field the shield distance of sheath becomes longer.

M. Hatami et al. (2008) studied the collisional effects in the case of plasma sheath magnetization consisting of two species of positive ions. It was supposed that the ions have different magnitudes of masses. Frequency of ion neutral collisional effects are connected to the plasma sheath magnetization. Model of three fluid hydrodynamics is used by them, and obtained the dimensionless equations, which is numerically solved. Likewise, they observed that with the increase of frequency of ion neutral collision, velocities of ion species fluctuations as well as the density distributions, should be shifted towards the edge of plasma sheath, and these fluctuations amplitude increases as compared to the collisionless case. Thus for collisional as well as collisionless plasma sheath magnetization, for the species of heavier ion, amplitude fluctuations growth, as well as the shift of these fluctuation are more as compared to that of lighter ion species. Similarly, with the increase of ion collision frequency, ion velocity fluctuations as well as density distribution becomes very much faster. Also, as each ion species distance from the sheath becomes greater than five times the Debye length of electron, completely disappear these fluctuations. Furthermore, there is decrease in the kinetic energy of the

species of both ion, as the collision frequency increases. At last,it was observed that the ion frequency collision increases, there quickly falls the density distribution of electron.

Yasserian et al. (2009) investigated the electronegative discharge in the presence of constant oblique magnetic field. The densities of electron, positive and negative ions for various strengths of field magnetization was solved. Also, velocity of positive ions profile, as well as electric potential was found. The electrons, as well as negative ions are distributed, according to the Boltzmann's distribution, whereas positive ions were explored by continuity, as well as momentum transfer equations. If the value of electro negativity is high and for the negative ions various values of the magnetic field constitute three kinds of discharge structure. These are: feeble, intermediate and intense magnetic field. If the strength of the field magnetization is very weak, there forms the uniform types of structure, for intermediate magnetic field, there emerges stratified structure of multiple layer and followed by oscillations of electric potential, and disappear these oscillations, for energetic magnetic field. Finally, they obtained the positive ion flux, which arrived in the cathode, as the function of the strength of magnetic field, and they compared the result with electro positive discharge.

Rana (2009) explained the plasma sheath structure, which was formed near the material wall, for Beryllium plasma ionization, in various levels. The density of electron which reaches to the material wall was almost same. As the level of ionization increases, the decreasing rate of ion density, moving towards the wall, increases also. It was observed that, 1.1 times the ion density decreases, as there is increase in the ionization level from 1 to 3. This phenomenon is also reflected in charge density, as well as potential, electric field etc. Finally, he concluded that the level of ionization plays the vital role in defining the structure of plasma sheath.

By the motivation of experiment related to magnetized target fusion Krasheninnikova & Tang (2010) carried out the systematic investigation of the balance force and equilibrium plasma flows. In the initial case, uniform full Maxwellian plasma consisting of equal temperature collisionless ions and electrons is allowed to interact with a fully absorbing material wall. The force balance of steady-state force of the entire plasma and its individual components illuminates the roles that the hydrodynamic, magnetic and electric forces play. With the decrease in magnetic field, there becomes prominent the electric force in areas where breaking of quasineutrality occurs. The significance of this study depends on the relation between electron and ion thermal Larmor radii as well as Debye length of plasma. Due to the analysis of the two fluid balance force, the comparative importance of the current of electron and ion in the magnetic or Lorentz force can be understood. Primarily, it tells that the current is carried by electrons. The direction of the electric field helps to confine the ions, but not the electrons, which are forced to carry a maximum current to confine magnetically themselves. In the regimes, where

the magnetic field is strong, the average velocity of particles parallel to the wall is diamagnetic. But, close to the wall, there is very low number density of ion, which not produces any contribution to the current. At last, the computational and analytical results was presented which can also be used to the plasma sheath, close to the tokamaks initial wall.

The electrostatic plasma sheath, containing dust grains which is nanosized and two species of positive ions is studied by Foroutan (2010). The concentration of two species of positive ions, the velocity of ions at the edge of sheath as well as the bias voltage was investigated. The results obtained by him show that, with the increase in sheath thickness, the density ratio of two species of positive ions also increases. For the dust particles which are nanosized, the dominant forces are ion drag, the electric force, action of neutral drag as well as gravity are neglected. By the ion drag force as well as electric force, there is increase in the dust velocity, but the number density of dust decreases. At the sheath edge, if the velocity and number density is same, the argon ions have larger number density near the wall, as compared to that of Helium ions. At the edge of sheath, the number density of dust increases with the Argon ions velocity, however it changes feebly with Helium ions Mach number. Initially there was fast decrease in the number density of dust with the small increment in the velocity of ions at the sheath edge. Finally, it was observed that the ions with incident flux were not dependent of the bias voltage.

By the fluid model, Yankun et al. (2011) explored Bohm criterion in plasma sheath magnetization. Upper and lower limits for the condition of sheath in various states of applied field magnetization was observed. From numerical simulation, the obtained results tells that the magnetic field affects the ion Mach number significantly. Due to the Lorentz force effect on the velocity of ion, the Mach number of ion varies with the angle of incidence of ions. Also, at the boundary of plasma-sheath, the electric field determines the criterion of sheath. Hence at last, they concluded that the fluid model can help to understand the criterion in a plasma sheath magnetization.

Duarte & Clemente (2011) studied the effects of electron inertia on the problem of planar sheath plasma. It was observed that, the generation of electron inertia in treatment of problem of classic sheath introduces that changes occurs to the floating plasma wall potential. In their model, at the wall, electrons were attaining sonic velocity. Due to this sonic velocity, there build the shock where velocity and density of electron, approach discontinuities, and there remained electric potential continuous. Finally, numerical computation in terms of electric potential, densities, and velocities of particles was presented. Also, they showed the result comparison, from literature related to Maxwell-Boltzmann distribution of electron.

By the application of KTS model, Chalise & Khanal (2012) observed the plasma sheath region in an oblique magnetization. It was monitered that the plasma- sheath magnetization had two clear regions i.e. magnetic feld dependent region as well as electric field dependent region. Magnetic field dominent region consists near to the sheath entrance whereas near to the absorbing wall electric field dominent region lies. The region related to the dependent of magnetic field, acceleration of particles occurs due to feeble electric field but due to magnetic field particles are gyrated. Because of the gyrating effect, path of the particles changes and the velocity of particles decreases towards the absorbing wall. At last, it was observed that sheath width decreases as the magnetic field increases. In their work, velocity variation perpendicular to the wall is considered, however, the velocities in perpendicular direction are considered to be constant.

By the application of kinetic Trajectory Simulation model, Gurung (2012) workd on the time-independent, non neutral, as well as collision less plasma sheath created near the wall, that have various presheath current densities. It was observed that, there is increment of density of electron at the material wall sharply as well as linearly, however, near the wall, density of ion without linearly as well as monotonically increases as correspond to the presheath density of current. He observed the result, which is applicable to control the particles flow near the wall, and method of controlling particles arriving to the plasma facing wall. Finally, in the region of sheath as well as at the absorbing wall, the parameters of plasma are influenced highly by the current density of presheath.

By the application of KTS model, Poudel (2012) learned the ion as well as electron density variations for various presheath, polytropic constants of ion. The distribution functions of species of particles was calculated, by solving the associated kinetic relations, along the corresponding particle of trajectories, in the collisionless case. It was monitored, the density of ion and electron plasma sheath, for three reasonable values of presheath, ion polytropic constants. In each case there is gradual decrease in ion as well as electron densities from entrance of sheath to the material wall. Also, he observed, electron density decreases much faster as compared to that of ion. Furthermore, in all the cases, the density of ion is greater, as compared to that of electron, the rate of falling of ion density is greater as compared to that of electron.

In the existence of electronegative ions, Yasserian & Aslaninejad (2012) studied the formation of plasma sheath in front of the material wall of magnetized plasma. To explore the particles species of plasma, they used the fluid equations. On applying Sagdeev potential, they investigated the collisional influence as well as the field magnetization on Bohm criterion. The profiles of space charge was obtained by them in existence of field magnetization on various frequencies of collision, and the concentration of electronegative ions. Peak of the space charge is raised by the collision and the field

magnetization, however, the electronegative ions damps the peak. Also, if the field magnetization is high, there is emergence of fluctuations in the profiles of space charge. At last, they obtained the actual current through the sheath region for various values of collision and field magnetization in electronegative, as well as electropositive plasmas.

By using the fluid model Driouch & Chatei (2013) studied the dusty plasma characteristics on a magnetized sheath with certain temperature of ion. In their work, they took fluid ions, hot electrons as well as cold fluid dust grains. The fluid model is solved numerically to obtain the information of sheath briefly with various temperatures of ion and observed significant change in the quantities, characterizing the sheath. Finally, in the collisional sheath, the action of temperature of ion is more obvious in dynamics of dust with uniform cross section.

M. M. Hatami (2013) used the two fluid model to investigate the properties of exact density of current, as well as positive space charge in the region of collisional magnetized plasma sheath. It was supposed that positive ions, have fixed temperature where as densities of electron follows the Boltzmann's distribution. With the increase in the frequency of ion-neutral collision, and the magnitude of external field magnetization, the current density increases across the sheath region. Likewise, with the increase in the frequency of ion neutral collision as well as the magnitude of field magnetization in the region of sheath, the accumulation of positive ions increases also. Finally, as the ion temperature increases, there is decrease in the current density in the region of sheath.

With the application of hydrodynamic equations, the criterion of the formation of sheath was investigated by M. M. Hatami & Shokri (2013), in a feeble electronegative plasma magnetization which consists of electrons, negative as well as positive ions. It was supposed that, at the sheath entrance, positive ions velocity was not normal to the material wall and there was formation of sheath region, as the positive ions velocity lies in the interval with specific upper and lower limits. The presentation of field magnetization affects both of upper and lower limits. In sheath region, they studied the charged particles of density distribution for the value of Mach number. Finally, monotonically reduction of the positive ion density distribution leading to the sheath formation occurs if and only if the mach number lies between upper and lower limits.

For sheaths kinetic theory, in one dimensional case surrounding, emitting surface of electron was studied by J. P. Sheehan et al. (2013). The ratio of temperature of plasma electron to emitted electron, affects the potential of sheath. This case arises, as the temperature of plasma electron is within the order of temperature of emitted electron in magnitude. If the temperature of plasma electron is equal to the temperature of emitted electron, in such case, potential of sheath tends to zero. The results obtained by them is validated in cell simulations of particle. They tested the theory by the measurements of

sheath surrounding, thermionically, emitting cathode, in after glow of rf plasma. Finally, it was predicted that the potential of sheath shrunk to zero if plasma electron cooled to the temperature of emitted electron.

J. Sheehan et al. (2014) studied the influence of temperature of emitted electron on the sheath of plasma. It was assumed that plasma electrons follows the relation of Boltzmann, and the emitted electrons are liberated with nearly zero energy. The ratio of plasma electron to emitted electron temperature affects the potential of sheath. Finally, the emissive potential of sheath is nearly to the energy of beam, only when the flux of emitted electron is less than the flux of beam.

In presence of dust, Moulick & Goswami (2014) studied the formation of sheath for collisional plasma. In common laboratory plasma, because of high thermal velocity of electrons, the dust acquires negative charges. The dust charging theory dealing with the issue is that of the orbit motion limited theory. But, the theory does not find its application when the ion neutral collisions are present significantly. Collision is modeled by constant mean free path model. The sheath is considered jointly with the bulk of the plasma and a smooth transition of the plasma profiles. The various plasma profiles such as the electrostatic force on the grain, the ion drag force along with the dust density and velocity are shown to vary spatially with increasing ion neutral collision.

In the existence of emission of secondary electron, Huang et al. (2015) developed the electrostatic particle-in-cell simulation code to search, the interaction between plasma and material surfaces. To incorporate the process of bombardment of ion on the surface of material, ions having kinetic energy are included in to the numerical simulation. Due to the further investigation, the influences of the emission of electron on sheath dynamics is induced by ions on the top of electrons.

1d3v KTS model of plasma was studied by Chalise & Khanal (2015a) in a plasma sheath magnetization. This can be used for modeling different situations of interest and high accuracy of results is obtained. To calculate the distribution function of ion trajectories of ion are followed. At the injection, electrons are considered to be a cut-off Maxwellian velocity distribution and analytically they get their density distribution. The potential profile is iterated towards the final time-independent and self consistent condition. They used the above result to learn plasma sheath region formed due to the presence of oblique field magnetization. Finally, their model provides the fundamental study of various types of plasma sheath magnetization and maximum exact results are obtained.

Fluid model of one-dimension of magnetized plasma wall transition region near the floating electrode with angle of magnetic field which was immersed in a plasma magnetization was studied by Gyergyek & Kovačič (2015). In case, the electrons, they assumed the Boltzmann equation. On the other hand, the positive ions obey the ion momentum

exchange equation and ion continuity equation. In this work, using the term of zero source, an extensive comparison of the results is obtained on one hand and on the other hand, non zero three different source terms is made. In total, four different terms of ion source were assumed. The zero source term as well as three different non-zero ion source terms. As they used the zero source term, there becomes very sensitive model to the secondary conditions, where in few cases, the solutions showed oscillations of maximum amplitude. When they used, any of the three non-zero ion source terms, those problems are eliminated, but the consistency of the model is also broken. Numerically, the equations in the entire magnetized plasma-wall transition region are solved. As in the case of ion temperature zero, the model can be solved even if there is selected a very small ion velocity as a boundary condition.

Chalise & Khanal (2015b) observed the kinetic energy of ion and thickness of sheath in plasma sheath magnetization. It was observed that moving ions having kinetic energy reaching to the material wall was controlled by the applied magnetic field strength. There is increment of kinetic energy of ion as we move towards the material wall, but in the case of electron kinetic energy decreases.

Jacquot et al. (2015) studied the modelling of propagation of full wave to integrated ICRH wave coupling/RF sheaths. Rectification of RF sheaths is the reason for operational limits for the Ion Cyclotron Range of Frequencies heating systems. To simulate this, the self-consistent waves and sheaths and for Ion Cyclotron Heating code is the set of coupled equations, which computes self-consistently the wave propagation and DC plasma biasing. Now, its propagation module of wave explains with the considered slow wave, which is the source of RF sheath oscillations. Likewise, the Ion Cyclotron Range of Frequencies, power coupling to the plasma is due to the fast wave. They proposed to replace this one wave equation by the full wave module in either 2D or 3D as a first step towards integrated modelling of RF sheaths as well as wave coupling. Finally, they got the dependable convergence with the profile of density up to the leading edge of antenna limiters.

In the oblique magnetic field, the Radio frequency sheaths was observed by Myra & D'Ippolito (2015). In front of a conducting surface, radio frequency sheaths is studied for plasma which is immersed in a magnetic field with the surface that makes an oblique angle. The one dimensional equations, which explaind the dynamics of non neutral Debye sheath and time-dependent magnetic presheath was developed. By the strength of magnetic field, Maxwell-Boltzmann electrons was employed by the model and they decided the mobility and magnetization of the ions and wave frequency of wave as well. They concentrated on the ion-cyclotron range of frequencies and solved the equations numerically to get the rectified dc voltage, the rf voltage and current respectively. The sheath voltage-current relation was used to get the rf sheath impendance. Generally,

the impedance has resistive and capacitive contributions, and generalized the model of previous sheath boundary condition.

Kshetri (2015) studied the electric field as well as magnetic field effect on the velocity of ion at the presheath-sheath boundary. By the method of Runge-Kutta, Lorentz's force equation was solved. It was found that magnetic field does not affect on the parallel component of velocity, where as there is maximum effect on the perpendicular gyration. By increasing the magnetic field, gyration frequency decreases and gyration amplitude changes also. Finally, it has been observed that as the time increases, gyration amplitude gradually decreases as well.

Joshi (2015) analyzed oscillations of electron plasma which was non-linear having large amplitude, where spatial variations are one dimensional. It was found that the ions formed the constant background of neutralization. Also, variation in number density, electric field as well as velocity was observed. Finally, he observed, for various time, the non linear evolution in number density. The profile of electric field as well as velocity show steeping nature, however there remains maximum amplitude constant.

The anode double layer of droplet shape and sheath formation of electron in magnetically constricted anode was studied by Chauhan et al. (2016). It was observed fireball of droplet shape and double layer of anode in a magnetically constricted anode. Using permanent magnets, the anode which was disc shaped constricted. On using high voltage in between the cathode and anode, plasma is created with the glow discharge. Droplet shaped glow was received whose size was large close to the anode. Finally, the role of field magnetization in the formation of the glow, its shape as well as the profile of plasma potential was explained.

By the application of fluid equations, the oblique field magnetization effect as well as ratio of ion densities on a multi-component plasma sheath was studied by Basnet (2015). Plasma consists of two species of positive ions having different masses with the ratio of ionization same. Numerically the dimensionless equations was solved with given initial boundary conditions. The results obtained by him show the density profile, lighter ion velocity profile, as well as heavier ion species begins to fluctuate. There occurs higher fluctuations of species of lighter ion as compared to that of species corresponding to heavier ion. Finally, he observed that as the concentration of Neon gas increases with respect to the Helium gas, there is decrease in the electrostatic sheath potential of the multi-component plasma sheath, however there is decrease in the amplitude density profile of species of ion.

The plasma sheath structure in the presence of oblique magnetic field was studied by Sapkota (2016). He supposed the ion neutral collision effect with limited temperature of ion. The field magnetization magnitude, temperature of ion, frequency of ion neutral

collision, space charge density as well as net density of current was studied. It was observed that as the ion temperature and strength of magnetic field increases, space charge density as well as exact current to the material wall also increases. Field magnetization increases the transverse drift. On the other hand temperature of ion causes to increase the longitudinal drift of ions. Finally, frequency of ion neutral collision has important effect, however particles are affected close to the sheath edge.

By the application of fluid hydrodynamics on the dusty plasma sheath magnetization, Acharya (2016) investigated the collision effects as well as densities ratio of ion to electron, positive ions and negative dust particles. The compiled equations was solved by Runge-Kutta method, and observed the velocity of ion, dust velocity, density of ion, electric field as well as potential also. It was observed that, as the collision frequency increases there is increase in the velocity of ion, however there is decrease in the ion density. Likewise, as the frequency of ion neutral collision increases there is increase in the electric field as well as potential also.

By the application of fluid hydrodynamics, Bashyal (2016) explored the pressure gradient force effect as well as obliqueness of field magnetization on feeble magnetized electronegative plasma. The plasma which is electronegative consists of electrons, negative as well as positive ions. She considered that with two different temperatures, electrons as well as negative ions obey the Boltzmann Distribution. The fluid equations to explore density, velocity as well as potential profile of ions was solved. The ion Mach number variation for various values of oblique magnetic field strength was observed. Her observation gives the magnetic field strength, as well as the obliqueness are critical factor on the criterion of sheath formation. The obliqueness of field magnetization minimize the flow velocity of ion but the wall potential increases. Finally, it was concluded that, as the value of oblique magnetic field strength increases, the Mach number of ions increases also.

Lin et al. (2016) studied the polytropic coefficient of ion in the collision-less case which contains hot ions. By analyzing the equation of ion energy and taking the kinetic effects, they showed that ion polytropic coefficient is approximately constant. Also, it was observed that the value of polytropic coefficient depends on the temperature of hot ion and its concentration in plasma. The ion saturation current density depend on the temperature of ion and concentration of ions having high temperature. The value of ion saturation current density significantly alter from the one obtained by applying the assumption of adiabatic ion flow.

When the space-crafts having high speed return to the atmosphere, there is formation of plasma sheath on its surface. At first, Cong et al. (2018) established the model of hyperbolic electron number density distribution. By analytic method, power reflection

coefficient, absorption coefficient and transmission coefficient was derived as well. At last, they compared the analytic method and Wentzel-Kramer-Brillouin method, about their limitations and applicability.

Using KTS model, Chaulagain (2017) studied the action of ion temperature variation in a plasma sheath magnetization consisting of two-ion species. He got the profile of ion densities, electron and total charge density as well as potential by collisionless, time independent plasma sheath. Close to the sheath entrance there is change in physical parameters slowly but close to the wall, exhibit steep gradient. Magnetic field quite lowers the density of ion in comparison to the case without the magnetic field. Because of the rise in thermal velocity, the density of ion increases as the ion temperature increases. In magnitude there is decrease in potential, as the ion temperature increases. Finally, at the wall with the increase in ion temperature, total charge density increases also.

Burby (2017) studied the fluids of ions and electrons which is frictionless, couples the two-fluid Maxwell system. If the frequencies of Langmuir waves, waves of light and cyclotron motion of single-particle are scaled asymptotically to be large, Maxwell system with two-fluid becomes fast-slow dynamical system. This system admits a single-fluid closure which is systimatically computed with any order of accuracy. Magnetohydrodynamics is reproduced by this closure in leading order estimation. The unlimited extended hierarchy of MHD models. It was geometrically interpreted the closure as an invariant slow manifold in the unlimited dimensional two-fluid phase space. By Lie transforms infinite dimensional, the Poisson bracket for all order closure in the closed type was obtained. Therefore, by truncating the single fluid Hamiltonian, the conservative truncation of single fluid closure was obtained.

From the surface of solid, the emitted electrons can affect noticeably the characteristics of surroundings of plasma sheath by modifying balance of current at the wall, Bohm criterion at the sheath edge and separation of charge in the region of sheath. Qing & Hu (2017) establish the static sheath model with cold ions, and moving electrons to stress the effect of various emitted total electron velocity distribution function on the classic solution of sheath as well as its transition structure. They found that, the solution of sheath as well as the threshold of coefficient of total emission of electron influences the total EEVDFs. Finally, from the obtained results, it was observed that as electron emission coefficient increases gradually from zero, there would not transit the sheath from classic sheath to space-charge limited sheath structure.

By using fluid model, Khadka (2017) studied the ionization ratio effect on multicomponent plasma sheath magnetization. Numerically, the fluid equations was solved to obtain the potential profile, velocity and density of ions. It was assumed the Helium and Argon

ions having ionization ratio different. As the ionization ratio increases, there is decrease in the density of ion. Also, with the increase in number of charge, the peak density shifted towards the edge of sheath. Finally, he observed that different ion temperatures creates ripples on depression and bump of density as well as velocity profile of lighter ions. On the other hand, there is increase in sheath potential as the ionization ratio increases also.

Yuan et al. (2018) investigated the sub-terahertz wave transmission in magnetized and unmagnetized plasma sheaths. On the transmission of wave, they studied the temporal evolution impacts of the plasma sheath. In the plasma sheath magnetization, the transmission of atmospheric window frequencies was discussed briefly. Likewise, the rates of power transmission for the left hand circular as well as the right hand circular modes in plasma sheath magnetization are obviously higher as well as lower as compared to those in unmagnetized plasma sheath. The power transmission rates of the mode of left hand circular increases with strength of external magnetic field and wave frequency. Similarly, both in magnetized and unmagnetized plasma sheath the power tranmission rate of left hand circular mode dependent with time because of the time-related evolution of plasma sheath.

Various applications of plasma involve the plasma coming into contact with the surface of liquid. Previous investigation of stability of such types of surface of liquid is neglected the existence of the region of sheath between the liquid and the bulk plasma. Strong electric fields as well as strong ion flows are existed in this region. To observe the instability condition, Holgate et al. (2018) assumed a linear perturbation investigation of interface of liquid-sheath. Such criterion exhibits surface of metal which is molten in tokamak edge plasmas are stable against the electric field. Finally, they concluded that liquid surface stabilization by bombardment of ion was encouraging for the existing development of technologies of plasma-liquid.

The hypersonic vehicle, which is surrounded by the plasma sheath is the dynamic and time varying medium to calculate directly the physical parameters with variation of time which is nearly impossible. For understanding the physical parameters with dynamic nature as well as their effect on the communication, it is important the time varying degree. Shi et al. (2018) proposed to detect the electronic density of plasma sheath time-varying characteristics, and wireless channel property. This method utilizes the constant envelope zero autocorrelation sequence and this has spread gain characteristics as well as outstanding autocorrelation. Theoretically they simulate under the specific time-varying radio channel which exhibits that the method proposed by them is capable to detect frequency of time variation up to 200 kHz. The results obtained experimentally in the radio frequency modulation discharge plasma device confirmed the detection ability of time variation, practically in dynamic plasma sheath. At the same time, phenomenon of

nonlinear of plasma sheath dynamics on signal of communication through the channel sounding result was observed.

Nakatsutsumi et al. (2018) monitared the lasers having high energy which is interacting with solid material produces number of electrons creating electric field surrounding the target material. In this electric fields, the accelerated beams of protons indicate specific properties. For long term multidisciplinary purpose that is for cancer therapy, current challenges to achieve energies of proton by raising the laser intensity on target. Finally, the numerical as well as experimental results showing that self generated magnetostatic fields on the surface of the target pose the basic limitation for enough intensities of laser.

Karki (2018) investigated the collision effect in plasma sheath in uniform and oblique field magnetization using fluid models in which pressure gradient effect is also taken. Numerically, fluid equations which are dimensionless are solved for given boundary conditions. It has been observed that there is significant effect in ion density as well as velocity and space charge density. Likewise, it was observed that there was increase in the magnitude of potential on the wall with the increase in frequency of collision and decrease in rate of density of electron shifts towards the entrance of sheath.

To identify the properties of plasma sheath, Fu et al. (2018) investigated the enhancement of electric field with presence of surface protrusion in the atmospheric microdischarges. The enhancement of electric field which is caused by surface protrusion is tested to adjust aspect ratio as well as size of protrusion. The enhancement of electric field depends on the aspect ratio of protrusion. Also, axial electric field in vacuum and discharges may become nonlinear with protrusion on cathode and they compared sheath thickness which is obtained by two methods. Likewise, they observed that if the aspect ratio increases, there is decrease in the thickness of sheath. On the other hand, as the protrusion size increases, there is slight decrease in thickness of sheath. Finally, they concluded that protrusion's aspect ratio effect, as well as the thickness of sheath is important as compared to that size of protrusion.

Regmi et al. (2018) analyzed the effect of carbon and tungsten surfaces to hydrogen plasma for various temperatures. For various ion temperatures by using kinetic trajectory simulation model, the absorption and reflection coefficient of ion was studied. Also, the total ion charge density as well as ion density distribution was studied. They observed that reflection and absorption coefficient of incident particles depends on the kinetic energy of ion. If their energy is high, they will be reflected less. For the carbon and tungsten wall, the reflection coefficient of ion at 1 eV is 0.0567 and 0.3970 respectively, whereas for the wall of carbon, the reflection coefficient of ion at 2 eV decreases to 0.0246 and for the wall of tungsten, the reflection coefficient of ion at 2 eV is 0.3402. Finally the absorption, and reflection from the surface facing plasma are influenced by

the temperature of impinging ions.

Badsi et al. (2018) developed the numerical method to capture sheaths which is stationary and the plasma forms near to the metallic wall. Their work is based on the bi-species (ion/electron) Vlasov- Ampere model. In their work, they addressed to know if numerical schemes which is classical can preserve stationary solutions with boundary conditions, since at the discrete level, these solutions are not the priory conserved. In the context of method of high order semi Lagrangian, interpolation close to the boundary of the domain requires the specific treatment. High velocity resolution, high order interpolation and very small time steps, it was able accurately to recover the equilibrium for comparatively long time.

Morales Crespo (2018) studied the effect of positive ion temperature on plasma wall transition. Electric potential from plasma to the wall was obtained by the formulation of model as an initial value problem, and few characteristics which is useful for the experimental application, for example positive current to voltage characteristics, the floating potential, saturation current density and the estimation of thickness of sheath. At last, it was analysed how these quantities depend on ionization degree and temperature of positive ion.

Plasma sheath which is electronegative and its behavior in the collisional plasma in the absence of magnetic field and consists of q-nonextensive electrons. Boltzmann distributed negative and positive ions. By assuming the positive ion neutral collisions, and neglecting the effects of collisions and ionization between negative and positive ions. Borgohain & Saharia (2018) derived the modified version of Bohm-sheath criterion, and floating potential by applying multifluid model. By the application of modified version of Bohm-sheath criterion, the characteristics of sheath like spatial density profiles, net space charge density as well as potential was investigated. They observed that with increase the value of q-nonextensivity, electronegativity and collisionality there is decrease in the thickness of sheath but sheath potential and net space charge density increases. Finally, it was observed that as the values of ratio of electron temperature to negative ion temperature increases, sheath thickness increases also but sheath potential and net space charge density decreases.

Falessi & Zonca (2018) derived the set of equations and described the macroscopic transport of particles as well as energy in the thermonuclear plasma. In their work, they analyzed particle as well as energy transport on the confinement time of energy in a plasma with magnetic field taking coulomb collisions as well as fluctuations on equal footing. The equations used by them hold at every point in space and not to involve any radial averaging operation. The derived equations allow for studying collisional, and turbulent transport self-consistently. By assuming separation of scale, the transport

equations was derived from the kinetic relations with the help of analysis of multiple scale perturbation, as well as spatio-temporal averaging. In their work, the evolution equations was obtained for the moments of the distribution function. Finally, the equations is derived for the transport of particles as well as energy by using first order gyrokinetics.

CHAPTER 3

3. MATERIALS AND METHODS

3.1 Single particle model

In plasma physics, single particle model is described as individual electron and ion move in the imposed electric as well as magnetic fields. Each particle motion is described by the Lorentz force. For many cases of practical view, the motion of each particle is treated as superposition of comparatively fast circular motion around the point, which is called the guiding centre.

In the very low density, devices like the alternating gradient synchrotron, only trajectory of the single particle is considered. Sometimes plasma behaves like fluids and sometimes behaves like individual particles collection (Chen, 2016). Here we discuss how the single particle behaves in the electric as well as magnetic field.

When the electric field is zero, there is only the cyclotron gyration of charged particle about the static magnetic field. We write the equation of motion as

$$m\frac{d\boldsymbol{v}}{dt} = q\boldsymbol{v} \times \boldsymbol{B} \tag{3.1}$$

Taking the magnetic field along the z-direction, we have

$$m\frac{dv_x}{dt} = qBv_y \tag{3.2}$$

$$m\frac{dv_y}{dt} = -qBv_x \tag{3.3}$$

$$m\frac{dv_z}{dt} = 0 \tag{3.4}$$

$$\frac{d^2v_x}{dt^2} + \omega_c^2 v_x = 0 \tag{3.5}$$

$$\frac{d^2v_y}{dt^2} + \omega_c^2 v_y = 0 \tag{3.6}$$

where ω_c is the cyclotron frequency which is defined as

$$\omega_c = \frac{|q|B}{m} \tag{3.7}$$

Conventionally, we choose the cyclotron frequency ω_c is always nonnegative. Then from equation (3.5) and (3.6), we get

$$v_{x,y} = v_\perp \exp(\pm i\omega_c t + i\delta_{x,y}) \tag{3.8}$$

where $\pm$ represents the sign of charge q. We choose the phase δ, such that

$$\frac{dx}{dt} = v_\perp e^{i\omega_c t} \tag{3.9}$$

The positive constant $v_\perp$ indicates the speed in plane perpendicular to the magnetic field $\boldsymbol{B}$. Then we have

$$\frac{dy}{dt} = \pm i v_\perp e^{i\omega_c t} \tag{3.10}$$

Integrating Equations (3.9) and (3.10), we get

$$x - x_0 = -i\frac{v_\perp}{\omega_c} e^{i\omega_c t} \tag{3.11}$$

$$y - y_0 = \pm\frac{v_\perp}{\omega_c} e^{i\omega_c t} \tag{3.12}$$

Thus the Larmor radius is defined as

$$r_L = \frac{m v_\perp}{|q|B} \tag{3.13}$$

As we take the real part of equation (3.11) and (3.12) then we have

$$x - x_0 = r_L \sin\omega_c t \tag{3.14}$$

$$y - y_0 = \pm r_L \cos\omega_c t \tag{3.15}$$

Figure 10 explains the fixed circular orbit, the guiding center (x_0, y_0). Gyration's direction is such that the field magnetization which is generated by charged particle is opposite to that of the externally imposed magnetic field. Therefore, particles of plasma tend to reduce the field magnetization and hence the plasmas are therefore diamagnetic.

If the electric field is present, it will be found that the motion will be the sum of the two motions i.e., Larmor gyration and guiding center's drift. Choosing $\boldsymbol{E}$ be lie in the $x - z$

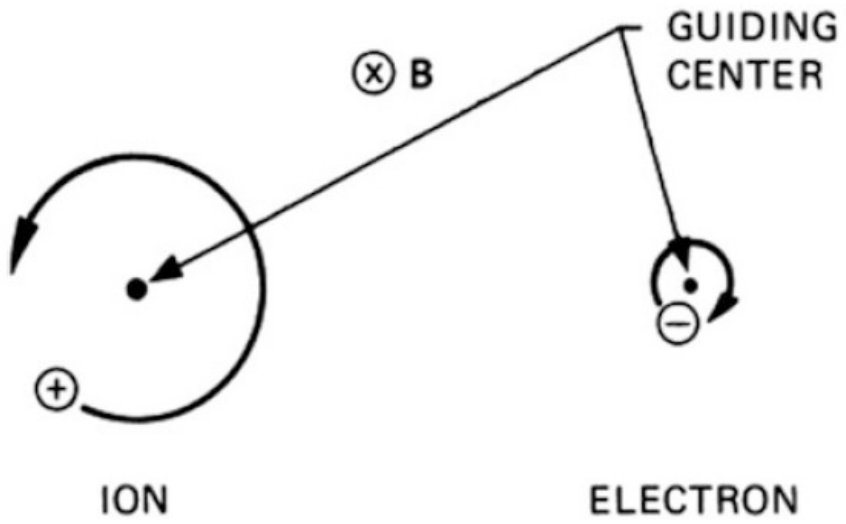

Figure 10: Larmor gyration in uniform magnetic field. (Source: Chen, 2016)

plane, such that $E_y = 0$. Now we write the equation of motion as

$$m\frac{d\boldsymbol{v}}{dt} = q\left[\boldsymbol{E} + \boldsymbol{v} \times \boldsymbol{B}\right] \tag{3.16}$$

For z-component we write

$$\frac{dv_z}{dt} = \frac{q}{m}E_z \tag{3.17}$$

$$\text{or} \quad v_z = \frac{qE_z}{m}t + v_z 0 \tag{3.18}$$

Equation (3.16) have transverse components as

$$\frac{dv_x}{dt} = \frac{q}{m}E_z \pm \omega_c v_y \tag{3.19}$$

$$\frac{dv_y}{dt} = 0 \mp \omega_c v_x \tag{3.20}$$

For constant electric field, differentiating above equation as

$$\frac{d^2v_x}{dt^2} = -\omega_c^2 v_x \tag{3.21}$$

$$\frac{d^2v_y}{dt^2} = -\omega_c^2\left(\frac{E_x}{B} + v_y\right) \tag{3.22}$$

This can be written as

$$\frac{d^2}{dt^2}\left(v_y + \frac{E_x}{B}\right) = -\omega_c^2\left(v_y + \frac{E_x}{B}\right) \tag{3.23}$$

Equation (3.9) and (3.10) can also be written as

$$v_x = v_\perp e^{i\omega_c t} \tag{3.24}$$

$$v_y = \pm i v e^{i\omega_c t} - \frac{E_x}{B} \tag{3.25}$$

To obtain the formula of the drift velocity v_E, we solve the equation (3.16) and omit the term of left hand side of this equation, then this equation becomes

$$[\boldsymbol{E} + \boldsymbol{v} \times \boldsymbol{B}] = 0 \tag{3.26}$$

Cross product is taken with $\boldsymbol{B}$, then we have

$$\boldsymbol{E} \times \boldsymbol{B} = \boldsymbol{v}B^2 - \boldsymbol{B}(\boldsymbol{v} \cdot \boldsymbol{B}) \tag{3.27}$$

According to this equation, transverse components are

$$\boldsymbol{v}_E = \boldsymbol{E} \times \boldsymbol{B}/B^2 \tag{3.28}$$

where v_E is the drift velocity.

Here $\boldsymbol{v}_E$ is independent with q, m and v. Following picture gives this reason. First half cycle of ion's orbit, from electric field, energy is gained, and increases in v as well as in r_L. Whereas in second half cycle, energy is lost and hence r_L decreases. The drift in v_E causes the difference in r_L on the left as well as right hand side of the orbit. There is gyration of negative electron in opposite direction, and gains energy also in the opposite direction as well. For the particles having same velocity but having different masses, the particle which is lighter will have r_L smaller and drift less per cycle. Anyway, the gyration frequency of such particles is also larger and hence two effects cancel exactly. The particles having the same mass but having different energy would have same cyclotron frequency ω_c. The particle which is slower one may have r_L smaller and gains minimum energy in the half cycle from $\boldsymbol{E}$. The particles which is less energetic, fractional change in Larmor radius r_L for the change in energy which is given is larger and hence canceled these two effects. With the changing pitch, in space, the orbit which is three dimensional is the slanted helix as shown in Figure 11.

3.2 Fluid model

To study the characteristics of plasma, it's parameters are used for three different approaches like single particle theory, fluid model and kinetic theory. For minimizing complexities in the kinetic theory, fluid model explain the macroscopic quantities which are based on plasma, such macroscopic quantities are density, mean velocity as well as

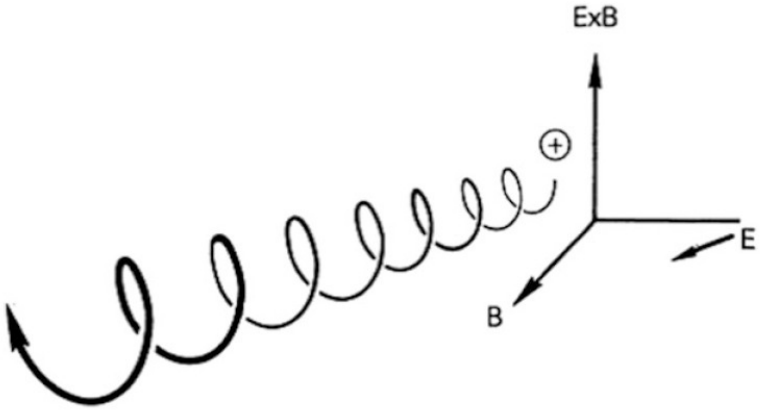

Figure 11: In space the real orbit of the gyrating particle. (Source: Chen, 2016)

energy.

Individual particles identity is neglected in the fluid model, and fluid element motion is taken only. In plasma, ions and electrons acts as the fluid. In actual case, there is validity of collisional fluid theory, but in our case we assumed the collisionless condition. More than 80% phenomena of plasma were explained by the fluid theory, and the fluid element motion is taken significantly, and hence the theory of single particle is neglected (Chen, 2016). The majority of the observed phenomenon is described by the fluid model. But some phenomena can not be described by this fluid model. In this case, velocity distribution function is considered, and we say such treatment as the kinetic theory.

The approach of single particle as we get to be terribly complex. We need approach of statistics because we would not follow every particle in the separate case. Providentially, it is not necessary because majority of observed plasma phenomena in the experiments should be briefly explained by the crude fluid model. In this case individual particles identity is removed and fluid elements motion is taken. In the case of ordinary fluid, particles collision keep the particles moving together in the fluid element. In the estimation of fluid, we assumed that the plasma is composed of either two or more than two interpenetrating fluids. In the case of only one species of the ion, we need two types of equations of the motion. One is the ion fluid which is positively charged, and other is the electron fluid having negative charge. The gas which is partially ionized, we also need the equation for fluid of the neutral atoms. By collisions, only neutral fluid interact with ions as well as electrons. Even if there is no collisions, ion as well as electron fluids interacts with each others, because there is generation of electric and magnetic fields.

3.2.1 Continuity equation

Suppose N is the number of particles in a volume V that can be changed as the surface contains either particles source or sink bounding the volume V. As the flux of particles

represents '$n\boldsymbol{u}'$', then from the divergence theorem, we have

$$\frac{\partial N}{\partial t} = \int \frac{\partial n}{\partial t} dV = -\int \nabla.(n\boldsymbol{u}) dV \tag{3.29}$$

For any volume, we have

$$\frac{\partial n}{\partial t} + \nabla.(n\boldsymbol{u}) = 0 \tag{3.30}$$

This equation is the continuity equation which explain the conservation of particles.

3.2.2 Momentum equation

In the electromagnetic field, for the charge particle moving with average velocity '$\boldsymbol{u}$', the equation of the motion is written as

$$mn\frac{d\boldsymbol{u}}{dt} = qn\left[\boldsymbol{E} + \boldsymbol{u} \times \boldsymbol{B}\right] \tag{3.31}$$

Suppose $\boldsymbol{S}(x,t)$ is the fluid element property in the $x-$space in one dimension. Then we write the rate of change of 'S' as

$$\frac{d\boldsymbol{S}}{dt} = \frac{\partial \boldsymbol{S}}{\partial t} + u_x \frac{\partial \boldsymbol{S}}{\partial x} \tag{3.32}$$

In three dimension, this is generalized as

$$\frac{d\boldsymbol{S}}{dt} = \frac{\partial \boldsymbol{S}}{\partial t} + (\boldsymbol{u} \cdot \nabla)\boldsymbol{S} \tag{3.33}$$

We say this equation as the connective derivative. Hence above equation (3.31) can be expressed as,

$$mn\left[\frac{\partial \boldsymbol{u}}{\partial t} + (\boldsymbol{u} \cdot \nabla)\boldsymbol{u}\right] = qn\left[\boldsymbol{E} + \boldsymbol{u} \times \boldsymbol{B}\right] \tag{3.34}$$

As we take the thermal motion, then at the right hand side of equation (3.34), we add the pressure gradient force, so that the resulting equation can be written as,

$$mn\left[\frac{\partial \boldsymbol{u}}{\partial t} + (\boldsymbol{u} \cdot \nabla)\boldsymbol{u}\right] = qn\left[\boldsymbol{E} + \boldsymbol{u} \times \boldsymbol{B}\right] - \nabla p \tag{3.35}$$

where $\nabla p = \nabla(nk_{\mathrm{B}}T)$ is the pressure gradient force which arises from random motion of particles.

3.2.3 Boltzmann relation

For $x-$component, the equation of motion of fluid is written as,

$$mn\left[\frac{\partial u_x}{\partial t} + (\boldsymbol{u}\cdot\nabla)u_x\right] = qnE_x - \frac{\partial p}{\partial x} \tag{3.36}$$

Convective term is very smaller then that the term $\partial u_x/\partial t$, therefore we remove this term, Hence

$$\frac{\partial u_x}{\partial t} = \frac{q}{m}E_x - \frac{k_\mathrm{B}}{mn}\frac{\partial n}{\partial x} \tag{3.37}$$

From this equation, it is clear that fluid is accelerated in the direction of $\boldsymbol{B}$ with the combined pressure gradient and electrostatic force. For electron, we take the limit as $m \to -e$, $q \to -e$ and $E = -\nabla\phi$, then

$$e\frac{\partial \phi}{\partial x} = \frac{k_\mathrm{B}T^\mathrm{e}}{n}\frac{\partial n}{\partial x} \tag{3.38}$$

Integrating this equation, we get

$$e\phi = k_\mathrm{B}T^\mathrm{e}\ln n + D \tag{3.39}$$

Boundary condition is used for $\phi = 0$, $n = n_0$, then we get

$$D = -k_\mathrm{B}T^\mathrm{e}\ln n_0 \tag{3.40}$$

This value is used in equation (3.39), we get

$$\begin{aligned} & k_\mathrm{B}T^\mathrm{e}\ln\frac{n}{n_0} = e\phi \\ \text{or}\quad & \ln\frac{n}{n_0} = \frac{e\phi}{k_\mathrm{B}T^\mathrm{e}} \\ \text{or}\quad & n = n_0 e^{e\phi/k_\mathrm{B}T^\mathrm{e}} \end{aligned} \tag{3.41}$$

This equation gives the required Boltzmann distribution for electrons

3.2.4 Poisson's equation

The relation between the electric field and gradient of scalar potential ϕ is

$$\boldsymbol{E} = -\nabla\phi \tag{3.42}$$

We can write the gauss law as

$$\nabla \cdot \boldsymbol{E} = \frac{\rho}{\varepsilon_0} \tag{3.43}$$

The equations (3.42) and (3.43) are combined, then we get

$$\nabla^2 \phi = -\frac{\rho}{\varepsilon_0} \tag{3.44}$$

This equation gives the relation between electric potential and total charge density and is called the Poisson's equation.

3.3 Basic concept of kinetic trajectory simulation

The fluid theory we have been using so far is the simplest description of plasma, it is indeed fortunate that this approximation is sufficiently accurate to describe the majority of observed phenomena. There are some phenomena, for which a fluid treatment is inadequate. For these, we need to consider the velocity distribution function $f(\boldsymbol{v})$ for each species, this treatment is called kinetic theory. Generally, the characteristic feature of the kinetic trajectory simulation (KTS) method is that the distribution function of the particle species involved are calculated directly by solving the related (collision less or collisional) kinetic equations along the respective collision less trajectories. Here we assume the electron and ion velocity distribution functions at the sheath edge to be shifted cut-off Maxwellian.

KTS is an iterative method for numerically calculating self consistent, time-independent kinetic plasma states in some given bounded spatial region. The plasma states are generally characterized by

- velocity distribution function $f(\boldsymbol{x}, \boldsymbol{v})$
- electric field $\boldsymbol{E}(\boldsymbol{x})$
- magnetic field $\boldsymbol{B}(\boldsymbol{x})$
- boundary conditions

At any given instant, each particle has a specific position and velocity. Hence we can characterize the instantaneous configuration of a large number of particles by specifying the density of particles at each point r,v in phase-space. The distribution function is the function prescribing the instantaneous density of particles in phase-space and is denoted by $f(\boldsymbol{r}, \boldsymbol{v}, t)$. Therefore, $f(\boldsymbol{r}, \boldsymbol{v}, t)d\boldsymbol{r}d\boldsymbol{v}$ is the number of particles at time t having positions in the range between $\boldsymbol{r}$ and $\boldsymbol{r} + d\boldsymbol{r}$ and velocities in the range between $\boldsymbol{v}$ and $\boldsymbol{v} + d\boldsymbol{v}$. As time progresses, the particle motion and acceleration causes the number

of particles in these $\boldsymbol{r}$ and $\boldsymbol{v}$ ranges to change and so f will change. In the general case of time-dependent, collisional kinetic theory, the Boltzmann equation for the particle species-s is

$$\frac{df^{\mathrm{s}}}{dt} = \left(\frac{\partial}{\partial t} + \boldsymbol{v}\cdot\frac{\partial}{\partial \boldsymbol{r}} + \boldsymbol{a}^{\mathrm{s}}\cdot\frac{\partial}{\partial \boldsymbol{v}}\right) f^{\mathrm{s}} = c^{s} \tag{3.45}$$

with

$$\boldsymbol{a}^{\mathrm{s}}(\boldsymbol{r},\boldsymbol{v},t) = \frac{q^{\mathrm{s}}}{m^{\mathrm{s}}}[\boldsymbol{E}(\boldsymbol{r},t) + \boldsymbol{v}\times\boldsymbol{B}(\boldsymbol{r},t)] \tag{3.46}$$

where $\boldsymbol{E}(\boldsymbol{r},t)$ and $\boldsymbol{B}(\boldsymbol{r},t)$ are the macroscopic electric and magnetic fields and c^{s} is the species-'s' collision integral term. The time derivative

$$\frac{d}{dt} \equiv \left(\frac{\partial}{\partial t} + \boldsymbol{v}\cdot\frac{\partial}{\partial \boldsymbol{r}} + \boldsymbol{a}\cdot\frac{\partial}{\partial \boldsymbol{v}}\right) \tag{3.47}$$

is the "Lagrangian" or total time derivative. The ion neutral collision frequency ν^{i} can be expressed as $\nu^{i} = n_n\sigma v_c^{i}$; where n_n is the neutral gas density σ is the constant collision crosssection and v_c^{i} is the ion collision velocity which depends on thermal velocity and average fluid velocity of ion. For the constant collision mean free path $\lambda^{i} = 1/n_n\sigma$, the collision mean free path of ion is larger then the dimension of our consider model. Therefore, plasma sheath can be considered as collision less(Riemann, 1981; Li et al., 2013). For the collision less cases, the equation (3.45) becomes "Vlasov equation", which is

$$\left(\frac{\partial}{\partial t} + \boldsymbol{v}\cdot\frac{\partial}{\partial \boldsymbol{r}} + \boldsymbol{a}^{\mathrm{s}}\cdot\frac{\partial}{\partial \boldsymbol{v}}\right) f^{\mathrm{s}} = 0 \tag{3.48}$$

i.e.,

$$\frac{df^{\mathrm{s}}}{dt} = 0 \implies f^{\mathrm{s}} = \text{constant}. \tag{3.49}$$

That is the velocity distribution function is constant for an observer which is moving along the collision less trajectory. Therefore, at each point the distribution function along the trajectory can be achieved if its value at one point is known.

3.4 Basic equations

We consider the one-dimensional, time-independent, collisionless, electrostatic problems, which is related to the basic equations as follows:

(a) In differential form, for electrons ($q = -e$), the velocity distribution function satisfies

the time-independent Vlasov equation as (Adhikari et al., 2019)

$$\left[\boldsymbol{v}\cdot\frac{\partial}{\partial\boldsymbol{r}}-\frac{e}{m^{\mathrm{e}}}\left(\boldsymbol{E}(\boldsymbol{r})+\boldsymbol{v}\times\boldsymbol{B}(\boldsymbol{r})\right)\cdot\frac{\partial}{\partial\boldsymbol{v}}\right]f^{\mathrm{e}}(\boldsymbol{r},\boldsymbol{v})=0 \tag{3.50}$$

In trajectory integrated forms, for electrons, the velocity distribution function is

$$f^{\mathrm{e}}(\boldsymbol{r},\boldsymbol{v})=f^{\mathrm{e}}_{\mathrm{st}}\left(\boldsymbol{r}^{\mathrm{e}}_{\mathrm{st}},\boldsymbol{v}^{\mathrm{e}}_{\mathrm{st}}\right), \tag{3.51}$$

where $f^{\mathrm{e}}_{\mathrm{st}}$ is the "starting distribution", $\boldsymbol{r}^{\mathrm{e}}_{\mathrm{st}}$ is starting configuration and $\boldsymbol{v}^{\mathrm{e}}_{\mathrm{st}}$ is the starting velocity of electrons. The equations of motion for electron are:

$$\frac{d\boldsymbol{r}^{\mathrm{e}}}{dt}=\boldsymbol{v}^{\mathrm{e}} \tag{3.52}$$

with components of velocity

$$\frac{dx^{\mathrm{e}}}{dt}=v^{\mathrm{e}}_x \tag{3.53}$$

$$\frac{dy^{\mathrm{e}}}{dt}=v^{\mathrm{e}}_y \tag{3.54}$$

$$\frac{dz^{\mathrm{e}}}{dt}=v^{\mathrm{e}}_z \tag{3.55}$$

and

$$\frac{d\boldsymbol{v}^{\mathrm{e}}}{dt}=\boldsymbol{a} \tag{3.56}$$

with components of acceleration

$$\frac{dv^{\mathrm{e}}_x}{dt}=a^{\mathrm{e}}_x \tag{3.57}$$

$$\frac{dv^{\mathrm{e}}_y}{dt}=a^{\mathrm{e}}_y \tag{3.58}$$

$$\frac{dv^{\mathrm{e}}_z}{dt}=a^{\mathrm{e}}_z \tag{3.59}$$

The macroscopic acceleration of electron is

$$\boldsymbol{a}^{\mathrm{e}}(\boldsymbol{r})=-\frac{e}{m^{\mathrm{e}}}\left[\boldsymbol{E}(\boldsymbol{r})+\boldsymbol{v}\times\boldsymbol{B}(\boldsymbol{r})\right] \tag{3.60}$$

with its components

$$a^{\mathrm{e}}_x=-\frac{e}{m^{\mathrm{e}}}\left[E(x)+(\boldsymbol{v}\times\boldsymbol{B}(\boldsymbol{r}))_x\right] \tag{3.61}$$

$$a^{\mathrm{e}}_y=-\frac{e}{m^{\mathrm{e}}}\left[E(y)+(\boldsymbol{v}\times\boldsymbol{B}(\boldsymbol{r}))_y\right] \tag{3.62}$$

$$a^{\mathrm{e}}_z=-\frac{e}{m^{\mathrm{e}}}\left[E(z)+(\boldsymbol{v}\times\boldsymbol{B}(\boldsymbol{r}))_z\right] \tag{3.63}$$

(b) Likewise, in differential form, the velocity distribution functions for singly charged ions satisfy the time independent Vlasov equations as (Adhikari et al., 2018)

$$\left[\boldsymbol{v}\cdot\frac{\partial}{\partial\boldsymbol{r}}+\frac{e}{m^{\mathrm{i}}}\left(\boldsymbol{E}(\boldsymbol{r})+\boldsymbol{v}\times\boldsymbol{B}(\boldsymbol{r})\right)\cdot\frac{\partial}{\partial\boldsymbol{v}}\right]f^{\mathrm{i}}(\boldsymbol{r},\boldsymbol{v})=0 \tag{3.64}$$

and in trajectory integrated forms as:

$$f^{\mathrm{i}}(\boldsymbol{r},\boldsymbol{v})=f^{\mathrm{i}}_{\mathrm{st}}\left(\boldsymbol{r}^{\mathrm{i}}_{\mathrm{st}},\boldsymbol{v}^{\mathrm{i}}_{\mathrm{st}}\right) \tag{3.65}$$

where $f^{\mathrm{i}}_{\mathrm{st}}$, $\boldsymbol{r}^{\mathrm{i}}_{\mathrm{st}}$ and $\boldsymbol{v}^{\mathrm{i}}_{\mathrm{st}}$ is the starting distribution, starting configuration and starting velocity of ions respectively. The ion equations of motion are

$$\frac{d\boldsymbol{r}^{\mathrm{i}}}{dt}=\boldsymbol{v}^{\mathrm{i}} \tag{3.66}$$

with components

$$\frac{dx^{\mathrm{i}}}{dt} = v^{\mathrm{i}}_x \tag{3.67}$$

$$\frac{dy^{\mathrm{i}}}{dt} = v^{\mathrm{i}}_y \tag{3.68}$$

$$\frac{dz^{\mathrm{i}}}{dt} = v^{\mathrm{i}}_z \tag{3.69}$$

and

$$\frac{d\boldsymbol{v}^{\mathrm{i}}}{dt}=\boldsymbol{a}^{\mathrm{i}} \tag{3.70}$$

with component of acceleration

$$\frac{dv^{\mathrm{i}}_x}{dt} = a^{\mathrm{i}}_x \tag{3.71}$$

$$\frac{dv^{\mathrm{i}}_y}{dt} = a^{\mathrm{i}}_y \tag{3.72}$$

$$\frac{dv^{\mathrm{i}}_z}{dt} = a^{\mathrm{i}}_z \tag{3.73}$$

The macroscopic acceleration is

$$\boldsymbol{a}^{\mathrm{i}}(\boldsymbol{r})=\frac{e}{m^e}\left[\boldsymbol{E}(\boldsymbol{r})+\boldsymbol{v}\times\boldsymbol{B}(\boldsymbol{r})\right] \tag{3.74}$$

with its components,

$$a_x^{\mathrm{i}} = \frac{e}{m^{\mathrm{e}}}\left[E(x) + (\boldsymbol{v} \times \boldsymbol{B}(\boldsymbol{r}))_x\right] \tag{3.75}$$

$$a_y^{\mathrm{i}} = \frac{e}{m^{\mathrm{e}}}\left[E(y) + (\boldsymbol{v} \times \boldsymbol{B}(\boldsymbol{r}))_y\right] \tag{3.76}$$

$$a_z^{\mathrm{i}} = \frac{e}{m^{\mathrm{e}}}\left[E(z) + (\boldsymbol{v} \times \boldsymbol{B}(\boldsymbol{r}))_z\right] \tag{3.77}$$

(c) The electric field is given as

$$\boldsymbol{E}(\boldsymbol{r}) = -\frac{d\phi(\boldsymbol{r})}{dr}, \tag{3.78}$$

where the electrostatic potential $\phi(\boldsymbol{r})$ is obtained from Poisson's equation

$$\frac{d^2\phi(\boldsymbol{r})}{dr^2} = -\frac{\rho(\boldsymbol{r})}{\varepsilon_0} \tag{3.79}$$

The space charge density is defined as

$$\rho(\boldsymbol{r}) = \sum_s q^{\mathrm{s}} n^{\mathrm{s}}(\boldsymbol{r}_j) \tag{3.80}$$

The electron and ion densities given as

$$n^{\mathrm{s}}(\boldsymbol{r}) = \int_{-\infty}^{+\infty} d^3v f^{\mathrm{s}}(r, \boldsymbol{v})\,; \quad s = (e, i) \tag{3.81}$$

The various components of velocity of ions in the plasma sheath have been computed using the Lorentz force equation (Chen, 2016)

$$\begin{aligned} &\boldsymbol{F} = q\left[\boldsymbol{E} + \boldsymbol{v} \times \boldsymbol{B}\right] \\ \text{or} \quad &\frac{d\boldsymbol{v}}{dt} = \frac{q}{m}\left[\boldsymbol{E} + \boldsymbol{v} \times \boldsymbol{B}\right] \end{aligned} \tag{3.82}$$

where q is the charge of ion having mass m, moving with velocity $\boldsymbol{v}$ with the magnetic field $\boldsymbol{B}$ and electric field $\boldsymbol{E}$.

The oscillatory motion of the ions under goes the damping phenomenon and the typical differential equation of damped harmonic oscillator is, (Simmons, 2016)

$$\frac{d^2v}{dt^2} + 2k\frac{dv}{dt} + \omega_0^2 v = 0 \tag{3.83}$$

where ω_0 is the natural frequency of the oscillating particle. By using equation (3.85), the equation of the damped harmonic oscillator is (Adhikari et al., 2016)

$$v(t) = v_{\mathrm{m}} + Ae^{-kt}\sin(\omega t + \psi) \tag{3.84}$$

where k is damping constant, A is amplitude, v_{m} is mean value and ψ is the phase angle. This equation is used to fit with the computed plot. The parameters v_m, A, k, ω and ψ are estimated from the corresponding plots. v_{m} = value of $v(t)$ at time t equal to one second, A = amplitude of $v(t)$ at time t equal to zero, ω = angular frequency = $2\pi f$, f = frequency of oscillation and ψ = phase angle.

To estimate k, first of all nature of the damped oscillation is carefully observed. From the graph maximum peak value of the velocity (v_1) at smaller time (t_1) as well as velocity (v_2) at longer time (t_2) are noted. Then, k is calculated using the following formula:

$$k = \frac{1}{(t_2 - t_1)} \ln\left(\frac{v_1 - v_{\mathrm{m}}}{v_2 - v_{\mathrm{m}}}\right) \tag{3.85}$$

If v is the velocity of the ion at any time t, then the equation of fitted curve is

$$v = v_0 e^{-t/\tau} \tag{3.86}$$

where v_0 is the initial value of v and τ is the characteristic time which can be written as

$$\tau = t_1 + \frac{v_1 - v}{v_2 - v} \triangle t \tag{3.87}$$

The stationary Child sheath thickness can be estimated according to the Child-Langmuir law as (Chen, 2016).

$$L_s^2 = \frac{4}{9}\epsilon_0 \sqrt{\frac{2e}{m^{\mathrm{i}}}} \frac{|\phi_w|^{3/2}}{J^i_{\mathrm{ps}}} \tag{3.88}$$

where J^i_{ps} is the ion current density at the presheath side.

The flux of particle species-s is,

$$\Gamma^s = \int d^3 v^s v^s f^s(x, \boldsymbol{v}^s). \tag{3.89}$$

By assuming the Boltzmann's distribution of electrons, the wall potential is obtained by equating the ion and electron fluxes at the wall (Adhikari et al., 2019) i.e.,

$$\Gamma^{\mathrm{i}} = \Gamma^{\mathrm{e}} \tag{3.90}$$

which yields,

$$\frac{e\phi_w}{k_{\mathrm{B}} T^{\mathrm{e}}} = \frac{1}{2} \ln\left[\frac{2\pi m^{\mathrm{e}}}{m^{\mathrm{i}}} \left(\frac{T^{\mathrm{e}}_{\mathrm{ps}} + \gamma^{\mathrm{i}} T^{\mathrm{i}}_{\mathrm{ps}}}{T^{\mathrm{e}}}\right)\right] \tag{3.91}$$

3.5 Plasma sheath model

The simulation region which is our region of interest bounded by two parallel planes at $x = 0$ and $x = L$ is shown in Figure 12. In the present work, the plasma consists singly charged hydrogen ions and electrons, are not in thermal equilibrium such that $T^e \neq T^i$, where T^e and T^i are electron and ion temperatures, respectively. The right hand boundary $x = L$ is specified as the "sheath entrance" whereas the left hand boundary $x = 0$ represents the non-emitting material wall. The uniform magnetic field is applied in $x - y$ plane which makes an angle θ with the line normal to the wall.

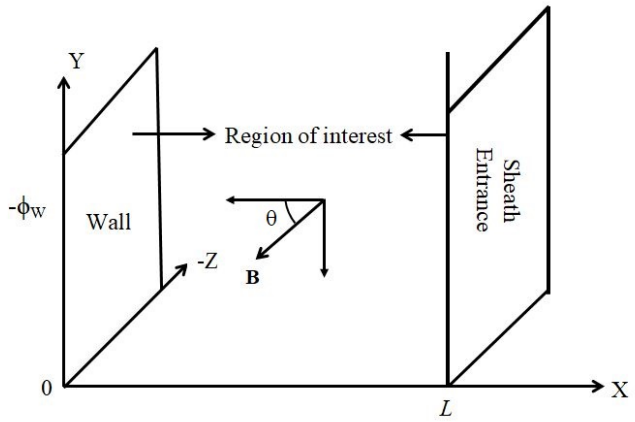

Figure 12: Plasma sheath model. (Source: Adhikari et al., 2019)

In the present work, we adopt the particle and field boundary conditions as;

(a) Particle boundary conditions

From the right hand boundary, the plasma particle enters the simulation region with cut-off Maxwellian velocity distributions functions and the distribution function satisfies the following conditions as:
At the left hand boundary,

$$f^s(x = 0, \boldsymbol{v} \geq 0) = 0; \qquad s = (e, i) \tag{3.92}$$

At the right hand boundary,

$$f^{\mathrm{e}}(x = L, \boldsymbol{v} \leq 0) = A^{\mathrm{e}} \exp\left[-\left(\frac{v_x^2 + v_y^2 + v_z^2}{v_{\mathrm{tf}}^{e^2}}\right)\right] \Theta[v_{\mathrm{cL}}^{\mathrm{e}} - v_x] \tag{3.93}$$

$$f^{\mathrm{i}}(x = L, \boldsymbol{v} \leq 0) = A^{\mathrm{i}} \exp\left[-\frac{[(v_x - v^{\mathrm{i}}_{\mathrm{mL}})^2 + v_y^2 + v_z^2]}{v_{\mathrm{tf}}^{e^2}}\right] \Theta(v^{\mathrm{i}}_{\mathrm{cL}} - v_x) \tag{3.94}$$

where the thermal velocity of particle species 's' is

$$\boldsymbol{v}^{\mathrm{s}}_{\mathrm{tf}} = \sqrt{\frac{2k_{\mathrm{B}}T^{\mathrm{s}}}{m^s}} \tag{3.95}$$

where $v^{\mathrm{i}}_{\mathrm{mL}}$ is the ion "Maxwellian-maximum" velocity at $x = L$ and $v^{\mathrm{i}}_{\mathrm{cL}}$ ($v^{\mathrm{i}}_{\mathrm{cL}} < 0$) is the ion cut-off velocity at $x = L$. The electron velocity distribution function at any position is

$$f^{\mathrm{e}}(x, \boldsymbol{v} \leq 0) = A^{\mathrm{e}} \exp\left[-\frac{v^2}{v_{\mathrm{tf}}^{\mathrm{e}\,2}} + \frac{e\phi(x)}{k_{\mathrm{B}}T^{\mathrm{e}}_{\mathrm{tf}}}\right] \Theta(v^{\mathrm{e}}_{\mathrm{c}}(x) - v_x), \tag{3.96}$$

where $\Theta(x)$ is a heaviside function and

$$v^{\mathrm{e}}_{\mathrm{c}}(x) = \sqrt{\frac{2e[\phi(x) - \phi_0]}{m^{\mathrm{e}}}} \tag{3.97}$$

is the cut-off velocity of electron at point x.
Likewise, for the ions velocity distribution function is,

$$f^{\mathrm{i}}(x = L, \boldsymbol{v}) = A^{\mathrm{i}} \exp\left[-\frac{[(v_x - v^{\mathrm{i}}_{\mathrm{mL}})^2 + v_y^2 + v_z^2]}{v_{\mathrm{tf}}^{e^2}}\right] \Theta(v^{\mathrm{i}}_{\mathrm{cL}} - v_x) \tag{3.98}$$

There are seven parameters A^{e}, $T^{\mathrm{e}}_{\mathrm{f}}$, $v^{\mathrm{e}}_{\mathrm{cL}}$, A^{i}, $T^{\mathrm{i}}_{\mathrm{f}}$, $v^{\mathrm{i}}_{\mathrm{mL}}$ and $v^{\mathrm{i}}_{\mathrm{cL}}$ in the right hand side of Equation (3.96) and Equation (3.98), they must be specified according to the physical situation considered. The density of particle species-s at $x = L$ is

$$n^{\mathrm{s}}_L = \int_{-\infty}^{+\infty} d^3v f^{\mathrm{s}}(L, \boldsymbol{v}). \tag{3.99}$$

At $x = L$, the electron density is,

$$\begin{aligned} n^{\mathrm{e}}_L &= \int_{-\infty}^{\infty} d^3v\ f^{\mathrm{e}}(L, \boldsymbol{v}) \\ &= A^{\mathrm{e}} \int_{-\infty}^{\infty} dv_x \int_{-\infty}^{\infty} dv_y \int_{-\infty}^{\infty} dv_z\ \exp\left[-\left(\frac{v_x^2 + v_y^2 + v_z^2}{v_{\mathrm{tf}}^{e^2}}\right)\right] \Theta[v^{\mathrm{e}}_{\mathrm{cL}} - v] \\ &= A^{\mathrm{e}} \int_{-\infty}^{v_{e,cL}} dv_x\ \exp\left[-\left(\frac{v_x}{v^{\mathrm{e}}_{\mathrm{tf}}}\right)^2\right] \int_{-\infty}^{\infty} dv_y\ \exp\left[-\left(\frac{v_y}{v^{\mathrm{e}}_{\mathrm{tf}}}\right)^2\right] \int_{-\infty}^{\infty} dv_z\ \exp\left[-\left(\frac{v_z}{v^{\mathrm{e}}_{\mathrm{tf}}}\right)^2\right] \end{aligned}$$

Using $v/v_{\rm tf}^{\rm e} = \xi$, we get

$$\begin{aligned} n_L^{\rm e} &= A^{\rm e} \int_{-\infty}^{v_{\rm cL}^{\rm e}/v_{\rm tf}^{e}} v_{tf}^{e} \exp\left(-\xi^2\right) d\xi \, \sqrt{\pi v_{tf}^{e^2}} \sqrt{\pi v_{tf}^{e^2}} \\ &= A^{\rm e} \pi \, {v_{\rm tf}^{\rm e}}^3 \left[\frac{\sqrt{\pi}}{2} + \frac{\sqrt{\pi}}{2} erf\left(\frac{v_{cL}^{e}}{v_{tf}^{e}} \right) \right] \\ &= \frac{A^{\rm e} \, \pi^{3/2} \, {v_{\rm tf}^{\rm e}}^3}{2} \, C^{\rm e}, \end{aligned}$$

where

$$C^{\rm e}(T_{\rm f}^{\rm e}, \phi_0) = 1 + erf\left(\frac{v_{cL}^{e}}{v_{\rm tf}^{\rm e}} \right) = 1 + erf \sqrt{\frac{-e\phi_0}{k_{\rm B} T_{\rm f}^{\rm e}}} \tag{3.100}$$

and "erf" represents the "Error function", which is defined as

$$erf(x) = \frac{2}{\sqrt{\pi}} \int_0^x d\xi \; \exp\left(-\xi^2\right) \tag{3.101}$$

The ion density at $x = L$ is,

$$\begin{aligned} n_L^{\rm i} &= \int_{-\infty}^{+\infty} d^3v f^{\rm i}(L, \boldsymbol{v}) = \int_{-\infty}^{+\infty} d^3v \exp\left[-\left(\frac{(v_x - v_{\rm mL}^{\rm i})^2 + v_y^2 + v_z^2}{{v_{\rm tf}^{\rm i}}^2} \right) \right] \Theta[v_{\rm cL}^{\rm i} - v_x] \\ &= A^{\rm i} \int_{-\infty}^{+\infty} dv_x \int_{-\infty}^{+\infty} dv_y \int_{-\infty}^{+\infty} dv_z \; \exp\left[-\left(\frac{(v_x - v_{\rm mL}^{\rm i})^2 + v_y^2 + v_z^2}{{v_{\rm tf}^{\rm i}}^2} \right) \right] \Theta[v_{\rm cL}^{\rm i} - v_x] \\ &= A^{\rm i} \int_{-\infty}^{v_{\rm cL}^{\rm i}} dv_x \exp\left[-\left(\frac{(v_x - v_{\rm mL}^{\rm i})}{v_{\rm tf}^{\rm i}} \right)^2 \right] \int_{-\infty}^{\infty} dv_y \; \exp\left[-\left(\frac{v_y}{v_{\rm tf}^{\rm i}} \right)^2 \right] \int_{-\infty}^{\infty} dv_z \; \exp\left[-\left(\frac{v_z}{v_{\rm tf}^{\rm i}} \right)^2 \right] \end{aligned} \tag{3.102}$$

Using $\left(v - v_{\rm mL}^{\rm i}\right)/v_{\rm tf}^{\rm i} = \xi$, we get

$$\begin{aligned} n_L^{\rm i} &= A^{\rm i} \int_{-\infty}^{(v_{\rm cL}^{\rm i} - v_{\rm mL}^{\rm i})/v_{\rm tf}^{\rm i}} v_{\rm tf}^{\rm i} \exp\left(-\xi^2\right) d\xi \, \sqrt{\pi v_{tf}^{i^2}} \sqrt{\pi v_{tf}^{i^2}} \\ &= A^{\rm i} \pi \, {v_{\rm tf}^{\rm i}}^3 \left[\frac{\sqrt{\pi}}{2} + \frac{\sqrt{\pi}}{2} erf\left(\frac{v_{\rm cL}^{\rm i} - v_{mL}^{i}}{v_{\rm tf}^{\rm i}} \right) \right] \\ &= \frac{A^{\rm i} \, \pi^{3/2} \, {v_{\rm tf}^{\rm i}}^3}{2} \left[1 + erf(\tau_{\rm cL}^{\rm i}) \right] \\ &= \frac{A^{\rm i} \, \pi^{3/2} \, {v_{\rm tf}^{\rm i}}^3}{2} \, C^{\rm i} \end{aligned}$$

where

$$C^{\mathrm{i}} = 1 + erf(\tau^{\mathrm{i}}_{\mathrm{cL}}) \quad \text{and} \quad \tau^{\mathrm{i}}_{\mathrm{cL}} = \left(\frac{v^{\mathrm{i}}_{\mathrm{cL}} - v^{i}_{mL}}{v^{\mathrm{i}}_{\mathrm{tf}}} \right)$$

The fluid velocity of species-s is given as

$$\boldsymbol{u}^{\mathrm{s}} = \frac{1}{n^{\mathrm{s}}_{L}} \int \boldsymbol{v} f^{s}(x, \boldsymbol{v}) d^3 v \tag{3.103}$$

Such that

$$\boldsymbol{u}^{\mathrm{e}}_{L} = -\left(\frac{v^{\mathrm{e}}_{t}}{\sqrt{\pi}} \frac{D^{\mathrm{e}}}{C^{\mathrm{e}}} \right) i \tag{3.104}$$

and

$$\boldsymbol{u}^{\mathrm{i}}_{L} = \left[v^{\mathrm{i}}_{xm,L} - \frac{v^{\mathrm{i}}_{t}}{\sqrt{\pi}} \frac{D^{\mathrm{i}}}{C^{\mathrm{i}}} \right] i \tag{3.105}$$

The presheath side electron temperature at $x = L$ is given as

$$T^{\mathrm{e}}_{L} = \frac{1}{3 n^{\mathrm{e}}_{L} k_{B}} \int \int \int d^3 v \, m^{\mathrm{e}} \left(v - u^{\mathrm{e}}_{L} \right)^2 f^{\mathrm{e}}(x, \boldsymbol{v}) \tag{3.106}$$

where

$$C^{\mathrm{e}} = 1 + erf \sqrt{\frac{-e\phi_0}{k_{\mathrm{B}} T^{\mathrm{e}}}}, \qquad D^{\mathrm{e}} = \exp\left(\frac{-e\phi_0}{k_{\mathrm{B}} T^{\mathrm{e}}} \right) \tag{3.107}$$

Likewise, the presheath side ion temperature at $x = L$ is given as

$$T^{\mathrm{i}}_{L} = \frac{1}{3 n^{\mathrm{i}}_{L} k_{\mathrm{B}}} \int \int \int d^3 v \, m^{\mathrm{i}} \left(v - u^{\mathrm{i}}_{L} \right)^2 f^{\mathrm{i}}(x, \boldsymbol{v}) \tag{3.108}$$

(b) Field boundary condition

The magnitude of electrostatic potential is chosen as zero at $x = L$ and a fixed negative constant value at $x = 0$ i.e.,

$$\phi(x = 0) = \phi_0 \text{ (constant)} < 0 \tag{3.109}$$

$$\phi(x = L) = 0 \tag{3.110}$$

Ourselves we restrict to the potential distribution, which decreases monotonically from $x = L$ to $x = 0$ such that the electric field always remains negative.

3.6 Presheath-sheath coupling

As the plasma flows towards the wall, it passes through the two specific regions like electric field which have large gradient, as well as weak gradient of variables. The "sheath" is the narrow region in which there is large gradient of electric field, as well as supersonic velocity, where as "presheath" is the region attached with the bulk plasma, having weak gradient of variables, and generally subsonic flow.

Sheath and presheath have different scale length and generally, are studied by using various approaches (Riemann, 1991, 2000). In our case it is important, to couple the different solutions at the side of presheath, and sheath. In our case, we present the presheath-sheath coupling mechanism for the unperturbed flow of plasma parameters at the presheath-sheath boundary. The coupling scheme satisfies an important requirements i.e.,quasineutrality condition, sheath edge singularity condition, continuity of first three moments and kinetic Bohm condition. The sheath side parameters n^{s}, T^{s} and u^{s} are coupled with the presheath side parameters $n^{\mathrm{s}}_{\mathrm{ps}}$, $T^{\mathrm{s}}_{\mathrm{ps}}$ and $u^{\mathrm{s}}_{\mathrm{ps}}$. The continuity of the physical parameters is given by

$$n^{\mathrm{e}}_{L} = n_{\mathrm{ps}}, \quad n^{\mathrm{i}}_{L} = n_{ps} \tag{3.111}$$

$$u^{\mathrm{e}}_{L} = u^{\mathrm{e}}_{\mathrm{ps}}, \quad u^{\mathrm{i}}_{L} = u^{\mathrm{i}}_{\mathrm{ps}} \tag{3.112}$$

$$T^{\mathrm{e}}_{L} = T^{\mathrm{e}}_{\mathrm{ps}}, \quad T^{\mathrm{i}}_{L} = T^{\mathrm{i}}_{\mathrm{ps}} \tag{3.113}$$

The coupling equations are

$$n^{\mathrm{e}}_{\mathrm{ps}} = n_{\mathrm{ps}} = 4A^{\mathrm{e}}C^{\mathrm{e}}\left(\frac{\pi k_{\mathrm{B}}T^{\mathrm{e}}}{2m^{\mathrm{e}}}\right)^{1.5} \tag{3.114}$$

$$n^{\mathrm{i}}_{\mathrm{ps}} = n_{\mathrm{ps}} = 4A^{\mathrm{i}}C^{\mathrm{i}}\left(\frac{\pi k_{\mathrm{B}}T^{\mathrm{i}}}{2m^{\mathrm{i}}}\right)^{1.5} \tag{3.115}$$

$$u^{\mathrm{e}}_{\mathrm{ps}} = -\sqrt{\frac{2k_{\mathrm{B}}T^{\mathrm{e}}}{\pi m^{\mathrm{e}}}}\frac{D^{\mathrm{e}}}{C^{\mathrm{e}}} \tag{3.116}$$

$$u_{\rm ps}^{\rm i} = v_{mL}^{\rm i} - \sqrt{\frac{2k_{\rm B}T^{\rm i}}{\pi m^{\rm i}}}\frac{D^{\rm i}}{C^{\rm i}} \tag{3.117}$$

$$T_{\rm ps}^{\rm e} = T^{\rm e}\left[1 - \frac{2}{3}\sqrt{\frac{-e\phi_0}{\pi k_{\rm B}T^{\rm e}}}\frac{D^{\rm e}}{C^{\rm e}} - \frac{2}{3\pi}\left(\frac{D^{\rm e}}{C^{\rm e}}\right)^2\right] \tag{3.118}$$

$$T_{\rm ps}^{\rm i} = T^{\rm i}\left[1 - \frac{2}{3}\frac{\tau_{cL}^{\rm i}}{\pi}\frac{D^{\rm i}}{C^{\rm i}} - \frac{2}{3\pi}\left(\frac{D^{\rm i}}{C^{\rm i}}\right)^2\right] \tag{3.119}$$

3.7 Bohm-Chodura criterion

To exist sheath, the in-streaming ion have to satisfy the condition, which we say "Bohm-Chodura Criterion". Here we derive Bohm criterion, which is satisfied by injected ion velocity distribution function, so that the formation of sheath is possible, whereas, we assumed the electron distribution to satisfy full Maxwellian. This case arises for without magnetic field or the applied magnetic field perpendicular to the wall.

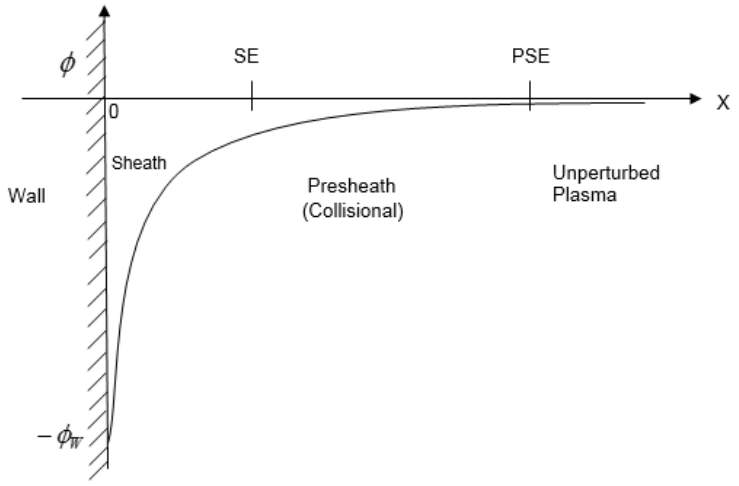

Figure 13: Potential profile monotonically decreasing from $x = L$ to $x = 0$. (Source: Khanal, 2003)

The Poisson's equation is written as

$$\frac{d^2\phi}{dx^2} = -\frac{\rho(\phi)}{\varepsilon_0}. \tag{3.120}$$

In Taylor' series, the above equation is expanded about $x \approx L$, we get

$$\left[\frac{d^2\phi}{dx^2}\right]_{x\to L} = -\frac{1}{\varepsilon_0}\left[\rho(\phi_0) + \phi\left[\frac{d\rho}{d\phi}\right]_{x\to L} + \frac{\phi^2}{2}\left[\frac{d^2\rho}{d\phi^2}\right]_{x\to L} + - - -\right] \tag{3.121}$$

If we assumed at the sheath entrance, the plasma is quasineutral, i.e. $\rho(x_L) = 0$, $n^{\mathrm{i}}_{\mathrm{ps}} = n^{\mathrm{e}}_{\mathrm{ps}}$. Then, using the quasineutrality condition, and neglecting second and higher order terms from Equation (3.121), we obtain

$$\left[\frac{d^2\phi}{dx^2}\right]_{x\to L} + \frac{\phi}{\epsilon_0}\left[\frac{d\rho}{d\phi}\right]_{x\to L} = 0. \tag{3.122}$$

But we have taken the potential profile which is monotonically decreasing towards the wall i.e., of the form $\phi(x \le L) \le 0$. Hence the Equation (3.122), will have non-oscillatory solution, only if

$$\left[\frac{d\rho}{d\phi}\right]_{x\to L} \le 0. \tag{3.123}$$

In terms of particle densities, we expressed the above relation as

$$\left[\frac{d\rho}{d\phi}\right]_{x\to L} = e\left[\frac{dn^{\mathrm{i}}}{d\phi} - \frac{dn^{\mathrm{e}}}{d\phi}\right]_{x\to L}. \tag{3.124}$$

At any point, the electron density including the potential profile, is given by

$$n^{\mathrm{e}}(\phi) = n^{\mathrm{e}}_L\, exp\left[\frac{e\phi}{k_{\mathrm{B}}T^{\mathrm{e}}_{\mathrm{f}}}\right]\left[\frac{1 + erf\sqrt{\frac{e(\phi-\phi_0)}{k_{\mathrm{B}}T^{\mathrm{e}}_{\mathrm{f}}}}}{1 + erf\sqrt{\frac{-e\phi_0}{k_{\mathrm{B}}T^{\mathrm{e}}_{\mathrm{f}}}}}\right]. \tag{3.125}$$

The above equation is differentiated with respect to ϕ which yields

$$\begin{aligned}\frac{dn^{\mathrm{e}}(\phi)}{d\phi} = {} & \frac{n^{\mathrm{e}}_L e}{k_{\mathrm{B}}T^{\mathrm{e}}_{\mathrm{f}}}\exp\left[\frac{e\phi}{k_{\mathrm{B}}T^{\mathrm{e}}_{\mathrm{f}}}\right]\left[\frac{1 + erf\sqrt{\frac{e(\phi-\phi_0)}{k_{\mathrm{B}}T^{\mathrm{e}}_{\mathrm{f}}}}}{1 + erf\sqrt{\frac{-e\phi_0}{k_{\mathrm{B}}T^{\mathrm{e}}_{\mathrm{f}}}}}\right] \\ & + \frac{n^{\mathrm{e}}_L e}{k_{\mathrm{B}}T^{\mathrm{e}}_{\mathrm{f}}}\exp\left[\frac{e\phi_0}{k_{\mathrm{B}}T^{e}_{f}}\right]\frac{\sqrt{\frac{k_{\mathrm{B}}T^{\mathrm{e}}_{\mathrm{f}}}{e\pi(\phi-\phi_0)}}}{1 + erf\sqrt{\frac{-e\phi_0}{k_{\mathrm{B}}T^{\mathrm{e}}_{\mathrm{f}}}}}\end{aligned} \tag{3.126}$$

But at $x \to L$, and $\phi \to 0$, above Equation (3.126) reduces to

$$\left[\frac{dn^{\mathrm{e}}(\phi)}{d\phi}\right]_{x\to L} = \frac{n^{\mathrm{e}}_L e}{k_{\mathrm{B}}T^{\mathrm{e}}_{\mathrm{f}}}\left[1 + \exp\left[\frac{e\phi_0}{k_{\mathrm{B}}T^{\mathrm{e}}_{\mathrm{f}}}\right]\frac{\sqrt{\frac{-k_{\mathrm{B}}T^{\mathrm{e}}_{\mathrm{f}}}{e\pi\phi_0}}}{1 + erf\sqrt{\frac{-e\phi_0}{k_{\mathrm{B}}T^{\mathrm{e}}_{\mathrm{f}}}}}\right]. \tag{3.127}$$

We have taken the ion density at any point x which is given by

$$n^{\mathrm{i}}(\phi) = \int_{-\infty}^{v_{\mathrm{cL}}^{\mathrm{i}}} \int_{-\infty}^{\infty} \int_{-\infty}^{\infty} d^3v \left[1 - \frac{2e\phi}{m^{\mathrm{i}}v^2}\right]^{-1/2} f_L^{\mathrm{i}}(v). \tag{3.128}$$

After differentiating the Equation (3.128), then we get

$$\frac{dn^{\mathrm{i}}(\phi)}{d\phi} = \int_{-\infty}^{v_{\mathrm{cL}}^{\mathrm{i}}} \int_{-\infty}^{\infty} \int_{-\infty}^{\infty} d^3v \frac{f_L^{\mathrm{i}}(v)}{v^2} \left[1 - \frac{2e\phi}{m^{\mathrm{i}}v^2}\right]^{3/2}. \tag{3.129}$$

As $2e\phi < m^{\mathrm{i}}v^2$ at $x \to L$, we expand the above relation to get

$$\left[\frac{dn^{\mathrm{i}}}{d\phi}\right]_{x\to L} = \frac{e}{m^{\mathrm{i}}} \int_{-\infty}^{v_{\mathrm{cL}}^{\mathrm{i}}} \int_{-\infty}^{\infty} \int_{-\infty}^{\infty} d^v \frac{f_L^{\mathrm{i}}(v)}{v^2} \left[1 + \frac{3e\phi}{m^{\mathrm{i}}v^2}\right]. \tag{3.130}$$

At $x \to L$

$$\left[\frac{dn^{\mathrm{i}}}{d\phi}\right]_{x\to L} \equiv \frac{e}{m^{\mathrm{i}}} \int_{-\infty}^{v_{\mathrm{cL}}^{\mathrm{i}}} \int_{-\infty}^{\infty} \int_{-\infty}^{\infty} d^3v \frac{f_L^{\mathrm{i}}(v)}{v^2}. \tag{3.131}$$

From Equations (3.124), (3.127) and (3.131) we get

$$\left[\frac{d\rho}{d\phi}\right]_{x\to L} = e^2 \left[\frac{1}{m^{\mathrm{i}}} \int_{-\infty}^{v_{\mathrm{cL}}^{\mathrm{i}}} \int_{-\infty}^{\infty} \int_{-\infty}^{\infty} d^3v \frac{f_L^{\mathrm{i}}(v)}{v^2} - \frac{n_L^{\mathrm{e}}}{k_{\mathrm{B}}T_{\mathrm{f}}^{\mathrm{e}}} \left(1 + \sqrt{\frac{-k_{\mathrm{B}}T_{\mathrm{f}}^{\mathrm{e}}}{e\pi\phi_0}} \frac{\exp\left(\frac{e\phi_0}{k_{\mathrm{B}}T_{\mathrm{f}}^{\mathrm{e}}}\right)}{1 + erf\sqrt{\frac{-e\phi_0}{k_{\mathrm{B}}T_{\mathrm{f}}^{\mathrm{e}}}}}\right)\right]. \tag{3.132}$$

Then after we can write,

$$\left\langle \frac{1}{v^2} \right\rangle_L^{\mathrm{i}} \leq \frac{1}{C_s^2} \left[1 + \sqrt{\frac{-k_{\mathrm{B}}T_{\mathrm{f}}^{\mathrm{e}}}{e\pi\phi_0}} \frac{\exp\left(\frac{e\phi_0}{k_{\mathrm{B}}T_{\mathrm{f}}^{\mathrm{e}}}\right)}{1 + erf\sqrt{\frac{-e\phi_0}{k_{\mathrm{B}}T_{\mathrm{f}}^{\mathrm{e}}}}}\right], \tag{3.133}$$

where

$$\left\langle \frac{1}{v^2} \right\rangle_L^{\mathrm{i}} \leq \frac{1}{n_L} \int_{-\infty}^{v_{i,cL}} \int_{-\infty}^{\infty} \int_{-\infty}^{\infty} d^3v \, \frac{f_L^{\mathrm{i}}(v)}{v^2} \tag{3.134}$$

and

$$C_s^2 = \frac{k_{\mathrm{B}}T_{\mathrm{f}}^{\mathrm{e}}}{m^{\mathrm{i}}}. \tag{3.135}$$

Hence the Bohm's criterion is

$$\left\langle \frac{1}{v^2} \right\rangle \leq \frac{1}{C_s^2} \tag{3.136}$$

3.8 Electron density distribution

Electron density is obtained at any grid point x_j by using distribution function of electron Equation (3.93) is

$$n_j^{\mathrm{e}} = n_L^{\mathrm{e}} \exp\left(\frac{e\phi_j}{kT_f^{\mathrm{e}}}\right)\left[\frac{1+erf\sqrt{\frac{e(\phi_j-\phi_0)}{kT_f^{\mathrm{e}}}}}{1+erf\sqrt{\frac{-e\phi_0}{kT_f^{\mathrm{e}}}}}\right] \tag{3.137}$$

where $n_j^{\mathrm{e}} = n^{\mathrm{e}}(x_j)$ and $\phi_j = \phi(x_j)$.
Therefore, the electron density at any point is obtained if the potential profile is known.

3.9 Discretization of the simulation region

We are interested, in the region between $x = 0$ and $x = L$, which we say 'simulation region'. In Figure 14, entire simulation region, is uniformly discretized in velocity space, as well as position. In such simulation region, the grid point of position, is represented as x_j ($j = 1, 2, 3, ;n_x$, with n_x the total number of grid points), whereas the separation between consecutive grid point, is represented by Δx. Our discretization, $j = 1$ and $j = n_x$, correspond to left-hand boundary ($x = 0$), and right-hand boundary ($x = L$) respectively. In the work of computations, we choose the region to be large enough, such that the grid size, is less than the Debye length, of the injected electrons. As the values of any quantity $q(x)$, at the grid points, are represented by $q_j = q(x_j)$, then its value at any other point 'x', between two grid points q_j and q_{j+1} may be approximated by linear interpolation, in the form as,

$$q(x) = \left(\frac{x_{j+1}-x}{\Delta x}\right) q_j + \left(\frac{x-x_j}{\Delta x}\right) q_{j+1} \tag{3.138}$$

where, $x_j \le x \le x_{j+1}$.
Next excellence approximation, is the second-order interpolation, between the points x_{j-1} and x_{j+1}.

At any point, suppose $q(x)$ be the value of any quantity. Then $q(x)$ at any point is approximated as below:

$$q_x = q_j + c(x-x_j) + d(x-x_j)^2 \tag{3.139}$$

and at point $x = x_{j-1}$ is

$$q_{j-1} = q_j - c\Delta x + d\Delta x^2 \tag{3.140}$$

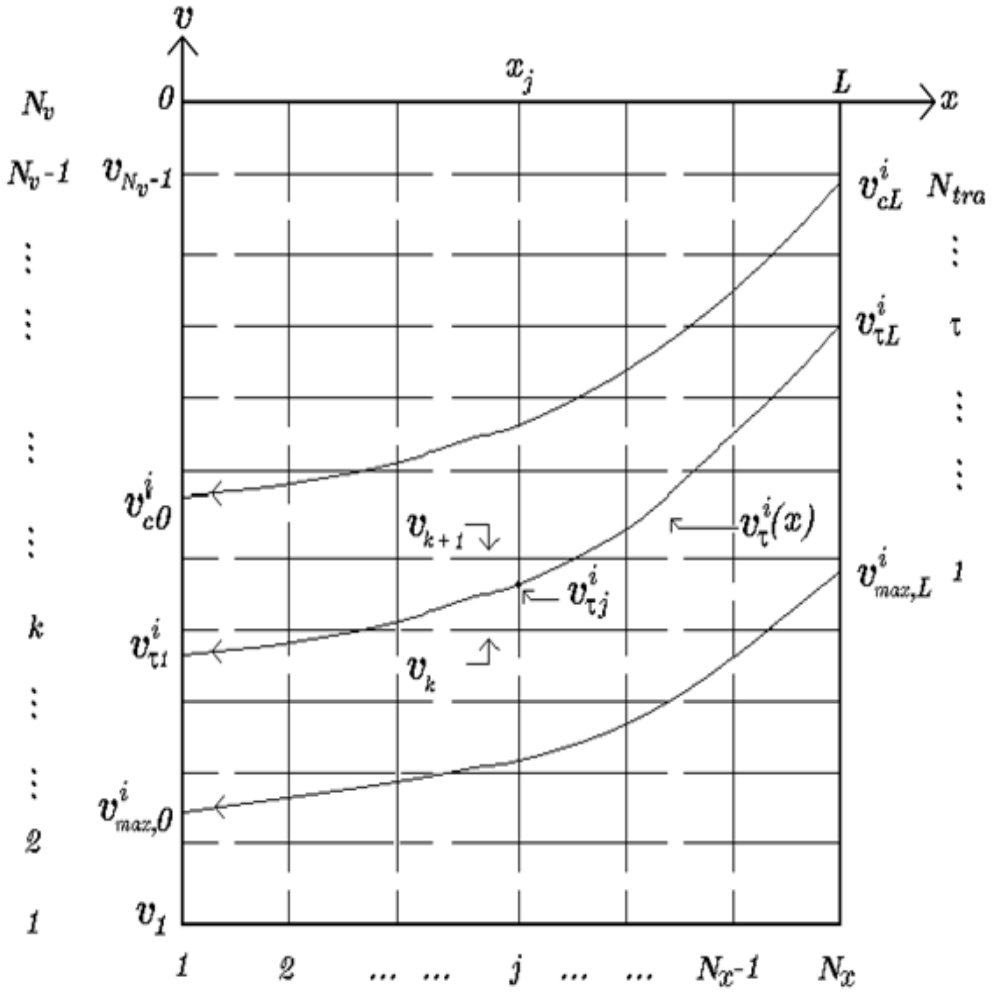

Figure 14: Schematic representation of the phase-space griding. (Source: Khanal, 2003)

Also at point $x = x_{j+1}$ is

$$q_{j+1} = q_j + c\Delta x + d\Delta x^2 \tag{3.141}$$

Equation(3.140) and (3.141) gives

$$c = \left(\frac{q_j - q_{j-1} + d(\Delta x)^2}{\Delta x} \right) \tag{3.142}$$

If we substitute the value of 'c' in equation(3.141), we get

$$q_{j+1} = q_j + \left[q_j - q_{j-1} + d(\Delta x)^2 \right] + d\Delta x^2 \tag{3.143}$$

On solving the above equation, we get

$$d = \left(\frac{q_{j+1} + q_{j-1} - 2q_j}{2(\Delta x)^2} \right) \tag{3.144}$$

If the value of 'd' is used, then we get the value of 'c' as below

$$c = \left(\frac{q_{j+1} - q_{j-1}}{2\Delta x} \right) \tag{3.145}$$

Substituting the value of 'c' and 'd' in above equation (3.139), we get

$$q(x) = q_j + (x - x_j) \left(\frac{q_{j+1} - q_{j-1}}{2\Delta x} \right) + \frac{1}{2}(x - x_j)^2 \left(\frac{q_{j+1} + q_{j-1} - 2q_j}{(\Delta x)^2} \right) \tag{3.146}$$

From this equation, the first, and second derivatives of any quantity $q(x)$, are approximated as shown below

$$\left(\frac{dq}{dx} \right)_j = \left(\frac{q_{j+1} - q_{j-1}}{2\Delta x} \right) \tag{3.147}$$

and

$$\left(\frac{d^2q}{dx^2} \right)_j = \left(\frac{q_{j+1} + q_{j-1} - 2q_j}{(\Delta x)^2} \right) \tag{3.148}$$

respectively.

3.10 Discretizing ion velocity

Figure 14 shows the velocity space of ion is uniformly discretized.The k^{th}, grid value of ion velocity, is represented like v_k, where $k = 1, 2, 3, \ldots, n_v$ with n_v the total number of velocity grid points. $k = 1$ and $k = n_v$, correspond to the fast, and the slow velocities of ion, in the discretization respectively. We consider, the ions with negative velocities in our simulation method. Setting $v_{n_v} = 0$ and choosing $|v_1|$ sufficiently large, such that the fastest moving ion, reaching the left-hand boundary, does not exceed this value, i.e. $|v_1| \geq |v^{\text{i}}_{max,0}|$. We select n_v to be sufficiently large, for the velocity grid size may be considerably less, as compared to that of thermal velocity of ion v^{i}_{tf}.

3.11 Ion trajectories

(a) discrete set of the injection velocities

Ions are injected, at the boundary of right-hand i.e., sheath entrance, $x = L$, in the range of velocity $-\infty < v \leq v^{\text{i}}_{cL}$. In the numerical implementation, this domain is

approximated by the finite $v^{\mathrm{i}}_{mL} \leq v \leq v^{\mathrm{i}}_{cL}$, and discretize the latter with n_{tra} equidistant, injection velocities of ion $v^{\mathrm{i}}_{\tau L}$ ($\tau = 1, 2, ..., n_{tra}$), where $\tau = 1$ and $\tau = n_{tra}$ correspond to the injection velocities, v^{i}_{mL} and v^{i}_{cL} respectively. Selection of v^{i}_{cL} is dependent on considering the problem and the maximum injection velocity, $v^{\mathrm{i}}_{max,L}$, is selected large enough, for the distribution function of ion, corresponding to velocities larger, than this velocity to be negligible. We use $v^{\mathrm{i}}_{mL} = v^{\mathrm{i}}_{cL} - 4v^{\mathrm{i}}_{tf}$, in our computations, where v^{i}_{tf} is the thermal velocity of ion.

(b) Discrete set of ion trajectories

At the boundary of right hand, $x = L$, the injection velocity, represents the ion trajectory velocity, at starting condition, in collisionless case, the n_{tra}, discrete injection velocities, $v^{\mathrm{i}}_{\tau L}$, is the n_{tra} related trajectories, which is labeled by the index 'τ'. The trajectory, corresponding to certain injection velocity is denoted by $v^{\mathrm{i}}_{\tau L}$ by $v^{\mathrm{i}}_{\tau}(L)$, and the velocity with which it crosses a grid point x_j is $v^{\mathrm{i}}_{\tau j} = v^{\mathrm{i}}_{\tau}\left(x_j\right)$, thus $v^{\mathrm{i}}_{\tau n_x} \equiv v^{\mathrm{i}}_{\tau L} = v^{\mathrm{i}}_{\tau}\left(L\right)$, in phase space. Velocities, v^{i}_{τ}, represent the ion trajectories intersections $v = v^{\mathrm{i}}_{\tau}\left(L\right)$, and the velocity, which crosses a grid point, $x = x_j$, $v^{\mathrm{i}}_{\tau j} = v^{\mathrm{i}}_{\tau}(x_j)$, is said to be "intersection velocities". Injection velocities of ion, $v^{\mathrm{i}}_{\tau L}$, are not dependent of the ion grid velocities, v_k, but we often choose them, such that each, $v^{\mathrm{i}}_{\tau L}$ coincide with one of the v_k's.

(c) Numerical calculation of ion trajectories

To calculate, the related velocity distribution functions, collision less trajectories is traced in KTS method. Trajectories of ion are considered in this section and hence omit the species index 'i'. To calculate the ion trajectory, we discretize equations of motion of ion Equation (3.66), Equation (3.70), Equation (3.71) and Equation (3.72) in time-centered manner as

$$\frac{x^{m+\frac{1}{2}} - x^{m-\frac{1}{2}}}{\Delta t} = v_x^m \tag{3.149}$$

and for change in v_x is

$$\begin{aligned}\frac{v_x^m - v_x^{m-1}}{\Delta t} = a_x^{m-\frac{1}{2}} &= \frac{e}{m^{\mathrm{i}}}\left[E\left(x^{m-\frac{1}{2}}\right) + (v \times B)_x^{m-\frac{1}{2}}\right] \\ &= \frac{e}{m^{\mathrm{i}}}E(x^{m-\frac{1}{2}}) - \frac{eB_0\sin\theta}{m^{\mathrm{i}}}v_z^{m-\frac{1}{2}}\end{aligned} \tag{3.150}$$

Change in v_y is

$$\frac{v_y^m - v_y^{m-1}}{\Delta t} = a_y^{m-\frac{1}{2}} = \frac{e}{m^{\mathrm{i}}}\left[0 + (v \times B)_y^{m-\frac{1}{2}}\right] = \frac{eB_0\cos\theta}{m^{\mathrm{i}}}v_z^{m-\frac{1}{2}} \tag{3.151}$$

For change in v_z is

$$\frac{v_z^m - v_z^{m-1}}{\Delta t} = a_z^{m-\frac{1}{2}} = \frac{e}{m^{\mathrm{i}}}\left[0 + (v \times B)_z^{m-\frac{1}{2}}\right]$$
$$= \frac{eB_0}{m^{\mathrm{i}}}\left(v_x^{m-\frac{1}{2}} \sin\theta - v_y^{m-\frac{1}{2}} \cos\theta\right) \tag{3.152}$$

respectively, here Δt, is the numerical, time-step size, $m \geq 0$, is the integer, such that the integral or half integral superscript $m \geq 0$, is such that, $v^m = v(t^m)$, $x^{m+\frac{1}{2}} = x\left(t^{m+\frac{1}{2}}\right)$, etc. Which corresponding to the total time elapsed, in steps of Δt, for the ion having injected at time zero at the boundary of right-hand. So, $m = 0$ corresponds to $t = 0$ with the injection (or starting) values

$$x^0 = L \quad \text{and} \quad v_x^0 = v_{\tau L}^{\mathrm{i}} \tag{3.153}$$

Positions selection at half integral times, as well as velocity at integral times in Equations (3.149), (3.150), (3.151)and(3.152) makes the time centered numerical scheme. Any step of time $m \geq 1$, with $x^{m-\frac{1}{2}}$ and v_x^{m-1} is given from the $(m-1)^{st}$ step, the new ion velocity is calculated from equation(3.150) as given below

$$v_x^m = v_x^{m-1} + \frac{e\Delta t}{m^{\mathrm{i}}} E(x^{m-\frac{1}{2}}) - \frac{eB_0 \Delta t \sin\theta}{m^{\mathrm{i}}} v_z^{m-\frac{1}{2}} \tag{3.154}$$

and we can also find new position of the ions from Equation (3.149)

$$x^{m+\frac{1}{2}} = x^{m-\frac{1}{2}} + \Delta t v_x^m \tag{3.155}$$

Electric field in Equation (3.154) at any point is obtained in the region of simulation by Equation (3.78). Therefore, there is ends up numerical scheme, with x-points at half-integral times, $\left(x^{m+\frac{1}{2}}\right)$ and velocities, at integral times, $\left(v_x^m\right)$ along a trajectory which is collisionless. Also, we can find, the ion velocity, at $x^{m+\frac{1}{2}}$ as given below equation

$$\frac{v_x^m + v_x^{m+1}}{2} = v_x^{m+\frac{1}{2}} \tag{3.156}$$

(d) Intersection velocities

Velocities which are at half integral time as in Equation(3.156), may not coincide, with the fixed grid points, x_j. To calculate the velocities of intersection for the τ^{th}, trajectory, at some inner grid point, x_j, the interpolation which is linear can be used as given below

$$v^{i}_{\tau j} = \frac{\left(x^{m-\frac{1}{2}} - x_j\right) v_x^{m+\frac{1}{2}} + \left(x_j - x^{m+\frac{1}{2}}\right) v_x^{m-\frac{1}{2}}}{\left(x^{m-\frac{1}{2}} - x^{m+\frac{1}{2}}\right)} \tag{3.157}$$

In this equation $x^{m-\frac{1}{2}}$ and $x^{m+\frac{1}{2}}$ are the adjacent points, along the trajectory on the right-hand side, and the left-hand side of the grid point x_j, respectively. We use the scheme of parabolic extrapolation, to calculate velocity of ion at the boundary of left-hand ($x = 0$). We consider the last three calculated points along the trajectory, which lie to the right-hand side, of the boundary of left-hand

$$\left[\left(x^{m-\frac{1}{2}}, v_x^{m-\frac{1}{2}}\right), \left(x^{m-\frac{3}{2}}, v_x^{m-\frac{3}{2}}\right) \quad \text{and} \quad \left(x^{m-\frac{5}{2}}, v_x^{m-\frac{5}{2}}\right)\right]$$

near the left-hand boundary, the ion velocity is approximated as

$$v(x) = v_x^{m-\frac{5}{2}} + c\left(x - x^{m-\frac{5}{2}}\right) + d\left(x - x^{m-\frac{5}{2}}\right)^2 \tag{3.158}$$

In this equation, 'c' and 'd' are constants and value of these constants are calculated. At the point $x = x^{m-\frac{1}{2}}$, velocity is approximated as below

$$\begin{aligned} v_x^{m-\frac{1}{2}} &= v_x^{m-\frac{5}{2}} + c\left(x^{m-\frac{1}{2}} - x^{m-\frac{5}{2}}\right) + d\left(x^{m-\frac{1}{2}} - x^{m-\frac{5}{2}}\right)^2 \\ \text{or} \quad c &= \frac{v_x^{m-\frac{1}{2}} - v_x^{m-\frac{5}{2}} - d\left(x^{m-\frac{1}{2}} - x^{m-\frac{5}{2}}\right)^2}{\left(x^{m-\frac{1}{2}} - x^{m-\frac{5}{2}}\right)} \end{aligned} \tag{3.159}$$

The velocity is approximated at the point $x = x^{m-\frac{3}{2}}$ as

$$v_x^{m-\frac{3}{2}} = v_x^{m-\frac{5}{2}} + c\left(x^{m-\frac{3}{2}} - x^{m-\frac{5}{2}}\right) + d\left(x^{m-\frac{3}{2}} - x^{m-\frac{5}{2}}\right)^2 \tag{3.160}$$

The value of 'c' is used from Equation (3.159) in Equation(3.160), then we get,

$$\begin{aligned} v_x^{m-\frac{3}{2}} = v_x^{m-\frac{5}{2}} + \left[\frac{v_x^{m-\frac{1}{2}} - v_x^{m-\frac{5}{2}} - c\left(x^{m-\frac{1}{2}} - x^{m-\frac{5}{2}}\right)^2}{\left(x^{m-\frac{1}{2}} - x^{m-\frac{5}{2}}\right)}\right]\left(x^{m-\frac{3}{2}} - x^{m-\frac{5}{2}}\right) \\ + d\left(x^{m-\frac{3}{2}} - x^{m-\frac{5}{2}}\right)^2 \end{aligned} \tag{3.161}$$

Then we obtain the value of 'd' from above equation as

$$d = \frac{\left(x^{m-\frac{5}{2}} - x^{m-\frac{3}{2}}\right)\left(v_x^{m-\frac{1}{2}} - v_x^{m-\frac{5}{2}}\right) - \left(x^{m-\frac{5}{2}} - x^{m-\frac{1}{2}}\right)\left(v_x^{m-\frac{3}{2}} - v_x^{m-\frac{5}{2}}\right)}{\left(x^{m-\frac{5}{2}} - x^{m-\frac{1}{2}}\right)\left(x^{m-\frac{5}{2}} - x^{m-\frac{3}{2}}\right)\left(x^{m-\frac{3}{2}} - x^{m-\frac{1}{2}}\right)} \tag{3.162}$$

This value of 'd' is used in Equation (3.159), then we get the value of 'c' as

$$c = \frac{\left(x^{m-\frac{5}{2}} - x^{m-\frac{3}{2}}\right)^2\left(v_x^{m-\frac{1}{2}} - v_x^{m-\frac{5}{2}}\right) - \left(x^{m-\frac{5}{2}} - x^{m-\frac{1}{2}}\right)^2\left(v_x^{m-\frac{3}{2}} - v_x^{m-\frac{5}{2}}\right)}{\left(x^{m-\frac{5}{2}} - x^{m-\frac{1}{2}}\right)\left(x^{m-\frac{5}{2}} - x^{m-\frac{3}{2}}\right)\left(x^{m-\frac{3}{2}} - x^{m-\frac{1}{2}}\right)} \tag{3.163}$$

If we used the value of the constants 'c' and 'd' from Equation(3.163) and Equation (3.162) on to the Equation (3.158), then we calculate the ion velocity at the left-hand boundary as,

$$v_\tau^{\mathrm{i}}(x=0) = v_x^{m-\frac{5}{2}} - cx^{m-\frac{5}{2}} + d\left(x^{m-\frac{5}{2}}\right)^2 \tag{3.164}$$

3.12 Ion velocity distribution function

Tracing the ion trajectories, for all n_{tra} injection velocities $v_{\tau L}^{\mathrm{i}}$, we can calculate the related, intersection velocities Equation (3.149), and the corresponding distribution functions, at all grid points x_j. The injection velocity, from where we start, are generally uniformly spaced, but the corresponding ion velocities, at the other grid points, $0 \leq x_j < L$, are spaced non uniformly, and generally not to be coincide with the grid velocities which is fixed, v_k. For our model there is not necessary, to know the ion distribution function, at these uniformly spaced, grid velocities.

The ion distribution function, can be calculated at the fixed grid points (position and velocity) by linear interpolation of the values, associated with the trajectory intersection points, to the closest desired grid points.

3.13 Ion density distribution

From the approach of distribution function, ion density distribution, $n^{\mathrm{i}}(x)$ is obtained as:

Distribution-function approach (DFA)

In the distribution function approach, the ion density distribution, $n^{\mathrm{i}}(x_j)$ is obtained with the help of integrating the ion velocity distribution function, over the velocity space. For the model of plasma we have chosen, we obtain the ion distribution function,

only at the intersection points $[x_j, v^{\mathrm{i}}_{\tau}(x_j)]$ and also be obtained, at the fixed grid points $[x_j, v_k]$ where there is given the distribution function. The ion density at x_j, where the distribution functions, $f^{\mathrm{i}}(x_j, v^{\mathrm{i}}_{\tau j})$, and the velocities of intersection of all n_{tra} trajectories of ion, $v^{\mathrm{i}}_{\tau j}$, are given, can be achieved by the following form of discretization
For first ion species

$$n^{\mathrm{i}}(x_j) = \frac{1}{2}\sum_{\tau=1}^{n_{tra}-1}\left[f^{\mathrm{i}}(x_j, v^{\mathrm{i}}_{\tau j}) + f^{\mathrm{i}}(x_j, v^{\mathrm{i}}_{\tau+1,j})\right]\left(v^{\mathrm{i}}_{\tau+1,j} - v^{\mathrm{i}}_{\tau j}\right) \tag{3.165}$$

and

$$n^{\mathrm{i}}(L) = \frac{1}{2}\sum_{\tau=1}^{n_{tra}-1}\left[f^{\mathrm{i}}(L, v^{\mathrm{i}}_{\tau j}) + f^{\mathrm{i}}(L, v^{\mathrm{i}}_{\tau+1,L})\right]\left(v^{\mathrm{i}}_{\tau+1,L} - v^{\mathrm{i}}_{\tau j}\right) \tag{3.166}$$

3.14 Solution of Poisson's equation

As the electron and ion densities are calculated, then from Equation (3.137) and Equation (3.166), we obtained the space charge density distribution by using

$$\rho(x_j) = \sum_s q^s n^s(x_j) = e[n^{\mathrm{i}}(x_j) - n^{\mathrm{e}}(x_j)] \tag{3.167}$$

Using the knowledge of space charge distribution, $\rho(x_j)$, from Equation (3.167), Poisson's Equation (3.79) is solved numerically to obtain the new potential distribution, $\phi(x_j)$. By using Equation(3.148), the discretized form of Poisson's equation is

$$\frac{\phi_{j+1} - 2\phi_j + \phi_{j-1}}{(\Delta x)^2} = -\frac{\rho_j}{\epsilon_o} \tag{3.168}$$

Here we write this equation, for all internal grid points, in the simulation region ($j = 2, 3, ..., n_x - 1$) which yields the following $n_x - 2$ equations, involving n_x unknowns, $\phi_1, \phi_2, ..., \phi_{n_x}$:

$$\begin{aligned}
&\phi_1 - 2\phi_2 + \phi_3 = -\frac{(\Delta x)^2}{\epsilon_o}\rho_2 \\
&\phi_2 - 2\phi_3 + \phi_4 = -\frac{(\Delta x)^2}{\epsilon_o}\rho_2 \\
&- - - - - - - - - - - - - \\
&\phi_{n_x-2} - 2\phi_{n_x-1} + \phi_{n_x} = -\frac{(\Delta x)^2}{\epsilon_o}\rho_{n_x-1}
\end{aligned} \tag{3.169}$$

At the two boundaries, the potential values have to be fixed as

$$\phi(x = L) = \phi_{n_x} = \phi_L \tag{3.170}$$

and

$$\phi(x = 0) = \phi_1 = \phi_0 \tag{3.171}$$

As the Equations (3.169), (3.170) and (3.171) is solved, we obtain the potential distribution, i.e. the potential values $\phi_1, \phi_2, ..., \phi_{n_x}$, this can be expressed as a single matrix equation as below

$$\begin{pmatrix} 1 & 0 & 0 & 0 & . & . & 0 \\ 1 & -2 & 1 & 0 & . & . & 0 \\ 0 & 1 & -2 & . & . & . & 0 \\ . & . & . & . & . & . & . \\ . & . & . & . & . & . & . \\ . & . & . & . & 1 & -2 & 1 \\ . & . & . & . & 0 & 0 & 1 \end{pmatrix} \times \begin{pmatrix} \phi_1 \\ \phi_2 \\ . \\ . \\ . \\ \phi_{n_x-1} \\ \phi_{n_x} \end{pmatrix} = \begin{pmatrix} \phi_o \\ -\frac{(\Delta x)^2}{\epsilon_o}\rho_2 \\ . \\ . \\ . \\ -\frac{(\Delta x)^2}{\epsilon_o}\rho_{n_x-1} \\ \phi_L \end{pmatrix} \tag{3.172}$$

The left-hand side, as well as at the right-hand side matrix are known. To solve the matrix equation, inverse of the first matrix, is multiplied with the right-hand side matrix, this is done by using the simple command in MATLAB programs.

3.15 Relaxation scheme

Exactly the solution of Poisson's equation converges for short systems (i.e., few Debye lengths). As the length of system increases, very small fluctuation, of the potential causes unphysical accumulation of the charges and hence the scheme, breaks down. Relaxation scheme is used to overcome this difficulty. Numerically exact potential distribution function $\phi_{ex}^{(m)}$, is obtained by solving Equation (3.172), which is linearly combined, with old potential distribution $\phi^{(m-1)}(x_j)$, to obtain the "re-adjusted" new potential distribution function $\phi^{(m)}(x_j)$, which is used exactly as the applicable result of m^{th} iteration:

$$\phi^{(m)}(x_j) = \omega\phi_{ex}^{(m)} + (1 - \omega)\phi^{(m-1)}(x_j) \tag{3.173}$$

with $0 < \omega < 2$, and ω is the relaxation parameter.

3.16 Electric field calculation

In this section, we discuss how the electric field is calculated, at all the grid points, from the potential profile which is given, and how we calculate the electric field for the points which are lying between two grid points.

(a) Electric field at the inner grid points:

At the inner grid points $j = 1, 2, \ldots, n_x - 1$, the electric field is obtained as follows,

$$E(x) = -\frac{\phi(x_{j+1}) - \phi(x_{j-1})}{2\Delta x} \tag{3.174}$$

(b) Electric field at the left-hand boundary:

Close to the left-hand boundary, $(x = 0)$, we consider, for the potential, the parabolic approximation as given below,

$$\phi(x) = \phi_1 + cx + dx^2 \tag{3.175}$$

where $\phi_0 = \phi_1$ is potential at $x = 0$. For second and third grid points, we have two equations, which are

$$\phi_2 = \phi_1 + c\Delta x + d(\Delta x)^2 \tag{3.176}$$

and

$$\phi_3 = \phi_1 + 2c\Delta x + 4d(\Delta x)^2 \tag{3.177}$$

respectively, from which the constants 'c' and 'd' is obtained as

$$c = -\frac{3\phi_1 - 4\phi_2 + \phi_3}{2\Delta x} \tag{3.178}$$

and

$$d = \frac{\phi_1 - 2\phi_2 + \phi_3}{2(\Delta x)^2} \tag{3.179}$$

We obtained, electric field near $x = 0$ by taking the derivative of Equation(3.175) as given below

$$E(x) = -\frac{d\phi(x)}{dx} = -c - 2dx \tag{3.180}$$

Hence, the electric field, at the left-hand boundary, is given by

$$E(x=0) = -c = \frac{3\phi_1 - 4\phi_2 + \phi_3}{2\Delta x} \tag{3.181}$$

(c) Electric field at the right-hand boundary:

Close to the right-hand boundary ($x = L$), let us consider for the potential, a parabolic approximation as given below

$$\phi(x) = \phi_{n_x-2} + y(x - x_{n_x-2}) + z(x - xn_x - 2)^2 \tag{3.182}$$

In this equation, ϕ_{n_x-2} is the potential at the grid point $x_{n_x-2} \equiv L - 2\Delta x$. For the grid points x_{n_x-1} and x_{n_x}, we have the equations as

$$\phi_{n_x-1} = \phi_{n_x-2} + y\Delta x + z(\Delta x)^2 \tag{3.183}$$

and

$$\phi_{n_x} = \phi_{n_x-2} + 2y\Delta x + 4z(\Delta x)^2 \tag{3.184}$$

respectively, the constants 'y' and 'z' can be obtained as follows:

$$y = -\frac{\phi_{n_x} - 4\phi_{n_x-1} + 3\phi_{n_x-2}}{2\Delta x} \tag{3.185}$$

and

$$z = \frac{\phi_{n_x} - 2\phi_{n_x-1} + \phi_{n_x-2}}{2(\Delta x)^2} \tag{3.186}$$

By taking the derivative of Equation (3.182), the electric field close to $x = L$ is obtained as

$$E(x) = -\frac{d\phi(x)}{dx} = -y - 2z(x - x_{n_{x-2}}) \tag{3.187}$$

Hence, at the right-hand boundary, the electric field is given as

$$E(x=L) = -y - 4z\Delta x = -\frac{3\phi_{n_x} - 4\phi_{n_x-1} + \phi_{n_x-2}}{2\Delta x} \tag{3.188}$$

(d) Electric field at any point in the simulation region:

As we calculated the electric field at every grid point, the electric field, at any point, in the simulation region is obtained by the linear interpolation between two nearest grid

points x_j and x_{j+1} as given below

$$E(x) = \frac{(x_{j+1} - x)E_j + (x - x_j)E_{j+1}}{\Delta x} \tag{3.189}$$

3.17 Iteration scheme

In our work, we are dealing only with collisionless and time independent cases. We take the initial-guess potential $\phi^{(0)}(x_j)$ as input to the main iteration block, which is the first iteration to the potential distribution $\phi^{(1)}(x_j)$. With the new potential as input, the main iteration block will be again invoked yielding $\phi^{(2)}(x_j)$, until the potential distribution has converged. The main iteration scheme is shown in the Figure 15. This iteration block carries out the m^{th} iteration (i.e. it calculates the new distributions, $\phi^m(x_j)$) for a given input (old) potential distribution, $\phi^{m-1}(x_j)$, by performing the three steps as follows.

Step 1: Analytically, the new electron density distribution, $n^{e(m)}(x_j)$ is calculated by using Equation (3.102). We calculate the new ion density $n^{i(m)}(x_j)$ by DFA approaches, by the help of Equation (3.131).

Step 2: From the new densities, $n^{e(m)}(x_j)$, as we obtained in step 1, we calculate the new space-charge density, $\rho^{(m)}(x_j)$, from Equation (3.81).

Step 3: By solving the matrix Equation (3.172), the new potential distribution, $\phi^{(m)}(x_j)$, is obtained numerically, with the new space-charge density, $\rho^{(m)}(x_j)$ which is inserted on the right-hand side.
The new potential distribution, $\phi^{(m)}(x_j)$, which is obtained in Step 3 of the main iteration block, is compared with the old potential distribution, $\phi^{(m-1)}(x_j)$ and we let the convergence to be reached if at each point x_j the condition

$$\mid \phi^{(m)}(x_j) - \phi^{(m-1)}(x_j) \mid \leqslant \delta \tag{3.190}$$

is satisfied, where δ is treated as the accuracy parameter.

3.18 Introduction to Runge-Kutta method

The ordinary differential equations can be reduced to the first order differential equations. The example of the second order equation is (Press et al., 2007)

$$\frac{d^2 f}{dx^2} + q(x)\frac{df}{dx} = r(x) \tag{3.191}$$

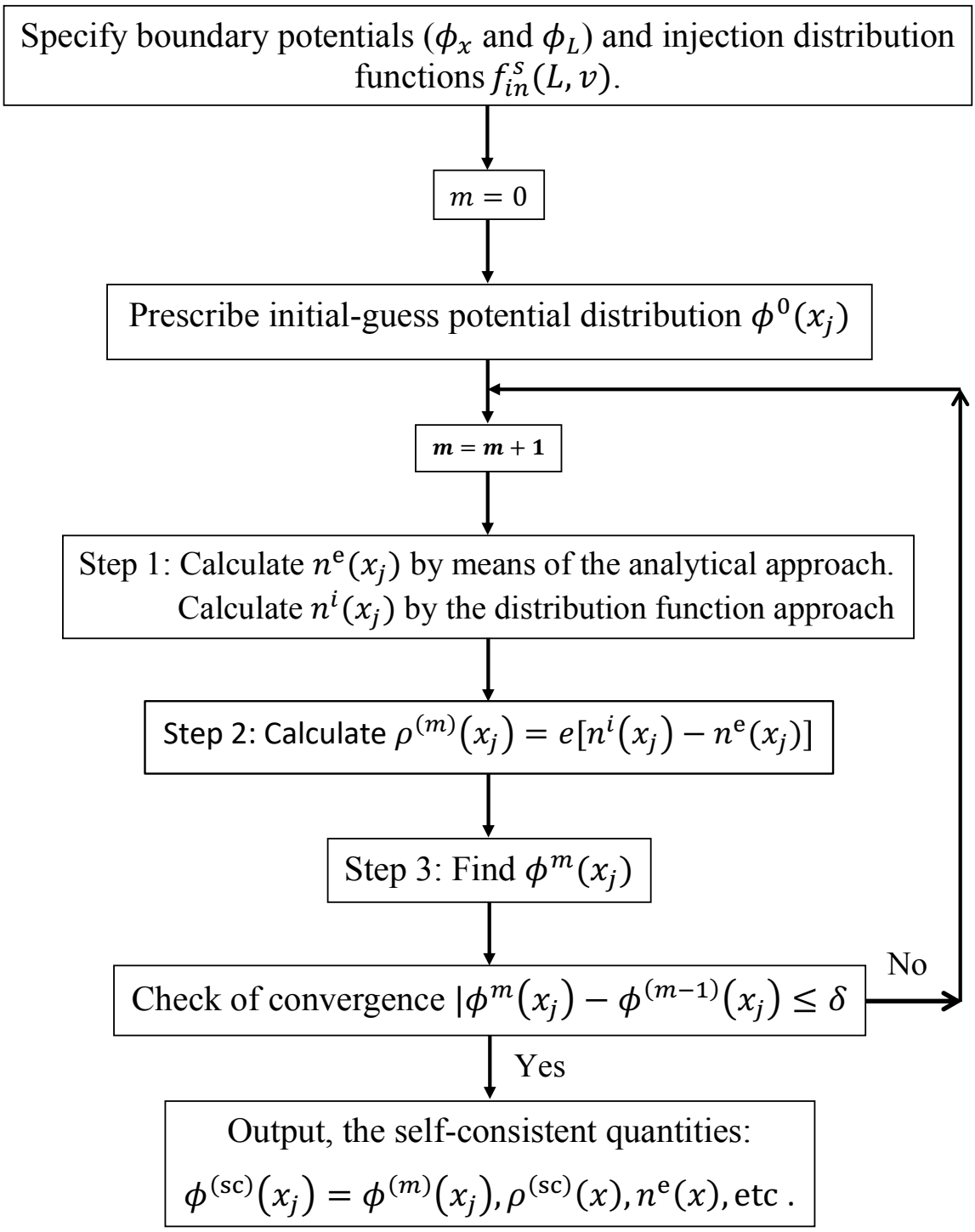

Figure 15: The Iteration Scheme (Khanal, 2003).

This equation is rewritten as the two first order equations as

$$\frac{df}{dx} = z(x) \tag{3.192}$$

$$\frac{dz}{dx} = r(x) - q(x)z(x) \tag{3.193}$$

Here in this equation z is the new variable. In the ordinary differential equations, the problem is reduced to the set of N coupled first order differential equations, for the functions $f_{\mathrm{i}}, i = 1, 2, \ldots, N$ having the form as

$$\frac{df_{\mathrm{i}}(x)}{dx} = S_{\mathrm{i}}(x, f_1, \ldots, y_N), \quad i = 1, \ldots, N \tag{3.194}$$

where the right hand side functions S_{i} are known.

The involving problem ODEs is not specified completely by its equation. Even in determining crucially , numerically how to attack the problem, is the nature of problem's boundary condition. In above Equation (3.49) boundary conditions are the algebraic conditions, on values of functions f_{i}.

For solving the initial value problems for ODEs, practically there are three types of numerical methods which are: Runge-Kutta methods, Richardson extrapolation and its particular implementation as the Bulirsch-Stoer methods and predictor-corrector methods.

But in this section, we discuss the numerical Runge-Kutta method which are used to solve the Lorentz force equation. Around 1900, two mathematicians Runge and Kutta enunciated this method. The increments of the function are calculated, once for all, with the help of formulas. Calculations of first increment are perfectly same, as for any other increment. Various types of differential equation formulas are discussed as given below (Scarborough, 1966).

(a) First-order equation

Suppose

$$\frac{dz}{dt} = f(t, z)$$

indicates, any first order equation, also let h indicates the interval, among equidistant values of t. As the starting values are z_0, t_0, then the first increment, in z is computed, from the formulas given below

$$\begin{aligned}
l_1 &= hf(t_0, z_0) \\
l_2 &= hf\left(t_0 + \frac{h}{2}, z_0 + \frac{l_1}{2}\right) \\
l_3 &= hf\left(t_0 + \frac{h}{2}, z_0 + \frac{l_2}{2}\right) \\
l_4 &= hf(t_0 + h, z_0 + l_3) \\
\triangle z &= \frac{1}{6}(l_1 + 2l_2 + 2l_3 + l_4)
\end{aligned} \tag{3.195}$$

Then,

$$t_1 = t_0 + h\,,\ z_1 = z_0 + \triangle z$$

For the interval of second, the increment in z, is computed in a same way, by means of the formulas given below

$$\begin{aligned} l_1 &= hf(z_1, t_1) \\ l_2 &= hf\left(t_1 + \frac{h}{2}, z_1 + \frac{l_1}{2}\right) \\ l_3 &= hf\left(t_1 + \frac{h}{2}, z_1 + \frac{l_2}{2}\right) \\ l_4 &= hf(t_1 + h, z_1 + l_3) \\ \triangle z &= \frac{1}{6}(l_1 + 2l_2 + 2l_3 + l_4) \end{aligned} \tag{3.196}$$

The increments for succeeding intervals are computed exactly the same way.

(b) Second-order equation

We suppose the differential equation of second order

$$\frac{d^2z}{dt^2} = f\left(t, z, \dot{z} = \frac{dz}{dt}\right)\,.$$

Suppose h denote the time interval, between equidistant values of t and t_0, x_0 and $\dot{z}(0)$ indicates the initial values of t, z and $\dot{z}$, as well. First increment numerical solution of equation above, is computed as

$$\begin{aligned} l_1 &= hf(t_n, z_n, \dot{z}_n) \\ l_2 &= hf\left(t_n + \frac{h}{2}, x_n + \frac{h}{2}\dot{z}_n + \frac{h}{8}l_1, \dot{z}_n + \frac{l_1}{2}\right) \\ l_3 &= hf\left(t_n + \frac{h}{2}, x_n + \frac{h}{2}\dot{x}_n + \frac{h}{8}l_2, \dot{x}_n + \frac{l_2}{2}\right) \\ l_4 &= hf\left(t_n + h, x_n + h\dot{z}_n + \frac{h}{2}l_3, \dot{z}_n + l_3\right) \\ \triangle z &= \dot{x}_n + \frac{1}{6}(l_1 + l_2 + l_3) \quad \text{and} \end{aligned} \tag{3.197}$$

$$\triangle \dot{z}_n = \frac{1}{6}(l_1 + 2l_2 + 2l_3 + l_4) \tag{3.198}$$

where $n = 0, 1, 2, \ldots$. Then

$$t_1 = t_0 + h\,, \quad z_1 = x_0 + \triangle z \quad \text{and} \quad \dot{z}_1 = \dot{z}_0 + \triangle \dot{z}\,.$$

CHAPTER 4

4. RESULTS AND DISCUSSION

In this chapter, the compiled set of kinetic equations in the section (3.1) to (3.25) are solved in MATLAB using KTS model and Ode45 for the given boundary conditions. To study the magnetized plasma sheath characteristics, ions velocity profile for different magnetic field and its obliqueness, has been investigated using Kinetic Trajectory Simulation Model. The obtained results are in well agreement with the previous 1d3v results.

At the entrance of the sheath, knowing the kinetic parameters initially, we solve the coupling of the kinetic presheath-sheath equations for the presheath parameters which are given. For this coupling scheme, the field boundary conditions are $\phi(x = L) = 0$ and $\phi(x = 0) = \phi_{\rm w} < 0$. We consider the numerical parameters as: $B = 100$ mT, $\theta = 5°$, mass of electron, $m_{\rm e} = 9.1\times10^{-31}$ kg, mass of hydrogen atom, $m_{\rm H} = 1.67\times10^{-27}$ kg, the simulasion region have dimension $15\lambda_{\rm D}^{\rm e}$, where $\lambda_{\rm D}^{\rm e}$ is the Debye length of the electron, $x/\lambda_{\rm D}^{\rm e}$ is the normalized distance and $n_{\rm ps} = 10^{20}$ m^{-3}. Here, we apply the KTS as well as numerical Runge- Kutta method to a plasma sheath problem, assuming the parameters at the presheath side of the sheath-presheath boundary to be given (fixed). The plasma parameters at the presheath side of the sheath-presheath boundary must to satisfy the quasineutrality condition, sheath edge singularity condition, continuity of first three moments and also the Bohm Chodura criterion.

Parameters $A^{\rm e}$, $T_{\rm f}^{\rm e}$, $v_{cL}^{\rm e}$, $A^{\rm i}$, $T_{\rm f}^{\rm i}$, $v_{mL}^{\rm i}$ and $v_{cL}^{\rm i}$ must be specified for the physical situation considered. In our calculation these parameter are imported from 1d3v coupling scheme. We consider the following parameters at the presheath side of the sheath-presheath boundary:

- Electron temperature as $(10 - 19)$ eV.
- Different values of the magnetic field are taken as 1 mT, 1.5 mT, 2 mT, 2.5 mT, 3 mT, 4.5 mT, 5 mT, 6 mT, 7.5 mT, 8 mT, 9 mT and 10.5 mT.
- Different values of the obliqueness of the field are taken as 30°, 60°, 75° and 90°.

4.1 Distribution function of ions

Ion species distribution function at the sheath entrance and the wall is shown in Figure 16(a) and 16(b). From this Figure, we see that velocity distribution function of ion is cut-off shifted half Maxwellian distribution. At the sheath entrance and wall, in magnitude, cut-off as well as Maxwellian maximum velocities are equal. However, as the ion flows towards the wall, its cut-off as well as Maxwellian maximum velocities increases from 1.907 v_t^i to 5.609 v_t^i.

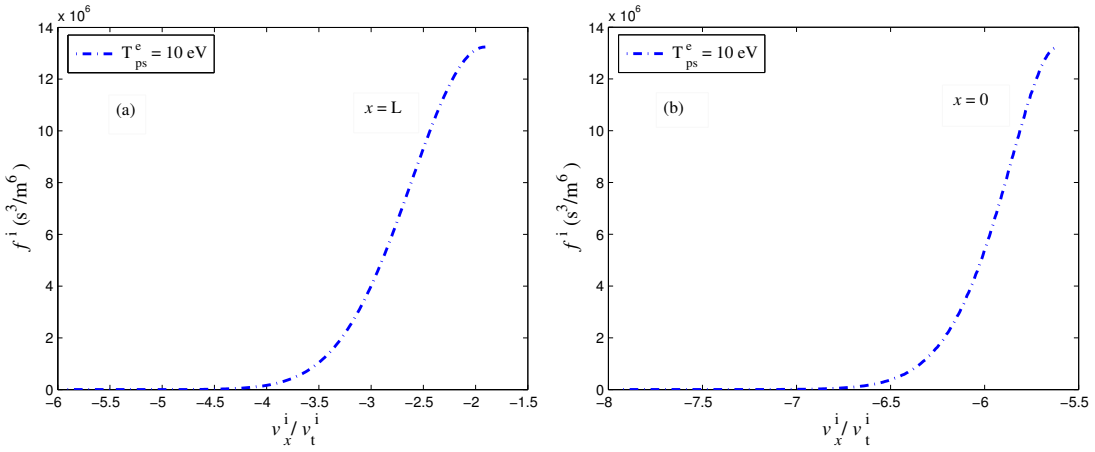

Figure 16: Ion velocity distributions function (a) at the sheath entrance and (b) at the wall

4.2 Potential profile

The effect of presheath electron temperature on potential profile is shown in Figure 17. The potential is monotonic function in the plasma wall transition region for two different values of electron temperature, which is consistent with the Debye shielding. With the increase in presheath electron temperature, the thermal velocity of electrons get increased and the density of electrons reaching the wall is higher resulting more negative potential developed on the wall. The simulated numerical values of the wall potential are -28.0844 V and -33.7013 V for presheath electron temperatures 10 eV and 12 eV however, the respective theoretical numerical values are -27.3155 V and -32.7786 V, respectively. The deviation of the simulated result from theoretical result is due to the fact that the cut-off Maxwellian distribution of electrons by the reflective wall. The density of electron given by our model is less as compared to that given by Boltzmann distribution that makes the absorbing wall more negative. Hence, in magnitude simulated value is high as compared to that of theoretical value which is nearly 3% in the magnitude.

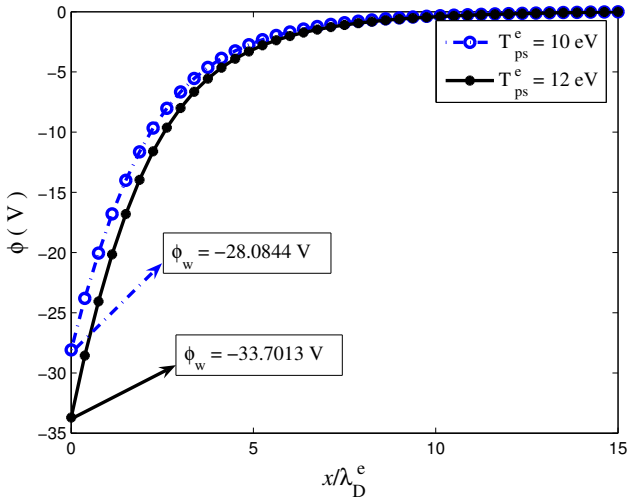

Figure 17: Potential profile as the function of normalized distance

4.3 Child-sheath thickness

Variation of Child-sheath thickness with presheath electron temperature is shown in Figure 18. From this plot, it has been observed that the thickness of sheath is influenced greatly by presheath electron temperature. With the increase in electron temperature at the presheath side, Child-sheath thickness increases.

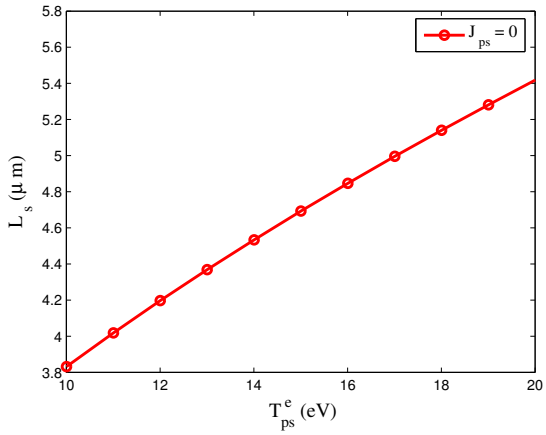

Figure 18: Child-sheath thickness as the function of presheath electron temperature

4.4 Ion and electron fluxes

The self-consistent ion and electron fluxes as the function of potential for two different values of presheath electron temperature are shown in the Figures 19 and 20, respectively. From these figures, it is seen that the ion and electron fluxes decrease towards the wall whereas the decrement rate of electron flux is more than ions. The electron flux is almost constant whereas that of ions are different such that the space charge density increases

to wards the wall.

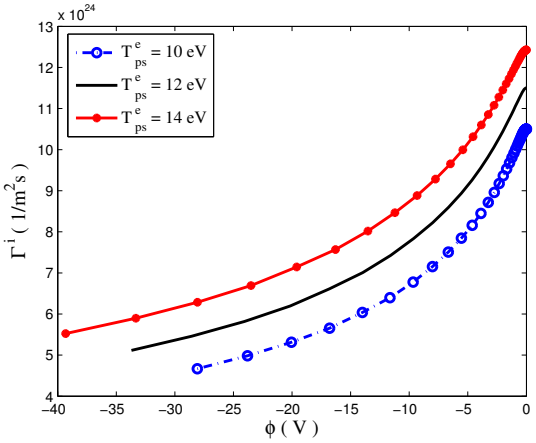

Figure 19: Ion flux as the function of potential for different values of presheath electron temperature

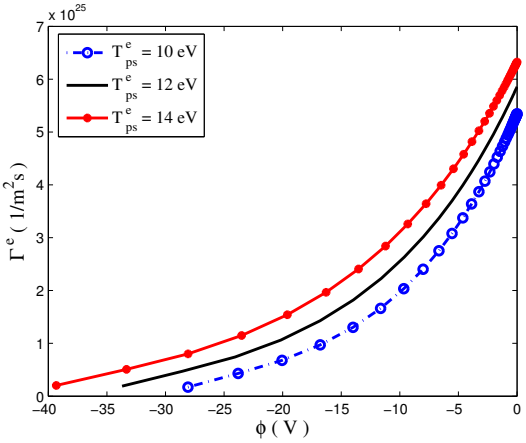

Figure 20: Electron flux as the function of potential for different values of presheath electron temperature

4.5 Presheath ion velocity profile

Figure 21 shows the presheath ion velocity as the function of temperature of ion at the presheath side for presheath electron temperature for different values (10 eV, 11 eV and 12 eV). The flows of the ion motion is feebly influenced by the residual electric field. Therefore, with the increase in presheath ion temperature, there is increment of the entrance ion velocity as well. Also, ions velocity is affected by the temperature of electron.

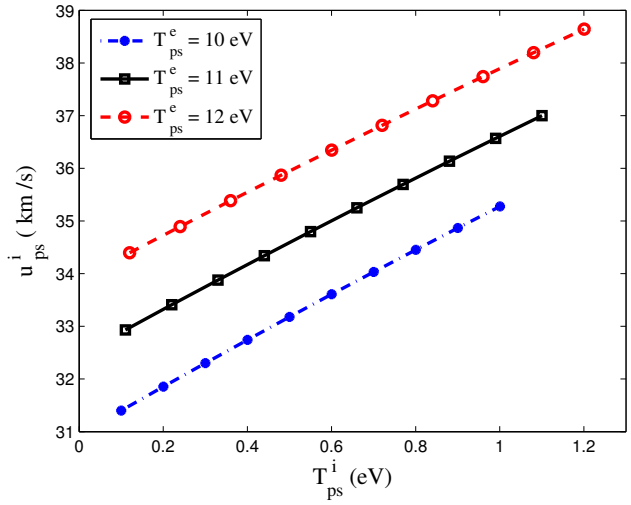

Figure 21: Presheath ion velocity as the function of presheath ion temperature for different values of presheath electron temperature

From Figure 22, we observe the coupling of ion temperature at the sheath side with respect to presheath ion temperature. From this plot, we see that with the increase of

ion temperature at the region of sheath, there is increase of presheath ion temperature as well.

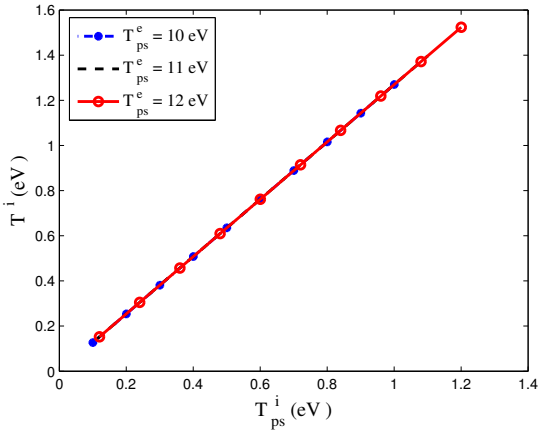

Figure 22: Variation of ion temperature as the function of presheath ion temperature

4.6 Comparison of kinetic approach and fluid approach

The self consistent potential profile for the electron temperature 10 eV is shown in Figure 23. In this picture red colour line shows the plot of fluid approach whereas the black colour shows the plot of kinetic approach. It has been observed that the simulated values of wall potential for kinetic approach and fluid approach are -28.08 eV and -26.08 eV respectively for presheath electron temperature 10 eV respectively. At the presheath region both fluid and kinetic approach works very well. In the sheath region the plasma parameters have sharp gradient so that fluid theory could not suitable to understand the sheath properties. Due to sharp variation, we need to know the distribution function each and every point which is incorporated by kinetic theory. However both models are qualitatively similar, quantitavily different Khanal (2003). It is more appropriate when the plot of kinetic approach move towards the wall instead of fluid approach.

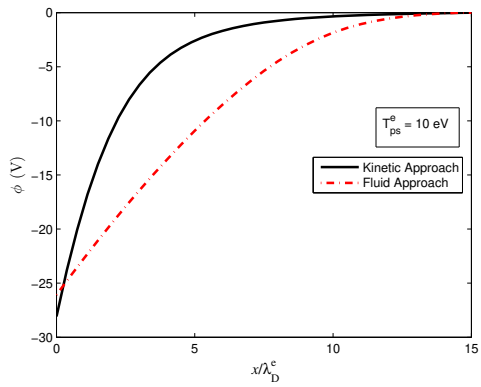

Figure 23: Potential profile as the function of normalized distance

4.7 Temporal ion velocity profile for different obliqueness of the magnetic field

The time dependency of velocity component of ions have been calculated for magnetic field 2.5 mT at different values of obliqueness of the field (0°, 30°, 45°, 60°, 75° and 90°). The results of calculation are shown in Figures 24 to 32. Figure 24(a) shows that the velocity along $z-$axis is independent of applied magnetic field. There is gyration of particles along x and $y-$axes. At initial condition of consideration of time there is more gyration along perpendicular axes. when further time increases, gyration frequency decreases gradually and after some time its value becomes negligible. After 0.6 second oscillation of each component of velocity become very negligible and each velocity component terminated to some mean value. The mean values of x, y and $z-$ component of velocity at angle 0° are observed to be 7.6 m/s, −54.6 m/s and 9794 m/s respectively. Initally the x and $y-$ component of velocity oscillate with maximum amplitude 13410 m/s, 12460 m/s and nearly 0 for $z-$ component respectively.

Figure 24(b) shows that as the obliqueness increases to 30° the mean values of x and y separated such that mean value of x is 28.14 m/s and y is 8059 m/s. The $z-$ component of velocity also shows some oscillations and its mean value becomes negative ie −1320 m/s. Also at obliqueness 30° the x, y and $z-$component of velocity oscillate with maximum amplitude 14378 m/s, 9061 m/s and 13230 m/s respectively

Figures 24(c) and 24(d) shows that at obliqueness 45° and 60° the mean values of x, y and $z-$component are −36.47 m/s, 11460 m/s, 7103 m/s and 27.36 m/s, 3816 m/s, 11710 m/s respectively. Also at obliqueness 45° and 60° the x, y and $z-$component of velocity oscillate with maximum amplitude 9830 m/s, 4786 m/s, 7747 m/s and 10303 m/s, 10522 m/s, 3360 m/s respectively

Similarly, Figures 24(e) and 24(f) show that at obliqueness 75° and 90° the mean values of x, y and $z-$ component of velocity are −12.01 m/s, −2103 m/s, 4789 m/s and −43.39 m/s, 3920 m/s, −1926 m/s respectively. Also the x, y and $z-$component of velocity oscillate with amplitude 15478 m/s, 13333 m/s, 5611 m/s and 14693 m/s, 13980 m/s, 13994 m/s respectively.

To estimate the parameters of the computed plot, we have calculated the mean value, maximum amplitude, damping constant, frequency of oscillation and the phase angle. For magnetic field 2.5 mT and angle (30° and 45°), we got damped oscillatory nature of each component of velocities as shown in Figures 25 to 30. The fitted plots are almost well matched with the computed plots. Figure 25 shows that the $x-$ component of velocity approximately has mean value 26 m/s, maximum amplitude 14910 m/s, damping constant 6.922 s^{-1}, frequency of oscillation 74.627 Hz and phase angle 0.773π radian. Similarly Figures 26 and 27 show that at the same value of magnetic field 2.5 mT and angle 30°, the y and $z-$ component of velocity has mean value, maximum

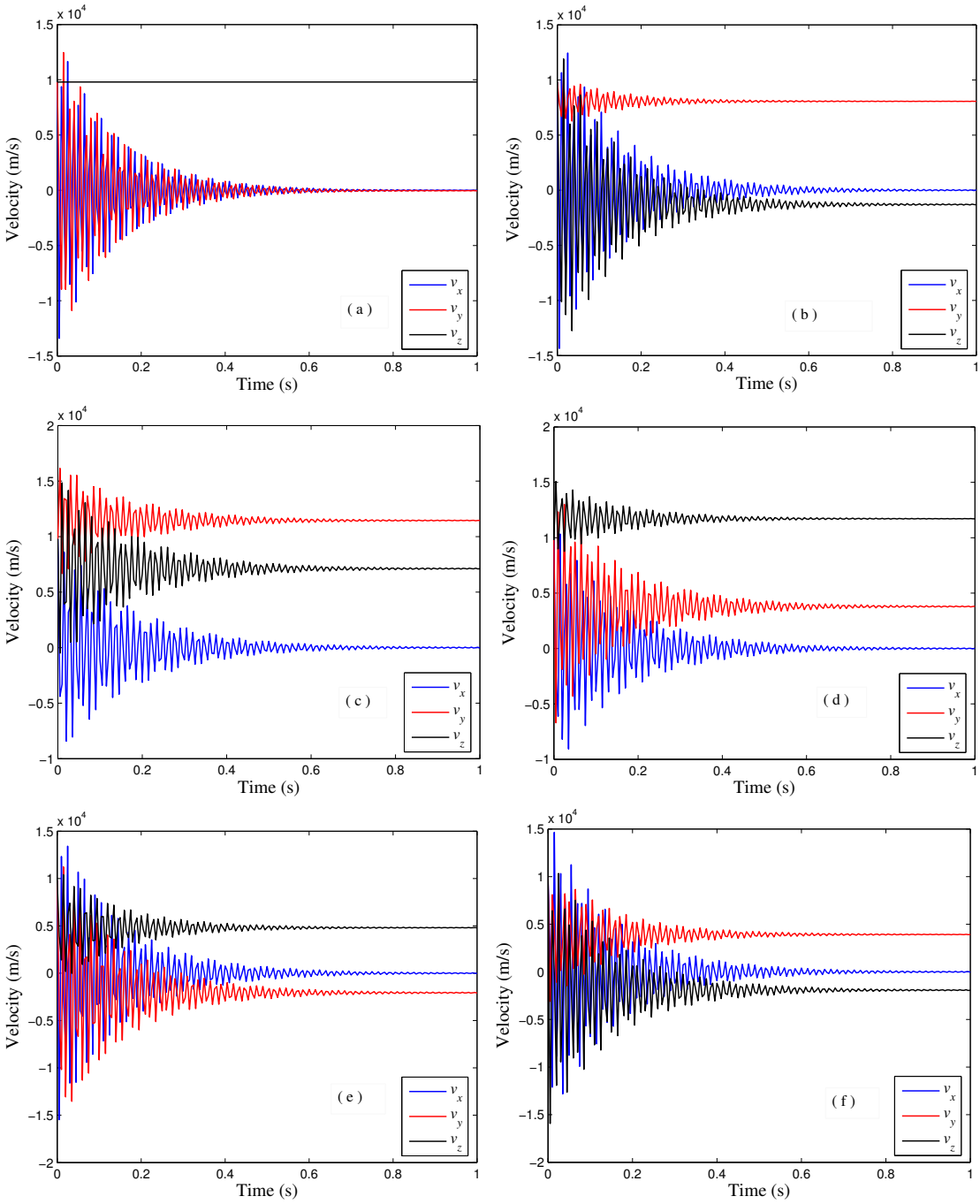

Figure 24: Variation of velocity with time at constant magnetic field 2.5 mT for different values of obliqueness (a) at angle 0°, (b) at angle 30°, (c) at angle 45°, (d) at angle 60°, (e) at angle 75° and (f) at angle 90° .

amplitude, damping constant, frequency of oscillation and phase angle as 8052 m/s, 2287 m/s, 6.665 s^{-1}, 74.667 Hz, 0.7244π radian and 1362 m/s, 14600 m/s, 6.4 s^{-1}, 74 Hz and 0.272π radian, respectively.

Figure 28 shows that at magnetic field 2.5 mT and angle 45°, the $x-$ component of velocity approximately has mean value 0, maximum amplitude 9794.2 m/s, damping constant 5.697 s^{-1}, frequency of oscillation 72 Hz and phase angle 0.5π radian. Also Figures 29 and 30 shows that at the same value of magnetic field 2.5 mT and angle 45°,

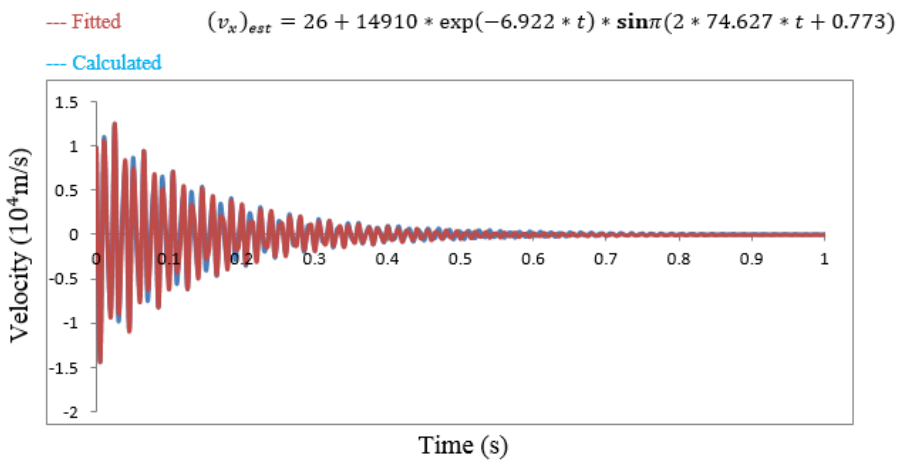

Figure 25: Damping of x- component of velocity with time at magnetic field 2.5 mT and angle 30°.

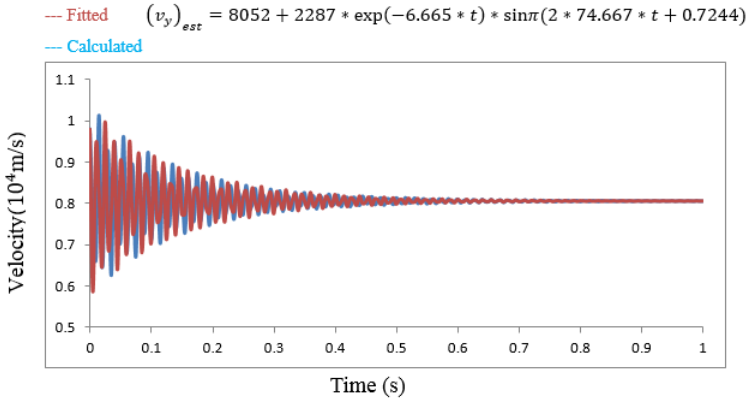

Figure 26: Damping of y- component of velocity with time at magnetic field 2.5 mT and angle 30°.

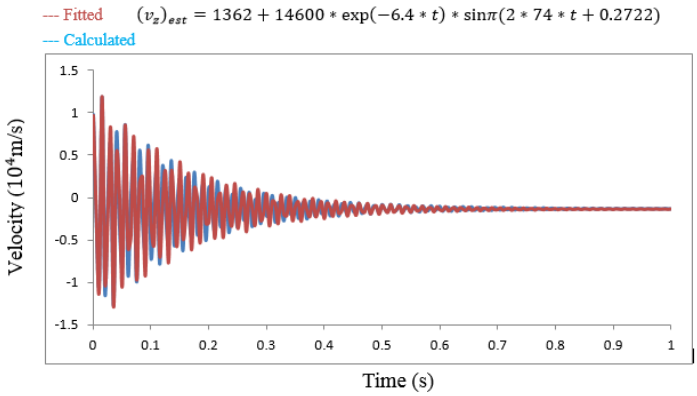

Figure 27: Damping of z- component of velocity with time at magnetic field 2.5 mT and angle 30°.

the y and $z-$ component of velocity has mean value, maximum amplitude, damping constant, frequency of oscillation and phase angle as 11435 m/s, 4815 m/s, 5.734 s^{-1},

72 Hz, 0.111π radian and 7137 m/s, 8200 m/s, 5.83 s^{-1}, 72 Hz, 0.9π radian respectively.

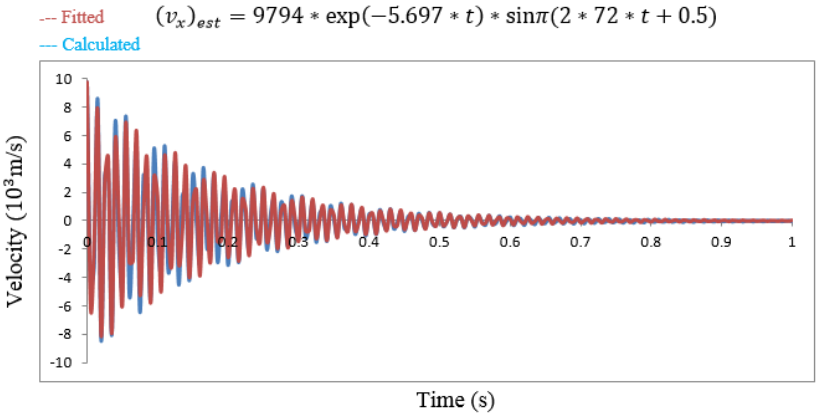

Figure 28: Damping of x- component of velocity with time at magnetic field 2.5 mT and angle 45°.

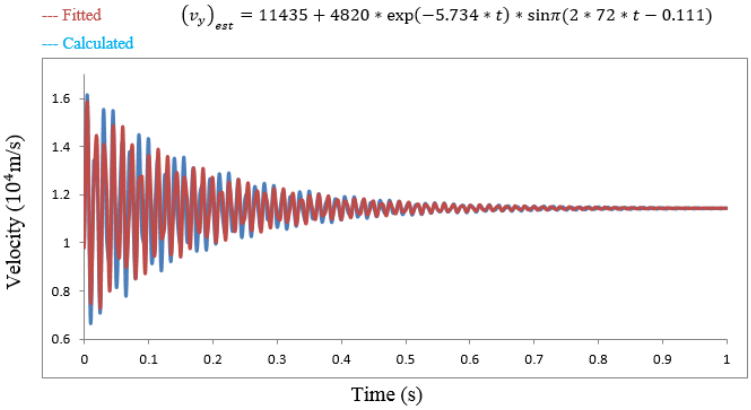

Figure 29: Damping of y- component of velocity with time at magnetic field 2.5 mT and angle 45°.

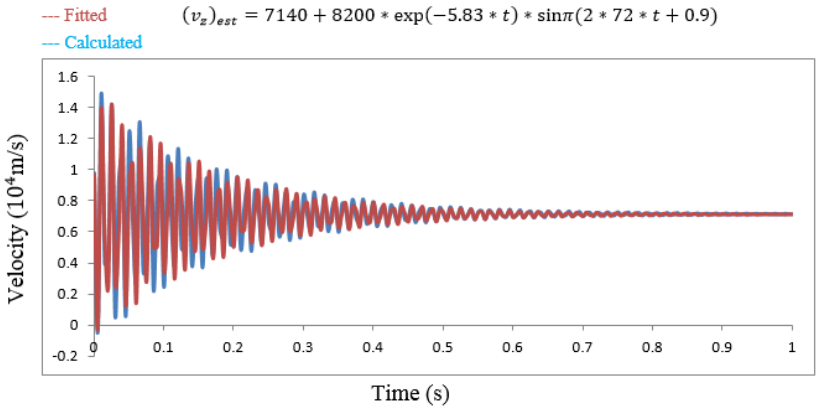

Figure 30: Damping of z- component of velocity with time at magnetic field 2.5 mT and angle 45°.

Table 1 shows the summery of observed data for mean value, maximum amplitude,

damping constant, frequency of oscillation and phase angle. The mean value of $x-$component of velocity at 30° is small but not equal to zero whereas at 45° mean value is zero. Mean value is maximum i.e 11435 m/s on $y-$component at 45° with respect to other components at different angles. Also at the same value of magnetic field 2.5 mT and angle 30° maximum and minimum amplitude is 14910 m/s and 2287 m/s on x and $y-$component respectively with respect to other components at different angles. At angle 30° for all component of velocity damping constant is slightly larger than at 45°. At angle 30° frequency of oscillation is greater with respect to x, y and $z-$components of other angles whereas at angle 45° frequency of oscillation is slightly smaller and constant compared to frequencies of other angles at different components. Similarly at angle 45°, phase angle at $y-$component is minimum i.e -0.111π radian than other components at different angles. On the other hand, at 45° phase angle at $z-$component is maximum i.e. 0.9π radian than other components at different angles.

Table 1: The observed data of mean value, amplitude, damping constant, frequency of oscillation and phase angle at magnetic field 2.5 mT. (Source: Adhikari et al., 2016)

Angle	Observed Mean value (m/s)			Observed Amplitude (m/s)			Damping constant (s^{-1})		
θ	v_x	v_y	v_z	v_x	v_y	v_z	v_x	v_y	v_z
30°	26	8052	1362	14910	2287	14600	6.9	6.7	6.4
45°	0	11435	7137	9794	4815	8200	5.697	5.7	5.8

Angle θ	Frequency of Oscillation (Hz)			Observed Phase angle (radian)		
	v_x	v_y	v_z	v_x	v_y	v_z
30^0	74.6	74.7	74	0.77π	0.7π	0.27π
45^0	72	72	72	0.5π	-0.11π	0.9π

The overall variation of mean value of velocity components at different obliqueness is shown in Figure 31 which shows mean value of component is nearly equal to zero for all angles at magnetic field 2.5 mT. The mean value of y and $z-$ components almost sinosodically varies with nearly complementary to each other with nearly equal amplitudes. The mean value of y and $z-$component of velocity is maximum i.e. 11460 m/s and 11710 m/s at angles 45° and 60° respectively. Figure 32 shows the overall variation of maximum amplitude of different component of velocity with respect to different obliqueness at magnetic field 2.5 mT . For x, y and $z-$ component of velocity the maximum amplitudes are 15478 m/s, 13980 m/s and 13994 m/s at angles 75°, 90° and 90° respectively. Similarly the minimum amplitudes are nearly 9830 m/s, 4786 m/s and zero at angles 45° and 0° respectively.

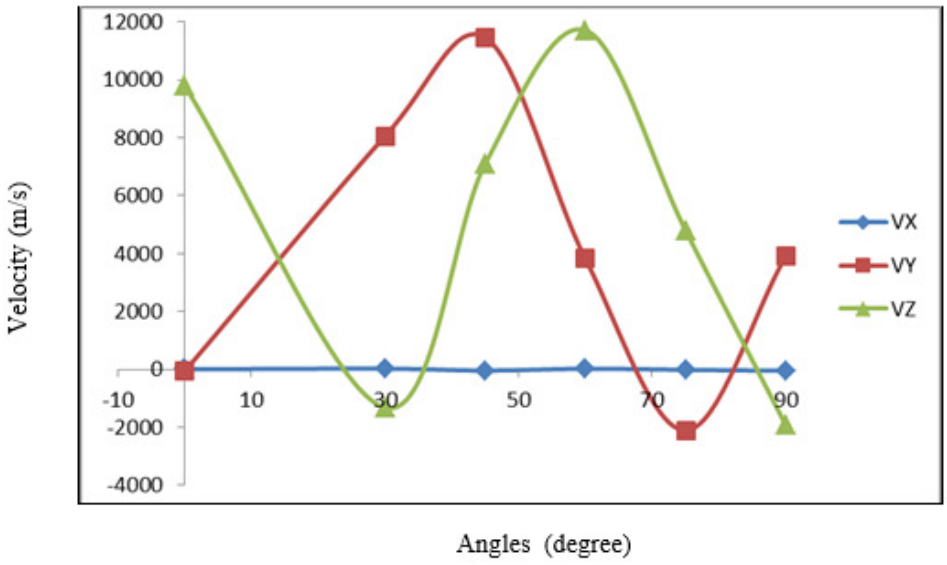

Figure 31: Variation of mean values of velocity with respect to angles at magnetic field 2.5 mT.

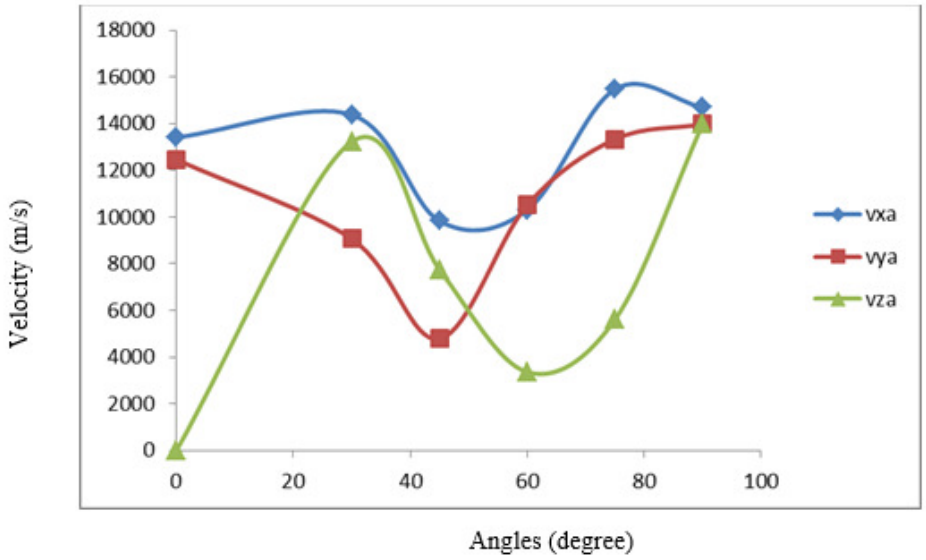

Figure 32: Variation of maximum amplitude of velocity with respect to angles at magnetic field 2.5 mT.

4.8 Temporal ions velocity profile for different magnitude of magnetic field

The temporal ion velocity profile variation have been calculated for different value of magnetic field and constant obliqueness 30° . The calculated results are shown in Figures 33 to 35.

Initially at magnetic field 1.5 mT, all the component of velocity shows oscillatory types nature as shown in Figure 33(a). Initially there is more gyration along perpendicular axes. When further time increases, there is gradually decrease of gyration frequency. At the same value of magnetic field, the mean value of all the component of velocity are

−45.21 m/s, 6863 m/s and 11490 m/s respectively. Also the x, y and $z-$component of velocity oscillate with maximum amplitude 9839 m/s, 7913 m/s and 4840 m/s respectively.

As the magnetic field is increased to 4.5 mT and 7.5 mT, the mean values of x, y and $z-$component of velocity are −0.1347 m/s, 6651 m/s, 11610 m/s and 0.001059 m/s, 6666 m/s, 11600 m/s respectively which is shown in Figures 33(b) and 33(c). Similarly, the x, y and $z-$component of velocity oscillate with maximum amplitude 9794 m/s, 7693 m/s, 4440 m/s and 9794 m/s, 7334 m/s, 4233 m/s respectively. Also at these values of magnetic field (4.5 mT, and 7.5 mT) frequency of oscillation decreases as compared to 1.5 mT. At magnetic field 4.5 mT, after 0.5 s oscillation of all the velocity component become negligible but for magnetic field 7.5 mT, oscillation of each component of velocity becomes negligible after 0.3 s.

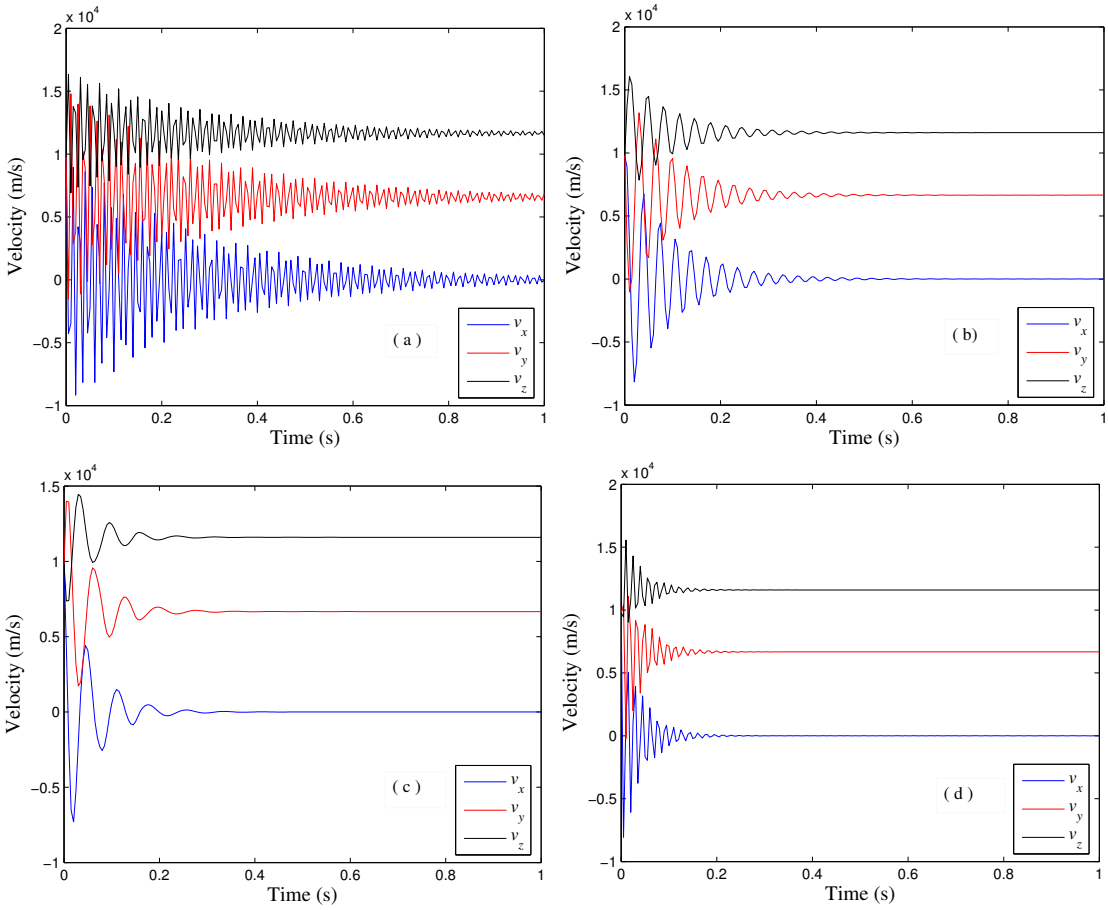

Figure 33: Variation of velocity with time at constant obliqueness 30° for different values of magnetic field (a) at 1.5 mT, (b) at 4.5 mT, (c) at 7.5 mT and (d) at 10.5 mT.

Finally, we calculate the mean values and maximum amplitude for magnetic field 10.5 mT. The mean values of x, y and $z-$component of velocity are −6.894 m/s, 6673 m/s and 11600 m/s respectively whereas the maximum amplitudes are 9794 m/s, 6879 m/s and 3970 m/s respectively, which is shown in Figure 33(d).

The overall variation of mean value of all the component of velocity for different values of magnetic field are shown in Figure 34. But when the field is greater than zero, the mean value of $x-$component is almost equal to zero. But at zero field mean values of y and $z-$component of velocities are nearly equal to 10000 m/s. For larger value of magnetic field, the two components of velocities are splitted with the mean value of y and $z-$component is almost constant around 6660 m/s and 11600 m/s respectively in the range of magnetic field from 2 mT to 10.5 mT.

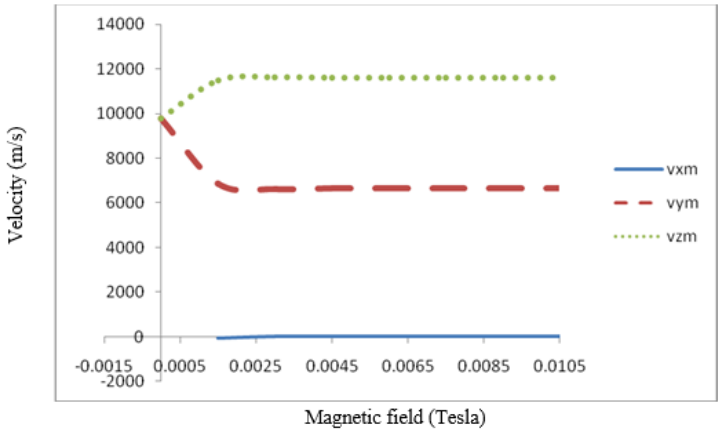

Figure 34: Variation of mean value of velocity with respect to magnetic field at angle 30°

Figure 35 shows the overall variation of maximum amplitude of all the component of velocity with respect to magnetic field. The maximum amplitude of $x-$component is constant around 9794 m/s whereas for y and $z-$component of velocity the maximum amplitudes are 8100 m/s and 4400 m/s respectively at magnetic field 1.5 mT. The minimum amplitudes of y and $z-$component are nearly equal to 4489 m/s and 2070 m/s respectively at magnetic field 6 mT.

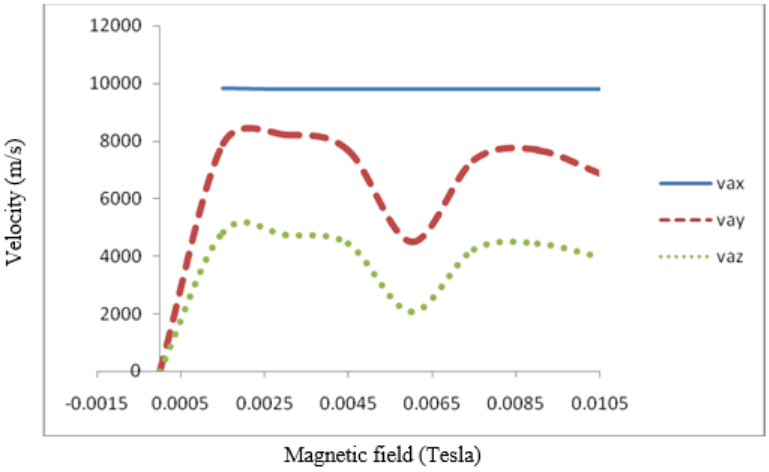

Figure 35: Variation of maximum amplitude of velocity with respect to magnetic field at angle 30°

4.9 Beat frequency of temporal ion velocity profile for different obliqueness of the magnetic field

Various components velocity of ion with time is calculated for constant magnetic field 2 mT at different obliqueness of the field (30°, 60° and 75°). Calculated results are shown in the Figures 36(a) to 36(c).

At obliqueness 30°, from Figure 36(a), the x, y and $z-$component of velocity varies sinosodially about the mean value of -106.9 m/s, 6639 m/s and 11620 m/s respectively with same oscillating frequency 100 Hz. These components show damping type oscillation with damping factor 4.3 s^{-1}, 4.5 s^{-1} and 4.2 s^{-1} respectively. Similarly at this angle, these components of velocity varies with maximum amplitude 9900.9 m/s, 3501 m/s and 2070 m/s respectively. Likewise, this figure shows that, for x, y and $z-$component, there forms 5.5, 5.2 and 5 beats in 1 second, so that their beat frequency is equal to 5.5 Hz, 5.2 Hz and 5 Hz. Also the first zero amplitude is obtained at about 0.2 second for $x-$component of velocity. On the other hand, around 0.1 second in y and $z-$component, we observe the first zero amplitude.

At angle 60°, Figure 36(b) shows that the x,y and $z-$component of velocity varies sinosodially having the mean value of -41.07 m/s, 11590 m/s and 6683 m/s respectively with frequency of oscillation 100 Hz. Like previous these components shows damping nature of oscillation as well with damping factor 4.4 s^{-1}, 4.7 s^{-1} and 4.2 s^{-1} respectively. Similarly at this value of angle, these components of velocity varies with the maximum amplitude 9835.07 m/s, 2630 m/s and 4747 m/s respectively. In addition, this figure shows that for these components of velocity, there forms 5.3, 5.6 and 5.7 beats in 1 second, so that their beat frequency is equal to 5.3 Hz, 5.6 Hz and 5.7 Hz. Likewise in $x-$component of velocity, the first zero amplitude is obtained at around 0.15 second whereas for y and $z-$component of velocity, the first zero amplitude is obtained at about 0.255 second.

Similarly at obliqueness 75°, the x, y and $z-$component of velocity varies sinosodially with mean value of -43.3 m/s, 11540 m/s and 3296 m/s respectively with the frequency of oscillation 100 Hz which is shown in Figure 36(c). Likewise, damping nature of oscillation shows by these components which have damping factor 4.5 s^{-1}, 4.2 s^{-1} and 5.5 s^{-1} respectively. Also at the same value of angle, these components of velocity varies with maximum amplitude 9750.74 m/s, 1850 m/s and 6498 m/s respectively. This figure shows that at an angle 75°, for x, y and $z-$component of velocity there is formation of 5.2, 5.6 and 5.6 beats in 1 second respectively, and hence their frequency of beat is equal to 5.2 Hz, 5.6 Hz and 5.6 Hz respectively. According to this figure, in $x-$component of velocity, at first the zero amplitude is obtained at around 0.28 second but in y and $z-$component of velocity, the first zero amplitude is obtained at about 0.4 second. Further

in each component of velocity, shoulder is obtained around 0.1 second.

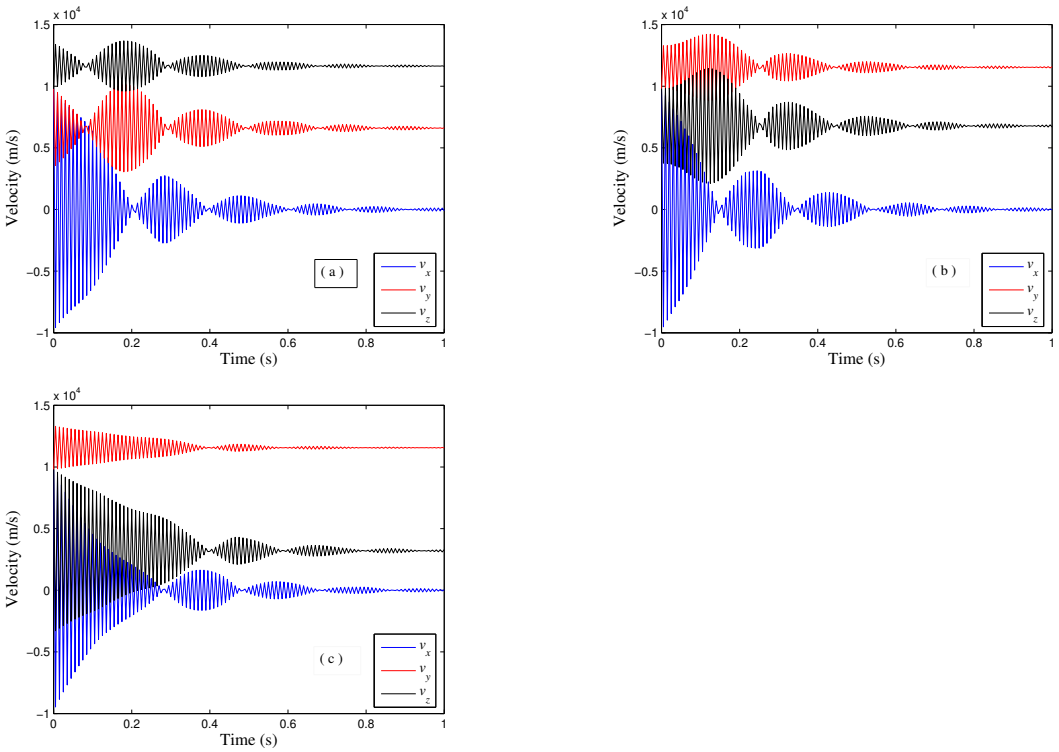

Figure 36: Variation of velocity with time at constant magnetic field 2 mT for different values of obliqueness (a) at 30°, (b) at 60° and (c) at 75°.

The summary of the observed data for mean value, maximum amplitude, damping constant, frequency of oscillation and beat frequency is shown in Table 2. For $x-$component, mean value of velocity at obliqueness of 30°, 60° and 75° is very small and negative as compared to that of other components. Mean value 11620 m/s which is maximum on

Table 2: The observed data of average value, amplitude, damping constant, frequency of oscillation and beat frequency at magnetic field 2 mT. (Source: Adhikari et al., 2018)

Angle	Observed mean value (m/s)			Observed maximum amplitude (m/s)			Damping factor (s^{-1})		
θ	v_x	v_y	v_z	v_x	v_y	v_z	v_x	v_y	v_z
30°	-106.9	6639	11620	9900.9	3501	2070	4.3	4.5	4.2
60°	-41.07	11590	6683	9835	2630	4747	4.4	4.7	4.2
75°	-43.3	11540	3296	9750.7	1850	6498	4.5	4.2	5.5

Angle	Frequency of oscillation (Hz)			Observed beat frequency (Hz)		
θ	v_x	v_y	v_z	v_x	v_y	v_z
30^0	100	100	100	5.5	5.2	5
60^0	100	100	100	5.3	5.6	5.7
75^0	100	100	100	5.2	5.6	5.6

the $z-$component at angle 30° with respect to the other components at different value of

obliqueness. Also at an angle 75°, amplitude 1850 m/s is minimum on the $y-$component whereas at the obliqueness 30°, amplitude 9900.9 m/s is maximum on x-component. At an angle 60°, the value of damping constant is maximum i.e. 4.7 s^{-1} on y-component. Frequency of oscillation is 100 Hz for each components of velocity at all the angle. Similarly, at angle 60°, beat frequency in the $z-$component is maximum 5.7 Hz in 1 s then the other components at different angles.

4.10 Modulation frequency of temporal ion velocity profile for different obliqueness of the field

The temporal dependence of variation of various components of ion velocity have been calculated for different obliqueness of the field (30°, 60° and 75°) and at constant magnetic field 6 mT. The results of calculation are shown in Figures 37(a) to 37(c).

In Figure 37(a) at obliqueness 30°, the x, y and $z-$component of velocity varies about the mean value of 0.0070 m/s, 6661 m/s and 11600 m/s respectively with same frequency of oscillation 100 Hz. Also these components show damping nature of oscillation with damping factor 13.8 s^{-1}, 13.1 s^{-1} and 13.0 s^{-1} respectively. Likewise, these component of velocity varies with maximum amplitude of 9793.993 m/s, 3138 m/s and 1550 m/s respectively. Also this figure shows that modulation frequency of x, y and $z-$component of velocity is same which is equal to 15.4 Hz respectively.

Figure 37(b) shows that at obliqueness 60°, the x, y and $z-$component of velocity varies about the average values of -0.008 m/s, 11570 m/s and 6718 m/s respectively with equal frequency of oscillation 100 Hz. Also these components show damping nature of oscillation with damping factor 15.2 s^{-1}, 13.7 s^{-1} and 12.3 s^{-1} respectively. Likewise, these component of velocity varies with maximum amplitude of 9794.008 m/s, 2650 m/s and 4632 m/s respectively. Also this figure shows that modulation frequency of x, y and $z-$component of velocity is 16.2 Hz, 15.8 Hz and 16.2 Hz respectively. At obliqueness 75°, the x, y and $z-$component of velocity varies about the average values of 0.0058 m/s, 11580 m/s and 3137 m/s respectively with equal frequency of oscillation 100 Hz as shown in Figure 37(c). Also these components show damping nature of oscillation with the damping factor as 12.9 s^{-1}, 14.9 s^{-1}, 14.1 s^{-1} respectively. Likewise, these component of velocity varies with the maximum amplitude of 9793.99 m/s, 1690 m/s and 6657 m/s. Also this figure shows that modulation frequency of x, y and $z-$component of velocity is 15.8 Hz, 16.0 Hz and 15.4 Hz respectively. Also in each component shoulder is obtained around 0.05 second.

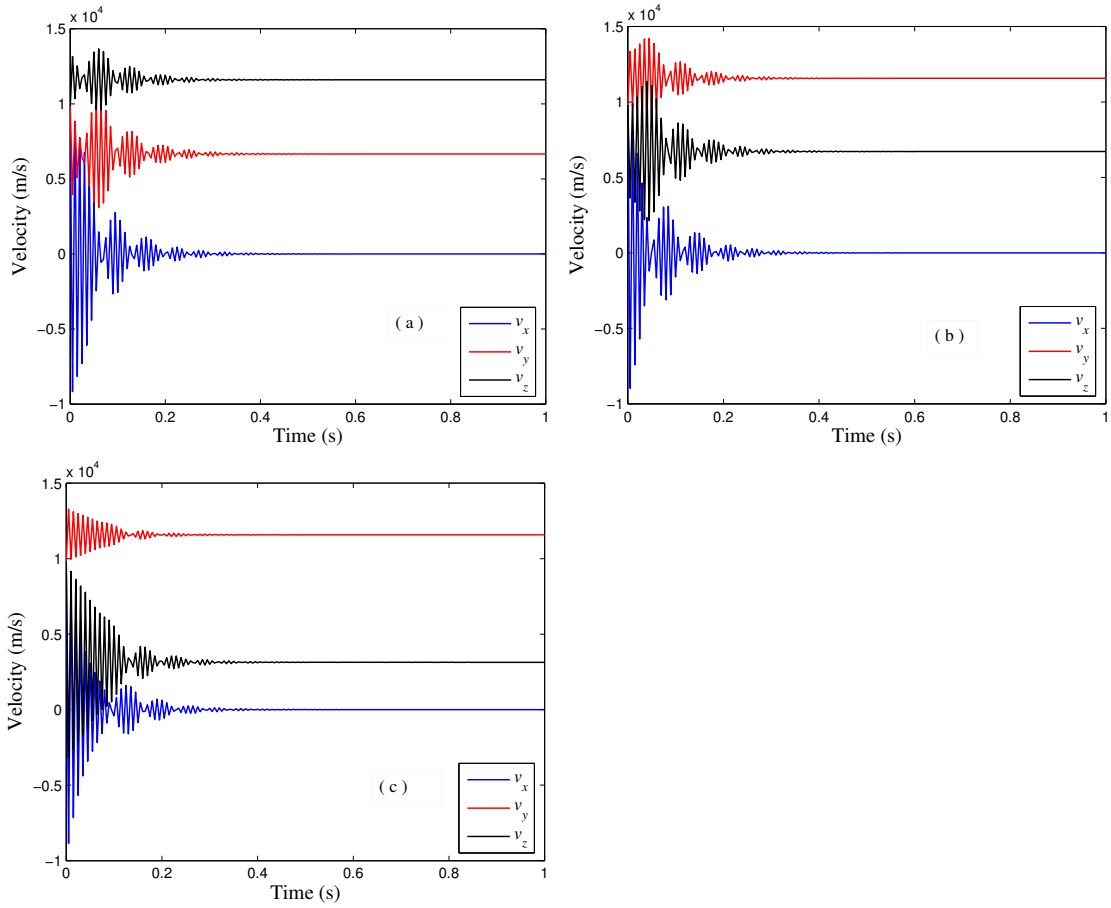

Figure 37: Variation of velocity with time at constant magnetic field 6 mT for different values of obliqueness (a) at 30° , (b) at 60° and (c) at 75° .

Table 3 shows the summary of observed data for average value, maximum amplitude, damping factor, frequency of oscillation and modulation frequency. The average value of $x-$component of velocity at obliqueness of 30°, 60° and 75° is small then other components. Mean value 11580 m/s is maximum on y-component at 75° with respect to other components at different angles. On $x-$component at angle 30° and 75°, amplitude 9793.99 m/s is maximum, whereas amplitude is minimum 1550 m/s for $z-$component at 30°. At angle 30° damping factor is minimum ie 13.0 /s on $z-$component. On the other hand at 75° for $y-$component damping factor is maximum i.e. 14.9 s^{-1} . Frequency of oscillation is the same i.e. 100 Hz for all component of velocity at each angle. Similarly, at angle 60° modulation frequency in the $x-$component and $z-$component is maximum (16.2 Hz) in 1 s than other components at different angles.

Table 3: The observed data of average value, amplitude, damping constant, frequency of oscillation and modulation frequency at magnetic field 6 mT

Angle	Observed mean value (m/s)			Observed maximum amplitude (m/s)			Damping factor (s^{-1})		
θ	v_x	v_y	v_z	v_x	v_y	v_z	v_x	v_y	v_z
30°	0.007	6661	11600	9794	3138	1550	13.8	13.1	13
60°	-0.008	11570	6718	9794	2650	4632	15.2	13.7	13.3
75°	0.0058	11580	3137	9794	1690	6657	12.9	14.9	14.1

Angle	Frequency of oscillation (Hz)			Observed modulation frequency (Hz)		
θ	v_x	v_y	v_z	v_x	v_y	v_z
30^0	100	100	100	15.4	15.4	15.4
60^0	100	100	100	16.2	15.8	16.2
75^0	100	100	100	15.8	16	15.4

4.11 Vector sum of oscillatory part of temporal velocity for different obliqueness of the magnetic field

At magnetic field 3 mT and angle 30°, the velocity of the ions at the sheath entrance is observed at various time as shown in Figure 38. Frequency of oscillation is almost equal ie 50 Hz for 30°, 60° and 90° . The oscillation amplitude of the velocity decreases as time increases and the mean value of each component of the velocity are obtained as 2.537 m/s, 6620 m/s and 11630 m/s respectively.

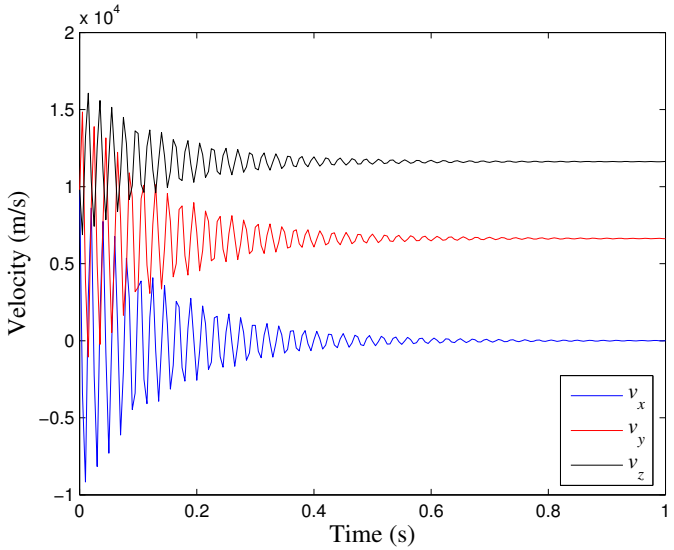

Figure 38: Velocity variation with time at magnetic field 3 mT and angle 30°.

As we computed the resultant of oscillatory part of all three component of the velocity, we found an exponential damping of the velocity as shown in Figure 39. The fitted curve in Figure 39 is almost matching with the computed plot. The equation of the fitted curve

is $v = v_0 e^{-t/\tau} = 10.456 \times 10^3 e^{-t/0.138}$ m/s, where v_0 is the initial value of v in m/s and τ is the characteristic time in second.

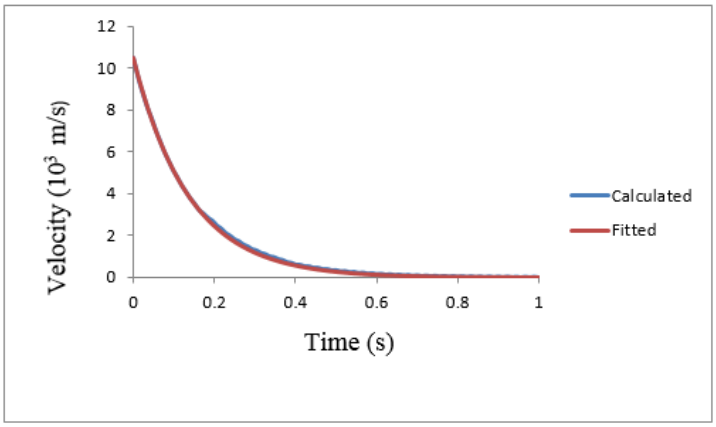

Figure 39: Oscillatory part of total velocity with respect to time at magnetic field 3 mT and angle 30°.

Like previous same magnetic field is applied in a plasma sheath at an angle 60°. The velocity of the ions at the sheath entrance is observed at various time as shown in Figure 40. With increase in time, the oscillation amplitude of the velocity decreases. The mean value of x, y and $z-$ component of the velocity were obtained as -7.35 m/s, 11550 m/s and 6757 m/s respectively.

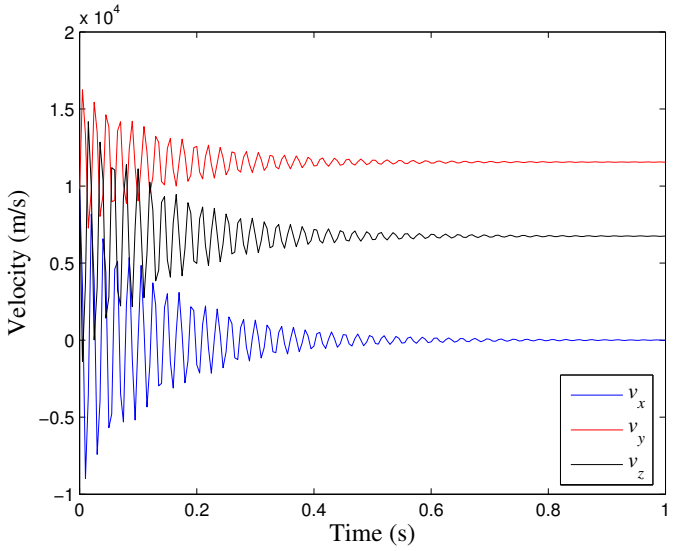

Figure 40: Velocity variation with time at magnetic field 3 mT and angle 60°.

When we computed the resultant of oscillatory part of all three component of the velocity, we found an exponential damping of the velocity as shown in Figure 41. The fitted curve in Figure 41 is almost matching with the computed plot. The equation of the fitted curve

is $v = v_0 e^{-t/\tau} = 10.41 \times 10^3 e^{-t/0.138}$ m/s, where v_0 is the initial value of v in metre per second and τ is the characteristic time in second.

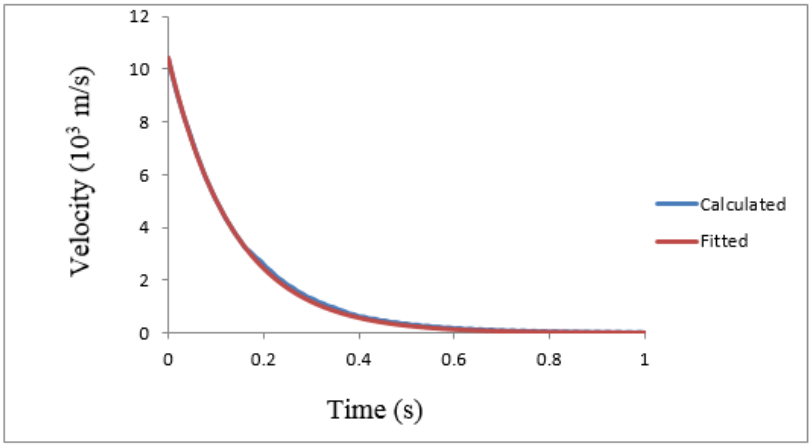

Figure 41: Oscillatory part of total velocity with respect to time at magnetic field 3 mT and angle 60°.

Similarly same magnetic field is applied in a plasma sheath at an angle 90° and at various time the velocity of the ions is observed as shown in Figure 42. The oscillation amplitude of the velocity decreases as time increases and the mean value of each component of the velocity were obtained as −772.5 m/s, 4415 m/s and −938.8 m/s respectively.

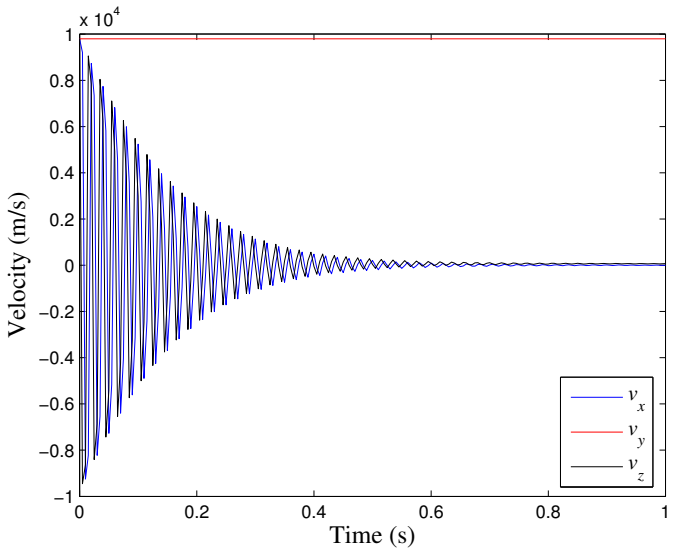

Figure 42: Velocity variation with time at magnetic field 3 mT and angle 90°.

When we computed the resultant of oscillatory part of all three component of the velocity, we found an exponential damping of the velocity as shown in Figure 43. The fitted curve in Figure 43 is almost matching with the computed plot. The equation of the fitted curve

is $v = v_0 e^{-t/\tau} = 14.984 \times 10^3 e^{-t/0.357}$ m/s, where v_0 is the initial value of v in metre per second and τ is the characteristic time in second.

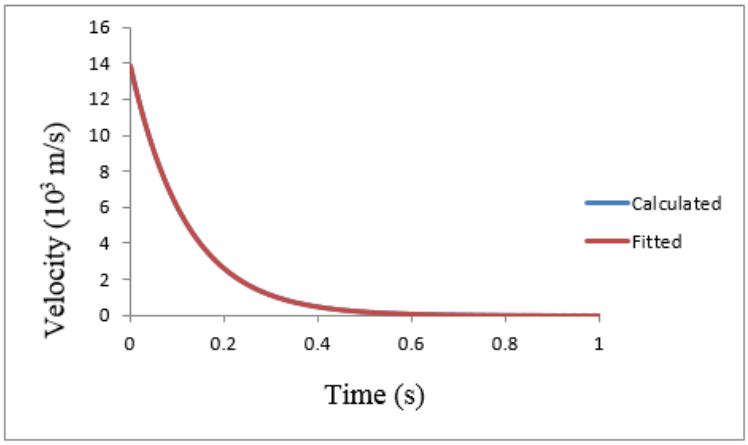

Figure 43: Oscillatory part of total velocity with respect to time at magnetic field 3 mT and angle 90°.

Figure 44 shows the dependence of oscillatory part of total velocity with time at constant magnetic field 3 mT and obliqueness 30°, 60° and 90°. As can be seen in Figure 44, the initial value of the velocity is greatest in obliqueness 90° and least in obliqueness 60°. On the other hand the characteristic time of damping is greatest at obliqueness of 90°.

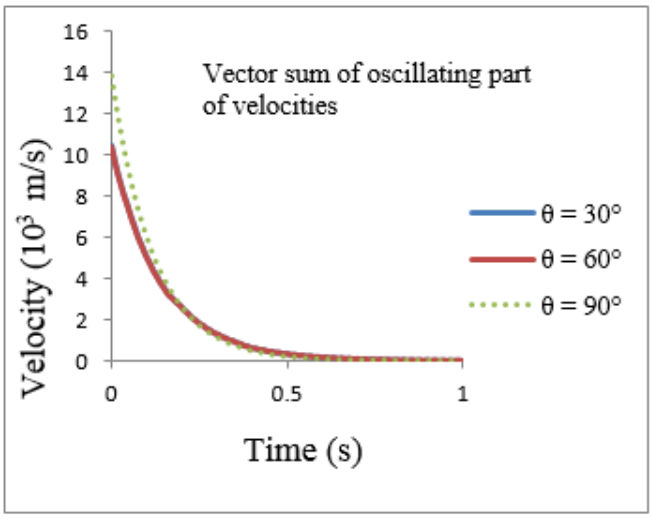

Figure 44: Variation of vector sum of Oscillatory part of total velocity with respect to time at magnetic field 3 mT and different angle

4.12 Vector sum of oscillatory part of temporal velocity for different value of magnetic field

As in Figure 45, at magnetic field 1 mT and angle 30°, the velocity of the ions at the sheath entrance is observed at different time interval . Frequency of oscillation of each component is almost equal ie 55.5 Hz . The oscillation amplitude of the velocity decreases as time increases and the mean value of each component of the velocity were obtained as −11.5 m/s, 6523 m/s and 11690 m/s respectively

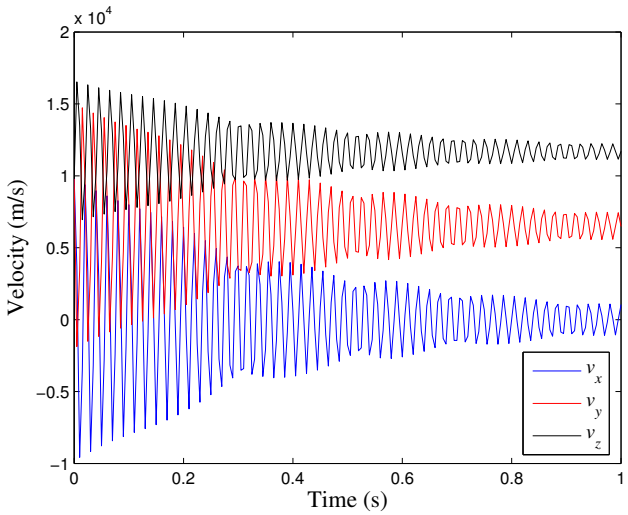

Figure 45: Velocity variation with time at magnetic field 1 mT and angle 30°.

As we computed the resultant of oscillatory part of all three component of the velocity, we found an exponential damping of the velocity as shown in Figure 46. The fitted curve in Figure 46 is almost matching with the computed plot. The equation of the fitted curve is $v = v_0 e^{-t/\tau} = 10.456 \times 10^3 e^{-t/0.414}$ m/s, where v_0 is the initial value of v in metre per second and τ is the characteristic time in second.

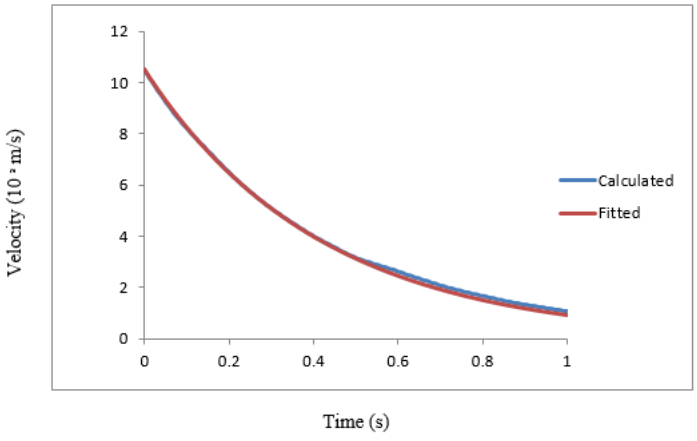

Figure 46: Oscillatory part of total velocity with respect to time at magnetic field 1 mT and angle 30°.

At magnetic field 3 mT and angle 30°, the velocity of the ions at the sheath entrance is observed at various time as shown in Figure 38. Frequency of oscillation of each component is equal to 52 Hz. The oscillation amplitude of the velocity decreases as time increases and the mean value of each component of the velocity were obtained as 2.5 m/s, 6620 m/s and 11630 m/s respectively. The resultant of oscillatory part of all the components of velocity found to be exponentially damped as shown in Figure 39. It is found that the fitted curve in Figure 39 is almost matching with the computed plot and the equation of the fitted curve is $v = v_0 e^{-t/\tau} = 10.456 \times 10^3 e^{-t/0.138}$ m/s; where v_0 is the initial value of v in metre per second and τ is the characteristic time in second.

At magnetic field 5 mT and angle 30°, the velocity of the ions at the sheath entrance is observed at various time as shown in Figure 47. Frequency of oscillation of each component is equal to 58.8 Hz. The oscillation amplitude of the velocity decreases as time increases and the mean value of each component of the velocity were obtained as 0.0548 m/s, 6655 m/s and 11610 m/s respectively.

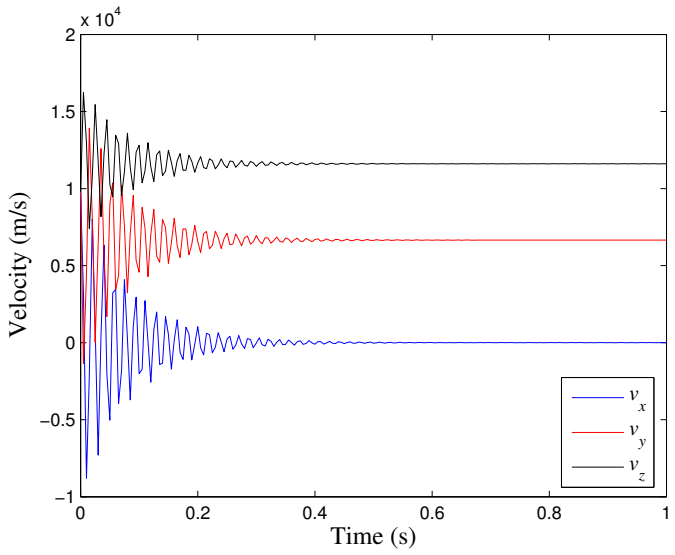

Figure 47: Variation of velocity with time at magnetic field 5 mT and angle 30°.

Like previous as we computed the resultant of oscillatory part of all three component of the velocity, we found an exponential damping of the velocity as shown in Figure 48. The fitted curve in Figure 48 is almost matching with the computed plot. The equation of the fitted curve is $v = v_0 e^{-t/\tau} = 13.802 \times 10^3 e^{-t/0.083}$ m/s, where v_0 is the initial value of v in metre per second and τ is the characteristic time in second.

Similarly, Figure 49 shows the variation of vector sum of oscillating part of total velocity with time at angle 30° and different magnetic field (1 mT, 3 mT and 5 mT). This figure shows that at obliqueness 30° initial velocity of the ions is almost same at different magnetic field. Likewise the damping rate of vector sum of oscillatory part of total

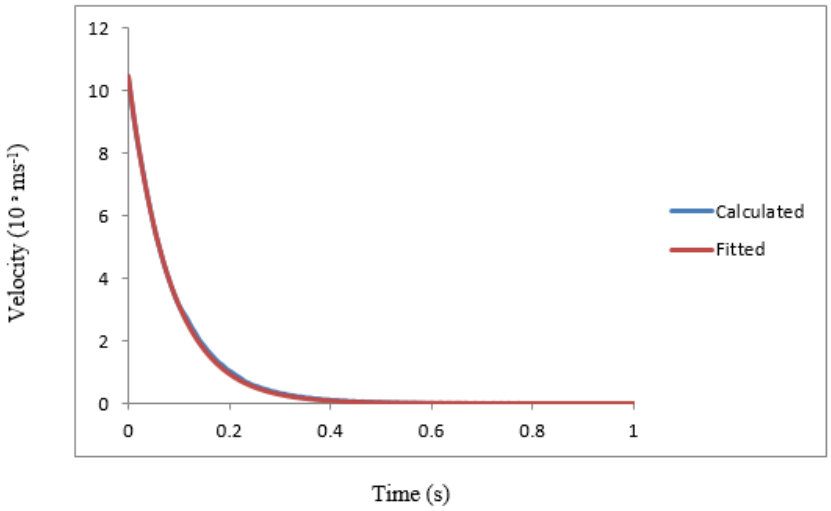

Figure 48: Oscillatory part of total velocity with respect to time at magnetic field 5 mT and angle 30°.

velocity increases from magnetic field 1 mT to 5 mT at obliqueness 30°.

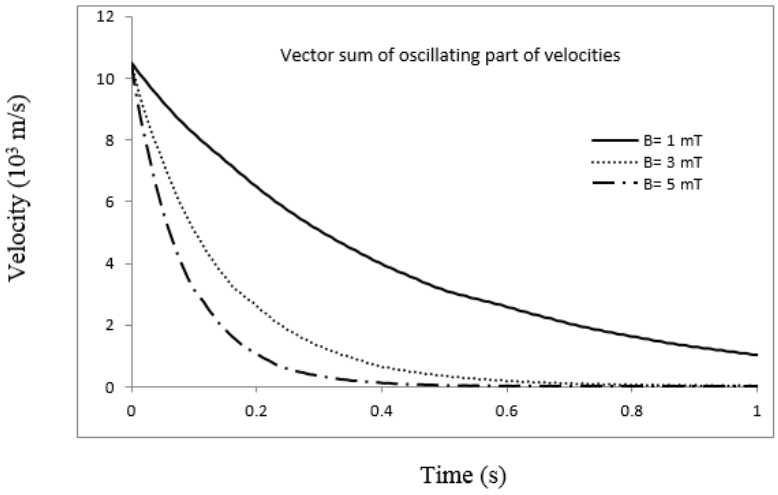

Figure 49: Variation of vector sum of Oscillatory part of total velocity with respect to time at angle 30° and different magnetic field.

CHAPTER 5

5. CONCLUSION AND RECOMMENDATIONS

5.1 Conclusion

The magnetized plasma sheath has been studied using the kinetic trajectory simulation (KTS) method, and also a scheme of presheath-sheath coupling is developed for magnetized plasma. The distribution function of ion and electron at the sheath entrance is assumed to be cut-off Maxwellian, and the sheath plasma is collisionless. The presheath parameters have significant effect on the parameters of sheath side and hence the particle and energy reaching the material wall. Both the electron and ion densities start decreasing from the sheath entrance towards the wall, where the space charge density has its maximum value. The potential decreases from sheath entrance towards the wall which increases for the increase of electron temperature at the presheath side. The value of the wall potential calculated by the simulation method is found to deviate from the theoretical value by nearly 3 % in magnitude. This discrepancy is due to the fact that, our distribution of electron is cut-off Maxwellian, rather than the Boltzmann distribution. The Child-sheath thickness, where the negative charge density is very low, increases with increase in electron temperature at the presheath. Likewise, there is significant effect of the presheath electron temperature on presheath ion velocity, and hence the wall potential increases in order to satisfy the Bohm-Chodura condition. Though the results obtained are qualitatively similar with previous literature, it is quantitavily different providing better insight into the sheath properties. The magnitude of wall potential increases from 56 V to 84 V, with the increment of presheath electron temperature from 20 eV to 30 eV respectively.

The earlier 1d1v KTS model was extended to include the effect of magnetic field by considering the velocity changes in all 3 dimensions. The governing presheath and sheath parameters, both evaluated at the presheth-sheath boundary were solved analytically for the purpose of coupling the two distinct regions of the plasma–wall transition. The extended model along with the coupling scheme was used to investigate the magnetized plasma sheath for varying magnitude and obliqueness of the magnetic field. It has been

observed that, the velocity of ions reaching the material wall can be controlled by the strength of applied magnetic field as well as its orientation. On changing the obliqueness of the field, the separation of the mean values as well as the maximum amplitude of all the three components of the velocity also change. It has been concluded that, the mean value of x-component (component normal to the wall) of velocity is nearly equal to zero for all angles at magnetic field 2.5 mT, whereas the mean value of y and z-components of velocity varies with almost equal amplitudes.

The time dependence of the velocity of ions in the magnetized plasma sheath has also been monitored. Angular dependence of mean value, maximum amplitude, damping constant, frequency of oscillation and phase angle of velocity components at magnetic field 2.5 mT with varying obliqueness have been studied. In conclusion, ion velocity at presheath-sheath boundary is well matched with the fitted damped oscillatory motion. As the obliqueness of the field changes the mean values, beat frequency as well as the maximum amplitude of the three components of the velocity also change but frequency of oscillation remains almost same. Modulation frequency of ions in a magnetized plasma sheath has been studied for different angle at constant magnetic field 6 mT. For different obliqueness, the average values, damping factor as well as frequency of oscillation change for all component of velocity. For y and z-components of velocity maximum amplitude changes but for x-component maximum amplitude remains constant. Frequency of oscillation of all velocity components of ions remains same, however, significant changes in the values of damping factor and modulation frequency for all components of velocity are observed. As the effect of magnetic field increases for increased obliqueness the ion velocity profiles exhibit shoulder nature. Such a shoulder is obtained at around 0.05 second at 75° for each component of velocity but not at 30° and 60°. For every increase in the magnitude of the magnetic the oscillation amplitude of the velocity decreases with time, and hence the mean values of different component of velocity changes as well. The computed and fitted values of the vector sum of oscillatory part of x, y and z-components of velocity of the ions are well matched. At angle 30°, damping rate of vector sum of oscillatory part of total velocity increases with the magnetic field increases from 1 mT to 5 mT. On the other hand vector sum of oscillating part of initial velocity is almost equal for magnetic field 1 mT, 3 mT and 5 mT at the same angle 30°. But for different obliqueness of the magnetic field, the initial velocity of the vector sum of oscillating part at 90° is greater than that at 30° and 60°.

The numerical parameters and boundary conditions required were taken from earlier works by LaBombard et al. (2005), Wesson & Campbell (2011), and Qingquan et al. (2018) and in the limiting cases, where the conditions are similar, our results agree with the reported results.

5.2 Recommendations

The results of our research work are in good agreement with previous works and this work provides the guideline for studying magnetized plasma-wall transition, using the kinetic approach. Being a kinetic approach, it provides better insight of various plasma parameters in a magnetized plasma sheath for different obliqueness, as well as magnitude of the magnetic field. This work is of importance in various plasma applications, where magnetic field plays role in production and confinement, for example, in fusion devices.

On the basis of the framework developed and obtained results, in future, this work can be extended further by considering the following cases:

- higher dimensional analysis (3d3v configuration of plasma)
- inclusion of collision term
- plasma having negative ions
- presence of dust in the plasma
- particle species having different temperatures
- multi-component plasma

CHAPTER 6

6. SUMMARY

6.1 Summary

Plasma is a quasineutral gas of charge and neutral particles which exhibits collective behavior. Because of its distinct behavior it is often termed as the fourth state of matter. It is of interest as it has found applications in diverse areas; controlled thermonuclear fusion, gaseous electronics, particle accelerators, medicine, and many more. In all practical applications plasma has to be confined within a finite volume and plasma-wall interaction plays the most important role in determining the overall plasma stability. We have extended the kinetic trajectory simulation (KTS) method to study magnetized plasma sheath, the thin layer formed next to the wall that separates core plasma from the wall. Assuming that, at the sheath entrance distribution functions of ion and electron to be cut-off Maxwellian the final self consistent states are obtained by solving the governing kinetic equations, iteratively. In order to satisfy the Bohm-Chodura condition, initial velocity of ions entering the sheath region is taken equal to the ion acoustic velocity. As the plasma sheath region is small compared to the collision mean free path and also the particle densities are less compared to the presheath region, the sheath region is assumed to be collisionsless.

In order to connect the sheath and presheath, which are usually studied using kinetic and fluid approaches; the coupling scheme has also been extended for magnetized cases. In a kinetic approach the distribution functions of individual particles are taken into account and since they contain more information than the fluid parameters, the results are of higher accuracy. In our case, the earlier KTS model is extended to include the effect of magnetic field by considering the velocity changes in all 3 dimensions. Also the coupling scheme that was earlier applicable for non-magnetic cases only is now reformulated so that it can couple any plasma with the sheath region. This was done by compiling and solving equations that involve governing presheath and sheath parameters, by satisfying all necessary conditions for the sheath formation.

The model developed is applicable, in principle, for all bounded plasmas and in the

present work it has been used to study magnetized plasma sheath that is formed in magnetic fusion devices. Such devices are of interest as they have the potential to generate huge amount of energy through the nuclear fusion. As different types of fusion devices are being studied and have made significant progresses still such devices are yet to produce energy for the use of common people. Among the one that has made significant progress is the so called Tokamaks, and in our work we have studied a plasma-wall transition problem that is similar to a fusion device. In order to do that we have taken the input numerical parameters and boundary conditions required to initiate our simulation from earlier relevant works. This is also helpful in comparing our results to those reported, and in the limiting cases, where the conditions are similar, our results agree with the reported results.

It has been observed that the presheath electron temperature affects the Child-sheath thickness, particle densities, particle velocities and hence the energy flux reaching the wall. Ion velocity at presheath-sheath boundary is affected by magnitude and obliqueness of the magnetic field. The velocity waves are damped in plasma without collisions in the time scale of the order of seconds. The effect is felt differently by various components of the velocity depending on their orientation with respect to the magnetic field. As the obliqueness of the field changes the mean values, beat frequency as well as the maximum amplitude of the three components of the velocity also change but frequency of oscillation remains almost the same. The work can be extended further by considering various types of plasma, considering collision, presence of dust, and in fully 3d3v geometry. As the results are in good agreement with previous works and the kinetic approach provides better insight this work is of importance in various plasma applications, where magnetic field plays role in production and confinement, especially in fusion devices.

REFERENCES

Acharya, S. K. (2016). *Fluid simulation of the ion-neutral collision effect on magnetized dusty plasma sheath* (M.Sc. Dissertation). Central Department of Physics, Institute of Science and Technology, Tribhuvan University, Kathmandu, Nepal.

Adhikari, B. R., Basnet, S., Lamichhane, H. P., & Khanal, R. (2018). Beat frequency and velocity variation of ions in a magnetized plasma sheath for different obliqueness of the magnetic field. *Journal of Institute of Science and Technology*, *23*, 88.

Adhikari, B. R., Basnet, S., Lamichhane, H. P., & Khanal, R. (2019). Presheath-sheath coupling for kinetic trajectory simulation of a magnetized plasma sheath. *AIP Advances*, *9*(5), 055123.

Adhikari, B. R., Lamichhane, H. P., & Khanal, R. (2016). Temporal dependence of components of velocity of ions in a magnetized plasma sheath for different obliqueness of the magnetic field. *5^{th} PSSI-plasma scholars colloquium*, 32.

Ahedo, E. (1999). Plasma–wall interaction in an oblique magnetic field: Model of the space-charge sheath for large potentials and small debye lengths. *Physics of Plasmas*, *6*(11), 4200.

Amemiya, H., & Bhattacharjee, S. (2006). Sheath formation criterion for negatively charged particles. *Journal of Physics D: Applied Physics*, *39*(17), 3773.

Atzeni, S., Meyer-Ter-Vehn, J., & Meyer-ter Vehn, J. (2004). *The physics of inertial fusion: Beam plasma interaction, hydrodynamics, hot dense matter*. Oxford University Press.

Badsi, M., Mehrenberger, M., & Navoret, L. (2018). Numerical stability of plasma sheath. *arXiv preprint arXiv:1802.05852*.

Bashyal, B. (2016). *Fluid simulation of the ion-neutral collision effect on magnetized dusty plasma sheath* (M.Sc. Dissertation). Central Department of Physics, Institute of Science and Technology, Tribhuvan University, Kathmandu, Nepal.

Basnet, S. (2015). *Study of multicomponent magnetized plasma sheath using fluid hydrodynamics* (M.Sc. Dissertation). Central Department of Physics, Institute of Science and Technology, Tribhuvan University, Kathmandu, Nepal.

Beilis, I. I., Keidar, M., & Goldsmith, S. (1997). Plasma-wall transition: The influence of the electron to ion current ratio on the magnetic presheath structure. *Physics of Plasmas*, *4*(10), 3461.

Bohm, D. (1949). *The characteristics of electrical discharges in magnetic fields*. ed. A. Guthrie and R. K. Wakerling. New York: McGraw-Hill.

Borgohain, D. R., & Saharia, K. (2018). Behavior of collisional sheath in electronegative plasma with q-nonextensive electron distribution. *Physics of Plasmas*, *25*(3), 032122.

Boyd, R. (1951). The mechanism of positive ion collection by a spherical probe in a dense gas. *Proceedings of the Physical Society. Section B*, *64*(9), 795.

Burby, J. W. (2017). Magnetohydrodynamic motion of a two-fluid plasma. *Physics of Plasmas*, *24*(8), 082104.

Chalise, R., & Khanal, R. (2012). A kinetic trajectory simulation model for magnetized plasma sheath. *Plasma Physics and Controlled Fusion*, *54*(9), 095006.

Chalise, R., & Khanal, R. (2015a). Self-consistent one dimension in space and three dimension in velocity kinetic trajectory simulation model of magnetized plasma-wall transition. *Physics of Plasmas*, *22*(11), 113505.

Chalise, R., & Khanal, R. (2015b). The study of kinetic energy of ion and sheath thickness in magnetized plasma sheath. *Journal of Materials Science and Engineering A*, *5*, 41.

Chauhan, S., Ranjan, M., Bandyopadhyay, M., & Mukherjee, S. (2016). Droplet shaped anode double layer and electron sheath formation in magnetically constricted anode. *Physics of Plasmas*, *23*(1), 013502.

Chaulagain, R. (2017). *Effect of temperature variation in two-ion species magnetized plasma sheath* (M.Sc. Dissertation). Central Department of Physics, Institute of Science and Technology, Tribhuvan University, Kathmandu, Nepal.

Chen, F. F. (2016). *Introduction to plasma physics and controlled fusion* (3rd ed.). Switzerland: Springer International Publishing.

Chodura, R. (1982). Plasma–wall transition in an oblique magnetic field. *The Physics of Fluids*, *25*(9), 1628.

Cong, C., Yun-yun, C., & Fen-ping, C. (2018). A comparative study on the propagation characteristics of electromagnetic waves in inhomogeneous plasma sheath. *Optik-International Journal for Light and Electron Optics*, *155*, 390.

Crookes, W. (1879). V. the bakerian lecture.—on the illumination of lines of molecular pressure, and the trajectory of molecules. *Philosophical Transactions of the Royal Society of London*, *170*, 135.

Dhakal, N. (2013). *Sheath structure for different density of the presheath plasma* (M.Sc. Dissertation). Central Department of Physics, Tribhuvan University, Kathmandu, Nepal.

Driouch, I., & Chatei, H. (2013). Fluid simulation of the ion temperature effects on a collisional magnetized sheath of a dusty plasma. *Journal of Applied Fluid Mechanics*, *6*(4), 511.

Duarte, V. N., & Clemente, R. A. (2011). Electron inertia effects on the planar plasma sheath problem. *Physics of Plasmas*, *18*(4), 043504.

Falessi, M. V., & Zonca, F. (2018). Gyrokinetic theory for particle and energy transport in fusion plasmas. *Physics of Plasmas*, *25*(3), 032306.

Foroutan, G. (2010). Fluid simulation of an electrostatic plasma sheath with two species of positive ions and charged nanoparticles. *Physics of Plasmas*, *17*(12), 123711.

Franklin, R. N. (1976). Plasma phenomena in gas discharges. *Oxford and New York, Clarendon Press*.

Franklin, R. N. (1989). Nomenclature for the plasma-sheath transition region. *Journal of Physics D: Applied Physics*, *22*(6), 860.

Franklin, R. N. (2000). Plasmas with more than one species of positive ion and the bohm criterion. *Journal of Physics D: Applied Physics*, *33*(24), 3186.

Fu, Y., Zhang, P., Verboncoeur, J. P., Christlieb, A. J., & Wang, X. (2018). Effect of surface protrusion on plasma sheath properties in atmospheric microdischarges. *Physics of Plasmas*, *25*(1), 013530.

Godyak, V. A., & Sternberg, N. (1990). Dynamic model of the electrode sheaths in symmetrically driven rf discharges. *Physical Review A*, *42*(4), 2299.

Goswami, M., & Ramachandran, H. (1999). A self-consistent analysis of a collisional presheath. *Physics of Plasmas*, *6*(12), 4522.

Gurung, J. B. (2012). *Plasma sheath structure for different presheath current densities* (M.Sc. Dissertation). Central Department of Physics, Institute of Science and Technology, Tribhuvan University, Kathmandu, Nepal.

Gyergyek, T., & Kovačič, J. (2015). Fluid model of the sheath in front of a floating electrode immersed in a magnetized plasma with oblique magnetic field: Some comments on ion source terms and ion temperature effects. *Physics of Plasmas*, *22*(4), 043502.

Hatami, M., Shokri, B., & Niknam, A. (2008). Collisional effects in magnetized plasma sheath with two species of positive ions. *Journal of Physics D: Applied Physics*, *42*(2), 025204.

Hatami, M. M. (2013). The properties of the space-charge and net current density in magnetized plasmas. *Plasma Science and Technology*, *15*(12), 1169.

Hatami, M. M., Niknam, A. R., Shokri, B., & Ghomi, H. (2008, May). Magnetized plasma sheath with two species of positive ions. *Physics of Plasmas*, *15*(5), 053508.

Hatami, M. M., & Shokri, B. (2013). Sheath formation criterion in magnetized electronegative plasmas with thermal ions. *Physics of Plasmas*, *20*(3), 033506.

Hatami, M. M., Shokri, B., & Niknam, A. R. (2008). Numerical investigation of the magnetized plasma sheath characteristics in the presence of negative ions. *Physics of Plasmas*, *15*(12), 123501.

Holgate, J. T., Coppins, M., & Allen, J. E. (2018). Electrohydrodynamic stability of a plasma-liquid interface. *Applied Physics Letters*, *112*(2), 024101.

Hu, P. N., & Ziering, S. (1966). Collisionless theory of a plasma sheath near an electrode. *The Physics of Fluids*, *9*(11), 2168.

Huang, C.-W., Chen, Y.-C., & Nishimura, Y. (2015). Particle-in-cell simulation of plasma sheath dynamics with kinetic ions. *IEEE Transactions on Plasma Science*, *43*(2), 675.

Jacquot, J., Bobkov, V., Colas, L., Heuraux, S., Křivská, A., Lu, L., ... Team, A. U. (2015). Full wave propagation modelling in view to integrated icrh wave coupling/rf sheaths modelling. *AIP Conference Proceedings*, *1689*(1), 050008.

Joshi, P. (2015). *Study of non linear oscillations of plasma electrons* (M.Sc. Dissertation). Central Department of Physics, Institute of Science and Technology, Tribhuvan University, Kathmandu, Nepal.

Joung, M., Cho, M., Namkung, W., Lho, T., Kim, D. C., Kim, J. S., ... Kim, G. H. (2007). Variation of plasma parameters on boundary conditions in an inductively coupled plasma source for hyperthermal neutral beam generation. *Physics of Plasmas*, *14*(10), 103502.

Karki, U. (2018). *Effect of collision in magnetized plasma sheath* (M.Sc. Dissertation). Central Department of Physics, Institute of Science and Technology, Tribhuvan University, Kathmandu, Nepal.

Kaw, P. K., & Bandyopadhyay, I. (2012). *The case for fusion. fusion physics*. (ed. M. Kikuchi, K. Lackner and M. Q. Tran) Vienna, Austria. IAEA Publication.

Khadka, K. (2017). *Effect of ionization ratio of two species of positive ions on magnetized plasma sheath* (M.Sc. Dissertation). Central Department of Physics, Institute of Science and Technology, Tribhuvan University, Kathmandu, Nepal.

Khanal, R. (2003). *A kinetic trajectory simulation model for bounded plasmas* (Ph.D. Thesis). Innsbruck University, Innsbruck, Austria.

Krasheninnikova, N. S., & Tang, X. (2010). Equilibrium properties of the plasma sheath with a magnetic field parallel to the wall. *Physics of Plasmas*, *17*(6), 063508.

Kshetri, V. S. (2015). *Study of ion velocity at presheath-sheath boundary for different electric and magnetic fields* (M.Sc. Dissertation). Central Department of Physics, Institute of Science and Technology, Tribhuvan University, Kathmandu, Nepal.

LaBombard, B., Hughes, J. W., Mossessian, D., Greenwald, M., Lipschultz, B., Terry, J. L., ... others (2005). Evidence for electromagnetic fluid drift turbulence controlling the edge plasma state in the alcator c-mod tokamak. *Nuclear Fusion*, *45*(12), 1658.

Langmuir, I. (1928). Oscillations in ionized gases. *Proceedings of the National Academy of Sciences*, *14*(8), 627.

Langmuir, I. (1929). The interaction of electron and positive ion space charges in cathode sheaths. *Physical Review*, *33*(6), 954.

Li, J.-j., Ma, J. X., & Wei, Z.-a. (2013). Sheath and boundary conditions in a collisional magnetized warm electronegative plasma. *Physics of Plasmas*, *20*(6), 063503.

Lin, B., Xiang, N., & Ou, J. (2016). The ion polytropic coefficient in a collisionless sheath containing hot ions. *Physics of Plasmas*, *23*(8), 083508.

Lindl, J. D. (1998). *Inertial confinement fusion: the quest for ignition and energy gain using indirect drive*. USA: American Institute of Physics.

Mathur, D. S. (2012). *Mechanics*. New Delhi, India: S. Chand & Co.

Mishra, A. (2006). *Sheath structure for different density of the presheath plasma* (M.Sc. Dissertation). Central Department of Physics, Tribhuvan University, Kathmandu, Nepal.

Morales Crespo, R. (2018). Positive ion temperature effect on the plasma-wall transition. *Physics of Plasmas*, *25*(6), 063509.

Moulick, R., & Goswami, K. S. (2014). Sheath formation under collisional conditions in presence of dust. *Physics of Plasmas*, *21*(8), 083702.

Myra, J. R., & D'Ippolito, D. A. (2015). Radio frequency sheaths in an oblique magnetic field. *Physics of Plasmas*, *22*(6), 062507.

Nakatsutsumi, M., Sentoku, Y., Korzhimanov, A., Chen, S., Buffechoux, S., Kon, A., ... others (2018). Self-generated surface magnetic fields inhibit laser-driven sheath acceleration of high-energy protons. *Nature communications*, *9*(1), 280.

Oksuz, L., & Hershkowitz, N. (2002). First experimental measurements of the plasma potential throughout the presheath and sheath at a boundary in a weakly collisional plasma. *Physical Review Letters*, *89*(14), 145001.

Pandey, B. P., Samarian, A., & Vladimirov, S. V. (2008). Plasma sheath in the presence of an oblique magnetic field. *Plasma Physics and Controlled Fusion*, *50*(5), 055003.

Persson, K.-B. (1962). Inertia-controlled ambipolar diffusion. *The Physics of Fluids*, *5*(12), 1625.

Poudel, T. (2012). *Effect of ion polytropic constant on particle densities in plasma sheath* (M.Sc. Dissertation). Central Department of Physics, Institute of Science and Technology, Tribhuvan University, Kathmandu, Nepal.

Press, W. H., Teukolsky, S. A., Vetterling, W. T., & Flannery, B. P. (2007). *Numerical recipes 3rd edition: The art of scientific computing* (3rd ed.). New York, United States of America: Cambridge University Press.

Qing, S., & Hu, Z. (2017). Effect of total emitted electron velocity distribution function on the plasma sheath near a floating wall. *AIP Advances*, *7*(8), 085220.

Qingquan, Y., Zhong, F., Guosheng, X. U., Ning, Y., Liang, C., Xiang, L., ... others (2018). Combined langmuir-magnetic probe measurements of type-i elmy filaments in the east tokamak. *Plasma Science and Technology*, *20*(6), 065101.

Rana, T. R. (2009). *Sheath structure for different levels of ionization of beryllium plasma* (M.Sc. Dissertation). Central Department of Physics, Institute of Science and Technology, Tribhuvan University, Kathmandu, Nepal.

Regmi, Y., Chalise, R., & Khanal, R. (2018). Response of carbon and tungsten surfaces to hydrogen plasma of different temperatures. *Physics of Plasmas*, *25*(4), 043521.

Riemann, K. U. (1981). Kinetic theory of the plasma sheath transition in a weakly ionized plasma. *The Physics of Fluids*, *24*(12), 2163.

Riemann, K. U. (1991). The bohm criterion and sheath formation. *Journal of Physics D: Applied Physics*, *24*(4), 493.

Riemann, K. U. (1994). Theory of the collisional presheath in an oblique magnetic field. *Physics of Plasmas*, *1*(3), 552.

Riemann, K. U. (1997). The influence of collisions on the plasma sheath transition. *Physics of Plasmas*, *4*(11), 4158.

Riemann, K. U. (2000). Theory of the plasma-sheath transition. *Journal of Technical Physics*, *41*(1), 89.

Riemann, K. U., Seebacher, J., Tskhakaya Sr, D. D., & Kuhn, S. (2005). The plasma–sheath matching problem. *Plasma Physics and Controlled Fusion*, *47*(11), 1949.

Sapkota, B. (2016). *Investigation of ion dynamics on collisional magnetized plasma sheath* (M.Sc. Dissertation). Central Department of Physics, Institute of Science and Technology, Tribhuvan University, Kathmandu, Nepal.

Scarborough, J. B. (1966). *Numerical mathematical physics* (6$^{\text{th}}$ ed.). New York, United States of America: Oxford and IBH Publishing.

Schupfer, N., Tskhakaya Sr, D. D., Khanal, R., Kuhn, S., Aumayr, F., da Silva, S. F., & Winter, H. P. (2006). Effect of particle-induced electron emission (piee) on the plasma sheath voltage. *Plasma Physics and Controlled Fusion*, *48*(8), 1093.

Sheehan, J., Kaganovich, I., Wang, H., Sydorenko, D., Raitses, Y., & Hershkowitz, N. (2014). Effects of emitted electron temperature on the plasma sheath. *Physics of Plasmas*, *21*(6), 063502.

Sheehan, J. P., Hershkowitz, N., Kaganovich, I. D., Wang, H., Raitses, Y., Barnat, E. V., ... Sydorenko, D. (2013). Kinetic theory of plasma sheaths surrounding electron-emitting surfaces. *Physical Review Letters*, *111*(7), 075002.

Shi, L., Yao, B., Zhao, L., Liu, X., Yang, M., & Liu, Y. (2018). An integrative time-varying frequency detection and channel sounding method for dynamic plasma sheath. *AIP Advances*, *8*(1), 015103.

Shoucri, M., Cardinali, A., Matte, J. P., & Spigler, R. (2004). Numerical study of plasma-wall transition using an eulerian vlasov code. *The European Physical Journal D-Atomic, Molecular, Optical and Plasma Physics*, *30*(1), 81.

Simmons, G. F. (2016). *Differential equations with applications and historical notes* (3$^{\text{rd}}$ ed.). New York, United States of America: CRC Press.

Smirnov, R., Takizuka, T., et al. (2007). Effect of oblique magnetic field on release conditions of dust particle from plasma-facing wall. *Research Report NIFS-Series*.

Stamate, E., & Sugai, H. (2005). Modal focusing effect of positive and negative ions by a three-dimensional plasma-sheath lens. *Physical Review Letters*, *94*(12), 125004.

Tiwari, R. K. (2006). *Propagation of ion acoustic waves in plasma presheath* (M.Sc. Dissertation). Central Department of Physics, Institute of Science and Technology, Tribhuvan University, Kathmandu, Nepal.

Tskhakaya, D., Eliasson, B., Shukla, P. K., & Kuhn, S. (2004). On the theory of plasma-wall transition layers. *Physics of Plasmas*, *11*(8), 3945.

Tskhakaya, D., Kuhn, S., Petržilka, V., & Khanal, R. (2002). Effects of energetic electrons on magnetized electrostatic plasma sheaths. *Physics of Plasmas*, *9*(6), 2486.

Wesson, J. (1997). Poloidal distribution of impurities in a rotating tokamak plasma. *Nuclear fusion*, *37*(5), 577.

Wesson, J., & Campbell, D. J. (2011). *Tokamaks* (Vol. 149). Oxford University Press.

Yankun, J., Xiu, Z., Huiping, L., & Minghui, Q. (2011). Bohm criterion in a magnetized plasma sheath. *Plasma Science and Technology*, *13*(5), 519.

Yasserian, K., & Aslaninejad, M. (2012). On the space-charge formation in a collisional magnetized electronegative plasma. *Physics of Plasmas*, *19*(7), 073507.

Yasserian, K., Aslaninejad, M., & Ghoranneviss, M. (2009). Structure of presheath-sheath in magnetized electronegative plasma. *Physics of Plasmas*, *16*(2), 023504.

Yu, D.-R., Wu, Z.-W., Ning, Z.-X., & Wang, X.-G. (2007). Measurement of sheath thickness by lining out grooves in the hall-type stationary plasma thrusters. *Physics Letters A*, *364*(2), 146.

Yuan, K., Shen, L., Yao, M., Deng, X., Chen, Z., & Hong, L. (2018). Studies on the transmission of sub-thz waves in magnetized inhomogeneous plasma sheath. *Physics of Plasmas*, *25*(1), 013302.

Zheng-Xiong, W., Jin-Yuan, L., Xiu, Z., Yue, L., & Xiao-Gang, W. (2003). Sheath structure of an electronegative plasma. *Chinese Physics Letters*, *20*(9), 1537.

Zou, X., Qiu, M., Liu, H., Zhang, L., Liu, J., & Gong, Y. (2008). The ion density distribution in a magnetized plasma sheath. *Vacuum*, *83*(1), 205.

APPENDIX

A. Publications

1) Adhikari, B. R., & Khanal, R. (2013a). Introduction to the plasma state of matter. *The Himalayan Physics, 4*(4), 60.

2) Adhikari, B. R., & Khanal, R. (2013b). Plasma sheath studies in Nepal. *Vivek, 9*, 292.

3) Adhikari, B. R., Lamichhane, H. P.,& Khanal, R. (2016). Temporal dependence of components of velocity of ions in a magnetized plasma sheath for different obliqueness of the magnetic field. *Proceedings of the 5th PSSI-plasma scholars colloquium*. Cuttak, India: Department of Physics, Ravenshaw University, p. 32.

4) Adhikari, B. R., Lamichhane, H. P., & Khanal, R. (2017). Progress in tokamak fusion research. *Symmetry, 11*, 49.

5) Adhikari, B. R., Basnet, S., Lamichhane, H. P.,& Khanal, R. (2018). Beat frequency and velocity variation of ions in a magnetized plasma sheath for different obliqueness of the magnetic field. *Journal of Institute of Science and Technology, 23*, 88.

6) Adhikari, B. R., Basnet, S., Lamichhane, H. P., & Khanal, R. (2019). Presheath-sheath coupling for kinetic trajectory simulation of a magnetized plasma sheath. *AIP Advances, 9*(5), 055123.

7) Adhikari, B. R., Basnet, S., Lamichhane, H. P.,& Khanal, R. (2019). Variation of velocity component of ions in a magnetized plasma sheath for different obliqueness of the magnetic field. *The Himalayan Physics, 8*, 71.

8) Adhikari, B. R., Basnet, S., Lamichhane, H. P., & Khanal, R. (2020). Variation of velocity of ions in a magnetized plasma sheath for different magnetic field. *Journal of Nepal Physical Society, 6*(1), 25.

9) Adhikari, B. R., Lamichhane, H. P., & Khanal, R. (2021). Modulation frequency and velocity variation of ions in a magnetized plasma sheath for different obliqueness of the field. *BIBECHANA*. (Accepted for publication)

B. Oral presentations

1) International Conference on Physics of Space and Materials (ICPSM-2017), 2-3 September, 2017, St. Xavier's College, Kathmandu, Nepal.

2) 5th PSSI-Plasma Scholars Colloquium (PSC-2016), 27-28 August 2016, Ravenshaw University, Cuttack, India.

3) Symposium on Plasma Physics and Material Science, 9 April, 2016 Central Department of Physics, Tribhuvan University, Kathmandu.

4) International Conference on Explorations in Physics (ICEP-2018), 29-31 May, 2018, Kathmandu, Nepal

C. Poster presentations

1) International Conference on Nano- Materials and Computational Physics, 27-28 December, 2018, Central Department of Physics, Tribhuvan University, Kirtipur, Nepal.

2) 2nd Young Scientists Summit-2017, 28-29 January, 2017, RECAST, Tribhuvan University, Kirtipur, Kathmandu, Nepal.

3) International Conference on Plasma Science, Technology and Application- 2016 (ICPSTA-2016), 20-21 January, 2016, Amity University, Lucknow, India.

4) 7th International Conference on the Frontiers of Plasma Physics and Technology (FPPT-7), 13-17 April, 2015, Kochi, India.

5) International Conference on Plasma Science and Applications (ICPSA-2014), 22-24 September, 2014, Kathmandu, Nepal.

D. Research visits

1) Plasma Lab. at Kathmandu University, Dhulikhel, Nepal, 22-24 September, 2014.

2) Saha Institute of Nuclear Physics, Kolkata, India, 23-25 October, 2013.

3) Plasma Lab at VIT University, Chennai, India, 03-10 July 2014.

4) Plasma Lab at Amity University, Lucknow, India, 20-23 January, 2016.

5) Advanced Plasma Lab at Ravenshaw University, Cuttak, India, 27-31 August, 2016.

E. Participation in research methodology lectures

1) Lecture series on Research Methodology delivered by Prof. Dr. Subodh R. Shenoy, TIFR, India during 6 November to 22 December 2017, Organized by Central Department of Physics, Tribhuvan University, Kirtipur, Nepal.

2) Training Workshop on Scientific Writing during 21-25 June 2018, organized by Research Cenre for Applied Science and Technology (RECAST), Tribhuvan University, Kathmandu, Nepal.

Presheath-sheath coupling for kinetic trajectory simulation of a magnetized plasma sheath

Cite as: AIP Advances 9, 055123 (2019); doi: 10.1063/1.5088107
Submitted: 8 January 2019 • Accepted: 15 May 2019 •
Published Online: 28 May 2019

Bhesha Raj Adhikari, Suresh Basnet,[a] Hari Prasad Lamichhane, and Raju Khanal

AFFILIATIONS

Central Department of Physics, Tribhuvan University, Kirtipur, Kathmandu 44613, Nepal

[a]Email: sbplasma1986@gmail.com

ABSTRACT

The coupling of presheath-sheath parameters is extended for the study of magnetized plasma sheath using the kinetic trajectory simulation (KTS) method, in which the final self-consistent states are obtained iteratively by solving the kinetic equations. In our case, it is assumed that the ion and electron velocity distribution functions are cut-off Maxwellians at the sheath entrance. The results show that the cut-off and Maxwellian maximum velocities have equal magnitudes at the sheath entrance and at wall. The presheath electron temperature has a considerable effect on the self-consistent potential profile which affects the Child sheath thickness. The latter increases from 3.8320 μm to 5.4190 μm when the presheath electron temperature increases from 10 eV to 20 eV. It is found that the number of ions reaching wall is higher than that of the electrons and hence the space charge density has its maximum value there. Furthermore, the temperature of ions in the sheath region increases with the increase in presheath ion temperature. Moreover, the cut-off distribution causes our simulation result to deviate from the theoretical result found for the Boltzmann distribution by about 3%. The coupling scheme presented here provides a basis for smooth transition of plasma parameters at the presheath-sheath interface. The proper understanding of the magnetized plasma-wall transition plays a vital role for further exploring the plasma sheath characteristics which has useful applications in fusion and industrial plasma devices.

I. INTRODUCTION

The kinetic trajectory simulation (KTS) method is used for the understanding of magnetized plasma sheath properties, and a scheme for its coupling with presheath is presented. It has a wide range of growing applications in various plasma fields such as plasma fusion device, sputtering, etching, etc.[1–8] As the magnetized plasma comes in contact with the material wall, a thin skinny space charge region is formed ("sheath") in the order of few Debye lengths.[9] In the sheath region, the potential has sharp gradient and the effect of this potential can be felt up to quasineutral plasma ("presheath"), which accelerates the ions in the presheath zone so that the marginal Bohm sheath criterion is satisfied.[10]

$$|u^i_{n,SE}| = c_s \equiv \left(T^e_{ps}/m^i\right)^{0.5} \tag{1}$$

The equation (1) is the simplest form of Bohm sheath condition for vanishing ion temperature. Moreover, the general hydrodynamic Bohm condition is written as[11]

$$|u^i_{n,SE}| = c_s \equiv \left[\left(T^e_{ps} + \gamma^i T^i_{ps}\right)/m^i\right]^{0.5} \tag{2}$$

where $u^i_{n,SE}$ is the ion fluid-velocity component normal to the wall, γ^i is ion polytropic constant, T^e_{ps} and T^i_{ps} are presheath electron and ion temperatures in (eV), respectively and m^i is the mass of positive ion.

The Bohm-Chodura criterion, which defines the magnetic presheath entrance (MPSE), can be written as[12]

$$|u^i_{||,MPSE}| = c_s \tag{3}$$

in which $u^i_{||,MPSE}$ is the ion fluid-velocity component parallel to the magnetic field at the MPSE.

H. Pedit and S. Kuhn[13] developed KTS method for two-dimensional bounded collisionless plasma. In this method, the velocity distribution function for the particle species can be calculated via their respective particle trajectories. K. U. Riemann[14] presented analytic solution for presheath-sheath transition for weakly ionized plasma using self-consistent kinetic theory. The exact sheath-presheath solutions are constructed by assuming the Boltzmann distribution for electrons and singly charged positive

ions in contact with a material wall. It is found that the sheath potential is monotonic and the ion distribution functions follow the half Maxwellian distribution inside the core plasma. A. V. Vasenkov and B. D. Shizgal[15] studied plasma sheath of a dc glow discharge using kinetic the approach. The electric field is calculated from the Poisson's equation using the velocity distribution functions. It is found that the ion distribution function varies strongly with the decrease in the ratio of the Debye length to the ion mean free path. S. D. Baalrud and C. C. Hegna[16] developed the kinetic Bohm condition based on the positive exponent velocity moments, which contrasted the conventional kinetic Bohm condition. The lower velocity particles are unimportant in the new theory whereas it dominates in the conventional theory. The collision is very important to determine the particle distribution functions throughout the presheath.

R. Chalise and R. Khanal[17,18] developed the kinetic trajectory simulation method for the time independent, collisionless $1d3v$ magnetized plasma sheaths. It is found that the magnetized plasma sheath has two distinct regions; magnetic field dominant region and electric field dominant region. The self-consistent potential sharply decreases towards the wall, which becomes prominent with increase in strength of the magnetic field. In their work, they used the coupling scheme developed for electrostatic cases.[19] In this work, we extend the presheath-sheath coupling scheme considering $1d3v$ magnetized plasma sheath, which is crucial to further enhance the KTS method.

II. BASIC PRINCIPLE OF KINETIC THEORY AND PLASMA SHEATH MODEL

The kinetic theory is the statistical treatment of the assembly of particles, from which measurable macroscopic variables can be derived by averaging over the particle distribution. The fluid theory is the simplest description of plasma which is generally preferred in the presheath region. On the other hand, in the sheath region, as the physical parameters have sharp gradients, the kinetic theory is preferred. The kinetic trajectory simulation (KTS) method is an iterative method for the numerical calculation of self-consistent, time-independent kinetic plasma bounded in the given spatial region.[17–19] In this method, the information of particles in the phase space is carried by the spatial and velocity dependence distribution functions $f^s(\vec{r},\vec{v})$, and this information at each and every point can be obtained by solving the collisionless kinetic equations along with respective particles trajectories, where 's' ($s = i$ for ion, e for electron). In the iteration scheme, the main iteration block carries out the m^{th} iteration for the given old potential distribution. The new ion velocity distribution function is obtained via numerical trajectory integration of the kinetic equation, based on the trajectories defined by the old electric field. In the present case we assume that the plasma is collisionless and hence the particle's distribution function is constant as the particles move in the phase space. The electron density is calculated analytically by assuming half Maxwellian distribution at the injection sheath entrance. The acceleration of a species-s in the presence of macroscopic electromagnetic force is

$$\vec{a}^s = \frac{q^s}{m^s}\left(\vec{E} + \vec{v} \times \vec{B}\right) \tag{4}$$

where q^s and m^s are charge and mass of the species-s. In the absence of collisions, the fundamental kinetic equation for the species-s is well-known Vlasov equation[9]

$$\frac{df^s}{dt} \equiv \left(\frac{\partial}{\partial t} + \vec{v}\cdot\nabla + \vec{a}^s(\vec{r},\vec{v},t)\cdot\nabla_v\right) f^s(\vec{r},\vec{v},t) = 0 \tag{5}$$

The relation between an electric field and the electrostatic potential $\phi(\vec{r})$ is

$$\vec{E}(\vec{r}) = -\nabla\phi(\vec{r}) \tag{6}$$

The electrostatic potential satisfies the Poisson's equation

$$\varepsilon_0\nabla^2\phi(\vec{r}) = -\rho(\vec{r}) \tag{7}$$

where

$$\rho(\vec{r}) = \sum_s q^s n^s(\vec{r}) \tag{8}$$

is the space charge density.

The number density of particle species-s is

$$n^s(\vec{r}) = \iiint f^s(\vec{r},\vec{v})d^3v \tag{9}$$

A. Planar sheath geometry

The schematic diagram of $1d3v$ planar sheath geometry is shown in Fig. 1. The magnetized plasma is bounded by two parallel planes at $x = L$ (the sheath entrance) and $x = 0$ (the material wall), which is our region of interest. The oblique magnetic field acts on the x-y plane and makes angle β with normal to the wall. In the present case, we consider the collisionless magnetized plasma consisting of singly charged electropositive ions (hydrogen) and electrons. The $1d1v$ electron and ion phase spaces in a monotonically decreasing potential towards the left-hand boundary (wall) are shown in Figs. 2 and 3, respectively.[19]

In Fig. 2, we assign the type-I trajectories for those electrons entering in to the simulation region at the right hand boundary with sufficiently negative velocities $v_x < -v_{xs}(x)$; however they can reach the left hand boundary; where $v_{xs}(x)$ is the electron separatrix, which separates the regions of passing electrons from those being reflected. The type-II trajectory represents those electrons injected at the starting point and their velocity becomes zero at the left hand boundary. The type-III implies the electrons enter the simulation region at the right hand boundary with velocities $-v_{xs}(x) < v_x < v_{xs}(x)$ and

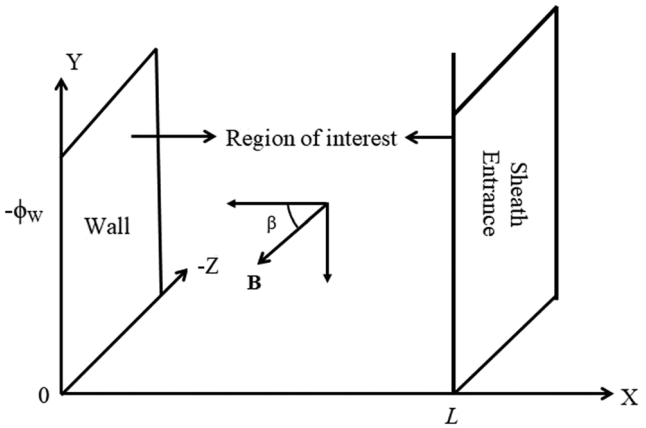

FIG. 1. Geometry of $1d3v$ plasma sheath model.

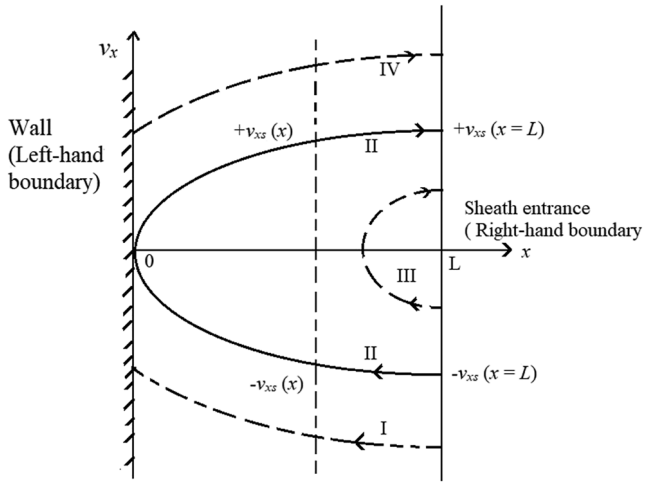

FIG. 2. Electron phase space in a potential decreasing monotonically towards the wall.

get reflected before reaching the left hand boundary. The type-IV trajectory is for those electrons, which enter the simulation region with positive velocities such that $v_{xs}(x) < v_x$ and they are accelerated towards the right hand boundary.

In Fig. 3, the type-I trajectory is for those ions enter the simulation region at the right-hand boundary with negative velocities $-v_{xs}(x) > v_x$. The type-II trajectory is assigned for those ions injected at the starting point whose velocity becomes zero at the right-hand boundary. The type-III trajectories are those ions, which enter the simulation region at the left-hand boundary with positive velocities $-v_{xs}(x) < v_x < v_{xs}(x)$ and get reflected before reaching the right-hand boundary. The type-IV trajectory is for those ions, which enter the simulation region with ion velocities $v_x > v_{xs}(x)$.

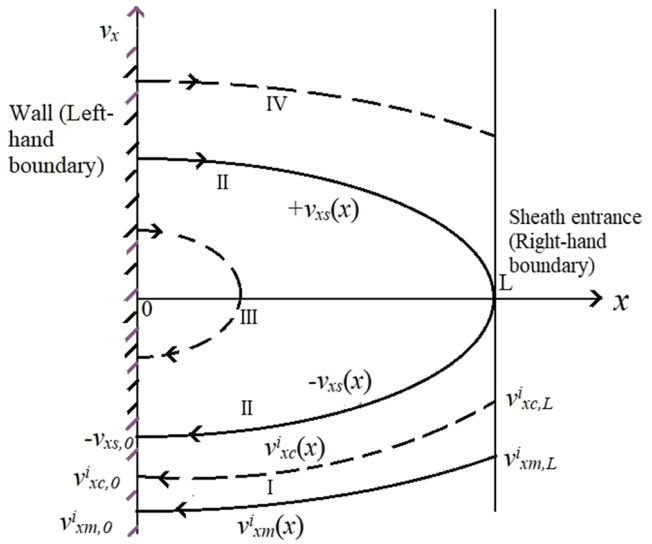

FIG. 3. Ion phase space in a potential decreasing monotonically towards the wall.

Likewise the phase spaces for $1d3v$ magnetized plasma are considered.

Due to absorbing properties of the material wall, the velocity distribution is cut-off Maxwellian. The electron velocity distribution function is

$$f^e(x,\vec{v}) = A^e \exp\left[-\left(\frac{v_x^2+v_y^2+v_z^2}{v_t^{e2}}\right)+\frac{e\phi}{k_B T^e}\right]\times H\left[v_c^e(x)-v_x\right] \tag{10}$$

in which A^e is the amplitude of the electron velocity distribution function, which is related to the presheath electron density, $v_t^s = (2k_BT^s/m^s)^{0.5}$ is the thermal velocity of species-s, T^s is the sheath side temperature of species-s, $v_c^e(x) = [2e(\phi(x)-\phi_w)/m^e]^{0.5}$ is the cut-off velocity of electron at x, ϕ_w is the wall potential, and $H(x)$ is Heaviside step function.

The ion velocity distribution function at $x = L$ is

$$f^i(x=L,\vec{v}) = A^i \exp\left[-\left(\frac{\left(v_x-v^i_{xm,L}\right)^2+v_y^2+v_z^2}{v_t^{i2}}\right)\right]\times H\left[v^i_{xc,L}-v_x\right] \tag{11}$$

in which A^i is the amplitude of the ion velocity distribution function, which is related to the presheath ion density, $v^i_{xm,L}$ and $v^i_{xc,L}$ are the Maxwellian-maximum and cut-off velocities, respectively at $x = L$.

The particle density of species-s at $x = L$ is

$$n_L^s = \frac{A^s v_t^{s^3}\pi^{3/2}}{2}C^s \tag{12}$$

The fluid velocity of species-s is given as

$$\vec{u}^s = \frac{1}{n_L^s}\int \vec{v} f^s(x,\vec{v})d^3v \tag{13}$$

Such that

$$\vec{u}_L^e = -\left(\frac{v_t^e}{\sqrt{\pi}}\frac{D^e}{C^e}\right)\hat{i} \tag{14}$$

and

$$\vec{u}_L^i = \left[v^i_{xm,L}-\frac{v_t^i}{\sqrt{\pi}}\frac{D^i}{C^i}\right]\hat{i} \tag{15}$$

The presheath side electron temperature at $x = L$ is given as

$$T_L^e = \frac{1}{3n_L^e k_B}\iiint d^3v m^e\left(v-u_L^e\right)^2 f^e(x,\vec{v}) \tag{16}$$

$$= T^e\left[1-\frac{2}{3}\sqrt{\frac{-e\phi_w}{\pi k_B T^e}}\frac{D^e}{C^e}-\frac{2}{3\pi}\frac{D^{e^2}}{C^{e^2}}\right] \tag{17}$$

in which $D^e = \exp\left(\frac{e\phi_w}{k_BT^e}\right)$ and $C^e = 1+erf\sqrt{\frac{-e\phi_w}{k_BT^e}}$.

Similarly, the presheath side ion temperature at $x = L$ is given as

$$T_L^i = \frac{1}{3n_L^i k_B}\iiint d^3v m^i\left(v-u_L^i\right)^2 f^i(x,\vec{v}) \tag{18}$$

$$= T^i\left[1 - \frac{2\tau_{cL}^i}{3\sqrt{\pi}}\frac{D^i}{C^i} - \frac{2}{3\pi}\frac{D^{i2}}{C^{i2}}\right] \tag{19}$$

in which $\tau_{cL}^i = \left(v_{xc,L}^i - v_{xm,L}^i\right)/v_t^i$, $D^i = \exp(-\tau_{cL}^{i\,2})$ and $C^i = 1 + erf(\tau_{cL}^i)$.

The analytic expression for electron density distribution is

$$n^e(x) = \iiint d^3v f^e(x,\vec{v}) \tag{20}$$

$$= n_L^e \exp\left(\frac{e\phi(x)}{k_B T^e}\right)\left\{\frac{1 + erf\left[\sqrt{\frac{e(\phi(x)-\phi_w)}{k_B T^e}}\right]}{1 + erf\left(\sqrt{\frac{-e\phi_w}{k_B T^e}}\right)}\right\} \tag{21}$$

B. Kinetic Bohm criterion for coupling scheme

The condition has to be satisfied by injected ion velocity distribution function so that the sheath is formed that shields quasineutral plasma. From the Poisson's equation (Eq. 7),

$$\varepsilon_0\frac{d^2\phi}{dx^2} = -\rho(\phi) \tag{22}$$

For the non-oscillating solution at $x \to L$,

$$\left[\frac{dn^i}{d\phi} - \frac{dn^e}{d\phi}\right]_{x\to L} = 0 \tag{23}$$

The conservation of ion energy reads

$$v_x = \sqrt{v_{xL}^2 - \frac{2e\phi}{m^i}} \tag{24}$$

where $v_{x\,L}$ is the velocity of ion at $x = L$.

For the ions, the equation (9) becomes

$$n^i = \iiint f^i(x,\vec{v})d^3v \tag{25}$$

Using equation (24) in equation (25) and differentiating with respect to ϕ yields,

$$\frac{dn^i}{d\phi} = \frac{e}{m^i}\int_{-\infty}^{v_{xc,L}^i}\int_{-\infty}^{\infty}\int_{-\infty}^{\infty}\frac{dv_x}{v_x^2}f^i(x=L,\vec{v})dv_y dv_z \times \left(1 - \frac{2e\phi}{m^i v_x^2}\right)^{-3/2} \tag{26}$$

At $x \to L$, $e\phi < m^i v_x^2$ and hence, the kinetic Bohm condition is

$$\int_{-\infty}^{v_{xc,L}^i}\int_{-\infty}^{\infty}\int_{-\infty}^{\infty}\frac{dv_x}{v_x^2}\exp\left[-\frac{\left(v_x - v_{xm,L}^i\right)^2 + v_y^2 + v_z^2}{v_t^{i2}}\right]dv_y dv_z = \frac{m^i n_L^e}{A^i k_B T^e}\left[1 + \sqrt{\frac{-k_B T^e}{e\pi\phi_w}}\frac{D^e}{C^e}\right] \tag{27}$$

C. Presheath-sheath coupling

In the presheath-sheath coupling mechanism, the sheath side parameters n^s, T^s and u^s are coupled with the presheath side parameters n_s^{ps}, T_s^{ps} and u_{ps}^s. For the unperturbed flow of plasma parameters at the presheath-sheath boundary, the coupling scheme satisfies an important requirement i.e., quasineutrality condition, sheath edge singularity condition, continuity of first three moments and kinetic Bohm condition. The continuity of the physical parameters is given by

$$n_L^e = n_{ps}, \quad n_L^i = n_{ps}, \tag{28}$$

$$u_L^e = u_{ps}^e, \quad u_L^i = u_{ps}^i, \tag{29}$$

$$T_L^e = T_{ps}^e, \quad T_L^i = T_{ps}^i, \tag{30}$$

The coupling equations are

$$n_{ps}^e = n_{ps} = 4A^e C^e\left(\frac{\pi k_B T^e}{2m^e}\right)^{1.5} \tag{31}$$

$$n_{ps}^i = n_{ps} = 4A^i C^i\left(\frac{\pi k_B T^i}{2m^i}\right)^{1.5} \tag{32}$$

$$u_{ps}^e = -\sqrt{\frac{2k_B T^e}{\pi m^e}}\frac{D^e}{C^e} \tag{33}$$

$$u_{ps}^i = v_{mL}^i - \sqrt{\frac{2k_B T^i}{\pi m^i}}\frac{D^i}{C^i} \tag{34}$$

$$T_{ps}^e = T^e\left[1 - \frac{2}{3}\sqrt{\frac{-e\phi_w}{\pi k_B T^e}}\frac{D^e}{C^e} - \frac{2}{3\pi}\frac{D^{e2}}{C^{e2}}\right] \tag{35}$$

$$T_{ps}^i = T^i\left[1 - \frac{2\tau_{cL}^i}{3\pi}\frac{D^i}{C^i} - \frac{2}{3\pi}\frac{D^{i2}}{C^{i2}}\right] \tag{36}$$

The one-dimensional stationary sheath thickness (L_s) can be estimated according to the Child–Langmuir law[9]

$$L_s^2 = \frac{4}{9}\varepsilon_0\sqrt{\frac{2e}{m^i}}\frac{|\phi_w|^{3/2}}{J_{ps}^i} \tag{37}$$

where $J_{ps}^i = n_{ps}eu_{ps}^i$ is the ion presheath current.

The flux of the particle species -s is

$$\Gamma^s = \iiint d^3v v f^s(x,\vec{v}) \tag{38}$$

Assuming the Boltzmann distribution of electrons, the analytical value of wall potential is obtained by equating the ion and electron fluxes i.e.

$$\Gamma^i = \Gamma^e \tag{39}$$

which yields,

$$\frac{e\phi_w}{k_B T^e} = \frac{1}{2}\ln\left[\frac{2\pi m^e}{m^i}\left(\frac{T_{ps}^e + \gamma^i T_{ps}^i}{T^e}\right)\right] \tag{40}$$

D. Numerical scheme in KTS

The region of interest, $x = 0$ to $x = L$ is discretized uniformly in configuration and velocity space as shown in Fig. 4. The vertical and horizontal solid lines represent the position and velocity grids, respectively. A position grid point is denoted by x_k; where $k = 1, 2, \ldots, n_x$ and n_x is the total number of grid points. The separation between consecutive grid points is denoted by Δx. In our simulation, we choose n_x to be large enough in such a way that the separation between consecutive gird points is always less than the electron Debye length. Similarly, we discretize v_y versus y and v_z versus z and generalize the $1d1v$ case for the $1d3v$ case.

In the KTS method, we trace the collisionless ion (particle) trajectories to calculate the respective velocity distribution function. For these calculations, we discretize the ion velocity in a time-centered manner.[18] For the given initial potential $\phi^{m-1}(x)$, the iteration scheme calculates a new potential distribution $\phi^m(x)$ in the following steps:

1st Step: By using equation (21), the new electron distribution $n^{em}(x)$ is calculated analytically and new ion density distribution $n^{im}(x)$ is calculated via the kinetic approach. Thus, a new space charge density $\rho^m(x)$ is then obtained.

2nd Step: Once the space charge density $\rho^m(x)$ is known, a new potential distribution $\phi_e^m(x)$ is calculated numerically by using Poisson's equation.

In order to get new input potential, we use the relaxation scheme as follows.[20] The numerically exact new potential function $\phi_e^m(x)$ is linearly combined with the old potential function $\phi^{m-1}(x)$ to obtain the new potential function $\phi^m(x)$, which is actually used as the relevant result of the m^{th} iteration[19]

$$\phi^m(x) = w\phi_e^m(x) + (1 - w)\phi^{m-1}(x) \tag{41}$$

where the relaxation parameter, w is taken as 0.08.

The re-adjusted new potential distribution $\phi^m(x)$ obtained in the second step of the iteration block is compared with the old potential distribution $\phi^{m-1}(x)$, and convergence is reached if the new and old potential distributions satisfy the condition

$$|\phi^m(x) - \phi^{m-1}(x)| \le \Delta\phi \tag{42}$$

with $\Delta\phi$ is defined as an accuracy parameter.

III. RESULTS AND DISCUSSION

In order to know the initial kinetic parameters at the sheath entrance, the presheath-sheath coupling equations are solved for the given presheath parameters. The field boundary condition to solve the basic equations for the coupling scheme are $\phi(x = L) = 0$ and $\phi(x = 0) = \phi_w < 0$. The physical parameters considered are; $B = 100$ mT, $\beta = 5°$, $m^e = 9.1093\times10^{-31}$ kg (mass of electron), $m_H = 1.6737\times10^{-27}$ kg (mass of hydrogen ion) and $n_{ps} = 10^{20}$ m^{-3} (plasma density). The length of simulation region is considered $15\times\lambda_D^e$, where $\lambda_D^e = \sqrt{\frac{\varepsilon_0 k_B T_{ps}^e}{n_{ps} e^2}}$ is the electron Debye length.

The velocity distribution function of ion species at the sheath entrance and the wall is displayed in Figs. 5(a) and 5(b), respectively, which is cut-off shifted half Maxwellian distribution. The cut-off and Maxwellian maximum velocities are equal in magnitudes at sheath entrance and at the wall; however, as the ion flows towards the wall its cut-off and Maxwellian maximum velocities increase from 1.9070 to 5.6090.

The self-consistent potential as the function of distance for two different values of presheath electron temperature is shown in Fig. 6. It is seen that the electrostatic sheath potential decreases monotonically towards the wall, which is consistent with Debye shielding. The thermal motion of electrons increases towards the sheath region for the rising electron temperature, and hence the potential sharply decreases towards the sheath region. It is found that the values of wall potential are -28.0844 V and -33.7013 V for two different values of presheath electron temperature 10 eV and 12 eV, respectively whereas by using equation (40), the corresponding analytical values are -27.3155 V and -32.7786 V, respectively. The deviation of simulation results from the analytical value is due to the fact that cut-off Maxwellian distribution of electrons by the reflective nature of

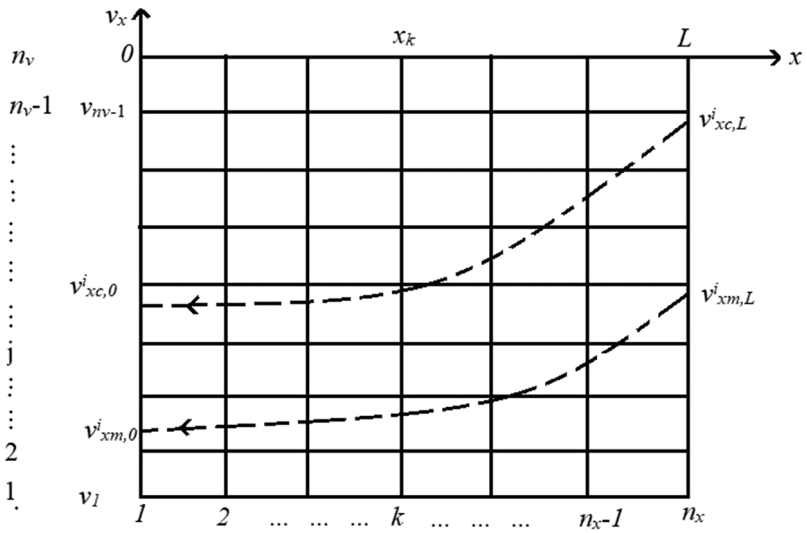

FIG. 4. Schematic representation of discretization of $1d1v$ phase-space.

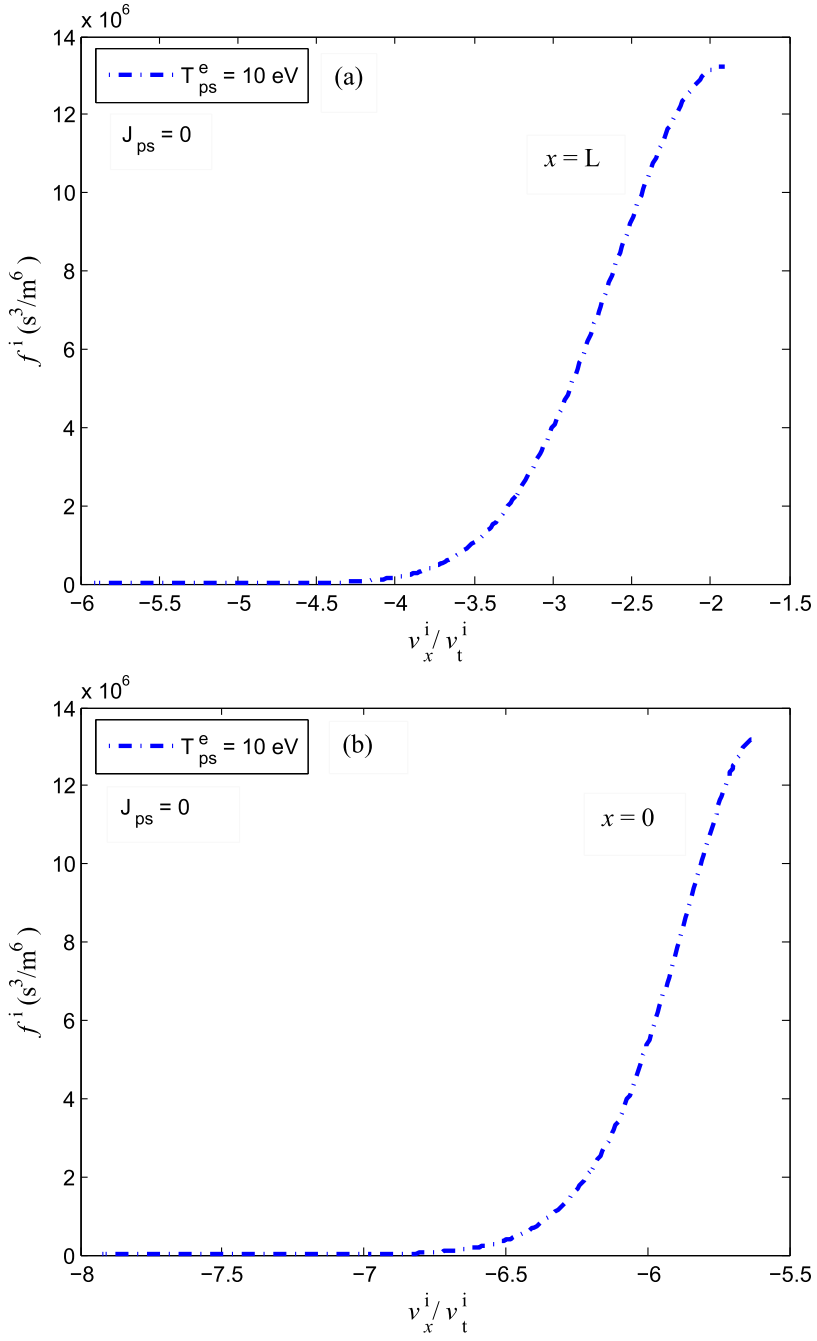

FIG. 5. (a) Ion velocity distributions function at the sheath entrance. (b) Ion velocity distributions function at the wall.

the wall and the corresponding distribution of electrons is given by equation (21). In the analytical prediction of wall potential (Eq. 40), we assume Boltzmann distribution of electrons

$$n^e = n_L^e \exp\left(\frac{e\phi}{k_B T^e}\right) \tag{43}$$

The kinetic Bohm's condition equation (27) becomes

$$M^i = 1 \tag{44}$$

where $M^i = \frac{u^i_{n,SE}}{c_s}$ is the ion Mach number.

The equation (44) is well-known Bohm condition, which is in agreement with previous literature.[21]

The electron density given by our model (Eq. 21) is less than that given by Boltzmann one (Eq. 43), which makes the wall more negative. Therefore, the magnitude of simulated value is higher than analytical value, which is approximately 3 % difference in magnitude.

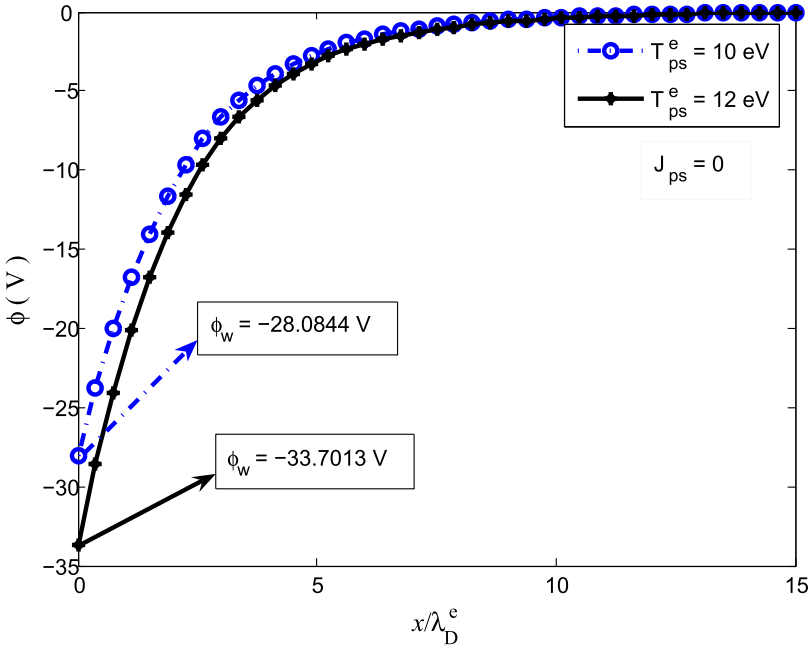

FIG. 6. Potential profile as the function of normalized distance.

Figure 7 shows the variation of sheath thickness as the function of presheath electron temperature. It is observed that the sheath thickness is highly influenced by the presheath electron temperature. As the prsheath electron temperature increases, the Child-sheath thickness begins to stretch. It implies the sharp decrement of electron flux towards the sheath region. The magnitude of wall potential has a higher value for the higher electron temperature. From equation (37), the increasing wall potential causes the increase in sheath thickness.

The self-consistent ion and electron fluxes as the function of potential for two different values of presheath electron temperature are shown in Figs. 8 and 9, respectively. It is seen that the ion and electron fluxes decrease towards the wall whereas the decrement rate of electron flux is more than ions. The electron

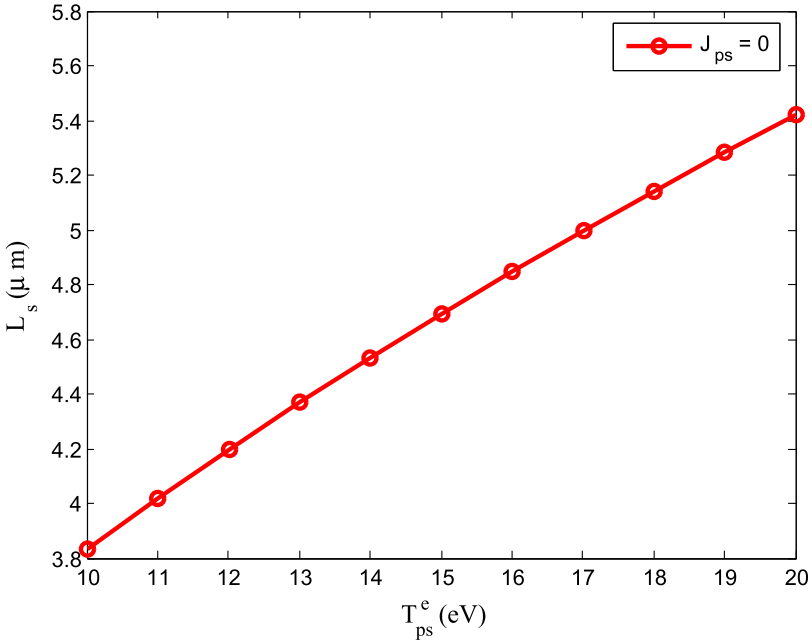

FIG. 7. Child-sheath thickness as the function of presheath electron temperature.

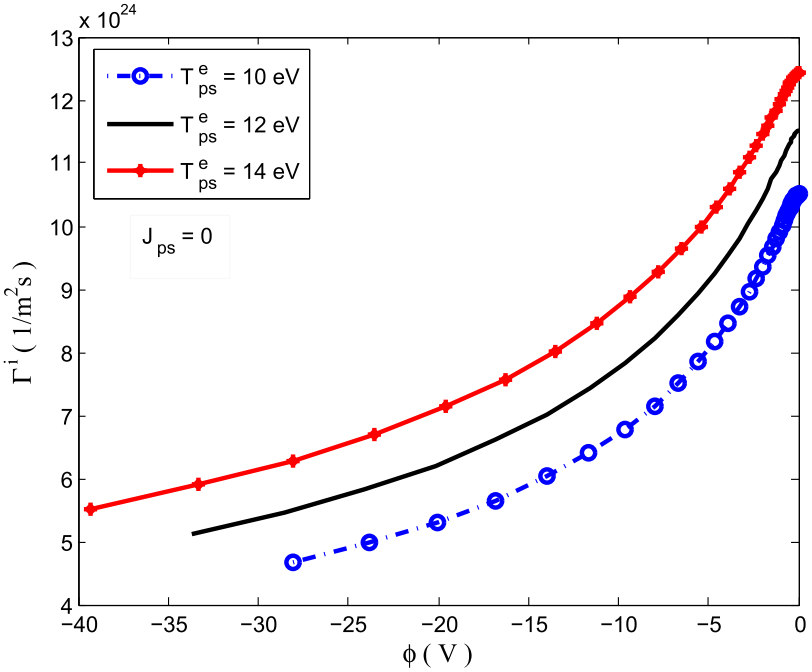

FIG. 8. Ion flux as the function of potential for different values of presheath electron temperature.

flux is almost constant the same whereas that of ions are different such that the space charge density increases towards the wall.

The residual electric field influences the motion of ion flow at the sheath entrance so as the presheath ion temperature increases, the entrance velocity of ions increases as shown in Fig. 10. In addition, the velocity of ions is affected by the electron temperature. The coupling of sheath side ion temperature with presheath ion temperature is shown in Fig. 11. It is seen that ion temperature increases at the sheath region for increasing presheath ion temperature. Thus, the coupling scheme ensures the smooth transition of plasma parameters at the presheath-sheath interfaces.

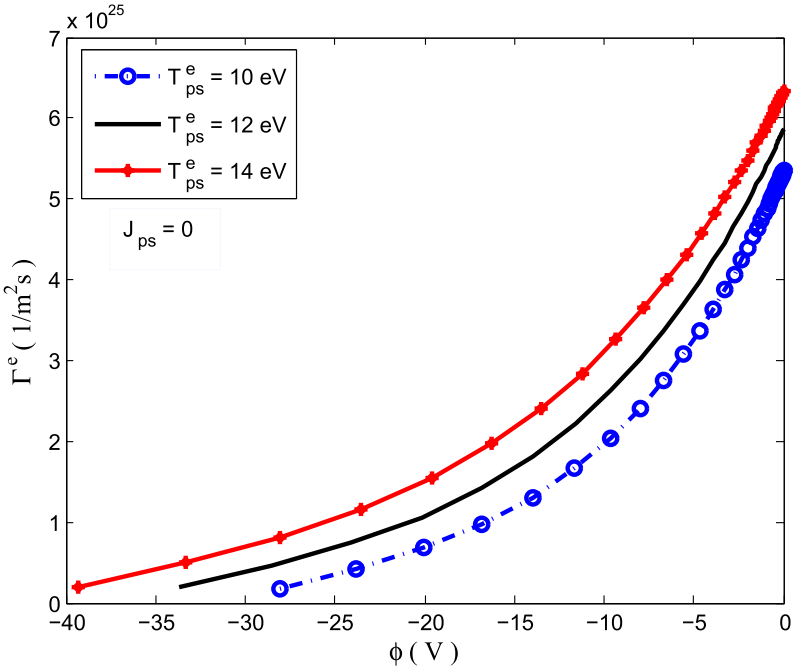

FIG. 9. Electron flux as the function of potential for different values of presheath electron temperature.

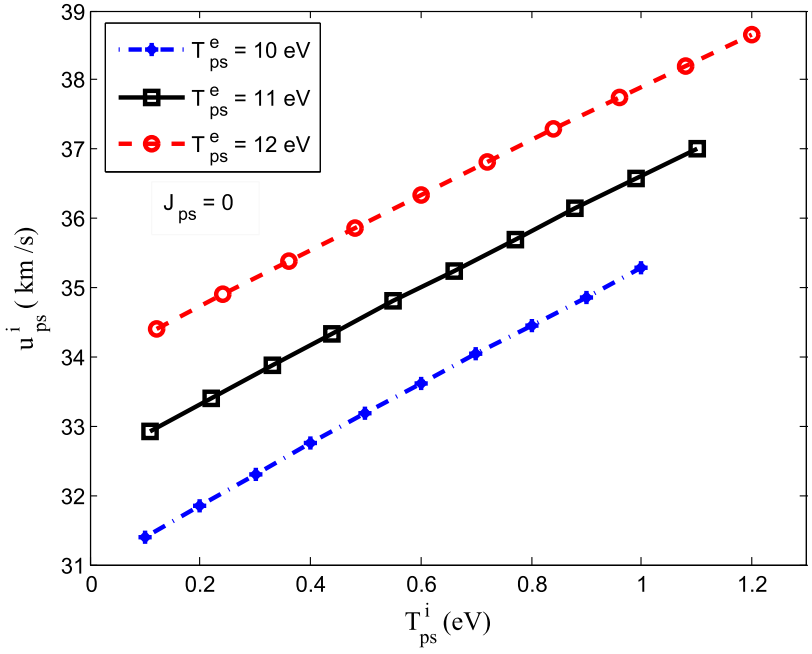

FIG. 10. Presheath ion velocity as the function of presheath ion temperature.

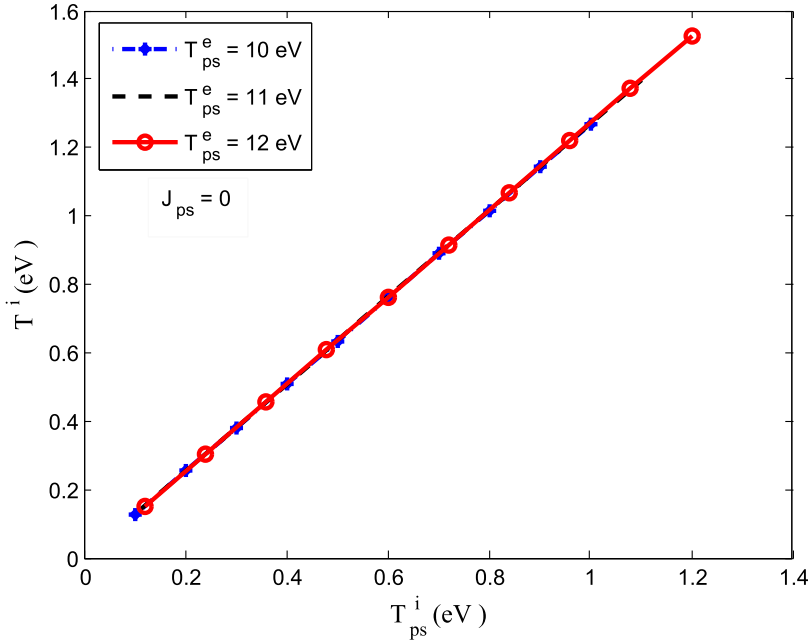

FIG. 11. Variation of ion temperature in the sheath side as the function of presheath ion temperature.

IV. CONCLUSIONS

We have developed the 1*d*3*v* presheath-sheath coupling scheme for the study of magnetized plasma sheath using kinetic trajectory simulation method. We assume that the ion and electron distribution functions are cut-off Maxwellian at the sheath entrance, where the quasineutrality, the sheath edge singularity condition, continuity of first three fluid moments and the kinetic Bohm condition are satisfied. The presheath side parameters have a considerable effect on the sheath side parameters. It is found that the cut-off and Maxwellian maximum velocities of ion have equal magnitudes at the injection point and the wall; however their values become higher at the wall than at the entrance. The potential profile decreases towards the wall and the slope of potential profile increases for the increase in presheath electron temperature. It is noted that the simulated value of wall potential is slightly deviated

from the theoretical value by about 3% in magnitude. This discrepancy arises due to the fact that our electron distribution is cut-off Maxwellian rather than Boltzmann distribution. The Child-sheath thickness increases with the increasing value of presheath electron temperature. The average thermal flux of ions and electrons across the *y-z* plane decrease towards the wall, however, the decrement of electrons flux is faster than ions. The space charge density has its maximum value at the wall, where the potential has a maximum value. In addition, the presheath electron temperature has a significant effect on the presheath ion velocity, and hence increases the wall potential to satisfy the marginal Bohm condition. The ion temperature on the sheath side increases with the increasing presheath ion temperature. Although the obtained results were qualitatively similar with previous literatures,[17,18] it is quantitatively different.

REFERENCES

[1] K. U. Riemann, J. Phys. D: Appl. Phys. **24**, 493 (1991).
[2] K. U. Riemann, Phys. Plasmas **4**, 4158 (1997).
[3] R. Khanal, S. Kuhn, S. Teodoru and D. D. Tskhakaya, Sr., 30th EPS Conference on Contr. Fusion and Plasma Phys., St. Petersburg, 27A, 1.171 (2003).
[4] K. U. Riemann, Phys. Plasmas **6**, 063508 (2006).
[5] R. N. Franklin, J. Phys. D: Appl. Phys. **36**, R309 (2003).
[6] S. Kuhn, K. U. Riemann, N. Jelic, D. D. Tskhakaya, Sr., and D. Tskhakaya, Jr., Phys. Plasmas **13**, 013503 (2006).
[7] S. Basnet and R. Khanal, AIP Advances **8**, 105321 (2018).
[8] P. C. Stangeby, Phys. Fluids **27**, 682 (1984).
[9] F. F. Chen, *Introduction to Plasma Physics and Controlled Fusion*, 3rd ed. (Springer, Switzerland, 2016).
[10] D. Bohm, in *The Characteristics of Electrical Discharges in Magnetic Field*, edited by A. Guthry and R. K. Wakerling (McGraw-Hill, NewYork, 1949).
[11] K. U. Riemann, J. Tech. Physics **41**, 89 (2000).
[12] R. Chodura, Phys. Fluids **25**, 1628 (1982).
[13] H. Pedit and S. Kuhn, Phys. Plasmas **1**, 13 (1994).
[14] K. U. Riemann, Phys. Fluids **24**, 2163 (1981).
[15] A. V. Vasenkov and B. D. Shizgal, Phys. Rev. E **63**, 046404 (2002).
[16] S. D. Baalrud and C. C. Hegna, Plasma Sources Sci. Technol. **20**, 025013 (2011).
[17] R. Chalise and R. Khanal, Plasma Phys. Control. Fusion **54**, 095006 (2012).
[18] R. Chalise and R. Khanal, Phys. Plasmas **22**, 113505 (2015).
[19] R. Khanal, A kinetic trajectory simulation model for bounded plasmas, PhD Thesis, University of Innsbruck, Austria (2003).
[20] W. H. Press, S. A. Teukolsky, W. T. Vetterling, and B. P. Flannery, *Numerical Recipes in C* (Cambridge University Press, 2002).
[21] X. Zou, M. Qiu, H. Liu, L. Zhang, J. Liu, and Y. Gong, Vacuum **83**, 205 (2008).

Temporal dependence of components of velocity of ions in a magnetized plasma sheath for different obliqueness of the magnetic field

B. R. Adhikari, H. P. Lamichhane and R. Khanal

Central Department of Physics, Tribhuvan University, Kirtipur, Kathmandu, Nepal

Received : 31st July 2016, Accepted : 21st August 2016

E-mail: b.r.adhikari@hotmail.com

Abstract. Time dependence of the velocity of ions in a magnetized plasma sheath has been numerically investigated by using a kinetic trajectory simulation model for varying obliqueness of magnetic field at constant magnitudes of magnetic and electric fields. Angular dependence of mean value, maximum amplitude, damping constant, frequency of oscillation and phase angle of velocity components at magnetic field 2.5 mT have been studied. At constant magnetic field, as the obliqueness of the field changes the separation of the mean values as well as the maximum amplitude of the different components of the velocity also changes. Ion velocity at presheath-sheath boundary is well matched with the fitted damped oscillatory motion.

24. Introduction

Temporal dependence of components of velocity of ions in a magnetized plasma sheath for different obliqueness of the magnetic field is recent field of research in plasma physics [1-4]. Now days, the sheath formed between magnetic plasma and a particle absorbing wall has received a significant attention [5-15]. As the plasma is confined in any closed surface, plasma interacts with the material surfaces which are very important in all plasma applications .so that the proper understanding of this interaction with the material surface is very important in all plasma applications [7]. If the plasma–wall interaction is well understood it will be possible to control heat loading, energy transfer and particle flow towards the wall and overall behaviour of plasma [3, 4].

The absorbing wall is charged up negatively due to the higher velocity of the plasma electrons. The plasma electrons have much more velocity as compared with that of the ions. Due to this reason negative potential is developed in the absorbing wall which attracts the ions and repels part of the electrons, forming a positive space charge region in front of the wall, which is 'sheath'. To exist such a sheath, the in streaming ions at the sheath edge have to satisfy the condition called the Bohm criterion [3, 16]. In its kinetic form this criterion reads

$$\left\langle \frac{1}{v^2} \right\rangle \leq \frac{1}{C_s^2} \qquad (1)$$

where, C_s is the ion-acoustic velocity and is given as

$$C_s = \sqrt{\frac{k(\gamma^i T_{PS}^i + \gamma^e T_{PS}^e)}{m^i}} \qquad (2)$$

In equation (2) k is Boltzmann constant, T_{ps}^i and T_{ps}^e the ion and electron temperatures at the presheath side of the sheath edge, γ^i and γ^e the ion and electron polytrophic constants respectively [1, 4].

In magnetized plasma sheath this study is very important to see the change in particle wall interaction as well as the particle dynamics. Plasma sheath is significantly influencing the charged particles and the energy flux to the wall, which modifies the absorption, emission impurities and all other characteristics in the plasma [7]. The Kinetic Trajectory Simulation (KTS) model [11,17] have been used to obtain solution to a non-neutral, time independent, collision less plasma sheath and hence we study the ion velocities in a magnetized plasma sheath for different obliqueness of the field. Also we used the equation of damped harmonic oscillator to fit with the computed plot.

This paper is organized as follows: In section 2 we discuss the basic principle of the KTS method in a simplified form. In this section we explain the distribution function in the collision less case. In section 3 we discuss about our magnetized plasma sheath model. In this section we apply Lorentz force equation which is solved by Runge-Kutta method in MATLAB using boundary condition. Also in this section, we use the damped harmonic oscillator equation which is used to fit with the computed plot. In section 4 we obtain the result in graphical form and we discuss about our result. Finally we summarize our work and draw conclusions.

25. Basic Principle of KTS Method

For numerically calculating self-consistent, time independent kinetic plasma states in some given bounded spatial region KTS method is used whose characteristic features is that the distribution functions of the particle species involved are calculated by solving the related (collision less or collisional) kinetic equations along the respective collision less particle trajectories.

The fundamental equation which $f(\vec{r},\vec{v},t)$ has to satisfy is the Boltzmann equation [7].

$$\frac{\partial f}{\partial t}+\vec{v}.\nabla f+\frac{\vec{F}}{m}.\nabla_v f=\left(\frac{df}{dt}\right)_c \qquad (3)$$

Where, $\vec{F}$ is the force acting on the particles and $\left(\frac{df}{dt}\right)_c$ is the time rate of change of f due to collisions. The symbol ∇ stands for the gradient in (x,y,z) space. The symbol ∇_v stands for the gradient in velocity space, and $f(\vec{r},\vec{v},t)$ is a velocity distribution function.

In collision less cases the equation is called the Vlasov equation

$$\frac{\partial f}{\partial t}+\vec{v}.\nabla f+\frac{q}{m}\left(\vec{E}+\vec{v}\times\vec{B}\right).\nabla_v f=0 \qquad (4)$$

In the KTS method we solve the kinetic equation along with other basic equations describing the plasma for given boundary and initial conditions.

26. Plasma sheath model

The *1d3v* model of magnetized plasma sheath is shown schematically in Figure 1.

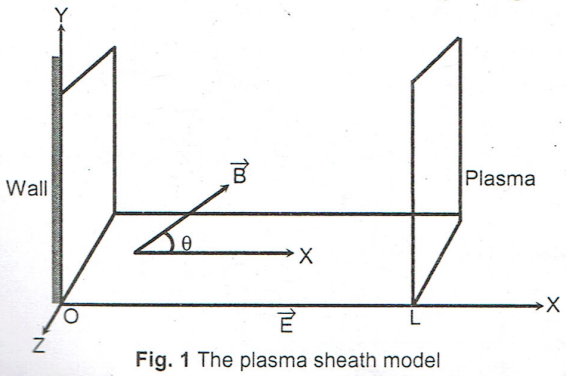

Fig. 1 The plasma sheath model

The simulation region considered is bounded by two parallel planes situated at x=0 and x=L and the plasma consists of only electrons and charged ions. These two parallel planes have specified x=L as the "plasma entrance" and an absorbing wall is specified by x=0. We assuming the angle between the oblique magnetic field with along the x-axis or electric field to be θ.The simulation region having two boundaries are perfectly absorbing and does not emit any particles. Consider the plasma particles enter the simulation region from the plasma entrance wall with cut off Maxwellian velocity distribution functions. Accordingly, the electron velocity distribution function is given by,

$$f^e(x,v) = A^e \exp\left[-\left(\frac{v_x^2 + v_y^2 + v_z^2}{v_t^{e2}}\right) + \frac{e\emptyset(x)}{kT^e}\right]\Theta[v_c^e(x) - v_x] \quad (5)$$

Where $v_c^e(x) = \sqrt{\frac{2e[\emptyset(x) - \emptyset_0]}{m^e}}$ is the electron cut off velocity at x, k is the Boltzmann constant and $\Theta(x)$ is the Heaviside function i.e.,

$\Theta(x) = 1$ if $x \geq 0$

$= 0$ otherwise (6)

The ion velocity distribution function at $x=L$ is given by,

$$f^i(L,v) = A^i \exp\left[-\left(\frac{(v_x - v_{mL}^i)^2 + v_y^2 + v_z^2}{v_t^{i2}}\right)\right]\Theta(v_{cL}^i - v_x) \quad (7)$$

Where $v_t^s = \sqrt{\frac{2kT^s}{m^s}}$ is the species-s (ion and electron) thermal velocity, v_{mL}^i is the ion "Maxwellian-maximum" velocity at $x=L$ and v_{cL}^i ($v_{cL}^i < 0$) is the ion cut off velocity at $x=L$. In the core plasma the particle distribution would obviously be Maxwellian, however, in case of sheath formation the ions are accelerated towards the wall so that they become shifted Maxwellian as given by equation (7). In addition, for the Bohm criterion to be satisfied by the ions they must have attained certain minimum velocity (v_{cL}^i) at the sheath entrance. As the electrons are retracted and reflected by the negative potential wall their distribution gets cut-off at the sheath entrance as given by equation (5).

As the starting parameters at the sheath entrance are known we solve the ion kinetic equations, for different discretized ion injection velocities up to the wall. This gives the ion velocities and their corresponding distribution function in the entire sheath region which on integration yields ion density distribution. Electron density distribution, on the other hand, is calculated analytically by using

$$n^e(x) = A^e \int_{-\infty}^{+\infty} dv_x \int_{-\infty}^{+\infty} dv_y \int_{-\infty}^{+\infty} [dv_z \left[-\left(\frac{v_x^2 + v_y^2 + v_z^2}{v_t^{e2}}\right)\right]\Theta(v_{cx}^e] - v_x) \quad (8)$$

which yield density in terms of potential as,

$$n^e(\emptyset) = n_L^e \exp\left[\frac{e\emptyset(x)}{kT^e}\right]\left[\frac{1 + erf\sqrt{\frac{e(\emptyset(x) - \emptyset_0)}{kT^e}}}{1 + erf\sqrt{\frac{-e\emptyset_0}{kT^e}}}\right] \quad (9)$$

Thus obtained ion and electron densities are used in Poisson equation, which results in new potential profile which is then iterated unless a final self-consistent profile is obtained. All required parametrs like ion density, velocity, etc. are obtained by solving the corresponding equations.

Due to the collisional force among the ions, the oscillatory motion of the ions under goes the damping phenomenon. The typical Differential equation of damped harmonic oscillator is [18]

$$\frac{d^2y}{dt^2} + 2k\frac{dy}{dt} + \omega_0^2 y = 0 \qquad (10)$$

where, ω_0 is the natural frequency of the oscillating particle.

The equation of damped harmonic oscillator is [18]

$$v(t) = v_m + Ae^{-kt}\sin(\omega t + \emptyset) \qquad (11)$$

where, k is damping constant, A is amplitude, v_m is mean value and $\emptyset$ is the phase angle. This equation is used to fit with the computed plot. The parameters v_m, A, k , ω and $\emptyset$ are estimated from the corresponding plots.

v_m = Value of v(t) at time t equal to 1 second,

k = Damping constant,

A = Amplitude of v(t) at time t equal to zero,

ω = angular frequency = 2πf, f = frequency of oscillation and

$\emptyset$ = Phase angle.

To estimate k, first of all nature of the damped oscillation is carefully observed. From the graph maximum peak values of the velocity (v_1) at smaller time (t_1) as well as velocity (v_2) at longer time (t_2) are noted. Then, k is calculated using following formula:

$$k = \frac{\ln\left(\frac{v_1 - v_m}{v_2 - v_m}\right)}{t_2 - t_1} \qquad (12)$$

27. Results and Discussion

The time dependency of the ion velocity with various obliqueness of the magnetic field has been computed using Runge-Kutta method programmed in MATLAB. To estimate the parameters of the computed plot we have calculated the mean value, maximum amplitude, damping constant, frequency of oscillation and the phase angle. For magnetic field 2.5 mT and angle (30°and 45°) we got damped oscillatory nature of each component of velocities as shown in figure (2-7). The fitted plots are almost well matched with the computed plots.

--- Fitted $(V_x)_{est} = 26 + 14910 * \exp(-6.922 * t) * sin\pi(2 * 74.627 * t + 0.773)$

--- Calculated

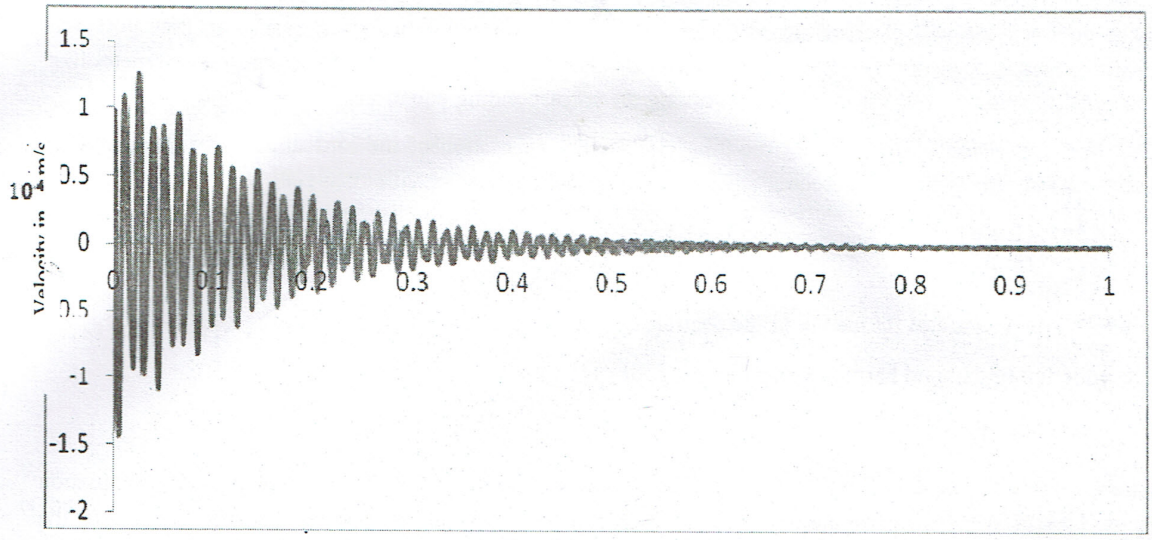

Fig. 2: Damping of x- component of velocity with time at magnetic field 2.5 mT, electric field 0.1 v/m and angle 30

--- Fitted $(V_y)_{est} = 8052 + 2287 * \exp(-6.665 * t) * \sin\pi(2 * 74.667 * t + 0.7244)$

--- Calculated

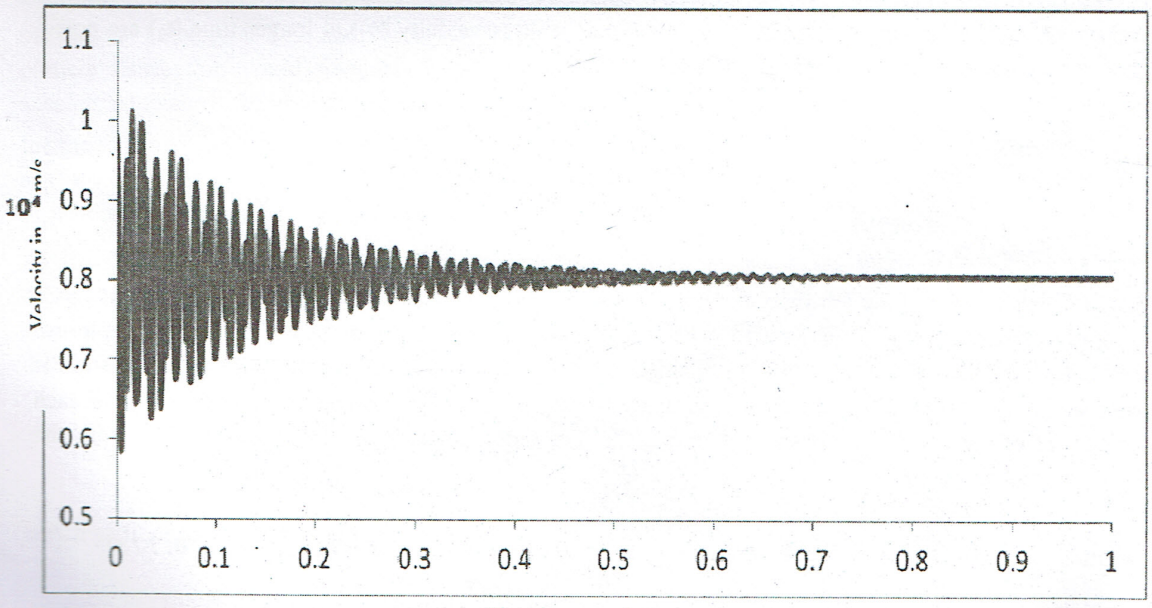

Fig. 3: Damping of y- component of velocity with time at magnetic field 2.5 mT, electric field 0.1 v/m and angle 30°.

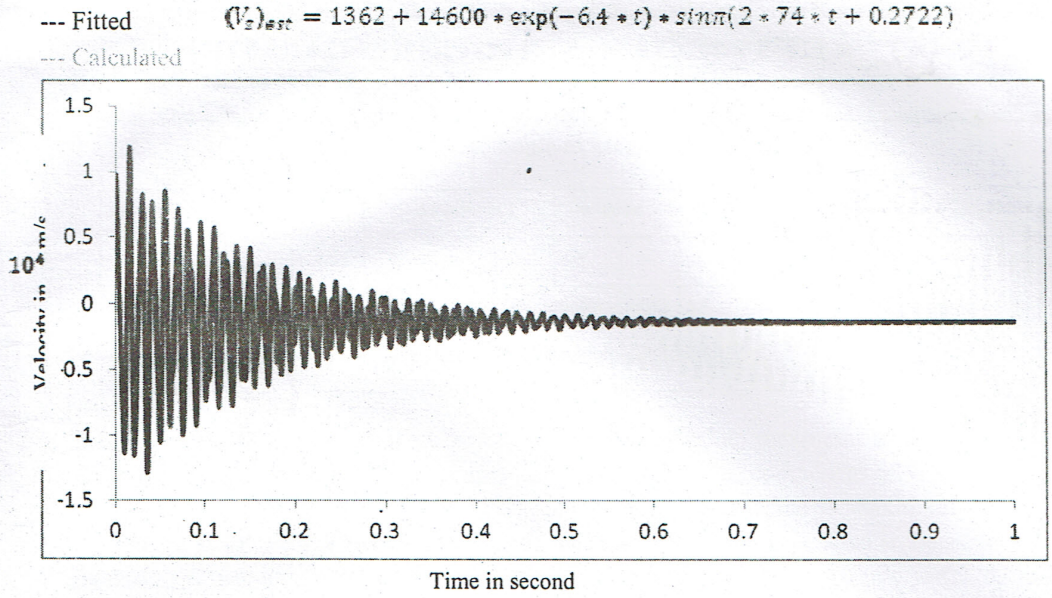

Fig. 4: Damping of z-component of velocity with time at magnetic field 2.5 mT, electric field 0.1 v/m and angle 30°.

Figure 2 shows that the x- component of velocity approximately has mean value 26 m/s, maximum amplitude 14910 m/s, damping constant 6.922 /sec, frequency of oscillation 74.627 Hz and phase angle 0.773π radian. Similarly Figure 3 and 4 show that at the samevalue of magnetic field 2.5 mT and angle 30° the y and z- component of velocity has mean value, maximum amplitude, damping constant, frequency of oscillation and phase angle as 8052 m/s, 2287 m/s, 6.665 /s, 74.667 Hz, 0.7244π radian and 1362 m/s, 14600 m/s, 6.4 /s, 74 Hz, 0.272π radian respectively.

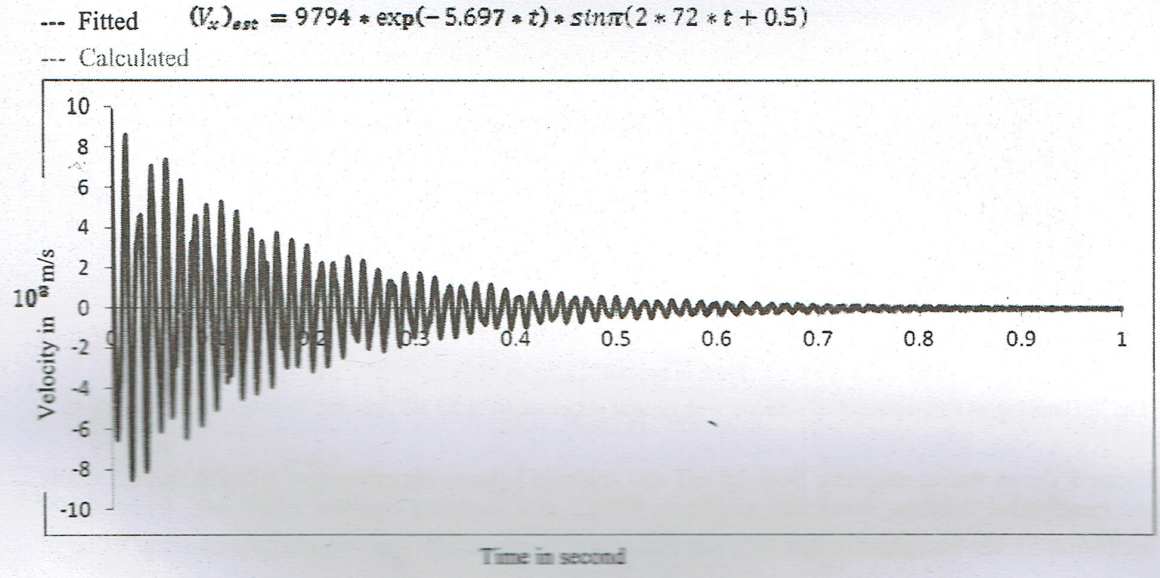

Fig. 5: Damping of x-component of velocity with time at magnetic field 2.5 mT, electric field 0.1 v/m and angle 45°.

--- Fitted $(V_y)_{est} = 11435 + 4820 * \exp(-5.734 * t) * sin\pi(2 * 72 * t - 0.111)$

--- Calculated

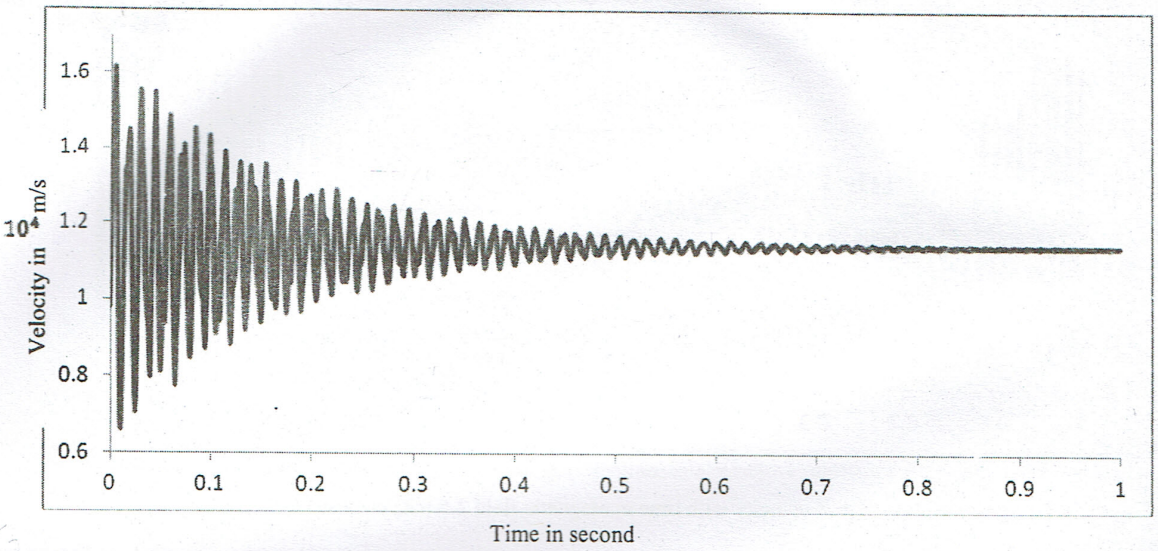

Fig. 6: Damping of y-component of velocity with time at magnetic field 2.5 mT, electric field 0.1 v/m and angle 45°.

--- Fitted $(V_z)_{est} = 7140 + 8200 * \exp(-5.83 * t) * sin\pi(2 * 72 * t + 0.9)$

--- Calculated

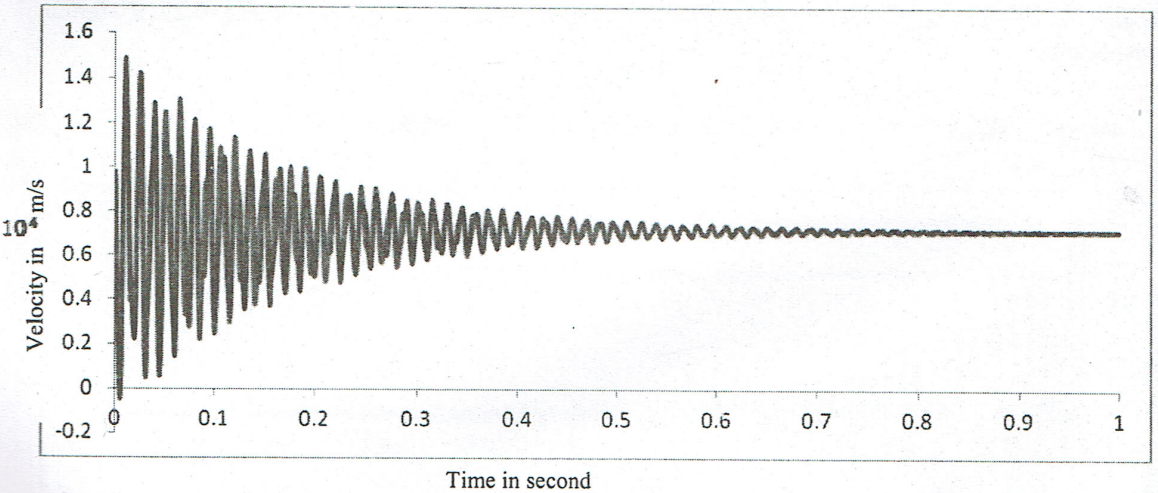

Fig. 7: Damping of z-component of velocity with time at magnetic field 2.5 mT, electric field 0.1 v/m and angle 45°.

Figure 5 shows that at magnetic field 2.5 mT and angle 45°, the x- component of velocity approximately has mean value 0 m/sec, maximum amplitude 9794.2 m/s, damping constant 5.697 /sec, frequency of oscillation 72 Hz and phase angle 0.5π radian. Also Figure 6 and 7 shows that at the same value of

magnetic field 2.5 mT and angle 45 ° the y and z- component of velocity has mean value, maximum amplitude, damping constant, frequency of oscillation and phase angle as 11435m/s, 4815 m/s, 5.734 /s, 72 Hz, 0.111π radian and 7137 m/s, 8200 m/s, 5.83 /s, 72 Hz, 0.9π radian respectively.

Table: The observed data of mean value, amplitude,Damping constant, Frequency of oscillation and Phase angle at magnetic field 2.5 mT

Theta	Mean Value			Amplitude			Damping constant			Frequency			Phase Angle		
	v_{xm}	v_{ym}	v_{zm}	v_{xa}	v_{ya}	v_{xa}	v_x	v_y	v_z	v_x	v_y	v_z	v_x	v_y	v_z
30°	26	8052	1362	14910	2287	14600	6.922	6.665	6.4	74.627	74.667	74	0.773π	0.724π	0.272π
45°	0	11435	7137	9794	4815	8200	5.6973	5.734	5.83	72	72	72	0.5π	-0.11π	0.9π

Table 1shows the summery of observed data for mean value, maximum amplitude, damping constant, frequency of oscillation and phase angle. The mean value of x- component of velocity at 30° is small but not equal to zero whereas at 45° mean value is zero. Mean value is maximum i.e 11435 m/s on y-component at 45° with respect to other components at different angles. Also at the same value of magnetic field 2.5 mT and angle 30° maximum and minimum amplitude is 14910 m/s and 2287 m/s on x and y-component respectively with respect to other components at different angles. At angle 30° for all component of velocity damping constant is slightly larger than at 45°. At angle 30° frequency of oscillation is greater with respect to x, y and z-components of other angles whereas at angle 45° frequency of oscillation is slightly smaller and constant compared to frequencies of other angles at different components. Similarly at angle 45°, phase angle at y-component is minimum i.e -0.111π radian than other components at different angles. On the other hand, at 45° phase angle at z-component is maximum i.e 0.9π radian than other components at different angles.

5. Conclusion

It has been observed that ion velocity at presheath-sheath boundary is greatly affected by obliqueness of the field. At constant magnetic field as the obliqueness of the field changes the separation of the mean values as well as the maximum amplitude of all the three component of the velocity also change. Angular dependence of mean value, maximum amplitude, damping constant, frequency of oscillation and phase angle of velocity components at magnetic field 2.5 mT has been observed. It is also observed that by applying the equation of damped harmonic oscillator, the fitted plot is almost well matched with the computed plot.

References

[1] Chodura R 1982 *Phys. Fluids* **25**,1628

[2] Chodura R 1986 *Plenum Publishing Corporation* 99

[3] Riemann KU 1991 J. *Physics. D: Appl. Phys.* **24**: 493

[4] Riemann KU 2000 *J. Tech. Phys. 41*: 89

[5] Hatami MM, Niknam AR, Shokri B and Ghomi H 2008 *Physics of Plasmas* **15**: 053058

[6] Zou X, Qiu M, Liu H, Zhang L, Liu J and Gong Y 2009 *Vacuum* **83**: 205

[7] Chalise R and Khanal R 2012 *Plasma Phys. Control Fusion* **54**:095006

[8] Gyergyek T and Kovacic J 2015 *Physics of Plasmas* **22**: 043502

[9] Huang CW, Chen YC and Nishimura Y 2015 *IEEE Transactions on Plasma Science* **43**: 675

[10] Moulik R and Goswami KS 2015 *Physics of Plasmas* **22**: 043701

[11] Chalise R and Khanal R 2015 *Physics of Plasmas* **22**: 113505

[12] Kubes P et.al 2015 *Physics of Plasmas* **22**: 062705

[13] Myra JR and D'lppolito DA 2015 *Physics of Plasmas* **22**: 062507

[14] Liberman MA, Lichtenberg AJ, Kawamura E and Chabert P 2016 *Physics of Plasmas* **23**: 013501

[15] Chauhan S, Ranjan M, Bandyopadhyay M and Mukherjee S 2016 *Physics of Plasmas* **23**: 013502.

[16] Bohm D 1949 *MC-Graw Hill*, **77**

[17] Khanal R 2002 A Kinetic Trajectory Simulation (KTS) Model for Bounded Plasma, Ph. D. Thesis, Innsbruck University, Austria.

[18] George F. Simmons, Differential Equations, *The McGraw-Hill*, Page No. 93-100, New York.

JNPS **6** *(1), 25-29 (2020)*
ISSN: 2392-473X (print)

Research Article

Variation of Velocity of Ions in a Magnetized Plasma Sheath for Different Magnetic Field

B. R. Adhikari[1,2,*], S. Basnet[2], H. P. Lamichhane[2] and R. Khanal[2]
[1] Department of Physics, Bhaktapur Multiple Campus, Tribhuvan University, Bhaktapur, Nepal
[2] Central Department of Physics, Tribhuvan University, Kirtipur, Kathmandu, Nepal
* Corresponding Email: b.r.adhikari@hotmail.com

Received: *11 Jan., 2020;* ***Revised:*** *30 Apr., 2020;* ***Accepted:*** *29 Jun., 2020*

Abstract

The kinetic trajectory simulation method has been used to study ion velocity profile in a plasma sheath for varying magnetic field at fixed obliqueness. As the electrons have higher velocity compared to that of ions the wall is charged up negatively with respect to the core plasma. The negative potential then attracts the ions and repels electrons forming a thin positive space charge region in front of the wall. This positive space charge region, known as the 'sheath' separates the negatively charged wall from the quasineutral 'presheath' plasma. The ions moving towards the wall have to satisfy the Bohm criterion to ensure the stability of the overall plasma. The mean value as well as oscillation frequency of velocity of ions change as the magnetic field is varied from 1.5 to 10.5 mT. The maximum amplitude of normal component of velocity is almost independent of the magnetic field but the maximum amplitude of other components of velocity change and shows oscillating nature as the magnetic field changes.

Keywords: Bohm criterion, Kinetic theory, Plasma-wall interaction, Presheath, Sheath.

1. INTRODUCTION

The understanding of plasma sheath is important for various practical applications of plasma as it is enclosed within a fixed volume [1]. The wall is charged up negatively with respect to the core plasma due to the high speed electrons reaching the wall earlier than the ions. Due to this reason,. The negative potential then attracts the ions and repels electrons forming a thin positive space charge region in front of the wall. This positive space charge region, known as the 'sheath' separates the negatively charged wall from the quasineutral 'presheath' plasma. The sheath structure and the overall plasma will be stable only if the ions moving towards the wall satisfy the Bohm criterion [2, 3]. Once the plasma-wall interaction is well understood it will be possible to control heat loading, energy transfer and particle flow towards the wall and overall bulk plasma behavior [4, 5].

The plasma sheath is one of the oldest problems in plasma [3, 6] and in recent years, the sheath formed between magnetized plasma and a particle absorbing wall has received a considerable amount of attention [7-11]. Irrespective of this, plasma sheath is significantly influencing the charged particles and the energy flux to the wall, which in turn considerably modifies the absorption, emission impurities and all other characteristics in the plasma [1, 11].

In typical boundary layer problems the sheath region is of several electron-Debye lengths, which is much smaller than the characteristic extension of the plasma. Such a sheath can only be formed, if the Bohm criterion [2, 4] is satisfied which demands that the ions enter the sheath region with a high velocity, which cannot be generated by thermal ion motion alone [4]. In its kinetic form the Bohm criterion in the presence of a magnetic field reads

$$\left\langle \frac{1}{v_{\parallel}^2} \right\rangle \leq \frac{1}{C_s^{\,2}} \quad \text{..... (1)}$$

where,

$$C_s = \sqrt{\frac{k(\gamma^i T_{PS}^i + \gamma^e T_{PS}^e)}{m^i}}$$

is the ion-acoustic velocity defined at the presheath side of the sheath edge, with k is Boltzmann

constant, γ^i and γ^e the ion and electron polytropic constants, respectively, T^i_{ps} and T^e_{ps} the ion and electron temperatures at the presheath side of the sheath edge, respectively and m^i is the mass of ion species [3, 5].

In this work, the velocity variation of ions in a magnetized plasma sheath for different magnitudes of magnetic field at constant obliqueness has been studied. This study is important to observe the particle dynamics change and the particle interaction with the material wall in a magnetized plasma sheath. The kinetic trajectory simulation (KTS) method [12] has been employed to obtain the solution to a non-neutral, collisionless plasma sheath.

2. METHODS AND MODEL

The Boltzmann kinetic equation that describes the particle motion in terms of the velocity distribution function is given as [7]

$$\frac{\partial f}{\partial t} + \vec{v}.\nabla f + \frac{\vec{F}}{m}.\nabla_v f = \left(\frac{df}{dt}\right)_c \quad \text{.....(2)}$$

where $\vec{F}$ the macroscopic forces that acts on the particles, and $\left(\frac{df}{dt}\right)_c$ is the rate of change of distribution function due to collisions. In the absence of collision equation (2) becomes the well-known Vlasov equation:

$$\frac{\partial f}{\partial t} + \vec{v}.\nabla f + \frac{q}{m}(\vec{E} + \vec{v}\times\vec{B}).\nabla_v f = 0 \quad \text{.....(3)}$$

This equation is valid in the plasma sheath region as its scale length is much smaller compared to the collision mean free path. In KTS method the Vlasov kinetic equation is solved to study bounded plasmas for given initial and boundary conditions [12-14]. At any point in the phase space, trajectory integration of the kinetic equations yield the respective particle distribution function at that point. As the distribution function is known, the particle density of the species '*s*' is calculated using

$$n^s(\vec{x}) = \int_{-\infty}^{+\infty} d^3v\, f^s(\vec{x},\vec{v}) \quad \text{.....(4)}$$

The geometry of the magnetized plasma sheath model for the present case is shown in Fig. 1. The region of interest is bounded by the two parallel planes, at $x = L$ (absorbing wall) and $x = 0$ (the plasma side, i.e., the sheath entrance). The oblique magnetic field lies on the *x*-*y* plane which makes an angle θ with the direction of electric filed such that the magnetic field can be expressed as

$$\vec{B} = B_0(\cos\theta\,\hat{x} + \sin\theta\,\hat{y}) \quad \text{.....(5)}$$

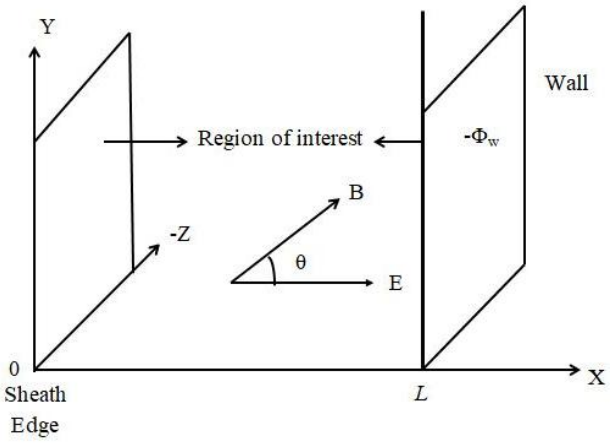

Fig. 1: *Geometry of the plasma sheath model.*

The plasma, consisting of electrons and singly charged ions, enters the simulation region with cut-off Maxwellian velocity distributions; the wall is perfectly absorbing. Thus, the velocity distribution function of electron is,

$$f^e(x,v) = A^e \exp\left[-\left(\frac{v_x^2 + v_y^2 + v_z^2}{v_{tf}^{e^2}}\right) + \frac{e\phi(\vec{x})}{kT_e}\right]\Theta\left[v^e_{cL}(x) - v_x\right] \quad \text{...(6)}$$

where $v^e_c(x) = \sqrt{\frac{2e[\phi(x) - \phi_0]}{m^e}}$ is the cut off velocity of electron at *x*, *k* is the Boltzmann constant and $\Theta(x)$ is the Heaviside function i.e.,

$$\Theta(x) = 1 \text{ if } x \geq 0 \quad \text{.....(7)}$$
$$= 0 \text{ otherwise.}$$

The ion velocity distribution function at $x = L$ is given as,

$$f^i(L,v) = A^i \exp\left[-\left(\frac{(v_x - v^i_{mL})^2 + v_y^{\,2} + v_z^{\,2}}{v_{tf}^{i\,2}}\right)\right]\ \Theta\left(v^i_{cL} - v_x\right) \quad \text{..(8)}$$

where, $v^s_{tf} = \sqrt{\frac{2kT^s}{m^s}}$ is the thermal velocity of particle species '*s*', v^i_{mL} is the Maxwellian-maximum velocity of ions at $x = L$ and v^i_{cL} ($v^i_{cL} < 0$) is the cut-off velocity of ions at $x = L$.

Once all the starting parameters at the sheath entrance are known the characteristic equations of motion are solved, for discretized ion injection velocities, up to the wall. This gives the ion velocities and their corresponding distribution function in the entire sheath region which on integration yields ion density distribution. For the velocity distribution given by equation (8), the ion density at any point within the sheath region is given as

$$n^i(x) = A^i \int_{-\infty}^{+\infty} dv_x \int_{-\infty}^{+\infty} dv_y \int_{-\infty}^{+\infty} dv_z \left[-\left(\frac{\left(v_x - v_{mL}^i\right)^2 + v_y^2 + v_z^2}{v_{tf}^{i^2}} \right) \right] \Theta\left(v_{cL}^i - v_x\right) \quad (9)$$

and the electron density is obtained analytically as

$$n^e(\phi) = n_L^e \exp\left[\frac{e\phi(x)}{kT_f^e} \right] \left[\frac{1 + erf\sqrt{\frac{e(\phi(x) - \phi_0)}{kT_f^e}}}{1 + erf\sqrt{\frac{-e\phi_0}{kT_f^e}}} \right] \quad (10)$$

The calculations are iterated self-consistently unless the resulting potential is stable which is verified by a pre-assigned accuracy parameter in the KTS method [12]. The various components of velocity of ions in the plasma sheath have been computed using Lorentz force equation

$$m^i \frac{d\vec{v}_i}{dt} = q\left[-\hat{x}\frac{\partial\phi}{\partial x} + \left(\vec{v}_i \times \vec{B}\right) \right] \quad \text{.....(11)}$$

where q is the charge and $\vec{v}_i$ is the ion velocity, and ϕ is the electrostatic potential.

3. RESULTS AND DISCUSSION

The results obtained by solving the related kinetic equations using the KTS method is presented for hydrogen plasma having temperature of 1 eV at the sheath entrance, where the electron temperature is 10 eV. The simulation region is 10 electron-Debye lengths which is discretized into 41 grid points. The ion velocity profile with time for different values of magnetic field (1.5 mT - 10.5 mT) at fixed obliqueness of 30 ° has been studied.

The temporal dependence of ion velocity for the magnetic field of 1.5 mT is shown in Fig. 2, which shows initially the ions spend more time gyrating. With the time, the frequency as well as amplitude of gyration decreases gradually. The mean values of x, y, and z-components of velocity are -45.21 m/s, 6863 m/s and 11490 m/s, respectively. The x, y and z-components of velocity oscillate with maximum amplitudes of 9839 m/s, 7913 m/s and 4840 m/s, respectively.

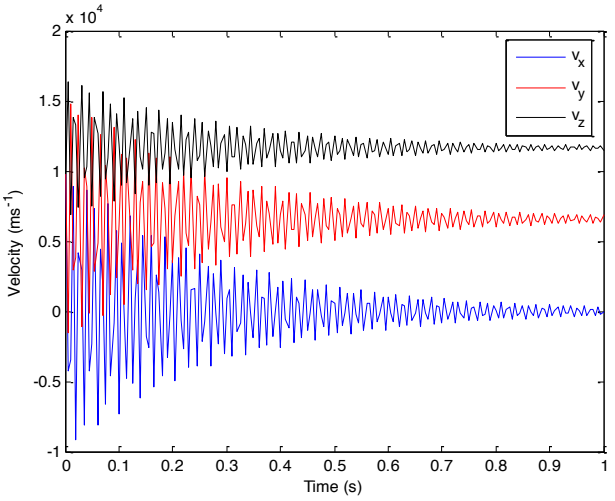

Fig. 2: *Velocity variation of ions with time for magnetic field 1.5 mT.*

Fig. 3 shows the velocity profile of ions at 4.5 mT magnetic field. The mean values of x, y and z-components of velocity are -0.1347 m/s, 6651 m/s and 11610 m/s, respectively. Compared to the case of 1.5 mT, as the strength of magnetic field increases, it is found that the mean values of x and z velocity components increased whereas the y-component is decreased. The amplitudes of oscillation of velocity is found to be 9794 m/s, 7693 m/s and 4440 m/s, respectively.

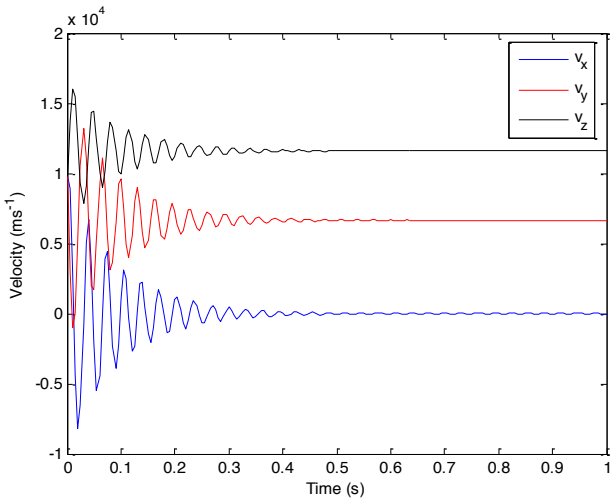

Fig. 3*: Velocity variation of ions with time for magnetic field 4.5 mT.*

Likewise, at 7.5 mT, the ion velocities are displayed in Fig. 4, in which the mean value of *x*-component is nearly equal to zero whereas *y* and *z*-components are 6666 m/s and 11600 m/s, respectively. However, maximum amplitude of the *x*-component velocity is the largest with 9794 m/s, compared to 7334 m/s, and 4233 m/s, of *y* and *z*-components, respectively. In comparison to 1.5 mT the frequency of oscillation decreases much faster for both 4.5 and 7.5 mT. The oscillation of each component of velocity becomes not significant after 0.5 second (in case of 4.5 mT; Fig. 3), and after 0.3 second (in case 7.5 mT; Fig. 4). Similar nature is shown for the magnetic field strength of 10.5 mT (Fig. 5) where the mean values of *x*, *y* and *z*-components are 10^{-4} m/s, 6673 m/s and 11600 m/s, and the maximum amplitudes of oscillation are 9794 m/s, 6879 m/s and 3970 m/s, respectively.

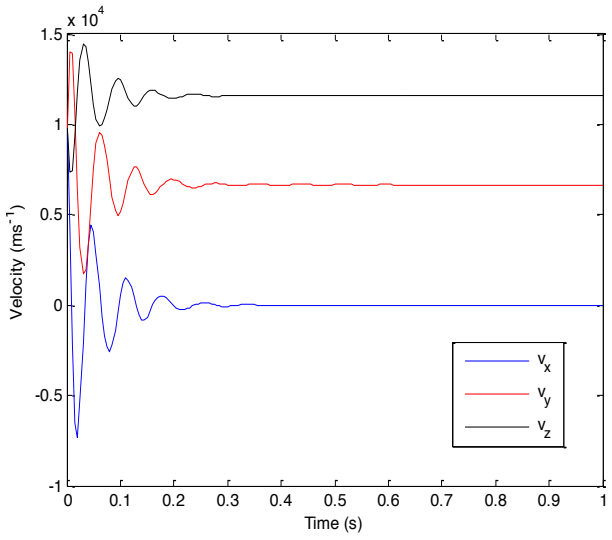

***Fig. 4**: Velocity variation of ions with time at magnetic field 7.5 mT.*

The overall variation of mean values of velocity components for different magnetic fields is displayed in Fig. 6. It is found that the mean value of *x*-component is almost zero, however the mean values of *y* and *z*-components differ with the field strength. The *y*-component of velocity is almost constant around 6660 m/s and the *z*-component is almost constant around 11600 m/s for the magnetic field beyond 2 mT.

Fig. 7 shows the overall variation of maximum amplitude of velocity components for different varying magnetic field. The maximum amplitude of *x*-component is constant around 9794 m/s. On the other hand the highest values of the maximum amplitude of *y* and *z*-components are around 8100 m/s and 4400 m/s, respectively at magnetic field of 1.5 mT whereas lowest values of the amplitudes are 4489 m/s and 2070 m/s respectively at magnetic field of 6 mT.

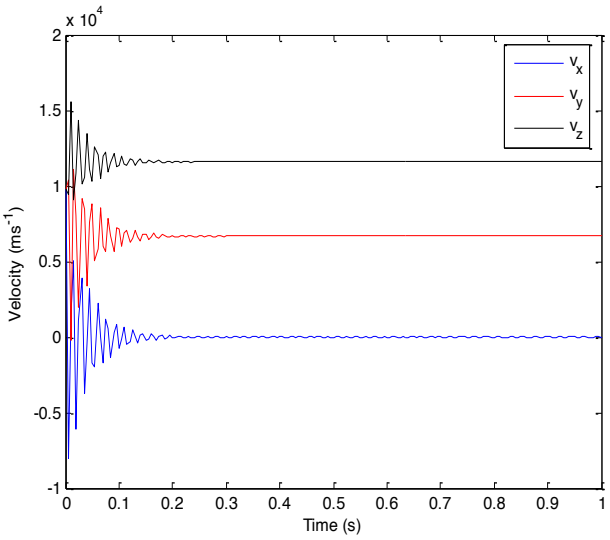

***Fig. 5**: Velocity variation of ions with time at magnetic field 10.5 mT.*

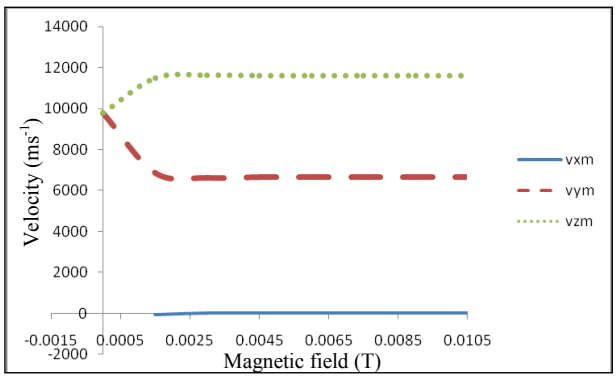

***Fig. 6**: Variation of mean value of velocity with respect to magnetic field at angle 30°.*

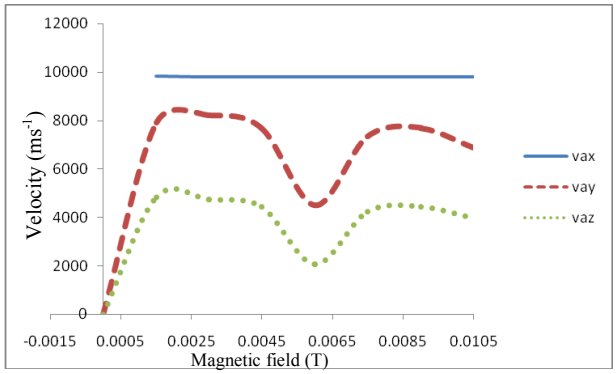

***Fig. 7**: Variation of maximum amplitude of velocity with respect to magnetic field at angle 30°.*

4. CONCLUSIONS

The variation of ion velocity in a magnetized plasma sheath for different magnitudes of magnetic field at constant obliqueness has been studied. The mean values as well as the frequency of oscillation of three component of velocity of ions changes

The variation of ion velocity in a magnetized plasma sheath, which consists of a single species of positive ions and electrons, was studied using kinetic theory. The temporal component of ion velocity oscillates and its oscillations as well as amplitudes are highly influenced by the magnetic field. After 0.5 second the oscillation of each component of velocity is negligible for the magnetic field 4.5 mT whereas the oscillation is negligible after 0.3 second for the magnetic field of 7.5 mT. When the magnetic field increases, the mean value of *y*-component decreases and attains 6660 m/s whereas the *z*-component is increased and attains 11600 m/s. The study is useful in understanding the exact particle behavior in magnetized plasma sheath region and can be important in material processing, plasma etching, confinement of plasma in fusion devices, surface treatment, lighting, medicine etc.

ACKNOWLEDGEMENT

B. R. Adhikari and S. Basnet would like to acknowledge the University Grants Commission, Nepal for PhD fellowships.

REFERENCES

[1] Chalise, R. and Khanal, R. A kinetic trajectory simulation model for magnetized plasma sheath. *Plasma Phys. Control. Fusion*, **54**, 095006-5pp (2012).

[2] Bohm, D. *Minimum ionic kinetic energy for a stable sheath*, in The Characteristics of Electrical Discharges in Magnetic Field, edited by Guthrie, A. and Wakerling, R. K., McGraw-Hill, New York (1949).

[3] Chodura, R. Plasma wall transition in an oblique magnetic field. *Phys. Fluids*, **25**, 1628-1633 (1982).

[4] Riemann, K. U. The Bohm criterion and sheath formation. *J. Phys. D: Appl. Phys.*, **24**, 493-518 (1991).

[5] Riemann, K. U. Theory of the plasma-sheath transition. *J. Tech. Phys.*, **41**, 89-121 (2000).

[6] Langmuir, I. Oscillations in ionized gases. *Proc. National Academy of Sciences*, **14**, 627-637 (1928).

[7] Liberman, M. A., Lichtenberg, A. J., Kawamura, E. and Chabert, P. Linear electromagnetic excitation of an asymmetric low pressure capacitive discharge with unequal sheath widths. *Phys. Plasmas*, **23(1),** 013501-7 (2016).

[8] Hatami, M. M. Sheath properties in two-temperature Non-Maxwellian electron plasmas. *IEEE Transactions on Plasma Science*, **46**, 868-874 (2018).

[9] Adhikari, B. R., Basnet, S., Lamichhane, H. P. and Khanal, R. Beat frequency and velocity variation of ions in a magnetized plasma sheath for different obliqueness of the magnetic field. *Journal of Institute of Science and Technology*, **23,** 88-92 (2018).

[10] Khoramabadi, M., Ghomi, H. and Shukla, P. K. Numerical investigation of the ion temperature effects on magnetized DC plasma sheath. *Journal of Applied Physics*, **109**, 073307-8 (2011).

[11] Basnet, S. and Khanal, R. Effects of collision and ion Mach number on magnetized plasma sheath with two species of positive ions. *AIP Advances*, **8**, 105321-9 (2018).

[12] Khanal, R. *A Kinetic Trajectory Simulation (KTS) Model for Bounded Plasma*, (Ph. D. Thesis). Innsbruck University, Innsbruck, Austria (2003).

[13] Chalise, R. and Khanal, R. Self consistent one dimension in space and three dimension in velocity kinetic trajectory simulation model of magnetized plasma wall transition. *Phys. Plasmas*, **22**, 01135021-5 (2015).

[14] Adhikari, B. R., Basnet, S., Lamichhane, H. P. and Khanal, R. Presheath-sheath coupling for kinetic trajectory simulation of a magnetized plasma sheath. *AIP Advances*, **9**, 055123-10 (2019).

Him. Phys. **8** 71-78, (2019)

Himalayan Physics

Variation of velocity component of ions in a magnetized plasma sheath for different obliqueness of the magnetic field

Research Article

Bhesha Raj Adhikari*, **Suresh Basnet, Hari Prasad Lamichhane, Raju Khanal**

Central Department of Physics, Tribhuvan University, Kirtipur, Kathmandu 44613, Nepal

Abstract: Frequency of oscillation and velocity variation of different component of ions in a magnetized plasma sheath has been numerically investigated by using a kinetic trajectory simulation model for varying obliqueness at constant magnetic field. By varying obliqueness average value, maximum amplitude, damping factor and frequency of oscillation of velocity components at magnetic field 8 mT have been studied. Due to the change in obliqueness of the field the average values as well as the maximum amplitude of the three components of the velocity also change but frequency of oscillation almost remains same. In this case also there is small change in damping factor as well.

Keywords: Magnetized plasma sheath • Bohm-Chodura condition • Frequency of oscillation • Kinetic theory • Mean value • Damping factor

1. Introduction

Velocity variation and frequency of oscillation of various components of ions for varying obliqueness is a new field of research [1–4]. Plasma sheath study is an old but now a days it is not a finished solved problem which is useful in different areas of plasma physics [5]. Works of both experiment and theory have been developed widely during the past several years and yet are still not fully understood [1–4, 6–10]. In recent years, the sheath formed between magnetic plasma and a particle absorbing wall has received a considerable amount of attention [6–15]. When the plasma is confined in any closed surface, it is obvious that the plasma interacts with the material surfaces so that the proper understanding of this interaction with the material surface is very important in all plasma applications (e.g. plasma confinement for fusion, sputtering, etching, surface treatment, etc) [8]. Once the plasma–wall interaction is well understood it will be possible to control heat loading, energy transfer and particle flow towards the wall and overall bulk plasma behaviour [3, 4].

To sheath, the in streaming ions at the sheath edge have to satisfy the condition called the Bohm criterion [3, 4, 6–17] . A magnetized plasma sheath is responsible for the flow of charged particles and energy towards the

* *Corresponding Author: b.r.adhikari@hotmail.com*

wall. In this work, we introduce and describe a new self consistent 1d3v Kinetic Trajectory Simulation (KTS) applicable for studying the magnetized PWT region.

The importance of this study is to see the change in the particle dynamics as well as the particle wall interaction in magnetized plasma sheath. Irrespective of this, plasma sheath is significantly influencing the charged particles and the energy flux to the wall, which in turn considerably modifies the absorption, emission impurities and all other characteristics in the plasma [8]. We have used the Kinetic Trajectory Simulation (KTS) model [13–17] to obtain solution to a non-neutral, time independent, collisionless plasma sheath and hence studied the ion velocities in a magnetized plasma sheath for different obliqueness of the field. This paper is organized as follows: In section 2 we discuss the basic principle of the KTS method in a simplified form. In this section we explain the distribution function in the collision less case. In section 3 we discuss about our magnetized plasma sheath model. In this section we apply Lorentz force equation which is solved by Runge-Kutta method in MATLAB using boundary condition. In section 4 we obtain the result in graphical form and we discuss about our result. Finally we summarize our work and draw conclusions.

2. Basic principle of KTS method

The fundamental equation which has to satisfy is the Boltzmann equation [8].

$$\frac{\partial f}{\partial t} + \vec{v}.\nabla f + \frac{\vec{F}}{m}.\nabla_v f = \left(\frac{df}{dt}\right)_c \tag{1}$$

where $\vec{F}$ is the force acting on the particles, and $\left(\frac{df}{dt}\right)_c$ is the time rate of change of f due to collisions. The symbol ∇ stands for the gradient in (x, y, z) space. The symbol ∇_v stands for the gradient in velocity space, and $f(\vec{r}, \vec{v}, t)$ is a velocity distribution function. In collisionless cases the equation is called the Vlasov equation:

$$\frac{\partial f}{\partial t} + \vec{v}.\nabla f + \frac{q}{m}(\vec{E} + \vec{v} \times \vec{B}).\nabla_v f = 0 \tag{2}$$

In the KTS method we solve the kinetic equation along with other basic equations describing the plasma for given boundary and initial conditions. The distribution function at any point along the trajectory can be obtained if its value at one point (i.e., at the boundary) is known. Then density of the species 's' is given by

$$n^s(\vec{x}) = \int_{-\infty}^{+\infty} d^3v f^s(\vec{x}, \vec{v}) \tag{3}$$

The space charge density is defined as

$$\rho(\vec{x}) = \sum_s q^s n^s(\vec{x}) \tag{4}$$

The electrostatic potential $\phi(x)$ is to be found from poisson's equation

$$\frac{d^2\phi(\vec{x})}{dx^2} = -\frac{\rho(\vec{x})}{\epsilon_0}, \tag{5}$$

and the electric field is given by

$$E(\vec{x}) = -\frac{d\phi(\vec{x})}{dx} \tag{6}$$

In our simulation, we solve Eqs. 1-6 along the collisionless trajectories for given boundary conditions.

3. Plasma sheath model

The 1d3v model of magnetized plasma sheath is shown schematically in Figure 1.

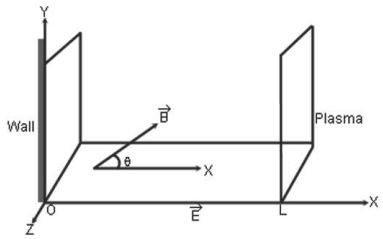

Figure 1. Schematic diagram of the plasma sheath model

The simulation region considered is bounded by two parallel planes situated at $x = 0$ and $x = L$ and the plasma consists of only electrons and singly charged ions. We have specified $x = L$ as the "sheath entrance" which separates the non-neutral, collision less sheath region ($x < L$) from the quasineutral collisional presheath region ($x > L$). Similarly, an absorbing wall is specified by $x = 0$. We assuming the angle between the oblique magnetic magnetic field with along the x-axis or electric field to be θ . The magnetic field lies in the x-y plane . We suppose the plasma particles (electrons and ions) enter the simulation region from the sheath entrance with cut off Maxwellian velocity distribution functions, the wall doesn't emit any particles and that both boundaries are perfectly absorbing. Accordingly, the electron velocity distribution function is given by

$$f^e(x,v) = A^e \exp\left[-\left(\frac{v_x^2 + V_y^2 + v_z^2}{v_{tf}^2}\right) + \frac{e\phi(\vec{x})}{kT_e}\right]\Theta\left[v_{cL}^e(x) - v_x\right] \tag{7}$$

where $v_c^e(x) = \sqrt{\frac{2e[\phi(x)-\phi_0]}{m^e}}$ is the electron cut off velocity at x, k is the Boltzmann constant and $\Theta(x)$ is the Heaviside function i.e.,

$$\Theta(x) = \begin{cases} 1 & \text{if} x \geq 0 \\ 0 & \text{otherwise.} \end{cases} \tag{8}$$

The ion velocity distribution function at $x = L$ is given by,

$$f^i(L,v) = A^i \exp\left[-\left(\frac{(v_x - v_{mL}^i)^2 + v_y^2 + v_z^2}{v_{tf}^{i2}}\right)\right]\Theta(v_{cL}^i - v_x) \tag{9}$$

where,$v_{tf}^{s} = \sqrt{\frac{2kT^5}{m^s}}$ is the species (ion and electron) thermal velocity, v_{ml}^{i} is the ion "Maxwellian-maximum" velocity at $x = L$ and v_{cL}^{i} ($v_{cL}^{i} < 0$) is the ion cut off velocity at $x = L$. In the core plasma the particle distribution would obviously be Maxwellian, however, in case of sheath formation the ions are accelerated towards the wall so that they become shifted Maxwellian as given by Eq. 9. In addition, for the Bohm criterion to be satisfied by the ions they must have attained certain minimum velocity (v_{cL}^{i}) at the sheath entrance. As the electrons are retracted and reflected by the negative potential wall their distribution gets cut-off at the sheath entrance as given by Eq. 7.

For the velocity distribution given by Eq. 9, we can evaluate Eq. 3 for electron density at $x = L$ as

$$n_L^e(x) = A^e \int_{-\infty}^{+\infty} dv_x \int_{-\infty}^{+\infty} dv_y \int_{-\infty}^{+\infty} dv_z \left[- \left(\frac{v_x^2 + v_y^2 + v_z^2}{v_{tf}^{e2}} \right) \right] \Theta(v_{cL}^e - v_x) \tag{10}$$

Now, from the velocity distribution function (Eqs. 9 and 3), we get ion density as

$$n_L^i = A^i \int_{-\infty}^{+\infty} dv_x \int_{-\infty}^{+\infty} dv_y \int_{-\infty}^{+\infty} dv_z \left[- \left(\frac{(v_x - v_{mL}^i)^2 + v_y^2 + v_z^2}{v_{tf}^{i2}} \right) \right] \Theta(v_{cL}^i - v_x) \tag{11}$$

In order to obtain the electron density profile, we require $\phi(x)$ to be known. In our calculation, we obtain $\phi(x)$ only at the grid points x_j so that we obtain the electron density at these points in terms of potential as

$$n^e(\phi) = n_L^e \exp\left[\frac{e\phi(x)}{kT_f^e} \right] \left[\frac{1 + erf\sqrt{\frac{e(\phi(x) - \phi_0)}{kT_f^e}}}{1 + erf\sqrt{\frac{-e\phi_0}{kT_f^e}}} \right] \tag{12}$$

Hence, one can obtain the electron density at any point if the potential profile is known. Different components of velocity of ions in the plasma sheath have been computed applying Lorentz force equation

$$\vec{F} = q(\vec{v} \times \vec{B}) + q\vec{E} \tag{13}$$

4. Results And Discussion

The time dependency of velocity component of ions have been calculated for magnetic field 8 mT at different obliqueness (30°, 60° and 75°) respectively. The results of calculation are shown Figs. 2 to 4. In Fig. 2 at angle 30° initial values of x, y, and z-component are same and started from the initial value equal to 9794 ms^{-1}. The x, y and z-component of velocity attains the average value of nearly equal to 0.0003 , 6668 and 11600 ms^{-1} respectively. Before getting the stabilized values (average values) the x-component of velocity oscillates with maximum amplitude as 2761.999 ms^{-1}. Similarly maximum amplitude of y and z-component is 3576 and 2060 ms^{-1} respectively. Each component has frequency of oscillation nearly equal to 10.5 , 10 and 10 Hz respectively. In addition, these components show damping nature of oscillation with damping factor 17.9, 18.3 and18.3 s^{-1} respectively.

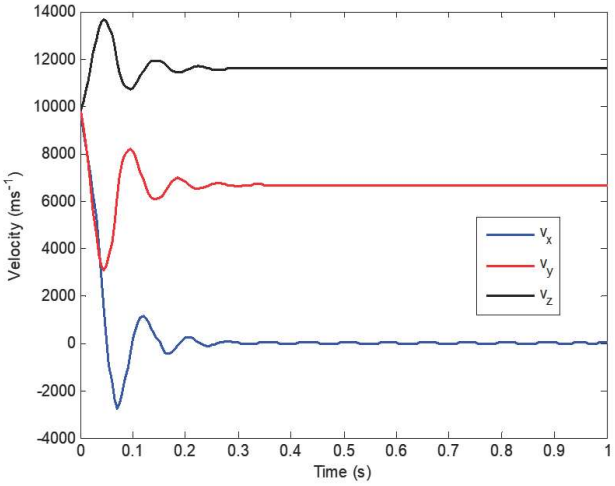

Figure 2. Variation of velocity with time at magnetic field 8mT and angle 30°

In Fig. 3 at angle 60° initial values of x, y and z-component are same and equal to 979ms^{-1}. In this figure y-component of velocity increased and the average value becomes equal to 11570ms^{-1} . But x and z-component of velocity attains the average values of -0.0008 and 6711ms^{-1} respectively. Before getting the average values each component oscillates with the maximum amplitude of 3113.99,1100 and 4619ms^{-1} respectively. Each component has frequency of oscillation nearly equal to 11.8,10 and 10.5 Hz respectively. Also,these components show damping nature of oscillation with damping factor 18.4,17 and 17.3s^{-1} respectively.

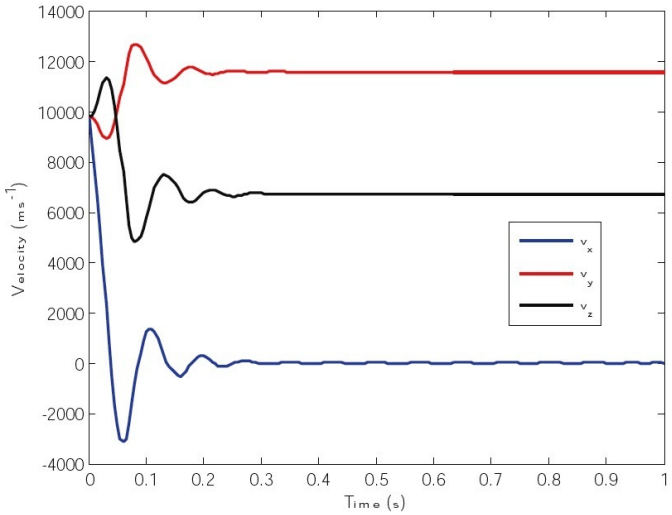

Figure 3. Variation of velocity with time at magnetic field 8 mT and angle 60°.

In Fig. 4, like previous also initial values of x, y and z-component are same and equal to 9794 ms^{-1}. The x and z-component of velocity decreases to the average values of 0.0004 and 3129 ms^{-1} respectively, whereas the the y-component of velocity increases to the average value of 11580 ms^{-1}. Before getting the average values each component oscillates with the maximum amplitude of 1605.99 , 290. and 1074 ms^{-1} respectively. Each component has frequency of oscillation nearly equal to 11.1 , 10.5 and 11.8 Hz respectively. These components also show damping nature of oscillation with damping factor 18.1, 17.6, and 17.8 s^{-1} respectively.

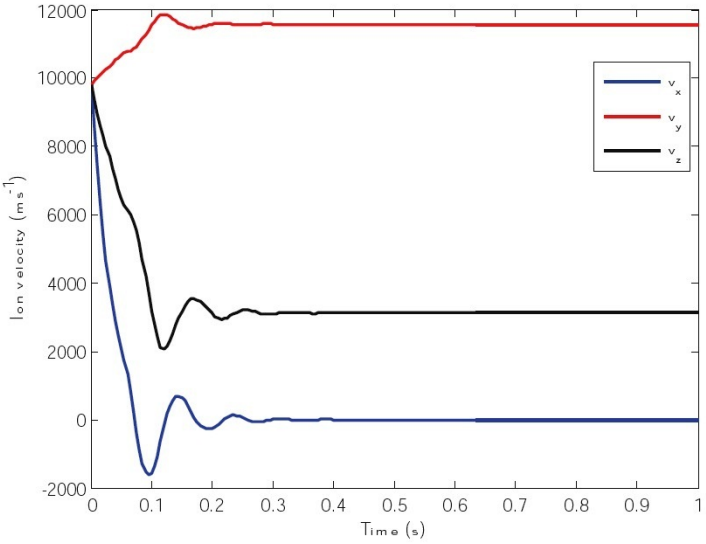

Figure 4. Variation of velocity with time at magnetic field 8 mT and angle 75°.

Table 1. The observed data of average value, amplitude, Damping constant and Frequency of oscillation at magnetic field 8 mT

Θ	Average value			Maximum amplitude			Damping factor			Frequency of oscillation		
	v_{xm}	v_{ym}	v_{zm}	v_{xz}	v_{yz}	v_{yz}	v_x	v_y	v_z	v_x	v_y	v_z
30°	0.0003	6668	11600	2761.99	3576	2060	17.9	18.3	18.3	10.5	10	10
60°	-0.0008	11570	6711	3113.999	1100	4619	18.4	17	17.3	11.8	10	10.5
75°	0.0004	11580	3129	1605.999	290	1074	18.1	17.6	17.8	11.1	10.5	11.8

Table 1 shows the summary of observed data for average value, maximum amplitude, damping factor and frequency of oscillation. Mean value (11600 ms^{-1}) is maximum on y-component at 30° with respect to other components at different angles. Also at angle 75° amplitude (290 m/s) is minimum on y-component whereas at angle 60° amplitude (4619 ms^{-1}) is maximum on z-component. At angle 60° damping factor is minimum ie 17 s^{-1} on y-component, on the other hand at 60° damping factor is maximum i.e. 18.4 s^{-1} on x-component.

5. Conclusions

It has been observed that ion velocity at presheath-sheath boundary is greatly affected by obliqueness of the field. At constant magnetic field as the obliqueness of the field changes the separation of the average values as well as the maximum amplitude of all the three component of the velocity also change but frequency of oscillation is almost constant. Angular dependence of average value, maximum amplitude, damping constant, frequency of oscillation of velocity components at magnetic field 8 mT has been observed. The study can be important in material processing, plasma etching and for confinement of plasma in fusion devices.

References

[1] Chodura R. Plasma–wall transition in an oblique magnetic field. The Physics of Fluids. 1982;25(9):1628–1633.

[2] Chodura R. Physics of Plasma-Wall Interactions in Controlled Fusion. Controlled Fusion, Plenum, New York. 1986;p. 99.

[3] Riemann KU. The Bohm criterion and sheath formation. Journal of Physics D: Applied Physics. 1991;24(4):493.

[4] Riemann K. Theory of the plasma-sheath transition. Journal of Technical Physics. 2000;41(1):89–121.

[5] Adhikari S, Moulick R, Goswami K. A dynamic analysis of the magnetized plasma sheath in a collisionless scenario with ion sources. Physics of Plasmas. 2017;24(8):083501.

[6] Hatami M, Niknam A, Shokri B, Ghomi H. Magnetized plasma sheath with two species of positive ions. Physics of plasmas. 2008;15(5):053508.

[7] Zou X, Qiu M, Liu H, Zhang L, Liu J, Gong Y. The ion density distribution in a magnetized plasma sheath. Vacuum. 2008;83(1):205–208.

[8] Chalise R, Khanal R. A kinetic trajectory simulation model for magnetized plasma sheath. Plasma Physics and Controlled Fusion. 2012;54(9):095006.

[9] Khoramabadi M, Ghomi H, Shukla PK. Numerical investigation of the ion temperature effects on magnetized DC plasma sheath. Journal of Applied Physics. 2011;109(7):073307.

[10] Gyergyek T, Kovačič J. Fluid model of the sheath in front of a floating electrode immersed in a magnetized plasma with oblique magnetic field: Some comments on ion source terms and ion temperature effects. Physics of Plasmas. 2015;22(4):043502.

[11] Huang CW, Chen YC, Nishimura Y. Particle-in-cell simulation of plasma sheath dynamics with kinetic ions. IEEE Transactions on Plasma Science. 2015;43(2):675–682.

[12] Moulick R, Goswami KS. Potential around a dust grain in collisional plasma. Physics of Plasmas. 2015;22(4):043701.

[13] Chalise R, Khanal R. Self-consistent one dimension in space and three dimension in velocity kinetic trajectory

simulation model of magnetized plasma-wall transition. Physics of Plasmas. 2015;22(11):113505.

[14] Lieberman M, Lichtenberg A, Kawamura E, Chabert P. Linear electromagnetic excitation of an asymmetric low pressure capacitive discharge with unequal sheath widths. Physics of Plasmas. 2016;23(1):013501.

[15] Chauhan S, Ranjan M, Bandyopadhyay M, Mukherjee S. Droplet shaped anode double layer and electron sheath formation in magnetically constricted anode. Physics of Plasmas. 2016;23(1):013502.

[16] Bohm D. The characteristics of electrical discharges in magnetic fields. Qualitative Description of the Arc Plasma in a Magnetic Field. 1949;.

[17] Khanal R. A kinetic trajectory simulation (KTS) model for bounded plasmas. na; 2002.

*Journal of Institute of Science and Technology 2018, **23**:88-92*
ISSN: 2469-9062 (print), 2467-9240 (e)
DOI: https://doi.org/10.3126/jist.v23i1.22201

Research Article

BEAT FREQUENCY AND VELOCITY VARIATION OF IONS IN A MAGNETIZED PLASMA SHEATH FOR DIFFERENT OBLIQUENESS OF THE MAGNETIC FIELD

B. R. Adhikari*, S. Basnet, H. P. Lamichhane, R. Khanal

Central Department of Physics, Tribhuvan University, Kirtipur, Kathmandu, Nepal
**Corresponding author: b.r.adhikari@hotmail.com*

(***Received:*** *August 8, 2018;* ***Revised****: December 22, 2018;* ***Accepted:*** *December 23, 2018)*

ABSTRACT

Beat frequency and velocity variation of ions in a magnetized plasma sheath has been numerically investigated by using a kinetic trajectory simulation (KTS) model for varying obliqueness of the external magnetic field in presence of an electric field. Angular dependence of mean value, maximum amplitude, damping constant, frequency of oscillation and beat frequency have been studied. As the obliqueness of the field changes the mean values, beat frequency as well as the maximum amplitude of the velocity components also change but frequency of oscillation remains almost the same.

Keywords: Plasma, Magnetized sheath, Bohm-Chodura condition, Kinetic theory, Beat frequency

INTRODUCTION

The study of beat frequency and velocity variation of ions in magnetized plasma sheath for varying obliqueness is one of the important problems for nearly all applications of plasma, where it is confined to a finite volume using magnetic fields (Chodura 1982, 1986, Riemann 1991, 2000). It is one of the most important problems of plasma. The correlative works, both of experiment and theory have been developed widely during the past several years and not yet fully understood (Chodura 1982, 1986, Riemann 1991, 2000, Hatami *et al.* 2008, Zou *et al.* 2009, Chalise & Khanal 2012, Khoramabadi *et al.* 2011, Gyergyek & Kovacic 2015). The sheath formed between magnetic plasma and a particle absorbing wall have received considerable amount of attention (Hatami *et al.* 2008, Zou *et al.* 2009, Chalise & Khanal 2012, Khoramabadi *et al.* 2011, Gyergyek & Kovacic 2015, Huang *et al.* 2015, Moulik & Goswami 2015, Chalise & Khanal 2015, Liberman *et al.* 2016, Chauhan *et al.* 2016). When the plasma is confined in any closed surface, the plasma interacts with the material surface so that the proper understanding of this interaction is very important in all plasma applications like in plasma confinement for fusion, sputtering, etching, surface treatment, etc (Chalise & Khanal 2012). Once the plasma-wall interaction is well understood it will be possible to control heat loading, energy transfer and particle flow towards the wall and overall bulk plasma behavior (Riemann 2000, Chalise & Khanal 2012). The wall is generally charged up negatively due to the higher velocity of the plasma electrons as compared with that of the ions. Due to this reason, negative potential is developed in the absorbing wall which attracts the ions and repels part of the electrons, forming a positive space charge region in front of the wall, which is 'sheath'. For the formation and stability of such a sheath, the in-streaming ions at the sheath edge has to satisfy a condition called the Bohm criterion (Bohm 1949), which for a magnetized plasma is modified by Chodura (1982, 1986).

In presence of an oblique magnetic field, the charged particles entering into the plasma sheath region oscillate and it has been observed that the ion velocity shows beat-like nature. The beat nature shown by ion velocity in a magnetized plasma sheath has been reported and analyzed for different obliqueness of the magnetic field using a kinetic trajectory simulation (KTS) model (Khanal 2003). The importance of this study is to observe the changes in the particle dynamics as well as the particle wall interaction in magnetized plasma sheaths.

METHODS AND MODEL

KTS is an iterative method for numerically calculating self-consistent, time independent kinetic plasma states in some given bounded spatial region originally developed for non-magnetic cases (Khanal 2003) which was extended to include oblique magnetic field by Chalise and Khanal (2012). The characteristics feature of the KTS method is that the distribution functions of the ions are calculated directly, by solving the related kinetic equations along the respective collisionless particle trajectories. The electron density profile is still obtained analytically considering its cut-off Maxwellian distribution by the negative wall.

The fundamental equation which $f(\vec{r},\vec{v},t)$ has to satisfy is the Boltzmann equation (Chalise & Khanal 2012).

$$\frac{\partial f}{\partial t}+\vec{v}.\nabla f+\frac{\vec{F}}{m}.\nabla_v f=\left(\frac{df}{dt_c}\right) \quad (1)$$

Where, $\vec{F}$ is the force acting on the particles and $\left(\frac{df}{dt}\right)_c$ is the time rate of change of f due to collisions. The symbol ∇ stands for the gradient in (x, y, z) space and ∇_v

stands for the gradient in velocity space, and $f(\vec{r},\vec{v},t)$ is a velocity distribution function. In collisionless cases the equation is called the Vlasov equation:

$$\frac{\partial f}{\partial t}+\vec{v}\cdot\nabla f+\frac{q}{m}(\vec{E}+\vec{v}\times\vec{B}).\nabla_v f=0 \qquad (2)$$

In the KTS method we solve the kinetic equation along with other basic equations describing the plasma for given boundary and initial conditions. The distribution function at any point along the trajectory can be obtained if its value at one point (i.e., at the boundary) is known. Then density of the species 's' is given by

$$n^s(\vec{x})=\int_{-\infty}^{\infty} d^3v\, f^s(\vec{x},\vec{v}) \qquad (3)$$

The space charge density is defined as

$$\rho(\vec{x})=\sum_s q^s n^s(\vec{x}) \qquad (4)$$

The electrostatic potential $\varphi(x)$ is to be found from Poisson's equation

$$\frac{d^2\phi(\vec{x})}{dx^2}=-\frac{\rho(\vec{x})}{\varepsilon_0}, \qquad (5)$$

and the electric field is given by

$$E(\vec{x})=-\frac{d\phi(\vec{x})}{dx} \qquad (6)$$

In present simulation, it solves equations (1)-(6) along the collisionless trajectories for given boundary conditions.

The *1d3v* model of magnetized plasma sheath is shown schematically in Fig. 1. The simulation region considered is bounded by two parallel planes situated at $x=0$ and $x=L$ and the plasma consists of only electrons and singly charged ions. It has specified $x=L$ as the "sheath entrance" which separates the non-neutral, collision less sheath region ($x < L$) from the quasineutral collisional presheath region ($x > L$).

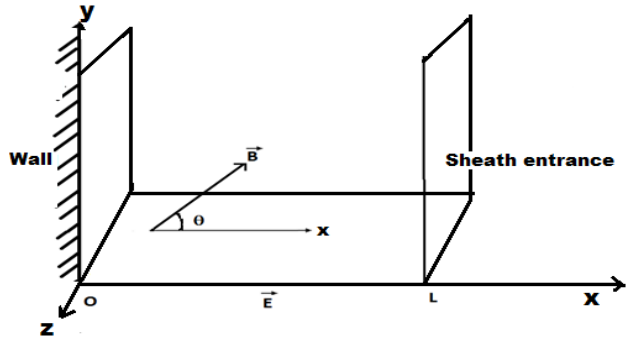

Fig. 1: Schematic diagram of the plasma sheath model

Similarly, an absorbing wall is specified by *x=0*. It is assumed that the angle made by the oblique magnetic field with the *x*-axis, which is the direction of the electric field, to be θ. The magnetic field lies in the *x-y* plane.

It is supposed that the plasma particles (electrons and ions) enter the simulation region from the sheath entrance with cut off Maxwellian velocity distribution functions, the wall doesn't emit any particles and that both boundaries are perfectly absorbing. Accordingly, the electron velocity distribution function is given by

$$f^e(x,v)=A^e\exp\left[-\left(\frac{v_x^2+v_y^2+v_z^2}{v_{tf}^{e^2}}\right)+\frac{e\phi(\vec{x})}{kT_e}\right]\Theta\left[v_{cL}^e(x)-v_x\right] \qquad (7)$$

where $v_c^e(x)=\sqrt{\frac{2e[\phi(x)-\phi_0]}{m^e}}$ is the electron cut off velocity at *x*, *k* is the Boltzmann constant and Θ (x) is the Heaviside function i.e.,

$$\Theta(x)=\begin{matrix}1 & if\ x\geq 0\\ 0 & otherwise.\end{matrix} \qquad (8)$$

The ion velocity distribution function at $x=L$ is given by,

$$f^i(L,v)=A^i\exp\left[-\left(\frac{(v_x-v_{mL}^i)^2+v_y^{\,2}+v_z^{\,2}}{v_{tf}^{i\,2}}\right)\right]\Theta\left(v_{cL}^i-v_x\right) \qquad (9)$$

where, $v_{tf}^s=\sqrt{\frac{2kT^s}{m^s}}$ is the species-s (ion and electron) thermal velocity, v_{ml}^i is the ion "Maxwellian-maximum" velocity at $x=L$ and v_{cL}^i (v_{cL}^i < 0) is the ion cut off velocity at $x=L$. In the core plasma the particle distribution would obviously be Maxwellian, however, in case of sheath formation the ions are accelerated towards the wall so that they become shifted Maxwellian as given by equation (9). In addition, for the Bohm criterion to be satisfied by the ions they must have attained certain minimum velocity (v_{cL}^i) at the sheath entrance. As the electrons are retracted and reflected by the negative potential wall their distribution gets cut-off at the sheath entrance as given by equation (7).

Once all the starting parameters at the sheath entrance are known we solve the ion kinetic equations, for different discretized ion injection velocities up to the wall. This gives the ion velocities and their corresponding distribution function in the entire sheath region which on integration yields ion density distribution. For the velocity distribution given by equation (9), we can evaluate equation (3) for electron density at $x=L$ as

$$n_L^e(x)=A^e\int_{=\infty}^{+\infty}dv_x\int_{-\infty}^{+\infty}dv_y\int_{-\infty}^{+\infty}dv_z\left[-\left(\frac{v_x^2+v_y^2+v_z^2}{v_{tf}^{e^2}}\right)\right]\Theta\left(v_{cL}^e-v_x\right) \qquad (10)$$

Now, from the velocity distribution function (9) and (3), we get ion density as

$$n_L^i = A^i \int_{-\infty}^{+\infty} dv_x \int_{-\infty}^{+\infty} dv_y \int_{-\infty}^{+\infty} dv_z \left[-\left(\frac{\left(v_x - v_{mL}^i\right)^2 + v_y^2 + v_z^2}{v_{tf}^{i^2}} \right) \right] \Theta\left(v_{cL}^i - v_x\right) \quad (11)$$

The average velocity for ions can be calculated by using

$$u_L^i = \frac{1}{n_L^i} \int_{-\infty}^{v_{cL}^i} \int_{-\infty}^{+\infty} \int_{-\infty}^{+\infty} \left(v_x \hat{i} + v_y \hat{j} + v_z \hat{k}\right) \times A^i \exp\left[-\left(\frac{\left(v_x - v_{mL}^i\right)^2 + v_y^2 + v_z^2}{v_{tf}^{i^2}} \right) \right] dv_x dv_y dv_z \quad (12)$$

and the average velocity for electrons is

$$u_L^e = \frac{1}{n_L^e} \int_{-\infty}^{v_{cL}^e} \int_{-\infty}^{+\infty} \int_{-\infty}^{+\infty} \left(v_x \hat{i} + v_y \hat{j} + v_z \hat{k}\right) \times A^e \exp\left[-\left(\frac{v_x^2 + v_y^2 + v_z^2}{v_{tf}^{e^2}} \right) \right] dv_x dv_y dv_z \quad (13)$$

The electron density profile, which is evaluated analytically, is given in terms of potential as

$$n^e(\phi) = n_L^e \exp\left[\frac{e\phi(x)}{kT_f^e} \right] \left[\frac{1 + erf\sqrt{\frac{e(\phi(x) - \phi_0)}{kT_f^e}}}{1 + erf\sqrt{\frac{-e\phi_0}{kT_f^e}}} \right] \quad (14)$$

RESULTS

The variation of various components of ion velocity with respect to time have been calculated numerically for magnetic field 2 mT at different obliqueness of the field (30°, 60° and 75°) and the results are shown in Figs 2 to 4. Figure 2 shows that at obliqueness 30°, the *x*-, *y*- and *z*-component of velocity sinosodially varied about the mean value of –106.9, 6639 and 11620 ms^{-1}, respectively, with same frequency of oscillation 100 Hz.

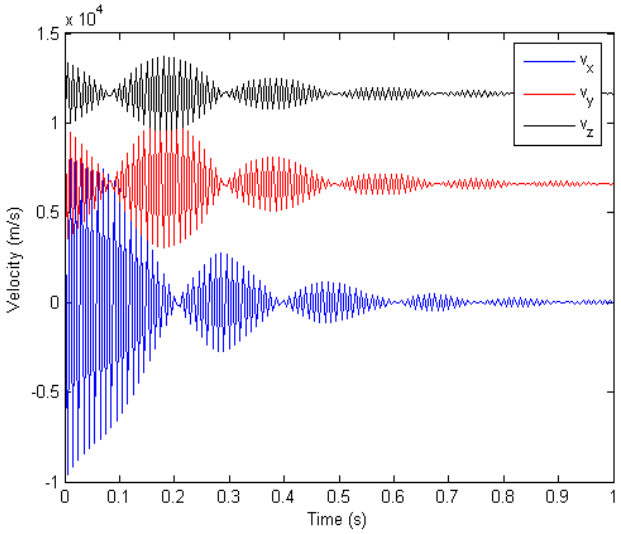

Fig. 2. Variation of velocity with time at magnetic field 2 mT and angle 30°

In addition, these components showed damping nature of oscillation with damping factor of 4.3, 4.5 and 4.2 s^{-1}, respectively. Like wise at the angle of 30°, the *x*-, *y*- and *z*-component of velocity varied with maximum amplitude of 9900.9, 3501 and 2070 ms^{-1}, respectively. The figure shows that, for *x*-, *y*- and *z*-component of velocity formed 5.5, 5.2 and 5.04 beats in *x*-, *y*- and *z*-component of velocity in 1 second, so that their beat frequency was equal to 5.5, 5.2 and 5.04 Hz. The first zero amplitude was obtained at about 0.2 second in *x*-component of velocity, whereas in *y*- and *z*-component of velocity the first zero amplitude was obtained at around 0.1 second.

Figure 3 shows that at angle 60°, the *x*-, *y*- and *z*-component of velocity sinosodially varied about the mean value of -41.07, 11590 and 6683 ms^{-1}, respectively, with constant frequency of oscillation 100 Hz. In addition, like previous these components also showed damping nature of oscillation with damping factor 4.4, 4.7 and 4.2 s^{-1}, respectively. Similarly, at the same angle, the *x*-, *y*- and *z*-component of velocity varied with maximum amplitude 9835.07, 2630 and 4747 ms^{-1}, respectively. Like wise this figure shows that for *x*-, *y*- and *z*-component of velocity, there formed 5.3, 5.6 and 5.7 beats in 1 second so that their beat frequency was equal to 5.3, 5.6 and 5.7 Hz. The first zero amplitude was obtained at around 0.15 second in *x*-component of velocity whereas in *y*- and *z*-component of velocity the first zero amplitude was obtained at around 0.255 second.

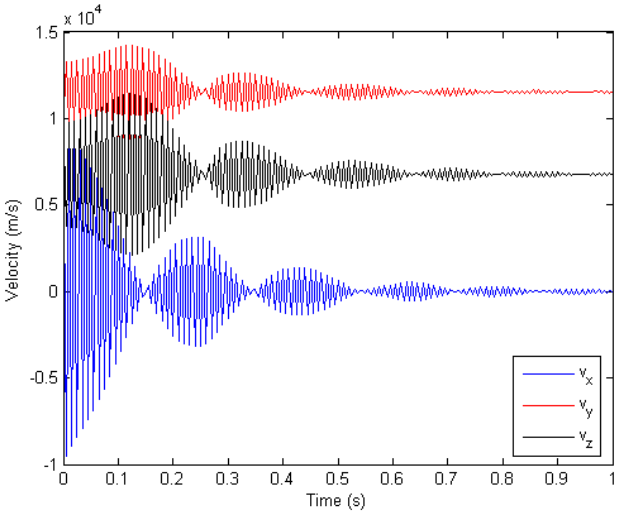

Fig. 3. Variation of velocity with time at magnetic field 2 mT and angle 60°

Figure 4 shows that the *x*-, *y*- and *z*-component of velocity sinosodially varied about the mean value of 43.26, 11540 and 3296 ms^{-1}, respectively, with frequency of oscillation 100 Hz at obliqueness 75°. In addition, these components showed damping nature of oscillation with damping factor of 4.5, 4.2 and 5.5 s^{-1}, respectively. The *x*-, *y*- and *z*-component of velocity varied with maximum amplitude

9750.74, 1850 and 6498 ms^{-1}, respectively, at the same value of obliqueness.

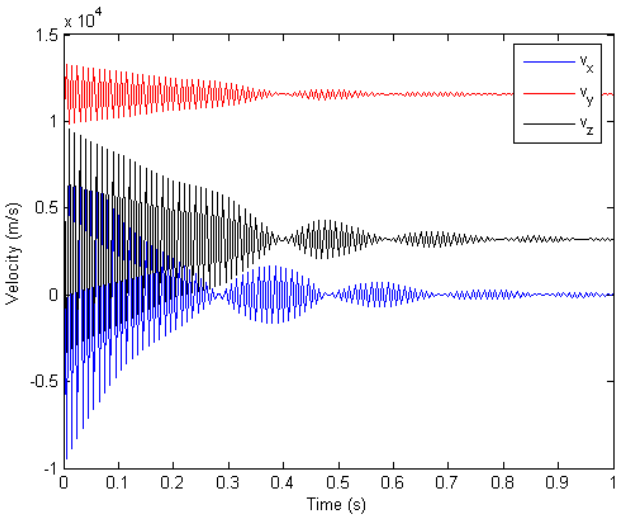

Fig. 4. Variation of velocity with time at magnetic field 2 mT and angle 75˚

Similarly, Fig. 4 shows that at an angle 75˚, for *x*-, *y*- and *z*-component of velocity there formed 5.2, 5.6 and 5.6 beats in 1 second, respectively, so that their beat frequency was equal to 5.2 , 5.6 and 5.6 Hz, respectively. Also in *x*-component of velocity, the first zero amplitude was obtained at around 0.28 second whereas in *y*- and *z*-component of velocity the first zero amplitude was obtained at around 0.4 second. Further in *x*-, *y*- and *z*-component of velocity shoulder was obtained at around 0.1 second.

DISCUSSION

Table 1 shows the summary of observed data for mean value, maximum amplitude, damping constant, frequency of oscillation and beat frequency. The mean value of *x*-component of velocity at obliqueness of 30˚, 60˚ and 75˚ was small and negative compared to other components. The negative sign was due to the geometry considered where the wall is at origin and the ions enter the sheath region from $x = L$ with negative velocity. Mean value (11620 ms^{-1}) was maximum of the *z*-component at 30˚ with respect to all other components at different angles.

Table 1. The observed data of mean value, amplitude, damping constant, frequency of oscillation and beat frequency (all values are in SI units) at magnetic field 2 mT

Theta	Mean Value			Amplitude			Damping constant			Frequency of oscillation			Beat frequency		
	v_{xm}	v_{ym}	v_{zm}	v_{xa}	v_{ya}	V_{za}	v_x	v_y	v_z	v_x	v_y	v_z	v_x	v_y	v_z
30°	–106.9	6639	11620	9900.9	3501	2070	4.3	4.5	4.2	100	100	100	5.5	5.2	5.0
60°	–41.1	11590	6683	9835.1	2630	4747	4.4	4.7	4.2	100	100	100	5.3	5.6	5.7
75°	–43.3	11540	3296	9750.7	1850	6498	4.5	4.2	5.5	100	100	100	5.2	5.6	5.6

Also at angle 75˚ amplitude (1850 ms^{-1}) was minimum of the *y*-component whereas at angle 30˚ amplitude (9900.9 ms^{-1}) was maximum of the *x*-component. At angle 60˚ damping constant was maximum i.e. 4.7 s^{-1} of the *y*-component. The beat frequency along the *z*-component was maximum (5.7 Hz) for the angle 60˚. As we were considering a uniform magnetic field the frequency of oscillation was same for all cases and presented here for the purpose of comparing with the beat frequency.

CONCLUSION

The beat nature shown by ion velocity in a uniform magnetized plasma sheath has been reported for the first time and has been analyzed for different obliqueness of the magnetic field. As the ions enter the sheath region they are guided by the magnetic field and hence start gyrating. As they move closer to the wall the electric field increases and the dominance of magnetic field ceases which causes the oscillation to have beat like nature. Thus the beat results primarily due to the combined effect of electric and magnetic fields. In present work we have studied the time evolution of ion velocity and the beat frequency for different obliqueness of the external uniform magnetic field. As the obliqueness of the field changes the separation of the mean values, beat frequency as well as the maximum amplitude of all the three component of the velocity changes. The study is useful in understanding the exact particle behavior when they travel in the sheath region and can be important in material processing, plasma etching and for confinement of plasma in fusion devices.

ACKNOWLEDGEMENT

One of the authors (BRA) would like to acknowledge the University Grants Commission-Nepal, Sanothimi, Nepal for Ph.D. Fellowship support.

REFERENCES

Bohm, D. 1949. *The characteristics of electrical discharges in magnetic fields*, Mc-Graw Hill, pp. 77.

Chalise, R. and Khanal, R. 2012. A kinetic trajectory simulation model for magnetized plasma sheath.

Plasma Physisics and Controlled Fusion **54**: 095006 (5pp).

Chalise, R. and Khanal, R. 2015. Self-consistent one dimension in space and three dimension in velocity kinetic trajectory simulation model of magnetized plasma-wall transition. *Physics of Plasmas* **22**: 113505 1-5.

Chauhan, S., Ranjan, M., Bandyopadhyay, M. and Mukherjee, S. 2016. Droplet shaped anode double layer and electron sheath formation in magnetically constricted anode. *Physics of Plasmas* **23:** 013502 1-9.

Chodura, R. 1982. Plasma wall transition in an oblique magnetic field. *Physics of Fluids* **25**: 1628-1633.

Chodura, R. 1986. *Physics of plasma-wall transition in controlled fusion*. In: D. E. Post and R. Behrisch (eds), Plenum Publishing Corporation, pp. 99.

Gyergyek, T. and Kovacic, J. 2015. Fluid model of the sheath in front of a floating electrode immersed in a magnetized plasma with oblique magnetic field: Some comments on ion source terms and ion temperature effects. *Physics of Plasmas* **22**: 0435021-0435024.

Hatami, M.M., Niknam, A.R., Shokri, B. and Ghomi, H. 2008. Magnetized plasma sheath with two species of positive ions. *Physics of Plasmas* **15**: 053058 1-5.

Huang, C.W., Chen. Y.C. and Nishimura, Y. 2015. Particle-in-cell simulation of plasma sheath dynamics with kinetic ions. *IEEE Transactions on Plasma Science* **43**: 675-682.

Khanal, R. 2003. *A kinetic trajectory simulation (KTS) model for bounded plasma*. Ph. D. Thesis, Innsbruck University, Austria.

Khoramabadi, M., Ghomi, H. and Shukla, P.K. 2011. Numerical investigation of the ion temperature effects on magnetized DC plasma sheath. *Journal of Applied Physics* **109**: 073307 1-8.

Liberman, M.A., Lichtenberg, A.J., Kawamura, E. and Chabert, P. 2016. Linear electromagnetic excitation of an asymmetric low pressure capacitive discharge with unequal sheath widths. *Physics of Plasmas* **23**(1): 013501-7.

Moulik, R. and Goswami, K.S. 2015. Potential around a dust grain in collisional plasma. *Physics of Plasmas* **22**: 043701-6.

Riemann, K.U. 1991. The Bohm criterion and sheath formation. *Journal of Physics D: Applied Physics* **24**: 493-518.

Riemann, K.U. 2000. Theory of the plasma-sheath transition The Bohm criterion and sheath formation. *Journal of Technical Physics* **41**: 89-121.

Zou, X., Qiu, M., Liu, H., Zhang, L., Liu, J. and Gong, Y. 2009. The ion density distribution in a magnetized plasma sheath. *Vacuum* **83**: 205-208.

Progress in Tokamak Fusion Research

B. R. Adhikari, H. P. Lamichhane and R. Khanal
Central Department of Physics, Tribhuvan University, Nepal

ABSTRACT

In nuclear fusion two light nuclei are fused together to create a larger nucleus plus a large amount of energy. For fusion to take place very high temperatures are required such that two positively charged nuclei come together overcoming the repulsive force. The temperature is so high that the fusion fuel is in the plasma state and its confinement is not an easy task. Two principal mechanisms for confining the fusion fuelare Magnetic Confinement Fusion (MCF) and Inertial Confinement Fusion (ICF). In MCF, plasma is confined using sophisticated magnetic field whereas in ICF high energy lasers are used to compress small pellets of plasma fuel to very high densities within their inertial position. A Tokamak is a device using magnetic field to confine plasma and has made significant progresses towards realizing fusion energy on earth. The progresses made in Tokamak fusion research and its progress is presented.

Introduction

Nuclear fusion is a process by which two light nuclei fuse together to form a heavier nucleus, and in doing so release considerable energy. In order to overcome the repulsive force that exists between the positive nuclei the fuels must be heated to very high temperatures before the fusion can start. In order to create fusion on earth the most convenientfusion reaction is that between deuterium (D) and tritium (T) as shown schematically in Figure 1.The D-T fusion is most conveniently achievable because the collision cross-section of the D-T fusion reactions is the highest and occurs at relatively lower temperature [1]. The temperature required is of the order of 10^8 K, which is even more than the temperature at the core of the sun.

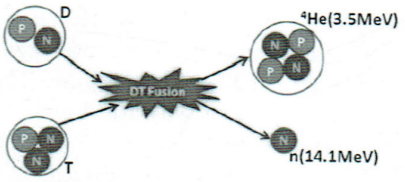

Figure 1: *Schematic of a D-T fusion reaction [1]*

As the temperature of any solid material is raised, its state changes from solid to liquid and then to gas. If we increase the temperature of a gas beyond a certain limit, it enters a regime where the thermal energy of its constituent particle is so great that the electrostatic forces which ordinarily bind electrons to atomic nuclei are overcome. Instead of hot gas composed of electrically neutral atoms, we then have a mixed population of charged and neutral particles. With increasing temperature the number of ionized particles increases and the ionized gas starts behaving differently. After the fraction of ionized particles is sufficiently high the ionized gas starts exhibiting collective behavior and the state of matter is plasma, and it is neither solid nor liquid nor gas. Plasma is thus defined as a quasineutral gas of charge and neutral particles which exhibits collective behavior [2]. Quasi-neutrality of plasma implies that the electron density and ion density are nearly equal and the collective behavior means that the motion of species depend not only on the local conditions but also on the state of the plasma far away from the point of interest.It is interesting to note that plasma can exist in diverse ranges of temperature and density ranges much lower as well as much higher than that of solid, liquid, and gas (as illustrated in Figure 2).

Nuclear fusion as the source of energy of the Sun and the stars was suggested many years ago [3] [4]. Since then, fusion energy is considered as one of the best potential sources of virtually unlimited energy for mankind [5]. Various methods for the realization of fusion energy were proposed and the most studied are Magnetic Confinement Fusion (MCF) and Inertial Confinement Fusion (ICF) [6] [7]. In MCF, the plasma is confined using a sophisticated magnetic field at very high temperatures, whereas in ICF high power lasers are used to compress small pellets of plasma fuel to very high densities within their inertial position. In both schemes it is desired to achieve the Lawson Criterion [5], which implies that more energy is produced through fusion reactions than the amount used up to start and maintain it [8]. In MCF, low density plasma is confined for longer period of time (few seconds to minutes), whereas in ICF high-density plasma is confined for few nanoseconds. Since nuclear fusion can potentially provide and almost unlimited source of energy, it is one of the most important scientific challenges man faces today [9].

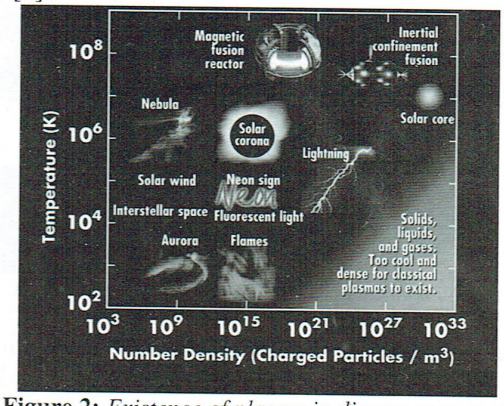

Figure 2: *Existence of plasma in diverse ranges of temperature and density [10]*

Tokamak and ITER

The most successful magnetic device, so far, for confining fusion plasma was invented in the late 1950s and is called 'Tokamak'[11]. The original idea of

Tokamak was given by Oleg Lavrentiev and invented in the 1950s by Nobel Laureates Igor Tamm and Andrei Sakharov. As obvious from its name a Tokamak uses powerful magnetic field configured in a sophisticated manner to confine thermonuclear plasma in the shape (Figure 3). Tokamaks have demonstrated better progresses as a fusion reactor especially in transport properties, operating density and stability of the fusion plasma which makes it the most promising approach for future commercial fusion reactors.

The Joint European Torus (JET), the world's largest Tokamak is also the most successful so far and serves as the milestone for the suitability of the Tokamak for future power production. In 1990s JET demonstrated controlled release of deuterium-tritium fusion power delivering 16 MW of fusion power using 10 MW as the input power [12]. It is worth considering the progress of magnetic confinement fusion research in terms of the fusion triple product achieved in various Tokamak devices (Figure 4). Since the start of Tokamak experiments in the 1960s, this product has increased by more than three orders of magnitude. Encouraged by the results fusion scientists from all over the world have come together in the construction of ITER (International Thermonuclear Experimental Reactor), which also means "the way" in Latin and hence the machine is expected to demonstrate the way forward for the construction and operation of future fusion power plants (Figure 5). ITER is an ambitious project whose initial concept was started in 19 November 1985 during Geneva Summit between the then US President Ronald Reagan and Soviet General Secretary Mikhail Gorbachov. As of now, the machine is designed to produce approximately 500 MW of fusion power sustained for more than 15 minutes by the fusion of about 0.5 g of deuterium - tritium mixture which corresponds to a gain of 10 with respect to the input power [13]. Construction of the facility began in 2007 in Cadarache of France, and the first plasma is expected to be produced in 2025.

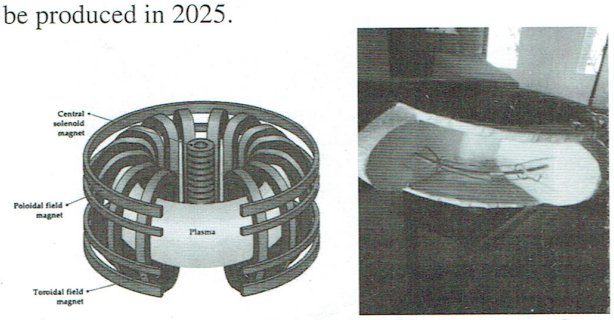

Figure 3: *Schematic of a Tokamak and a prototype at Central Department of Physics, Kirtipur*

Sun and stars are producing fusion energy for billions of years and nuclear fusion has already been tested as a nuclear weapon (so called hydrogen bomb) but unfortunately it is taking longer than expected for its realization of harnessing as an energy source. As fusion is clean, safeand virtually inexhaustible it is still a challenge for scientists and will be worth spending time and money for its research.

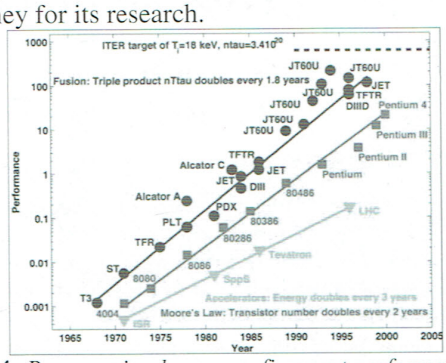

Figure 4: *Progress in plasma confinement performance* [13]

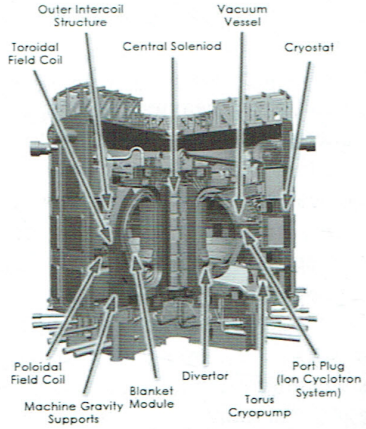

Figure 5: *Schematic diagram of ITER showing important components [13]*

Sometimes people argue that "*fusion is impossible*" but it has already been demonstrated in JET and many other devices across the globe and the progresses being made in construction of ITER is encouraging. The success of ITER will not only pave way for future fusion power plants but also demonstrates how science can bring people together to work for the betterment of mankind. As of now we can only hope that everything goes well as planned and fusion energy becomes available and for that we just need to push that date forward as quickly as possible.

References

[1] P. K. Kaw and I. Bandyopadhyay, *Fusion Physics*, Edited by M. Kikuchi, K. Lackner and M. Tran, IAEA, Vienna (2012).
[2] F. F. Chen. *Introduction to Plasma Physics and Controlled Fusion* (Third edition), Springer, Switzerland (2016).
[3] H. A. Bethe, Phys. Rev. **55**, 434 (1939).
[4] A. S. Eddington, *The Internal Constitution of the Stars*, Cambridge University Press (1926).
[5] W. J. Hogan and E. Bertel, *Energy from Inertial Fusion*, IAEA, Vienna (1995).
[6] N. G. Basov and O. N. Krokhin, Sov. Phys. JETP**19**, 123 (1964)
[7] J. Nuckolls et al, Nature **239**, 139 (1972).
[8] M. R. O'Brien and D.C. Robinson, *Plasma Physics*, Edited by R. Dendy, Cambridge University Press (1996).
[9] J. A. Bittencourt, *Fundamentals of Plasma Physics* (Third edition), Springer, NewYork (2004).
[10] https://lasers.llnl.gov/science/understanding-the-universe/plasma-physics (July 2017).
[11] J. Wesson, *Tokamaks*, Oxford University Press (1997)
[12] http://www.ccfe.ac.uk/jet.aspx (July 2017)
[13] https://www.iter.org/newsline/53/1589 (July 2017).

Introduction to the Plasma State of Matter

B. R. Adhikari and *R. Khanal
Central Department of Physics, Tribhuvan University, Kirtipur, Nepal
Department of Physics, Bhaktapur Multiple Campus, Tribhuvan University, Bhaktapur, Nepal
*plasmanepal@hotmail.com

Abstract: *Plasma is a quasineutral gas of charge and neutral particles which exhibits collective behavior. Because of its distinct behavior it is often termed as the fourth state of matter. It is of interest as it has found applications in diverse areas such as, controlled thermonuclear fusion, gas lasers, lightning, medicine, space science, electronics, etc. In this article we present an introduction to the plasma state of matter and discuss some of its applications.*

Keywords: plasma, quasineutrality, collective behavior, Debye shielding, plasma frequency, controlled thermonuclear fusion

1. INTRODUCTION

As the temperature of any solid material is raised, its state changes from solid to liquid and then to gas. If we increase the temperature of a gas beyond a certain limit, it enters a regime where the thermal energy of its constituent particle is so great that the electrostatic forces which ordinarily bind electrons to atomic nuclei are overcome. Instead of hot gas composed of electrically neutral atoms, we then have a mixed population of charged and neutral particles. With increasing temperature the number of ionized particles increases and the ionized gas starts behaving differently. After the fraction of ionized particles is sufficiently high the ionized gas starts exhibiting the collective behavior and the state of matter is plasma, and it is neither solid nor liquid nor gas. Plasma is thus defined as a quasineutral gas of charge and neutral particles which exhibits collective behavior. Quasineutrality of plasma implies that the electron density n_e is nearly equal to the ion density n_i so that $n_i \approx n_e \approx n$, where n is the common density of plasma particles called the plasma density; but the plasma is not so neutral that all the interesting electromagnetic phenomena vanish. The collective behavior implies that the motion of species depend not only on the local conditions but also on the state of the plasma far away from the point of interest [1]

The word "plasma" is derives from Greek and means something molded or fabricated. The existence of "the fourth state of matter" was first identified by Sir William Crookes in 1879 , however, the term plasma was introduced by I. Langmuir in 1928 to describe the state of matter in the positive column of glow discharge tube [2]. Plasma is thus an ionized gas, satisfying certain criteria to be discussed in next Sections; however any ionized gas cannot be called plasma.

2. DEBYE SHIELDING

Plasma possesses a special ability to shield out external potentials that are applied to it within a very small region. The external potential (ϕ_0) applied to a plasma is distributed into the plasma as

$$\phi(x) = \phi_o e^{-\frac{|x|}{\lambda_D}} \qquad (1)$$

where, λ_D is the Debye length expressed as

$$\lambda_D = \left(\frac{\varepsilon_0 k T_e}{n e^2}\right)^{\frac{1}{2}} \qquad (2)$$

ε_0 is the permittivity of free space, T_e is the electron temperature, e is the electronic charge and k is the Boltzmann constant.

The Debye length is an important physical property for the description of plasma. It provides a measure of the distance over which the influence of external potential is felt by the other charged particles inside the plasma. From equation (1) it is obvious that the charged particles arrange themselves in such a way that the external electrostatic fields are shielded within a distance of the order of a few Debye lengths.

This property is called the Debye shielding and for plasma to exhibit the collective behavior the Debye length must be much smaller than its characteristic length so that the majority of plasma particle are not influenced by the external potential. Consequently, charge in the plasma interacts collectively only with the charges those lie inside its Debye sphere, its effect on the other charges being effectively negligible.

For the Debye shielding to be a statistically valid concept the number of particles inside a Debye sphere must be sufficiently large [3], i.e.,

$$N_D = \frac{4}{3}\frac{\pi}{n^{1/2}}\left(\frac{\varepsilon_0 k T_e}{e^2}\right)^{\frac{3}{2}} \qquad (3)$$

must be very large.

3. PLASMA OSCILLATION

If the electrons in a quasineutral plasma are displaced from its equilibrium position an electric field will be built in such a direction such that it will try to restore the neutrality of the plasma by pulling the electrons back to their original positions. As the ions are massive compared to the electrons they form a uniform background. Due to inertia, the electrons will overshoot and oscillate about their equilibrium positions with a characteristic frequency, which is known as plasma frequency. This oscillation is so fast that the massive ions do not have time to respond to the oscillating electric field and may be considered as fixed. On solving the basic fluid equations for a plasma with singly charged ions the electron-plasma frequency ω_p is [1]

$$\omega_p = \left(\frac{ne^2}{\varepsilon_0 m_e}\right)^2 \qquad (4)$$

where m_e stands for mass of an electron . For the properties of the plasma to be determined by electromagnetic rather than hydrodynamic collision the plasma frequency must be large compared to the ordinary collision frequency.

4. CRITERION FOR PLASMA

As already mentioned, all the plasma are ionized gases, however, not all ionized gases are plasma. The conditions an ionized gas must satisfy to be called plasma are:

i) $\lambda_D < L$, where L is the dimension of plasma in question.

ii) $N_D >>> 1$

iii) $\omega_p \omega_c > 1$, where ω_c is the collision frequency of electrons with neutral

It is often said that more than 99% of the matter in the visible universe is in plasma state, however, the state of matter is almost not present on earth. A rare example of naturally occurring high temperature plasma on earth is lightning. This type of plasma can also be generated artificially using a high voltage, high temperature arc, which is the basis for the corona discharge process and for the plasma torch used to vaporize and redeposit metals. As soon as we start moving outside from the earth surface, e.g., the ionosphere is dominated by plasma. Although the plasma state is very rare on earth it is interesting to note that our solar system is dominated by plasma, as the Sun is in plasma state. Other examples where plasmas can be found are in stars, lightening, solar wind, fusion devices, welding arcs, neon signs, aurora, nebulae, galaxies, etc.

It is often a misconception that plasma is always hot. It is interesting to note that plasmas can exist in diverse ranges of temperature and density as shown in Fig. 1. Low temperature plasmas, used in surface modification and organic cleaning, are ionized gases generated at pressures between 0.1 and 2 Torr [4]. Thus plasma can exist at density and temperature both having ranges much lower as well as much higher than that of solid, liquid, and gaseous states of matter. Because of this diverse nature it has found applications in various fields, some of which are discussed below.

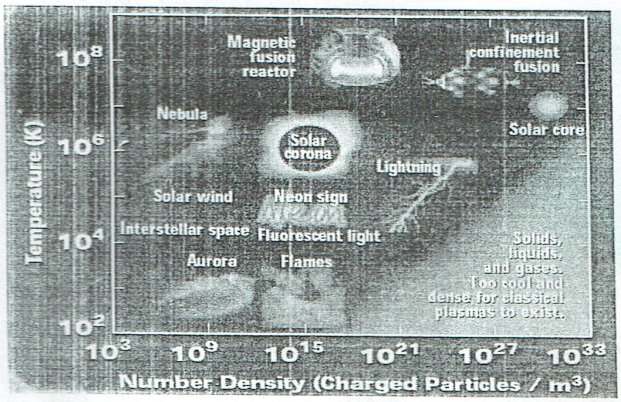

Fig. 1: Existence of plasma in diverse ranges of temperature and density

5. APPLICATIONS OF PLASMA

Because of its diverse nature plasma finds application in various fields such controlled thermonuclear fusion, surface treatment, biomedical applications, lighting, medicine, electronics, transportation and space propulsion, display technology, space physics, solid state plasma, gas lasers, etc. Some of the important and interesting applications of plasma in various fields are discussed here.

6. CONTROLLED THERMONUCLEAR FUSION:

Nuclear fusion as the source of energy of the Sun and stars was suggested many years ago [5-7]. Since then, fusion energy is considered as one of the best potential sources of virtually unlimited energy for mankind. Since nuclear fusion can potentially provide and almost unlimited source of energy, it is one of the most important scientific challenges man faces today. The most suitable reaction for the best utilization of the fusion energy as the potential sources of virtually unlimited energy for mankind is the one involving deuterium (D) and tritium (T) as:

$$D + T \rightarrow {}^4He + n + 17.6\ MeV$$

The Lawson criterion for a useful nuclear fusion reaction suggests that the cross-sections for the fusion reaction is appreciable for very high incident energies which corresponds to the temperature of the order of 10^8 K. This is much higher than the temperature at the core of the Sun and hence it is not easy confining the fusion fuels. This is in fact the problem faced by scientists which is not yet fully resolved and hence the fusion power could not be produced for commercial uses, so far. On the other hand the problem of heating and containing such plasma is responsible for the rapid growth of plasma physics since 1950s.

The schemes for realization of fusion energy on earth can be categorized into two main schemes, namely Magnetic Confinement Fusion (MCF) and Inertial Confinement Fusion (ICF) [8-10]. In MCF, the plasma is confined using a sophisticated nested magnetic field lines, where as in ICF, high power lasers (and in some cases high power particle beams) are used to compress small pellets of plasma fuel to very high densities and temperature within a time of the order of nanoseconds. Among various magnetic confinement schemes the most successful device so far is 'Tokamak', a doughnut shaped magnetic chamber initiated in former Soviet Union in early 50s. Based on various experiments the next generation Tokamak named "International Thermonuclear Experimental Reactor (ITER)", an international nuclear fusion research project to built the largest and most advanced experimental Takamak ever built, is currently under construction at Cadarache in France. The first operation of ITER is expected to be in 2020 [11].

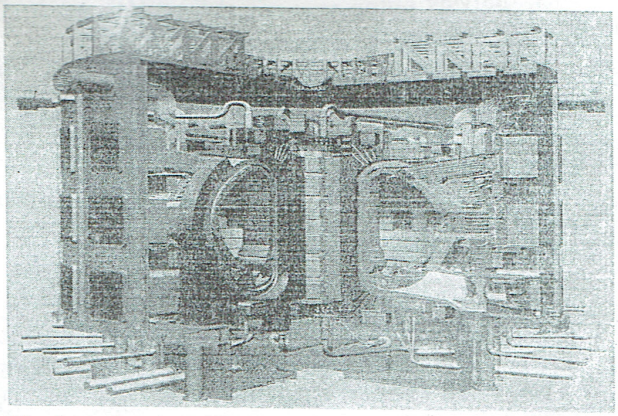

Fig. 2: Artist's impression of the International Thermonuclear Experimental Reactor (ITER)

7. PLASMA SURFACE TREATMENT:

Various plasma processes have been developed to attain a variety of specific surface properties and here we discuss some of the applications that are

also being studied in the plasma research lab at Kathmandu University, Dhulikhel, Nepal.

7.1 Surface Cleaning:

Plasma treatment is a safe and environmentally friendly alternative to traditional cleaning methods. A wide variety of industries utilize gas plasma treatment to remove organic surface contamination from materials that require critical cleaning. The active species in the oxygen combined with UV energy creates a chemical reaction with the surface contaminants, resulting in their volatilization and removal from the reaction chamber. Applications include cleaning of circuit boards for improved wire bonding, removal of organic contamination from glass slides and flat panels, cleaning of medical devices and other materials such as various metals and ceramics.

7.2 Adhesion promotion:

Improving adhesion between two surfaces is a common application. Good adhesion requires strong interfacial forces via chemical compatibility and chemical bonding. Plasma surface treatment can also assist in creating chemically active functional groups, such as amine, carbonyl, hydroxyl and carboxyl groups, to improve interfacial adhesion. Common applications include pre-treatment for medical catheters, cardiovascular stents, syringe components, dialysis pump parts and plastic films for drug bags. Plasma is also used to improve bond ability on substrates, such as glass, polymers, ceramics and various metals.

7.3 Controlling surface energies:

Plasma processing can also be used to tailor surface energies. Hydrophilic and hydrophobic surfaces can be created on polymers through interaction with a gas plasma. Using oxygen to create hydroxil functionality increases the wettability of a surface. This process has been used to enhance the performance of a catheter by creating a wettable surface on the polymer tubing. Similarly, surfaces can be specifically engineered to modify protein binding and improve blood compatibility. Common applications include tissue culture wares, filtration or separation media and contact lenses.

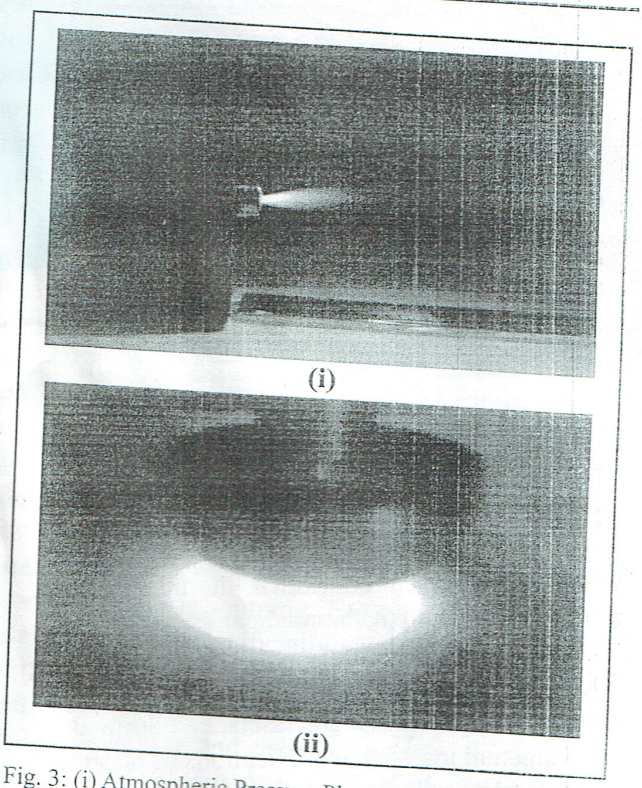

Fig. 3: (i) Atmospheric Pressure Plasma Jet and (ii) Dielectric Barrier Discharge (DBD) in Nitrogen

7.4 Improving biocompatibility:

Biomaterials that come in contact with blood or protein require special surface treatments to enhance biocompatibility. Amine functional groups, which are attached by ammonia plasma treatment, act as hooks for anticoagulants, such as heparin, and thereby decrease thrombogenicity. Synthetic polymer implant materials can be surface activated using radio frequency plasma techniques to enable covalent immobilization of cell binding peptides derived from the extra-cellular matrix proteins: fibronectin and laminin. The resulting grafted peptides can promote complete coverage of a surface with a monolayer of intact, healthy endothelial cells to form a natural, blood compatible surface.

7.5 Enhancing performance:

Surface crosslinking is often used to enhance the performance of polymers. The activity of the plasma creates a higher crosslinking density within the material to depths of a few thousand angstroms. The

resulting increase in hardness and chemical resistance can enhance performance in many applications.

8. PLASMA LIGHTING

The most prevalent man-made plasmas on our planet are the plasmas in lamps. There are primarily two types of plasma-based light sources, fluorescent lamps and high-intensity arc lamps. Fluorescent lamps find widespread use in homes, industry and commercial settings. High-intensity sources are widely used in industrial and commercial settings as well as for outdoor and security lighting near homes and public areas. Inside every fluorescent lamp there lurks plasma. It is the plasma that converts electrical power to a form that causes the lamp's phosphor coating to produce the light we see. The phosphor is the white coating on the lamp wall. A fluorescent lamp is shown here with part of the phosphor coating removed to reveal the blue plasma glow inside. The plasma generates ultraviolet light which in turn excites the phosphor coating inside the glass envelope. The phosphor emits a single color of visible light. Each pixel consists of three sub-pixels, one each of red, green and blue. By combining these primary colors at varying intensities, all colors can be formed.

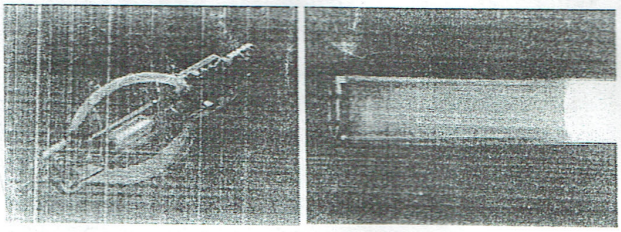

Fig. 3: Plasma lightning

9. BIOMEDICAL APPLICATIONS:

Although many synthetic biomaterials have physical properties that meet and even exceed those of natural body tissue, they can often cause adverse physiological reactions such as infection, inflammation and thrombosis formation. Through surface modification, biocompatibility as well as biofunctionality can be achieved without changing the bulk properties of the material. There are many ways by which to alter the interaction of biomaterials with their physiological environments, of these, plasma surface modification provides device manufacturers with a flexible, safe and environmentally friendly process that is extremely effective. Plasma surface modification is used for a variety of biomedical applications like Bioseparation, Sterilization, Ocular prostheses, Orthopaedic applications, Tissue culturing, etc.

10. CONCLUSION

The materials in our immediate surroundings are mostly solid, liquid and gas; however; the plasma state of matter dominates in our universe. It is the stuff in our sun and other stars and of the vast interstellar space. Plasma has found applications in lightning, computer chip manufacturing, spaceship propulsion, and many more. In the future it will likely be the stuff of electric power generated from fusion. Nuclear Fusion provides one of the major options for the truly sustainable or long term energy source. The fusion fuels are virtually inexhaustible and readily available throughout the world. Fusion power plant operation is inherently safe and has no risk of long-lived radioactive waste. Realizing these reactions to produce energy on earth is still a grand challenge to scientists and engineers. Though a steady progress has been made still several scientific and technological advances are necessary before the dream of commercial electricity production will become a reality.

REFERENCES

[1] A. S. Eddington, The Internal Constitution of the Stars, Cambridge University Press (1926)

[2] F. F. Chen. Introduction to Plasma Physics and Controlled Fusion (Second edition), Plenum Press, New York (1984)

[3] H. A. Bethe and C. L. Crictchfield, Phys. Rev. **54**, 248 (1938)

[4] H. A. Bethe, Phys. Rev. **55**, 434 (1939)

[5] I. Langmuir, Phys. Rev. **23**, 954 (1929)

[6] J. A. Bittencourt, Fundamentals of Plasma Physics (Third edition), Springer, New York (2004)

[7] J. Nuckolls et al, Nature **239**, 139 (1972)

[8] N. G. Basov and O. N. Krokhin, Sov. Phys.-JETP **19**, 123 (1964)

[9] V. B. Rozanov et al, Energy from Inertial Fusion, IAEA, Vienna, (1995)

[10] www.plasmas. org

[11] www.iter.org

Vivek, Volume-9 (2013), 292-300

Plasma Sheath Studies in Nepal

***B. R. Adhikari and R. Khanal**

Central Department of Physics, Tribhuvan University, Kirtipur
*Department of Physics, Bhaktapur Multiple Campus, Bhaktapur
Correspondance: b.r.adhikari@hotmail.com

Abstract

The plasma state of matter, also called the fourth state of matter, shows some peculiar properties next to a material wall. Due to the higher velocity of the electrons compared with that of ions, the wall is charged up negatively with respect to the surrounding plasma. The negative potential then attracts the ions and repels electrons, forming a positive space charge region in front of the wall. This positive – space – charge region, known as the "sheath" separates the negatively charged wall from the quasineutral "presheath" plasma. The plane which separates the sheath and presheath region is called sheath edge,where the in-streaming ions have to satisfy the "Bohm Criterion" to ensure the stability of the overall plasma. Various works on plasma sheath and related areas are being done in Nepal and here we present a review of plasma sheath studies in Nepal.

Key Words: Sheath, Presheath, sheath edge, ion-acoustic velocity, Bohm Criterion,

Introduction

As the temperature of any solid material is raised, its state changes from solid to liquid and then to gas. If we increase the temperature of a gas beyond a certain limit, it enters a regime where the thermal energy of its constituent particle is so great that the electrostatic forces which ordinarily bind electrons to atomic nuclei are overcome. Instead of hot gas composed of electrically neutral atoms, we then have a mixed population of charged and neutral particles. With increasing temperature the number of ionized particles increases and the ionized gas starts behaving differently. This is plasma, and it is neither solid nor liquid nor gas.

The word "plasma" comes from Greek and means something molded or fabricated [1]. The existence of "the fourth state of matter" was first identified by Sir William Crookes in 1879, however, the term plasma was introduced by I. Langmuir in 1928 to describe the state of matter in the positive column of glow discharge tube [2]. Any ionized gas cannot be called plasma of course; there is always some degree of ionization in any gas. Plasma is defined as a quasineutral gas of charge and neutral particles which exhibits collective behavior. Among various applications the plasma studies and research has gained momentum because of its applications in fusion energy.

Various methods for the terrestrial realization of fusion energy can be categorized into two main schemes, namely Magnetic Confinement Fusion (MCF) and Internal Confinement fusion (ICF). In MCF, the plasma is confined using a magnetic field with nested flux surface at very high temperatures, whereas in ICF lasers are used to compress small pellets of plasma fuel to very high densities. In MCF, low-density plasma is confined for a longer period of time, whereas in ICF a high density plasma is confined for a very short period of time.The most successful magnetic device for confining plasma was invented in the former Soviet Union in the late 1950s and is

Mr. Adhikar is Lecturer of Physics & Dr. Khanal is Associate Professor of Physics.

led a Tokamak. After the successful experimental demonstration of tritium burning, in the at European Torus in 1991, producing a peak fusion power of 1.7 MW, the magnetic confinement eme has gained further momentum towards the realization of fusion energy[3].

such fusion devices and wherever plasma comes in contact with a material wall, the plasma ion near the wall plays an important role in determining the overall plasma properties. As a ult of the higher velocity of the plasma electrons compared with that of the ions, the wall is rged up negatively with respect to the surrounding plasma. The negative potential then attracts ions and repels part of the electrons, forming a positive space charge region in front of the ll. This positive – space – charge region, known as the "sheath" separates the negatively charged ll from the quasineutral "presheath" plasma. The plane which separates the sheath and presheath ion is called sheath edge, where the in-streaming ions have to satisfy the" Bohm Criterion" to ure the stability of the overall plasma. Various works on plasma sheath and related areas are ng done in Nepal and here we present a review of plasma sheath studies in Nepal.

sma Sheath and the Bohm Criterion

cause of the shielding effect of the plasma, the negative potential of the solid surface will have stronger effect only in the sheath region, which extended only a small distance (a few Debye gths) away from the wall. For such a sheath to exist, the instreaming ions at the sheath edge e to satisfy a condition called the "Bohm criterion" [4] [5] [6] [7].

nsider a simple one dimensional model without magnetic field. Supposes there is no appreciable ctric field inside the plasma, we can then let the potential ϕ be zero there. When ions and ctrons hit the wall they recombine and are lost.

ce the electrons have much higher thermal velocities than ions they are lost faster and leave plasma with a net positive charge. The plasma must ther have a potential positive with respect he wall, i.e. the wall potential ϕ_w is negative. This potential cannot be distributed over the ire plasma, since Debye shielding will confine the potential variation to a layer of the order of eral Debye length in thickness. This layer, which must exist on all cold walls with which the sma is in contact, is called a sheath

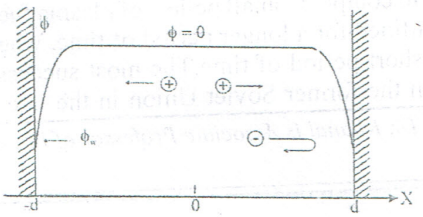

Fig. 1: Plasma potential profile near the wall

shown in figure 1, the plasma potential ϕ, forms sheath near the wall so that electrons are lected. The columb barrier $e\phi_w$ adjusts itself so that equal number of electrons and ions reach wall per second.

ferring to the figure 1, if $u(x)$ is the ion velocity, conservation of the energy requires:

$$\frac{1}{2}mu^2 + e\phi(x) = \frac{1}{2}mu_0^2$$

$$u = \sqrt{u_0^2 - \frac{2e\phi}{m}} \tag{1}$$

The ion equation of continuity then gives the ion density n_i in terms of the density n_0 in the main plasma:

$$n_0 u_0 = n_i(x) u_i(x) \tag{2}$$

Equation (1) and (2):

$$n_i(x) = n_0\left[1 - \frac{2e\phi}{mu_0^2}\right]^{-1/2} \tag{3}$$

In steady state, the electrons will follow the Boltzman distribution closely:

$$n_e(x) = n_0 e^{e\phi/kT_e} \tag{4}$$

Poisson's equation is then,

$$\frac{d^2\phi}{dx^2} = -4\pi e(n_i - n_e)$$

$$= 4\pi e n_0\left[e^{e\phi/kT_e} - (1 - \frac{2e\phi}{mu_0^2})^{-1/2}\right] \tag{5}$$

Normalizing on

$$\chi = -\frac{e\phi}{kT_e}, \xi = \frac{x}{\lambda_D} = x\sqrt{\frac{4\pi n_0 e^2}{kT_e}} \;\&\; \mu = \frac{u_0}{\sqrt{\frac{kT_e}{m}}} \tag{6}$$

Equation (5) is

$$\frac{d^2\chi}{d\xi^2} = (1 + \frac{2\chi}{\mu^2})^{-1/2} - e^{-\chi} \tag{7}$$

This is nonlinear equation. Equation (7) can be integrated once by multiplying χ'

$$\int_0^{\xi} \chi'\chi''d\xi_1 = \int_0^{\xi}(1+\frac{2\chi}{\mu^2})^{-1/2}\chi'd\xi_1 - \int_0^{\xi} e^{-\chi}\chi'd\xi_1$$

$$\int_0^{\xi}\frac{1}{2}\frac{d}{d\xi_1}(\chi')^2 d\xi_1 = \int_0^{\xi}\mu^2\frac{d}{d\xi_1}(1+\frac{2\chi}{\mu^2})^{1/2}d\xi_1 + \int_0^{\xi}\frac{d}{d\xi_1}(e^{-\chi})d\xi$$

Since $\chi = 0$ at $\xi = 0 (\Rightarrow \phi = 0 \text{ as } x \to 0)$ then Integrations yield:

$$\frac{1}{2}[(\chi')^2 - (\chi_0')^2] = \mu^2[(1+\frac{2\chi}{\mu^2})^{1/2} - 1] + e^{-\chi} - 1 \qquad (8)$$

If E = 0 in the plasma, we must set $\chi_0' = 0$ at $\xi = 0$ .Further integration to find χ have to be done numerically, but whatever it may yield, the R.H.S of equation (8) must be positive for all χ In particular for $\chi < 1$, we can expand the R.H.S of equation (8)

$$\mu^2[1+\frac{\chi}{\mu^2} - \frac{1}{2}\frac{\chi^2}{\mu^4} + \ldots\ldots - 1] + 1 - \chi + \frac{\chi^2}{2} - \ldots - 1 \geq 0$$

or, $$\frac{\chi^2}{2}(1-\frac{1}{\mu^2}) \geq 0$$

or, $$\mu^2 \geq 1 \qquad (9)$$

This implies that the ions must enter the sheath region with a velocity greater than the acoustic velocity v_s. This inequality is known as the Bohm sheath criterion. The physical reason for the Bohm criterion is easily seen form a plot of the ions and electron densities Versus .

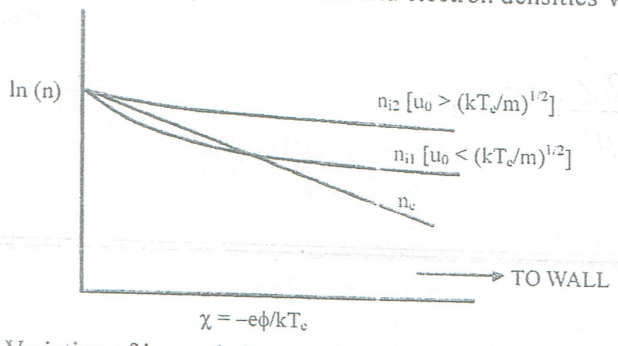

Fig-2 : Variation of ion and electron dens ty with normalized potential

Fig 2 shows the variation of ion and electron density (logarithmic scale) with normalized potential in a sheath. The ion density is drawn for two cases u_0 greater than and u_0 less than the critical velocity.

$$\left\langle \frac{1}{v^2} \right\rangle \leq \frac{1}{C_s^2} \tag{10}$$

In the Kinetic form the Bohm criterion reads

where $\langle\ \rangle$ denotes averaging over the ion distribution function and

$$C_s = \sqrt{\frac{k(\gamma^i T^i_{PS} + \gamma^e T^e_{PS})}{m^i}} \tag{11}$$

is the ion-acoustic velocity defined at the presheath side of the sheath edge, with k as Boltzmann constant, γ^i and γ^e the ion and electron polytropic constants, respectively, and T^i_{ps} and T^e_{ps} the ion and electron temperatures at the presheath side of the sheath edge, respectively [6] [7].

This condition (10) demands that ions enter the sheath region with a high velocity, which cannot be generated simply by the thermal motion of the ions. Consequently, the ions must be accelerated by an electric field penetrating deep into the presheath region. It also ensures that the potential profile to be non-oscillatory in the sheath.

Given figure 3 shows the geometry of the model for the plasma - wall transition. The plasma state is assumed to depend on the coordinate x perpendicular to the wall only. The electric field E is parallel to the x direction and the magnetic field **B** makes an angle ψ to x-axis. At x = L there is a particle absorbing wall. The plane x = 0 separates the plasma pre-sheath x<0 with a weak electric field from the transition zone x > 0 to the wall, where E is appreciable. The plasma x<0 is assumed to contain sources which maintain stationary particle fluxes across x=0. The transition zone x>0 is assumed to be collisionless.

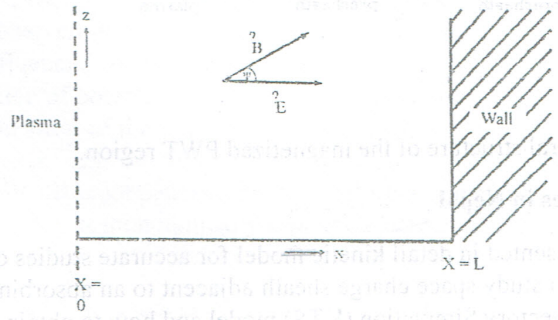

Fig.3: The bounded plasma model for the plasma-wall transition

In case of an oblique magnetic field, for the smooth start of the particle at a plasma side the flow velocity of the in-streaming plasma v has to exceed a certain limit, [8]

i.e. $v \geq C_s \cos \psi$ (12)

his is the Bohm – Chodura condition. The spatial reg on extending from the bulk plasma upto ıe solid surface will be referred to as the plasma wall transition (PWT) region.

ı the presence of a non vanishing oblique magnetic field, the presheath region consists of two arts: the collisional presheath (adjacent to the bulk plasma) and the magnetic presheath (adjacent) the sheath) [8], [5], [9]. The general structure of the PWT region in the presence of an oblique ıagnetic field is shown schematically in figure 4.

ı the collisional presheath region, the physical variables have weak gradients and the ions are ccelerated along the magnetic field towards the magnetic presheath so as to satisfy the Bohm-ıodura criterion [8]

: $<v_{11}>$ e" C_s (13)

/here $<v_{11}>$ denotes the ion velocity parallel to the magnetic field averaged over the ion distribution inction.

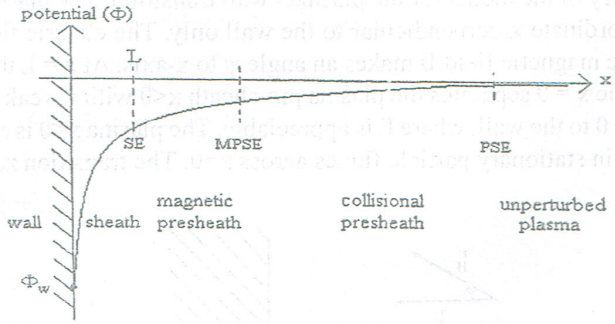

Figure. 4: General structure of the magnetized PWT region.

leview on Plasma Sheath studies in Nepal

.. Khanal [10] developed and presented in detail kinetic model for accurate studies of bounded lamas. He had used this model to study space charge sheath adjacent to an absorbing wall. He escribed extensively Kinetic Trajectory Simulation (KTS) model and how to obtain from it the inal self-consistent, time-independent state. He had devised and demonstrated this model only or 1d1v, time-independent and collisionless cases and had applied this model to the special case f a 1d1v single emitter plasma diode for the purpose of testing and comparison. Finally, in a ıajor new application, he had used this KTS model to study a space charge sheath adjacent to an bsorbing wall and bordering, on a presheath describec in a two fluid model. The solution of the elated presheath-sheath coupling problem is developed by him and the 'standard' one (having oltzmann distributed electrons) shows qualitative agreement but also some discrepancies due to ıe different electron distributions.

R.Khanal[11] studied the scheme for coupling(matching) a quasineutral two-fluied (electron-ion) presheath solution to a non-neutral,collisionless kinetic sheath solution.

Joshi [12] studied about the plasma sheath structure for different potential at the material wall using a kinetic model. He observed that the ion and electron density decreases monotonically from the sheath entrance towards the wall in all cases. Neupane [13] studied the plasma sheath structure for the increasing mass of the in-streaming ions. He had observed that fewer ions reach the wall on increasing the mass of the ions. Bhattarai[14] studied the effect on the plasma sheath structure due to the temperature variation of the in-streaming particles. He has been observed that the sheath structure is influenced by variation of presheath ion temperature. Tiwari [15] studied the propagation of ion acoustic wave in plasma presheath he observed that the non-neutral space charge layer do not serve as a layer for string reflaction of the acoustic waves. Mahendra [16] studied about the effect on the plasma sheath structure due to the temperature variation of the sheath length. He had observed that the majority of the potential drop occurs in the immediate vicinity of the wall for all sheath lengths but the potential decreases faster near the sheath entrance in case of short system lengths. Mishra [17] studied plasma sheath structure for different density of the presheath plasma. She had observed that the ion and electron density decreases monotonically from the sheath entrance towards the wall in all cases. The electron density decreases much faster than that of ions and hence the total charge density increases towards the wall.

Giri [18] studied the plasma sheath structure for different values of ion polytropic constant at different ion-electron temperature ratios. He found that the potential drop occurs in theimmediate neighborhood of the wall and the magnitude of the potential drop increases with increasing ion polytropic constant. The electric field is always negative in the sheath region and its magnitude increases towards the wall. K.N. Sharma [19] studied the effect of ion-induced electrons emission on the plasma sheath voltage for different values of ion induced electrons emission coefficient. D. Subba [20] studied the kinetic analysis for a smooth matching of the pre-sheath and the sheath using an intermediate scale.

Awasthi [21] studied kinetic energy distribution of electron and ion in the plasma sheath at different wall potentials. He has observed that the kinetic energy of the ions and electrons reaching the material wall is highly influenced by the potential applied to the wall. T. Rana [22] studied the sheath structure i.e. variation of potential distribution, charged density, density distribution, etc. for different levels of ionization of the plasma for given presheath parameters. V. Kaphle [23] studied the sheath structure for zinc oxide by providing the sufficient temperature in front of an absorbing material wall with different plasma densities at the pre-sheath side . He noticed that the ion and electron densities decrease monotonically from the sheath entrance towards the wall in all cases.

Gurung [24] studied non-neutral time independent and collision less plasma sheath formed infront of an absorbing material wall for different presheath current densities. He found that electron density at the wall increases linearly and sharply whereas ion density at the wall increases non

linearly and monotonically with respect to the presheath current density. T. Chetry [25] studied the variation in the ion and the electron densities for different presheath ion polytropic constants fed at the presheath entrance using a kinetic trajectory simulation model. Dhungana [26] studied the sheath structure for different electron temperatures at the presheath using the kinetic trajectory simulation model which is an iterative scheme of solving kinetic equation along the particle trajectories. He observed that the sheath structure is greatly affected by the variation of presheath electron temperature.

Recently, Chalise and Khanal [27] have studied the magnetized plasma sheath using a KTS. In their work they have considered velocity variation perpendicular to the wall, however the velocities in perpendicular direction are considered to be constant.

Conclusion

The potential profile differs for varying magnetic field and orientation. The potential is almost constant near the sheath entrance and has sharp gradient close to the wall. It has been observed that the potential decreases when the angle and magnetic field increases.

Our work is expected to provide a basis for studying all types of magnetized plasmas using the kinetic approach, detail and in-depth analysis of kinetic trajectory stimulation for the study of plasma sheath, to identify some problems of interest which could be tackled in future investigations to develop and evaluate the solution of pre-sheath sheath couplingg problem in great detail and may thus serve as a guide line for similar investigations in the future. This study is also helpful to extend 1d1v KTS model to 1d3v as well as 3d3v model.

References

[1] F. F. Chen. Introduction to Plasma Physics and Controlled Fusion (Second edition), Plenum Press, New York (1984)
[2] I. Langmuir, Phys. Rev. 23, 954 (1929)
[3] JET Team, Nuclear Fusion 32 (2), 187 (1992)
[4] D. Bohm, The Characteristics of Electrical Discharges in Magnetic Fields, Edited by A. Guthry and P.K. Wakerling, MC-Graw Hill, P.77 (1949)
[5] R. Chodura, Physics of Plasma-wall Transition in controlled Fusion, Edited by D.E. Post and R. Behrisch Plenum Publishing Corporation P. 99 (1986)
[6] K. U. Riemann, J. Physics. D: Appl. Phys. 24, 493 (1991)
[7] K. U. Riemann, J. Tech. Phys. 41 (1), 89 (2000)
[8] R. Chodura, Phys. Fluids 25 (9), 1628 (1982)
[9] P. C. Stangeby, The Plasma boundary of Magnitude Fusion Devices, IOP Publishing Ltd. (2000).
[10] R. Khanal, A Kinetic Trajectory Simulation (KTS) Model for Bounded Plasma, Ph. D. Thesis, Innsbruck University, Austria (2002)
[11] R. Khanal, A scheme for coupling a fluid presheath solution to a kinetic sheath solution, Scientific World, 3, Page 3, (2005)

[12] R. P. Joshi, Study of Plasma Sheath Structure for Different Potentials at the Material Wall, M.Sc. Thesis, Central Department of Physics, Tribhuvan University, Kirtipur, Nepal (2006)
[13] P. Neupane, Effect on the Plasma sheath Structure Due to the variation of the Mass of in-streaming ions, M.Sc. Thesis, Central Department of Physics, Tribhuvan University, Kirtipur, Nepal (2006)
[14] S. K. Bhattarai, Effect on the Plasma Sheath Structure due to the temperature variation of the In-streaming Particles, M Sc. Thesis, Central Department of Physics, Tribhuvan University, Kirtipur, Nepal (2006)
[15] R. K. Tiwari, Propagation of Ion Acoustic wave in Plasma Presheath, M. Sc. Thesis, Central Department of Physics, Tribhuvan University, Kirtipur, Nepal (2006)
[16] D. C. Mahendra, Effect on the Plasma Sheath Structure due to the Variation of the Sheath Length, M. Sc Thesis, Central Department of Physics, Tribhuvan University, Kirtipur, Nepal (2006)
[17] A. Mishra, Sheath Structure for Different Density of the Presheath Plasma, M. Sc Thesis, Central Department of Physics, Tribhuvan University, Kirtipur, Nepal (2006)
[18] P. Giri, Study of Plasma Sheath Structure for Different Values of the Ion Polytropic Constant, M. Sc Thesis, Central Department of Physics, Tribhuvan University, Kirtipur, Nepal (2007)
[19] K. N. Sharma, The Effect of Ion Induced Electrons Emission on the Plasma Sheath Voltage for Different Values of Ion Induced Electrons Emission Coefficient, M. Sc Thesis, Central Department of Physics, Tribhuvan University, Kirtipur, Nepal (2007)
[20] D. Subba, Kinetic Analysis for a Smooth Matching of the Presheath and The Sheath using an Intermediate Scale, M. Sc Thesis, Central Department of Physics, Tribhuvan University, Kirtipur, Nepal (2007)
[21] A. Awasthi, Kinetic Energy distribution of Electron and Ion in the Plasma Sheath at Different Wall Potential, M.Sc. Thesis, Central Department of Physics, Tribhuvan University, Kirtipur, Nepal (2009)
[22] T. Rana, Sheath Structure for different levels of Ionization of Berylleum Plasma, M. Sc. Thesis, Central Department of Physics, Tribhuvan University, Kirtipur, Nepal (2009)
[23] V. Kaphle, Sheath Structure for Zinc Oxide by providing the sufficient temperature in front of an absorbing material wall with different plasma densities, M. Sc. Thesis, Central Department of Physics, Tribhuvan University, Kirtipur, Nepal (2009)
[24] S. JB Gurung, Plasma Sheath Structure for different Presheath Current densities, M. Sc. Thesis, Central Department of Physics, Tribhuvan University, Kirtipur, Nepal (2012)
[25] T. Chetry, Effect of Ion Polytropic Constant on Particle densities in Plasma Sheath, M. Sc. Thesis, Central Department of Physics, Tribhuvan University, Kirtipur, Nepal (2012)
[26] S. Dhungana, Plasma Sheath Structure for Different Presheath Electron Temperature, M.Sc. Thesis, Central Department of Physics, Tribhuvan University, Kirtipur, Nepal (2012)
[27] R. Chalise and R. Khanal, Plasma Phys. Control Fusion 54 (2012)

BIBECHANA
ISSN 2091-0762 (Print), 2382-5340 (Online)
Journal homepage: http://nepjol.info/index.php/BIBECHANA
Publisher: Department of Physics, Mahendra Morang A.M. Campus, TU, Biratnagar, Nepal

Modulation frequency and velocity variation of ions in a magnetized plasma sheath for different obliqueness of the field

Bhesha Raj Adhikari [1,2,]*, Hari Prasad Lamichhane[1], Raju Khanal[1]
[1] Central Department of Physics, Tribhuvan University, Kirtipur, Kathmandu, Nepal
[2] Department of Physics, Bhaktapur Multiple Campus, Tribhuvan University, Bhaktapur, Nepal
* Email: b.r.adhikari@hotmail.com

Article Information:
Received: May 29, 2020
Accepted: August 1, 2020

Keywords:
Bohm criterion
Kinetic theory
Sheath
Presheath
Modulation frequency
Damping constant

ABSTRACT
The understanding of ion dynamics in magnetized plasma sheath is crucial for all applications of plasma. The velocity variation as well as modulation frequency of ions in a magnetized plasma sheath has been studied for different obliqueness of magnetic field. The governing Lorentz force equation has been solved numerically for the given boundary conditions as applicable in kinetic simulation of the sheath. For different obliqueness of the magnetic field, the average values, maximum amplitude, damping factor as well as frequency of oscillation are studied. The oscillating velocity components change at different rates depending on their orientation with respect to the field direction. Significant changes in the damping factor and modulation frequency has been observed for all components of velocity; however, the frequency of oscillation remains same. As the obliqueness increases, shoulder natures in the components of velocity are observed.

DOI: https://doi.org/10.3126/bibechana.v18i1.29171

1. Introduction

The formation of non-neutral region in the vicinity of material wall is a ubiquitous feature of bounded plasma and it has wide range of growing applications in diverse fields (e.g. plasma confinement for fusion, sputtering, etching, surface treatment etc.) [1]. In plasma, the thermal velocity of electrons is higher as compared to that of the ions. Due to this, the wall is charged up negatively with respect to the core plasma. Therefore, negative potential attracts the ions and repels electrons forming a thin positive space charge region near to the wall. This positive space charge region, known as the 'sheath' separates the negatively charged material wall from the quasineutral 'presheath' plasma. The in-streaming ions have to satisfy the Bohm criterion to ensure the stability of the overall plasma [2, 3]. The problem related to sheath is one of the oldest problems in plasma physics [3, 4] and once the plasma-wall interaction is well understood it will be possible to control heat loading, energy transfer and particle flow towards the wall and overall bulk plasma behavior [5 - 7].

The problem of sheath formation whenever it faces a material surface, its nature and evolution with time is significant for all plasma applications. This is a topic of interest and various works are reported recently as well; however, the study of modulation frequency as well as the time evolution of the ion velocity profile in a magnetized plasma sheath for varying obliqueness is still lacking [8-10]. This work focuses in the time variation of ion velocity, which shows oscillating nature, and its modulation frequency in a magnetized plasma sheath for different obliqueness of the field. The governing Lorentz force equation are formulated and solved numerically for the given boundary conditions as applicable in kinetic trajectory simulation (KTS) method of the sheath region [8, 11, 12].

In typical boundary layer problems, the sheath region is of several electron-Debye lengths which is much smaller than the characteristic extension of the plasma. Such a sheath can only be formed, if the Bohm criterion [2, 5] is satisfied which demands that the ions enter the sheath region with a high velocity, which cannot be generated by thermal ion motion alone [5]. In the presence of a magnetic field, in kinetic form, the Bohm criterion reads

$$\left\langle \frac{1}{v_{\parallel}^2} \right\rangle \leq \frac{1}{C_s^{\,2}} \tag{1}$$

where,

$C_s = \sqrt{\frac{k(\gamma^i T_{PS}^i + \gamma^e T_{PS}^e)}{m^i}}$ is the ion-acoustic velocity defined at the presheath side of the sheath edge, with k is Boltzmann constant, γ^i and γ^e the ion and electron polytropic constants, respectively, T_{ps}^i and T_{ps}^e the ion and electron temperatures at the presheath side of the sheath edge, respectively and m^i is the mass of ion species.

2. Model and basic equations

The 1d3v model of magnetized plasma sheath is shown schematically in Fig. 1. The region of interest is bounded by two parallel planes at $x = 0$ and $x = L$, and the plasma consists of only electrons and singly charged ions. The plane at $x = L$ represents the "sheath entrance" that faces the plasma side and $x = 0$ is the material wall, assumed to be non-emitting in the present case. The uniform magnetic field $\vec{B}$ acts on the *xy*-plane which makes an angle θ with the normal to the wall. In the presence of oblique magnetic field, the presheath consist of two distinct regions: collisional presheath and magnetic presheath [3, 13]. The general schematic diagram of magnetized plasma-wall transition region is shown in Fig. 2 [11].

As the sheath region is characterized by sharp gradients in a small scale of the order of electron-Debye lengths, it is usually treated kinetically, where the particle distribution are governed by the Boltzmann equation [1]

$$\frac{\partial f}{\partial t} + \vec{v}.\nabla f + \frac{\vec{F}}{m}.\nabla_v f = \left(\frac{\partial f}{\partial t}\right)_c \tag{2}$$

where $\vec{F}$ is the macroscopic force acting on the particles, and $\left(\frac{\partial f}{\partial t}\right)_c$ is the time rate of change of distribution function $f(\vec{r}, \vec{v}, t)$ due to collisions. The symbol ∇ represents the usual space-gradient operator whereas the symbol ∇_v represents the gradient in velocity space. For collisionless cases, suitable for sheath region as their dimension are much less than the mean free path, the equation (2) changes to so called Vlasov equation:

$$\frac{\partial f}{\partial t} + \vec{v}.\nabla f + \frac{q}{m}(\vec{E} + \vec{v} \times \vec{B}).\nabla_v f = 0 \tag{3}$$

In the KTS method, the kinetic equations are solved along with other basic equations describing the plasma for given boundary and initial conditions. The distribution function at any point along the trajectory can be obtained if its value at one point (i.e., at the boundary) is known. Density of the species '*s*' is then given by

$$n^s(\vec{x}) = \int_{-\infty}^{+\infty} d^3v f^s(\vec{x},\vec{v}), \quad (4)$$

which then yields the space charge density as

$$\rho(\vec{x}) = \sum_s q^s n^s(\vec{x}). \quad (5)$$

Thus obtained space charge density is then used in the Poisson's equation to obtain the electrostatic potential $\phi(x)$

$$\frac{d^2\phi(\vec{x})}{dx^2} = -\frac{\rho(\vec{x})}{\varepsilon_0}, \quad (6)$$

and the electric field is given by

$$E(\vec{x}) = -\frac{d\phi(\vec{x})}{dx} \quad (7)$$

The kinetic equations (3)-(7) are solved along the collisionless trajectories for given boundary conditions. The ion velocity in the plasma sheath are computed using the Lorentz force equation

$$m\frac{d\vec{v}}{dt} = q\left[\vec{E} + (\vec{v}\times\vec{B})\right] \quad (8)$$

where q is the charge of ion species whose mass is m.

The components of equation (8) are

$$\frac{dv_x}{dt} = \frac{qE}{m} - \frac{qBv_z\sin\theta}{m} \quad (9)$$

$$\frac{dv_y}{dt} = \frac{qBv_z\cos\theta}{m} \quad (10)$$

$$\frac{dv_z}{dt} = \frac{qBv_x\sin\theta}{m} - \frac{qBv_y\cos\theta}{m} \quad (11)$$

Since the magnetic field is dominating near the sheath entrance over the electric field, which is almost zero, the ions gyrate as they move slowly forward towards the wall. As the ions move towards the wall from the sheath entrance the electric field starts dominating, and hence the gyration decreases, and the equation of the damped harmonic oscillator can be is written as [14]

$$v(t) = v_m + Ae^{-kt}\sin(\omega t + \alpha) \quad (12)$$

where k, A, ω and α are damping constant, amplitude, frequency of oscillation and phase angle, respectively. The damping constant of oscillating velocity components defined by equation (9) can be expressed as [14]

$$k = \frac{\ln\left(\frac{v_1 - v_m}{v_2 - v_m}\right)}{t_2 - t_1} \quad (13)$$

where v_1 and v_2 are the resultant velocity at time t_1 and t_2, respectively and v_m is the mean value of oscillating parts of velocity.

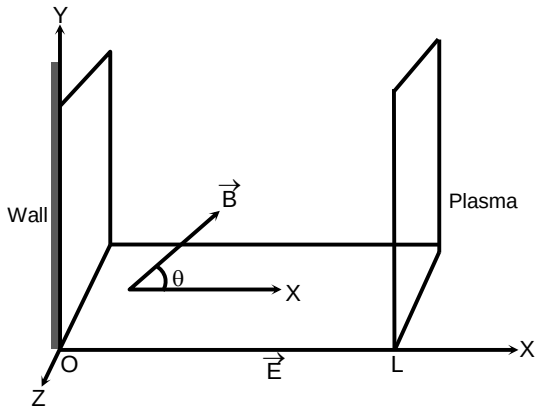

Fig. 1: Schematic geometry of the plasma-wall interaction model.

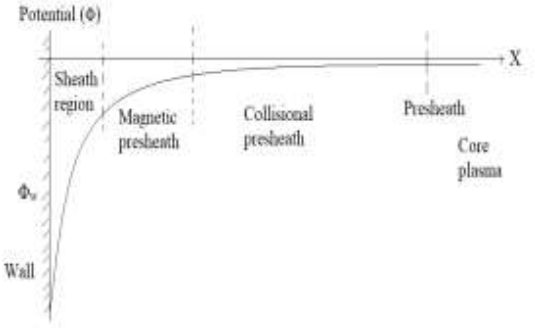

Fig. 2: Schematic diagram of magnetized plasma-wall transition region.

3. Results and Discussion

In order to study the temporal variation of velocity, the equations (9)-(11) are solved by using Runge-Kutta method for the given boundary conditions.

Furthermore, the amplitude of oscillation, damping factor, oscillation frequency and mean value are obtained by solving the equations (12) and (13) numerically. The temporal dependence of all three components of ion velocity have been calculated at constant magnetic field of 6 mT and for three different obliqueness of the field (30°, 60° and 75°), shown in Figs. 3, 4, and 5, respectively. For the obliqueness of 30°, the *x*, *y* and *z*-component of velocity varies about the mean value of 0.007 m/s, 6661 m/s and 11600 m/s respectively with same frequency of oscillation 100 Hz (Fig. 3). Also these components show damping nature of oscillation with damping factor 13.8 s^{-1}, 13.1 s^{-1} and 13.0 s^{-1}, respectively. Likewise, these component of velocity varies with maximum amplitude of 9794 m/s, 3138 m/s and 1550 m/s, respectively. It also shows that the modulation frequency of *x*, *y* and *z*-component of velocity is same which is equal to 15.4 Hz.

Fig. 4 shows that at obliqueness 60°, the *x*, *y* and *z*-component of velocity varies about the average values of -0.008 m/s, 11570 m/s and 6718 m/s, respectively with same frequency of oscillation, 100 Hz. Also these components show damping nature of oscillation with damping factor of 15.2 s^{-1}, 13.7 s^{-1} and 12.3 s^{-1} respectively. Likewise, these components of velocity vary with maximum amplitude of 9794 m/s, 2650 m/s and 4632 m/s, respectively. The modulation frequency of *x*, *y* and *z*-component of velocity for this case is 16.2 Hz, 15.8 Hz and 16.2 Hz, respectively.

At obliqueness of 75°, the *x*, *y* and *z*-component of velocity varies about the average values of 0.0058 m/s, 11580 m/s and 3137 m/s respectively, with same frequency of oscillation 100 Hz as shown in Fig. 5. Also these components show damping nature of oscillation with the damping factor as 12.9 s^{-1}, 14.9 s^{-1}, and 14.1 s^{-1}, respectively. Likewise, these component of velocity varies with the maximum amplitude of 9794 m/s, 1690 m/s and 6657 m/s, respectively. The modulation frequency of *x*, *y* and *z*-components of velocity are 15.8 Hz, 16.0 Hz and 15.4 Hz, respectively. In this case, of obliqueness 75°, shoulder nature in the velocity components are observed around 0.05 second which was not the case when the angles were smaller.

The obtained results are summarized in Table 1, where the average value, maximum amplitude, damping factor, frequency of oscillation and modulation frequency of all three component of ion velocity at obliqueness of 30°, 60° and 75°. The *y*-component of mean value (11580 m/s) is maximum at 75° compared to other angles. The amplitude is maximum (9793.99 m/s) of the *x*-component in two cases, when the angles are 30° and 75°, whereas amplitude is minimum (1550 m/s) for *z*-component at 30°. The damping factor of the *z*-component is minimum (13.0 s^{-1}) when the angle is 30°, on the other hand it is maximum for *y*-component (14.9 s^{-1}) at 75°. Similarly, modulation frequency in the *x*-component and *z*-component is maximum (16.2 Hz) at angle 60°, whereas frequency of oscillation remained same for all components of velocity for each cases considered.

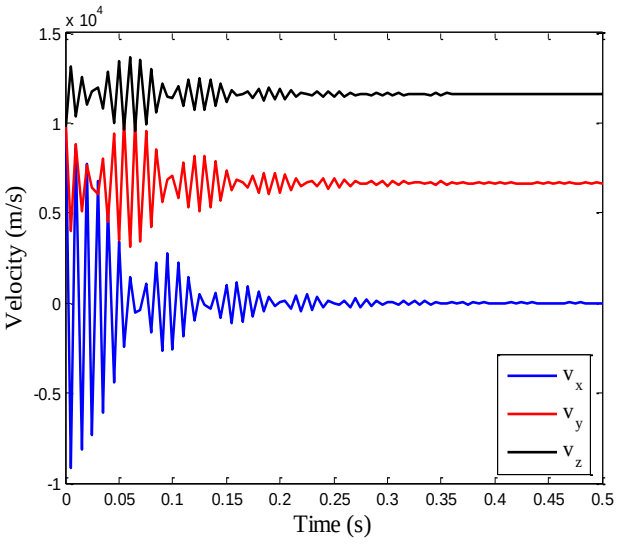

Fig. 3: Temporal variation of velocity of ions for a magnetic field of 6 mT at angle 30°.

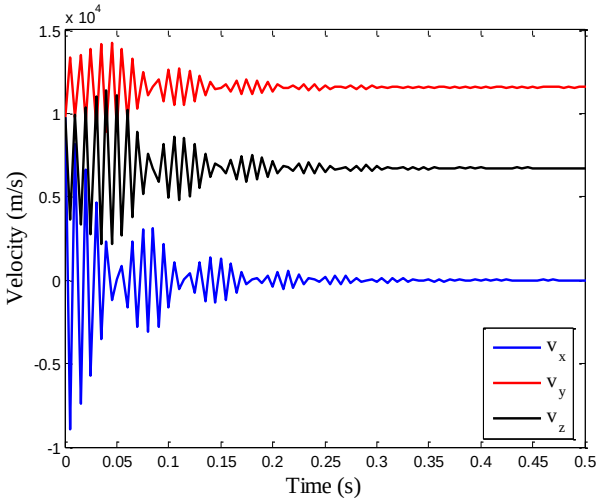

Fig. 4: Temporal variation of velocity of ions for a magnetic field of 6 mT at angle 60°.

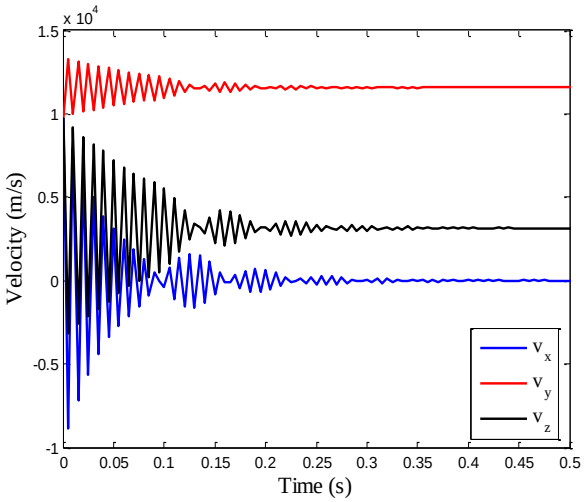

Fig. 5: Temporal variation of velocity of ions for a magnetic field of 6 mT at angle 75°.

Table 1: The average value, maximum amplitude, damping factor, frequency of oscillation and modulation frequency of ion velocity

θ	**Average Value** (m/s)			**Maximum Amplitude** (m/s)			**Damping factor** (s^{-1})			**Frequency of oscillation** (Hz)			**Modulation frequency** (Hz)		
	v_{xm}	v_{ym}	v_{zm}	v_{xa}	v_{ya}	V_{za}	v_x	v_y	v_z	v_x	v_y	v_z	v_x	v_y	v_z
30°	0.007	6661	11600	9793.99	3138	1550	13.8	13.1	13.0	100	100	100	15.4	15.4	15.4
60°	-0.008	11570	6718	9794	2650	4632	15.2	13.7	13.3	100	100	100	16.2	15.8	16.2
75°	0.0058	11580	3137	9793.99	1690	6657	12.9	14.9	14.1	100	100	100	15.8	16	15.4

4. Conclusions

Velocity variation as well as modulation frequency of ions in a magnetized plasma sheath has been studied for different obliqueness of magnetic field. It has been observed that the ion velocity at presheath-sheath boundary is affected by varying the obliqueness of the field. Various parameters like average ion velocity, amplitude, modulation frequency, and the damping factor can be controlled by varying the obliqueness. However, the frequency of oscillation is independent of obliqueness of magnetic field. The changes in these parameters results due to the change in contribution of the magnetic field with obliqueness. Present work is useful in understanding the time evolution of the particles velocities, and hence, exact particle behavior in magnetized plasma sheath region which is important in diverse plasma applications: material processing, surface treatment, plasma etching, confinement of plasma in fusion devices, and many more.

Acknowledgement

B. R. Adhikari would like to acknowledge the University Grants Commission, Nepal for the Ph. D.

fellowship. The authors warmly thank Mr. Suresh Basnet for fruitful discussions.

References

[1] R. Chalise and R. Khanal, A kinetic trajectory simulation model for magnetized plasma sheath, Plasma Phys, Control. Fusion 54 (2012) 095006 (5pp). https://doi.org/10.1088/0741-3335/54/9/095006

[2] D. Bohm, The characteristics of electrical discharges in magnetic fields, Edited by A. Guthry and P.K. Wakerling, MC-Graw Hill, 1949.

[3] R. Chodura, Plasma wall transition in an oblique magnetic field, Phys. Fluids 25 (1982) 1628-1633. https://doi.org/10.1063/1.863955

[4] I. Langmuir, Oscillations in ionized gases, Proc. National Academy of Sciences 14 (1928) 627-637.

[5] K. U. Riemann, The Bohm criterion and sheath formation, J. Phys. D: Appl. Phys. 24 (1991) 493-518. https://doi.org/10.1088/0022-3727/24/4/001

[6] K. U. Riemann, Theory of the plasma-sheath transition, J. Tech. Phys. 41 (2000) 89-121.

[7] M. M. Hatami, A. R. Niknam, B. Shokri and H. Ghomi, Magnetized plasma sheath with two species of positive ions, Phys. Plasmas 15 (2008) 053058 (5pp). https://doi.org/10.1063/1.2918319

[8] B. R. Adhikari, S. Basnet, H. P. Lamichhane and R. Khanal, Presheath-sheath coupling for kinetic trajectory simulation of a magnetized plasma sheath, AIP Advances 9 (2019) 055123 (10pp). https://doi.org/10.1063/1.5088107

[9] R. Moulick, S. Adhikari and K. S. Goswami, Sheath formation in collisional, low pressure, and magnetized plasma, Phys. Plasmas 26 (2019) 043512 (10pp). https://doi.org/10.1063/1.5090537

[10] S. Basnet, A. Sarma and R. Khanal, Effect of presheath electron temperature on magnetized plasma-wall transition and wall sputtering by plasma having two species of positive ions, Physica Scripta 95(2020) 065601 (11pp). https://doi.org/10.1088/1402-4896/ab7b89

[11] R. Khanal, A Kinetic trajectory simulation model for bounded plasma, Ph. D. Thesis. Innsbruck University, Austria (2003).

[12] R. Chalise and R. Khanal, Self consistent one dimension in space and three dimension in velocity kinetic trajectory simulation model of magnetized plasma wall transition, Phys. Plasmas 22 (2015) 113505 (5pp). https://doi.org/10.1063/1.4934601

[13] P. C. Stangeby, The plasma boundary of magnetic fusion devices, IOP Publishing Ltd (2000).

[14] G. F. Simmons, Differential equations with applications and historical notes, Tata McGraw-Hill, New Delhi (1991).

Bhesha Raj Adhikari

Central Department of Physics, Tribhuvan University, Kathmandu, Nepal

participated and presented a paper entitled

"Presheath-Sheath Coupling for Kinetic Trajectory Simulation of a Magnetized Plasma Sheath"

in the

Symposium on Plasma Physics and Material Science (SPPMS 2019)

held at the

Central Department of Physics, Tribhuvan University, Kirtipur, Kathmandu, Nepal.

2 July, 2019

Prof. Dr. Raju Khanal
Program Coordinator
SPPMS 2019

Tribhuvan University
Central Department of Physics
Kirtipur

INTERNATIONAL CONFERENCE ON
EXPLORATIONS IN PHYSICS (ICEP-2018)

29-31 May, 2018, Kathmandu, Nepal

Bhesh Raj Adhikari

Central Department of Physics, Tribhuvan University, Kirtipur, Kathmandu, Nepal

Contributed an oral presentation entitled

Modulation Frequency and Velocity Variation of Ions in a Magnetized Plasma Sheath for Different Obliqueness of the Field

during the conference

Chief Guest
Prof. Dr. Jiba Raj Pokharel
Vice Chancellor, NAST

Campus Chief
Rajesh Mahaju
Amrit Campus

SOC Chair
Assoc. Prof. Dr. Leela Pradhan Joshi
Amrit Campus

Organized by

Research Centre for Applied Science and Technology (RECAST), TU

Training Workshop on Scientific Writing

June 21–25, 2018

RECAST, Tribhuvan University (TU), Kathmandu, Nepal

Supported by

University Grants Commission (UGC)

Certificate of Participation

This certificate is bestowed to

BHESHA RAJ ADHIKARI

for the successful participation in **Training Workshop on Scientific Writing.**

Sudha

Prof Dr Sudha Tripathi

Rector

Tribhuvan University

Prof Dr Rameshwar Adhikari

Executive Director

RECAST

St. Xavier's College

The Physics department of St. Xavier's College, Kathmandu would like to award this certificate to

Bhesh Raj Adhikari

for his/her presentation on

VELOCITY VARIATION OF IONS IN A MAGNETIZED PLASMA SHEATH FOR DIFFERENT OBLIQUENESS OF THE FIELD

in the

International Conference on Physics of Space and Materials

held on September 2-3, 2017.

MR. DRABINDRA PANDIT
HEAD OF DEPARTMENT
PHYSICS

PROF. DR JIBA RAJ POKHAREL
VICE CHANCELLOR
NAST
CHIEF GUEST

FR. JIJU VARGHESE
PRINCIPAL

ST. XAVIER'S | COLLEGE | KATHMANDU

Lecture Series on

Research Methodology

6 November – 22 December 2017

Central Department of Physics
Tribhuvan University, Kirtipur, Nepal

Participation Certificate

Bhesh Raj Adhikari

Central Department of physics T.U.

participated in 21 hours lecture series on
Research Methodology delivered by Prof. Dr. Subodh R. Shenoy,
TIFR, India during 6 November to 22 December 2017.

Subodh R. Shenoy

Prof. Dr. Subodh R. Shenoy
Guest Speaker
Tata Institute of Fundamental Research, India

Prof. Dr. Binil Aryal
Head
CDP, TU, Kirtipur

International conference on
Nano-Materials and Computational Physics
27-28 December 2017
Central Department of Physics
Tribhuvan University, Kirtipur, Nepal

Participation Certificate

Bhesh Raj Adhikari

Central Department of Physics, T.U., Kirtipur

participated the conference during 27-28 December 2017 and contributed oral/poster presentation entitled

Study of beat frequency and velocity variation of ions in magnetized plasma sheath

Prof. Dr. Ram Pd Khatiwada	***Dr. Gopi Chandra Kaphle***	***Prof. Dr. Binil Aryal***
Dean	Secretary	Head
IoST, Tribhuvan University, Kirtipur	Organizing Committee	CDP, TU, Kirtipur

AMITY UNIVERSITY

LUCKNOW CAMPUS

INTERNATIONAL CONFERENCE ON

PLASMA SCIENCE, TECHNOLOGY & APPLICATION 2016

January 20 & 21, 2016

CERTIFICATE

This is to certify that Prof./Dr./Mr./Ms Bhesha Raj Adhikari of Tribhuvan University, Nepal presented an Oral/Poster Paper titled Velocity Variation of Ions in MPS in **International conference on Plasma Science, Technology and Application 2016,** during January 20-21, 2016, at Amity University, Lucknow Campus

Prof. (Dr.) Asita Kulshreshtha
Convener
ICPSTA-2016

Prof. (Dr.) H. K. Dwivedi
Director, Amity School of Applied Sciences
Amity University, Lucknow Campus

Maj Gen K. K. Ohri, AVSM (Retd.)
Pro Vice Chancellor
Amity University, Lucknow Campus

In collaboration with CSIR - CENTRAL ELECTRONICS ENGINEERING RESEARCH INSTITUTE (CEERI), PILANI, INDIA

Organised by AMITY SCHOOL OF APPLIED SCIENCES

5TH PSSI-PLASMA SCHOLARS COLLOQUIUM (PSC-2016)

ORGANIZED BY

DEPARTMENT OF PHYSICS RAVENSHAW UNIVERSITY

AND

PLASMA SCIENCE SOCIETY OF INDIA

27-28 AUG 2016

This is to certify that Dr/Mr/Ms. B.R. Adhikari of Central Dept. of Phy., Tribhuvan University., Nepal has participated in 5thPSSI-PLASMA SCHOLARS COLLOQUIUM (PSC-2016) being held at Raevnshaw University,Cuttack, and presented a paper (ORAL/POSTER) entitled Temporal dependency of components obliqueness of the magnetic field

Prof Rabindranath Pal
(President , PSSI)

Dr.(Mrs) Rita Paikaray
(Convenor , PSSI-2016)

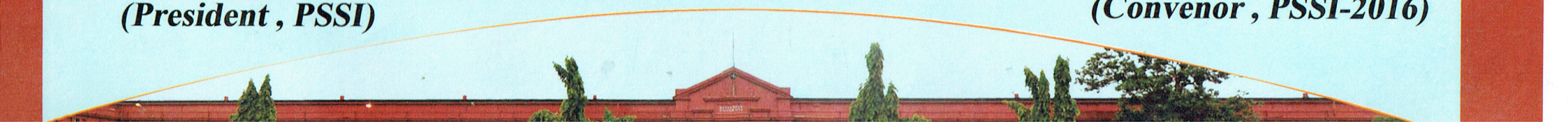

FPPT
Connecting innovative Theories

7th INTERNATIONAL CONFERENCE ON THE FRONTIERS OF PLASMA PHYSICS AND TECHNOLOGY (FPPT-7)

14-17 April 2015, Kochi (Near to Cochin), India

CERTIFICATE OF ATTENDANCE

This is to certify **Dr. B. R. Adhikari** has actively participated in the conference and presented a poster on "***Study Of Kinetic Energy Of Ion And Electron In Magnetized Plasma Sheath***".

We thank him for his valuable contribution and wish him all the success in future.

International Conference on the Frontiers of Plasma Physics and Technology FPPT

Kochi
17th April 2015

Prof. Tara Desai
Coference Director

Conference is organized in cooperation with the

International Atomic Energy Agency	Facility for Antiproton and Ion Research Germany	Technical University of Darmstadt Germany	Technical University of Vienna Austria

Conference is hosted by
PG and Research Department of Physics, Mar Athanasius college, Kothamangalam,
Mahatma Gandhi University, Kerala, India.

VIT®
UNIVERSITY
(Estd. u/s 3 of UGC Act 1956)
www.vit.ac.in
Vellore • Chennai
CHENNAI CAMPUS
Vandalur - Kelambakkam Road, Chennai - 600127

Sponsored by

CERTIFICATE OF PARTICIPATION

This is to certify that Mr/Ms/Dr ....Bhesha Raj Adhikari.....

of ..Tribhuvan University, Kathmandu.....has ~~participated~~ / presented a

~~oral~~ / poster in the 3rd PSSI-PLASMA SCHOLARS COLLOQUIUM (PSC-2014) & NATIONAL WORKSHOP ON EXPLORING PLASMA TECHNOLOGY FOR MATERIAL PROCESSING organized by Division of Physics, School of Advanced Sciences, VIT Chennai during 3 - 5th July 2014.

Bsarma.

Dr. Bornali Sarma
Co-Convener

Dr. Arun K. Sarma
Convener

VIT – A place to learn; A chance to grow

icpsa

International Conference on Plasma Science and Applications 2014

Bhesh Raj Adhikari

Central Department of Physics, Tribhuvan University, Kirtipur, Nepal

participated and presented a poster entitled

"Study of Kinetic Energy of Ion and Electron in Magnetized Plasma Sheath"

in the

International Conference on Plasma Science and Application (ICPSA2014)

held during **September 22 - 24, 2014** at

Kathmandu University, Dhulikhel, Nepal.

Prof. Dr. Deepak Prasad Subedi **Program Coordinator** **Kathmandu University**	**Dr. Raju Khanal** **Program Coordinator** **Tribhuvan University**	**Dr. Rajdeep Singh Rawat** **President** **Asian African Association for Plasma Training (AAAPT)**

INTI International University
LAUREATE INTERNATIONAL UNIVERSITIES

IPFS
Institute for Plasma Focus Studies

A A A P T
Asian-African Association for Plasma Training

CERTIFICATE

awarded to

Bhesh Raj Adhikari

Central Department of Physics, TU, Kirtipur

for actively participating in

The Numerical Experiment Workshop on Plasma Focus (NEW PF 2013)

held at

Kathmandu University, Dhulikhel, Nepal

September 27 – October 02, 2013

Dr. Deepak Prasad Subedi
Program Coordinator
Kathmandu University
Dhulikhel, Nepal

Prof. Saw Sor Heoh
Director
Centre for Plasma Research
INTI International University
Nilai, Malaysia

Prof. Lee Sing
Director
Institute for Plasma Focus Studies
Melbourne, Australia